

Approach for the Development of Suspensions with Integrated Electric Motors

Von der Fakultät Konstruktions-, Produktions- und Fahrzeugtechnik der
Universität Stuttgart zur Erlangung der Würde eines Doktors der
Ingenieurwissenschaften (Dr.-Ing.) genehmigte Abhandlung

Vorgelegt von
Meng Wang
aus Hebei, China

Hauptberichter: Prof. Dr. -Ing. Horst E. Friedrich

Mitberichter: Prof. Dr. -Ing. Eckhard Kirchner

Tag der mündlichen Prüfung: 06. May 2020

Institut für Verbrennungsmotoren und Kraftfahrwesen, Universität Stuttgart

Angefertigt am Institut für Fahrzeugkonzepte,
Deutsches Zentrum für Luft- und Raumfahrt (DLR) e.V. Stuttgart

2020

Acknowledgments

The author would like to thank his supervisors Prof. Dr. -Ing. Friedrich and Prof. Dr. -Ing. Kirchner for their consistent support and patience to his Ph.D study. The author is sincerely thankful to his advisor Dr. Elmar Beeh for his encouragement and guidance with his professional knowledge. Without their support, this thesis would not be completed.

I am grateful to have these colleagues, who provided me honest communication and exchange of learning experience: Dr. Zhou Ping, Dr. Andreas Höfer, Dr. Diego Schierle, Dr. Jens König, Dr. Gerhard Kopp and so on. I wish to thank the support of colleagues in laboratory of DLR FK, who helped me to complete the test and acquired the useful data in this work: Michael Kriescher, Philipp Straßburger, Cedric Rieger and so on. I wish to thank these friendly colleagues: David Krüger, Lucia Areces Fernandez, Marco Münster, Erik Chowson, Thomas Grünheid and so on, who let me enjoy the work in DLR FK. You are already my best friends in Germany. I want to mention Moritz Fisher, Dr. Bernd Propfe, Dr. Martin Redelbach who help me quickly accommodate the living and work in Germany. In my daily work I have been blessed with a friendly and cheerful group: DLR FK. I wish to thank all the colleagues who have given me help and encouragement.

Finally, I would like to thank my family member for supporting and understanding me throughout my study at university.

Kurzfassung

Das Konzeptdesign ist eine innovative und strategische Phase in der Produktentwicklung. In dieser Phase sind die Konzepterstellung und Entscheidung entscheidend für die folgende Produktentwicklung. Jedoch sind die realisierbaren Designkonzepte zu generieren und dann eine richtige Entscheidung zu treffen eine Herausforderung, da es sich um ein multidisziplinäres Design und unzureichende Informationen handelt. In der Konzeptionsphase von Elektrofahrzeugen ist Leichtbau ein Thema, das nicht ignoriert werden kann und von hoher Priorität ist. Die Kombination der Antriebseinheit in den Lenker ist eine effektive technische Lösung, um den Systemleichtbau zu erreichen und gleichzeitig die geringe Zunahme der ungefederten Masse zu realisieren. Allerdings sind hier folgende Fragen zu untersuchen: Wie die mit Elektromotoren integrierten Fahrwerkskonzepte unter Berücksichtigung der komplexen Funktionen, mehreren Designparameter und komplizierten Beziehungen systematisch generiert und bewertet werden können? Wie eine Strukturleichtbau der Achse für dieses kombinierte Konzept gestaltet werden kann? Wie die Fahrdynamik des Fahrzeugs mit diesem Fahrwerk bewertet wird?

In dieser Arbeit wird eine Design Methodik für die Entwicklung von mit Elektromotoren integrierten Fahrwerkskonzept vorgestellt.

Zunächst wird ein neuer Ansatz für die Funktionen Integration auf der Basis der Axiomatic Design vorgeschlagen. Bei diesem Ansatz wird die Funktion Integration formelhaft und explizit durch Matrixgleichungen beschrieben. Die Systemfunktionen, entsprechenden Parameter und ihre Beziehungen können in den Designmatrizen untersucht werden. Dieser Ansatz wird dann auf die Entwicklung von Fahrwerkskonzepten angewendet, die die Funktionen von Elektromotoren integrieren. Die generierten Konzepte werden durch die Vergleiche ihren Matrizen nach den Axiomen in Axiomatic Design bewertet und ausgewählt.

Anschließend wird ein Referenzfahrwerk getestet und die Parameter als Benchmark für die Entwicklung des Fahrwerkskonzepts verwendet. Die Designmatrix des Fahrwerkskonzept dient als Anleitung für nachfolgende Entwicklungen. Die Designvariablen in der Matrix werden in der Reihenfolge bestimmt, in der die mathematischen Matrixgleichungen gelöst werden.

Um die Systemmasse weiter zu reduzieren, wird die Topologieoptimierung für das Design der Fahrwerkstruktur unter der Berücksichtigung von kinematischen und elastokinematischen Zielen eingesetzt. Auf Basis von der Strukturtopologie wird eine aus Stahlrohren mit unterschiedlichen Dicken bestehende Leichtbaustruktur ausgelegt. Die Eigenschaften des Fahrwerkskonzeptes werden mit dem Referenzfahrwerk verglichen.

Um die Vertikal- und Rolldynamik des Fahrwerkskonzeptes zu untersuchen, werden ein analytisches Modell für die Fahrdynamik der Hinterachse und ein Straßenmodell für zweispurige Unregelmäßigkeiten gemäß den Straßenoberflächenprofile von ISO-8608 entwickelt. Diese Modelle können auf die Simulation der Fahr- und Rolldynamik des Zielfahrzeugs mit dem Konzept der Hinterachse angewendet werden. Die Fahrdynamik des Fahrzeugs mit dem neuen Fahrwerk wird mit dem Referenzfahrwerk verglichen.

Abstract

Conceptual design is an innovative and strategic phase in the process of product development. In this phase the concept generation and decision-making are critical to the following product development. However, it is a challenge to generate the realizable design concepts and then make a right decision because of involved multidisciplinary design and insufficient information. Lightweight design is a non-negligible and high priority subject in the concept design phase of electric vehicles. Combining the drive unit into suspension links is an effective engineering solution to achieve system lightweight while realizing the low increase of the unsprung mass. However, these questions arise from this idea: how the suspension concepts with integrated electric motors can be systematically generated and evaluated with consideration of complex functions, multiple design parameters and their intricate relationships? How an axle structure can be designed to be lightweight and suit this combined concept? How the ride dynamics of the vehicle with this suspension is evaluated?

This thesis presents a design methodology for the development of suspension concepts in which links are combined with electric motors.

Firstly, a new approach for concept design to integrating the functions based on the Axiomatic Design is proposed. In this approach, the integration process is formulaically and explicitly expressed by matrix equations. The system functions, corresponding parameters and their relationships can be investigated in the design matrices. This approach is then applied to the design of suspension concepts which integrate the functions of electric motors. The generated concepts are evaluated and selected by comparing their design matrices according to the Axioms introduced in Axiomatic Design.

Subsequently, a reference suspension is tested and the parameters are used as the benchmark for the development of the suspension concept. The design matrix of the

suspension concept is further to guide the subsequent engineering development. The design variables in the matrix are determined in the order in which the mathematical matrix equations are solved.

To further reduce the system mass, a topological design approach considering the suspension kinematics and compliance is proposed for the design of suspension structure. On the basis of the structure topology, a lightweight linkage consisting of steel tubes with different thickness is achieved. The characteristics of the suspension concept are compared with the reference suspension.

In order to investigate the vertical and roll dynamics of the concept suspension, an analytical model for the rear-axle vehicle dynamics and a road model for double lane irregularities in accordance with the ISO road standards are developed. These models can simulate the ride and roll dynamics of the target vehicle with the concept rear-axle on the ISO standard road surface. The ride dynamics with the new suspension is compared with the reference suspension.

Contents

Acknowledgments.....	iv
Kurzfassung	v
Abstract.....	vii
Contents.....	ix
List of Tables.....	xv
List of Figures.....	xvii
1 Introduction.....	1
1.1 Background.....	1
1.2 Overview of suspensions with integrated electric motors.....	2
1.2.1 Drive systems integrated into wheels (In-wheel motor)	3
1.2.2 Drive systems integrated into arms (Wheel-close motor).....	5
1.3 Overview of design theories and models	8
1.3.1 Development process	8
1.3.2 Design model und theories	9
1.3.3 Comparison of design methods.....	13
1.4 Research statement.....	14
1.5 Outline	17
2 Research target interpretation and requirement setting.....	21
2.1 Research target interpretation.....	21
2.1.1 Functional integration in the conceptual design phase.....	21
2.1.2 Structural design approach oriented to the concept suspension	22
2.1.3 Analytical model for ride dynamics	24

2.2	Technology status.....	26
2.2.1	Traditional suspension systems.....	26
2.2.2	Electric motors used for EVs.....	29
2.3	Requirements setting	30
2.3.1	Specification of the target car.....	30
2.3.2	Preliminary requirements for the suspension concept.....	33
3	A concept design approach based on Axiomatic Design for functional integration	37
3.1	AD method.....	38
3.2	Approach interpretation and illustration with an example of 3×3 matrices	41
3.2.1	Approach interpretation	41
3.2.2	Approach illustration with an example of 3×3 matrices	43
4	Concept design of suspensions with integrated electric motors using the proposed approach.....	51
4.1	Functional decomposition of the electric motor and suspension	52
4.1.1	Function decomposition of electric motors.....	52
4.1.2	Function decomposition of suspensions	54
4.2	Functional integration.....	59
4.2.1	Common functions	59
4.2.2	Functional integration based on design equation	60
4.3	Concept generation based on design equation.....	65
4.3.1	Conception based on McPherson suspensions.....	66
4.3.2	Conception based on double wishbone suspensions.....	70
4.3.3	Conception based on trapezoidal-link suspensions.....	72

4.3.4	Conception based on twist beam suspensions	76
4.3.5	Conception based on De-Dion suspensions	79
4.3.6	Conception based on multilink suspensions with one longitudinal arm	82
4.4	Comparison and evaluation	86
4.5	Design sequence on the basis of DM	90
5	Power and torque requirement of the powertrain	95
6	Investigation of the reference twist beam axle	105
6.1	Investigation of the reference rear axle by the test bench	105
6.1.1	Test rig	105
6.1.2	Testing cases	106
6.2	FEM model of the twist beam axle	107
6.2.1	CAD model	107
6.2.2	FEM modelling	108
6.3	Model validation	110
6.4	K&C analysis of reference twist beam axle	112
7	Structure optimization design considering K&C performance and geometric non-linearity	117
7.1	Structure optimization methods	118
7.2	Proposed approach	119
7.2.1	Geometric non-linearity	120
7.2.2	Wheel alignment vectors	122
7.3	Application to topological optimization of a concept suspension	124
7.3.1	Load cases	124
7.3.2	Optimization procedure	124

7.3.3	Mathematical model	126
7.3.4	Implementation with full constraints.....	127
7.3.5	Implementation without kinematic constraints.....	132
7.4	Implementation of size optimizations.....	133
7.4.1	Problem formulation	134
7.4.2	Implementation.....	135
7.5	Result comparisons.....	137
8	Modelling and analyzing ride dynamics of the concept suspension	141
8.1	Ride dynamics system.....	141
8.2	Ride dynamics model.....	144
8.2.1	Analytical models of vehicle ride dynamics	144
8.2.2	Modelling of the concept suspension	145
8.2.3	Modelling of the reference suspension.....	150
8.2.4	Simulink model.....	153
8.3	Road surface profile Model.....	155
8.3.1	The description of the stochastic road irregularities	155
8.3.2	Coherence of two road lanes	156
8.3.3	Modelling of two road lanes	158
8.3.4	Program and validation of road surface model	162
8.4	Ride dynamics analysis	164
8.4.1	Setting model parameters.....	165
8.4.2	Comparison of the ride dynamic response.....	167
8.4.3	Parameter sensitivity to vertical ride response	170
8.5	Conclusion.....	172

9	Conclusions and recommendations.....	175
9.1	Conclusions.....	175
9.2	Scientific contributions.....	176
9.3	Recommendations.....	177
	Bibliography.....	179
	Appendices.....	199
A.	Data of economic EVs in the market and concepts.....	199
B.	Vehicular three-dimensional reference system.....	200
C.	Data of the electric motor AMK DT5-26-10-POW.....	201
D.	Functional integration in case 2 and case 3.....	202
E.	Graphed classification of standard ISO roads.....	205
F.	Data of the suspension mass.....	206

List of Tables

Table 1.1: Characteristics of design methods.....	14
Table 2.1: NVH investigation methods and frequency scope	25
Table 2.2: Suspension classification and characteristics.....	27
Table 2.3: Characteristics of electric motors used for EVs.....	30
Table 2.4: Parameters of target car.....	33
Table 2.5: Preliminary K&C requirements.....	34
Table 4.1: New concepts generated by integrating common functions of suspension links and electric motors	66
Table 4.2: Effects of joints on required motions of McPherson suspensions	67
Table 4.3: Effects of joints on required motions of double wishbone suspensions.....	70
Table 4.4: Effects of joints on required motions of trapezoidal-link rear suspensions ..	73
Table 4.5: Effects of joints on required motions of multi-link suspensions	83
Table 4.6: Feasibility of the new concepts	86
Table 4.7: Integration feasibility comparison - Cross effects of DPm1 1, DPm2 1, DPm2 2, DPm2 3 and DPms2 1 on new suspension concepts.....	87
Table 5.1: Requirement of the Powertrain	100
Table 6.1: Important K&C parameters for twist beam axles.....	113
Table 7.1: Definition of loading conditions.....	130
Table 7.2: Definition of the constraints for the optimization	131
Table 7.3: Definition of the constraints for the optimization	134
Table 7.4: Results of the size optimization.....	137
Table 7.5: Comparison of K&C characteristics of reference and concept suspensions	138
Table 8.1: Key model parameters of vehicle dynamics	154
Table 8.2: Road classification (ISO 8608: 1995(E), 1995).....	156
Table 8.3: Parameters of the benchmark car	165
Table 8.4: Parameters of the target car.....	167
Table A.1: Investigation of economic EVs in the market and concepts	199

Table C.1: <i>Motor specification of the AMK DT5-26-10-POW (AMK Antriebs- und Steuerungstechnik GmbH Co. KG, 2012)</i>	201
Table F.1: <i>Data of suspension mass</i>	206

List of Figures

Figure 1.1: <i>Wheel hub motors</i> (Fischer, 2014) (Vijayenthiran, 2008) (Sterbak, 2007) (Wöstmann, 2011).....	4
Figure 1.2: <i>Schaeffler Wheel Module</i> (Harkort, et al., 2018).....	5
Figure 1.3: <i>Electric Twist Beam (eTB) from ZF AG</i> (Buchmeier, 2014).....	6
Figure 1.4: <i>In-Wheel-Transmission of the project FAIR from DLR</i> (Poetter, 2013).....	7
Figure 1.5: <i>Drive device for driving a wheel for electric vehicles</i> (Mair, et al., 2014).....	7
Figure 1.6: <i>Suspension system for electric vehicles in patent US 7413203 B2</i> (Kurata, 2008).....	8
Figure 1.7: <i>Engineering design process</i> (Priest & Sanchez, 2001) (Baxter, 1995).....	9
Figure 1.8: <i>General approach to product design and development</i> (VDI-Guideline 2221, 1993).....	12
Figure 1.9: <i>Engineering design theories and lightweight strategy in product design process</i>	16
Figure 1.10: <i>Outline of thesis</i>	19
Figure 2.1: <i>Market status and trends of suspension technology</i>	29
Figure 2.2: <i>Power-to-mass ratio of electric motors used for EVs</i>	31
Figure 2.3: <i>Torque-to-mass ratio of electric motors used for electric cars</i>	31
Figure 2.4: <i>Investigation of economic EVs in the market and in the concepts</i>	32
Figure 3.1: <i>Axiomatic Design Framework: domain and mapping</i> (Suh, 1990).....	38
Figure 3.2: <i>Function decomposition and zig-zagging process</i> (Gebala & Suh, 1992) ...	39
Figure 3.3: <i>Framework of functional integration process based on AD</i>	42
Figure 3.4: <i>An example of decomposition and combination</i>	43
Figure 3.5: <i>Functional integration process of two complex systems</i>	48
Figure 4.1: <i>Function decomposition of electric motors</i>	53
Figure 4.2: <i>Function decomposition of suspensions</i>	57
Figure 4.3: <i>Quarter-car suspension system</i>	58
Figure 4.4: <i>Decomposition of McPherson suspensions</i>	66

Figure 4.5: Concept 1 by combining the McPherson suspension with an electric motor	68
Figure 4.6: Decomposition of double wishbone suspensions	70
Figure 4.7: Concept 2 by combining the double wishbone suspension with an electric motor	71
Figure 4.8: Decomposition of trapezoidal-link rear suspensions	73
Figure 4.9: Concept 4 by combining the trapezoidal-link rear suspension with an electric motor	74
Figure 4.10: Decomposition of twist beam suspensions	76
Figure 4.11: Concept 6 by combining the twist beam suspension with electric motors	77
Figure 4.12: Decomposition of De-Dion suspensions	80
Figure 4.13: Concept 8 by combining the De-Dion axle with electric motors	81
Figure 4.14: Decomposition of multilink suspensions with a longitudinal arm	83
Figure 4.15: Concept 10 by combining the longitudinal arm with an electric motor	84
Figure 4.16: Nominal weighting factor of design criteria	89
Figure 4.17: Scoring of suspension concepts based on design criteria	89
Figure 4.18: Synthesis evaluation of suspension concepts	90
Figure 5.1: Wheel power and torque characteristics of the EV and its acceleration	97
Figure 5.2: Acceleration time of target vehicle with different wheel torque and power	99
Figure 5.3: Required wheel torque and power for vehicle acceleration	99
Figure 5.4: Dual motor powertrain	101
Figure 5.5: Drive unit construction	103
Figure 6.1: Test rig for the reference twist beam axle	106
Figure 6.2: Testing of the twist beam axle	106
Figure 6.3: CAD modelling of the twist beam axle	107
Figure 6.4: CAD model of bushings	109
Figure 6.5: FE model of bushings	109
Figure 6.6: FE model of the twist beam axle	110
Figure 6.7: simulations of twist beam axle	110

Figure 6.8: Simulated results compared with the experimental results	111
Figure 6.9: Load cases for the reference rear axle simulation.....	112
Figure 6.10: K&C characteristics from FEM simulation	114
Figure 7.1: ESL method	120
Figure 7.2: Defining the suspension K&C performance by a vector	123
Figure 7.3: Flowchart of the optimization procedure.....	125
Figure 7.4: Topological design space	128
Figure 7.5: Suspension arm combined with the electric motor	128
Figure 7.6: Iteration histories of objective function and constraint violation	131
Figure 7.7: Result of topological optimization considering K&C characteristics	132
Figure 7.8: Iteration histories of camber angle and toe angles.....	132
Figure 7.9: Result of topological optimization without kinematics constraints	134
Figure 7.10: Conceptual structure assembled by steel tubes based on the design topology	135
Figure 7.11: Iteration histories of objective function and constraint violation in size optimization.....	136
Figure 7.12: Iteration histories of camber angle and toe angles	136
Figure 7.13: Concept suspension with lightweight linkages.....	137
Figure 8.1: Description of the vehicle ride dynamics system of a passive suspension .	142
Figure 8.2: Development path of the Roll plane model	146
Figure 8.3: Model of quarter target vehicle with the concept suspension.....	147
Figure 8.4: Model of quarter benchmark vehicle with the reference suspension.....	152
Figure 8.5: Structure of the Simulink model	153
Figure 8.6: Overview of the Simulink model.....	154
Figure 8.7: Road PSDs of C-level road roughness on the left and right sides	163
Figure 8.8: Time domain road profile of the left and right tracks	163
Figure 8.9: Comparison of the road PSDs of B-level road simulated on the left and right sides with the ISO 8608 standards.....	164

Figure 8.10: Validation of the coherence of the C-level road with the specified coherence function.....	164
Figure 8.11: Comparison of the vehicle dynamic responses on standard ISO road surface of class C	168
Figure 8.12: Vehicle dynamic responses speed 10 m/s on standard ISO road surface class C.....	170
Figure 8.13: Comparisons of the rms vertical ride response of sprung mass with the benchmark suspension and the concept suspension	170
Figure 8.14: Rms ride performance of sprung mass with different torsion stiffness.....	171
Figure 8.15: Rms wheel load fluctuation of the concept suspension with different unsprung mass	171
Figure 8.16: Rms ride performance of sprung mass with different reaction torque in gear engagement.....	172
Figure 8.17: Top view of the whole suspension concept.....	173
Figure 8.18: Front view of the concept suspension.....	173
Figure B.1: Vehicular three-dimensional reference system (ISO 4130: 1978, 1978)	200
Figure C.1: Technology performance of the AMK DT5-26-10-POW (AMK Antriebs- und Steuerungstechnik GmbH Co. KG, 2012)	201
Figure E.1: Classification of standard ISO roads (ISO 8608: 1995(E), 1995)	205

Abbreviations

AC	Alternating Current.
AD method	Axiomatic Design Method
CA	Customer Domain
CAD	Computer-Aided Design
CAE	Computer-Aided Engineering
C-K	Concept-Knowledge
CSD	Cross Spectral Density
CV	Constant velocity
DC	Direct Current
DFT	discrete Fourier transform
DM	Design Matrix
DOF	Degree of Freedom
DP	Design Parameter
DSM	Design Structure Matrix
D&D	Design and Development
ESM	Electrically excited Synchronous Machine
ESL	Equivalent Static Load Method
EV	Electric Vehicle
FEM	Finite Element Method
FFT	Fast Fourier Transformation
FR	Functional Domain
HEV	Hybrid Electric Vehicle
IFFT	Inverse Fast Fourier Transformation
IM	Induction Motor
K&C	Kinematics and Compliance
MBS	Multi-Body Simulation
NPD	New Product Development

NVH	Noise Vibration and Harshness
OEM	Original Equipment Manufacturer
PMSM	Permanent Magnet Synchronous Motor
PSD	Power Spectrum Density
PV	Process Domain
RMS	Root Mean Square
SEA	Statistical Energy Analysis
SIMP	Solid Isotropic Material with Penalization method
TIPS	Theory of Inventive Problem Solving

Notation

A_v	Projected frontal area of the vehicle
$[A]$	Design matrix
a	Acceleration
a_{01}	Acceleration in the constant-torque region
a_{12}	Acceleration in the constant-power region
C_{mech}	Utilization factor
C	Stiffness matrix
c	Safety coefficient
c_1	Wheel stiffness
c_2	Suspension stiffness
c'_2	Equivalent spring stiffness
c_k	Torsion stiffness of the suspension structure
c_w	Drag coefficient
D	Diameter of tube elements
D_R	Diameter of the rotor
D_m	Coil diameter
D_s	Diameter of the stator
d	Diameter of the wheel
d_m	Average pitch diameter of teeth
E	Finite index set
e	Sub-domain in the structural design domain
F_A	Aerodynamic resistance
F_a	Axial component of the force
F_B	Force on the pivot point B
F_D	Damping force
F_d	Driving force on the wheel
F_e	Vibration force from the electric motor

F_F	Spring force
F_G	Gradient resistance
F_g	Vertical force on gear meshing
F_I	Acceleration resistance
F_k	Force caused by the torsion stiffness
$F_{Req,wheel}$	Required wheel driving force
F_T	Total resistance force
F_{Roll}	Rolling resistance
F_R	Reaction force from the wheel center
F_r	Radial component of the force on the driving gear
F_t	Tangential component of the force
F_Z	Vertical force caused by rolling of the tire on uneven grounds
$F(\omega)$	Frequency domain signal
f	Time frequency
$f(t)$	Time domain signal
f_{eq}	Vector of nodal forces associated to the external loads
f_{eq}^t	Vector of nodal forces associated with time step
f_{obj}	Objective function
f_R	Coefficient of rolling resistance
f_{Sges}	Distance from the total gravity center of the axle and wheel to the point B
G	Shear Modulus
$G_q(n_0)$	Fitted vertical displacement PSD
$G_q(n)$	Road spatial PSD
$G_{ll}(\omega)$	Auto-PSD of $h_l(t)$ in time frequency domain
$G_{lnn}(\omega) /$ $G_{luu}(\omega)$	Auto-PSD of $n_l(t)$ and $u_l(t)$ in time frequency domain respective
$G_{lnu}(\omega), G_{lun}(\omega)$	Cross-PSD of $n_l(t)$ and $u_l(t)$ in time frequency domain
$G_{lnn}(n) / G_{luu}(n)$	Auto-PSD of $n_l(t) / u_l(t)$ in spatial frequency domain respective

$G_{ll}(n) / G_{rr}(n)$	Auto-PSD of $h_l(t) / h_r(t)$ in spatial frequency domain respective
$G_{rl}(\omega)$	Cross-PSD of $h_r(t)$ and $h_l(t)$ in time frequency domain
g	Standard gravity
g_i	Constraint function for topological optimization
H	Correlative coefficient
H_k	DFT of h_m
$H_{hr}(\Omega)$	Displacement spectrum of $h_r(l_r)$
$H_{hr}^*(\Omega)$	Complex conjugates of the displacement spectrum $H_{hr}(\Omega)$
$h_l(t)$	Road roughness of the left side in time domain
$H_{ln}(\omega)$	Fourier transform of $n_l(t)$
$H_{lu}(\omega)$	Fourier transform of $u_l(t)$
$H_{lh}(\omega)$	Fourier transform of $h_l(t)$
h	Road excitation
h_i	Equilibrium function for topological optimization
$h_r(l_r)$	Road irregularity on the right side
$h_r(t)$	Road roughness of the right side in time domain
I	Finite index set
i	Vehicle front/rear mass distribution
i_B	The radius of the moment of inertia of the axle and the wheel
i_b	Ratio of bevel gears
i_f	Number of active coils
i_p	Ratio of planetary gear set
J_B	Moment inertia around point B
J_L	Moment of inertia of trailing arm around the gravity center
\mathbf{K}	Damping matrix
k	Different loading conditions
k_2	Suspension damping
k'_2	Equivalent damping

L	Road profile with a length L
L_R	Rotor length
L_S	Length of stators
l	Wheelbase
l_D	Longitudinal distance from the damper position to the pivot B
l_e	Longitudinal distance from gravity center of the electric motors to pivot B
l_F	Longitudinal distance from the spring position to the pivot B
l_g	Longitudinal distance between the driving gear center and driven gear center
l_L	Longitudinal distance from the wheel center to the pivot B
l_S	Longitudinal distance from gravity center of the trailing arms to pivot B
M	Mass matrix
M_g	Reaction rotational torque on the gear box
m_1	Unsprung mass
m_2	Sprung mass
m_a	Mass of the whole axle
m_L	Total mass of the trailing arm
m_R	Mass of parts fixedly connected with the wheel
m_v	Vehicle mass
n	Spatial frequency
n_{el}	Number of elements of the domain in topological optimization
n_0	Reference spatial frequency
n_k	Frequency at the k^{th} point
n_r	Rotational speed
n_{upper}	Upper limit of the road spatial frequency
$n_l(t)$	Signal caused from system input $h_r(t)$
p	Number of pole pairs

P_{mech}	Rated power of electric motor
P_0	Constant power on the wheels
R_g	Gear pitch circle of the driven bevel gear
R_w	Radius of the wheel
r	Wheel radius
s	Wheel track
\mathbf{s}_p	Wheel alignment vector
$[s_x, s_y, s_z]$	Wheel alignment vector components along x, y and z axes
t	Time
T	Time interval
T_{Req}	Required torque of vehicle
T_g	Torque on the gear
T_0	Constant torque on the wheels
u	Sub-structural domain
\mathbf{u}	Vector of nodal displacement
\mathbf{u}^t	Vector of nodal displacement associated with time step
$u_l(t)$	Noise signal
v	Vehicle speed
v_1	Rated speed of electric motor/vehicle
w	Road undulation exponent
w^k	Weight factor corresponding to different loading conditions
x_{hom}	General solution to homogenous differential equation
x_{part}	Particular solution
\mathbf{Z}	Maximal structural design domain
\ddot{z}_2	Vehicle body vibrational acceleration
\dot{z}_2	Vehicle body vibrational speed
z_2	Vehicle body vibrational displacement
\ddot{z}_1	Wheel vertical acceleration
\dot{z}_1	Wheel vibrational speed in the vertical direction

z_1	Wheel vibrational displacement in the vertical direction
\ddot{z}_L	Acceleration of trailing arm
z_l	Vertical motion of gravity center of the trailing arm
α	Pressure angles of the gear
β	Road grade angle
β_g	Spiral angle of the gear
γ_h	Coherence of the left and right road paths
δ	Bevel angle of the gear
η_p	Damping ration of suspension system
θ_{toe}	Toe angle
θ_{camber}	Camber angle
λ	Mass factor
λ_p	Natural frequency of suspension system
λ_r	Relative length
μ_R	Frictional coefficient between rear tire and road
ν	Poisson's ratio
ρ_A	Air density
$\boldsymbol{\rho}$	element density vector
ρ_i	Continuous densities of the i^{th} element
τ_p	Pole pitch
φ_2	Rotated angle of unsprung mass m_2
φ_L	Rotated angle of the trailing arm
ω	Angular frequency
ω_2	Rotational speed of sprung mass around the front axle
ω_L	Rotation speed of trailing arm around pivot point B
Δl	Road segment
$\Phi_{hrr}(\Omega)$	Auto-PSD of the right road
$\Phi_{hll}(\Omega)$	Auto-PSD of the left road
$\Phi_{lr}(\Omega)$	Cross spectral density (CSD) of the left and right road

Ω	Angular spatial frequency
Ω_p	Reference angular frequency

1 Introduction

1.1 Background

In the development history of vehicles, suspensions have been constantly improved to meet changing technology requirements of vehicles in different time.

At the beginning of the 20th century, the automotive suspensions consisted of only rigid axles and springs without shock absorbers, like the Benz 11/40 (1912-1914) and Benz 6/18 PS (1921) (Oswald, 1987). With the development of more powerful engines, cars became faster, but at the same time their mass increased; importantly, with the differential integrated to the rigid axle the unsprung mass was also increased dramatically. In order to cope with higher speeds and larger sprung and unsprung masses and to improve ride comfort, engineers used shock absorbers to damp the rebound force of springs (Daimler AG, 2008); a surge of innovations in suspension technology followed in the 1930s. Independent suspensions, which allow each wheel on an axle to move (i.e., reacting to bumps in roads) independently, made their debut during this wave of suspension innovation, as can be seen in the suspensions used in the Benz Typ 170 and 380 (Barthel & Lingnau, 1986) for instance. This invention not only improved the ride comfort and safety, but also enhanced the stability of the vehicle due to a better axle kinematics and compliance (K&C) performance.

With growing demand for improved vehicle ride comfort and safety as well as handling and stability, electromechanical technologies in suspensions are rapidly developed. By semi-active suspensions or active suspensions the spring or damper or both can be adjusted through a control system, e.g. the Adaptive Damping System and Active Electromagnetic System (Gysen, et al., 2010). Those systems control actuators to adjust the suspension spring rate or damping with response to the road feedback signals or driving situation (Daimler AG, 2008) (HAĆ, 2010). Compared to passive suspensions ride comfort and the dynamic of vehicles are significantly improved with semi-active or active suspensions (Koch, 2010).

At present, the hybrid electric vehicle (HEV) and electric vehicle (EV) are considered to represent the technology trend of the automotive industry facing the increasingly severe environmental and energy issues. However, a bulky battery package and limited driving range restrict the development of the HEVs and EVs. That being the case, lightweight design is an effective way to reduce vehicle energy consumption so as to improve the driving range. For the design of automotive suspensions, combining the electric drive system to the suspension system is an effective solution to significantly reduce the total system mass and system space occupation through the functional sharing of suspension arms and electric motor cases and elimination of joint shafts, subframe, engine mounts, and so on.

1.2 Overview of suspensions with integrated electric motors

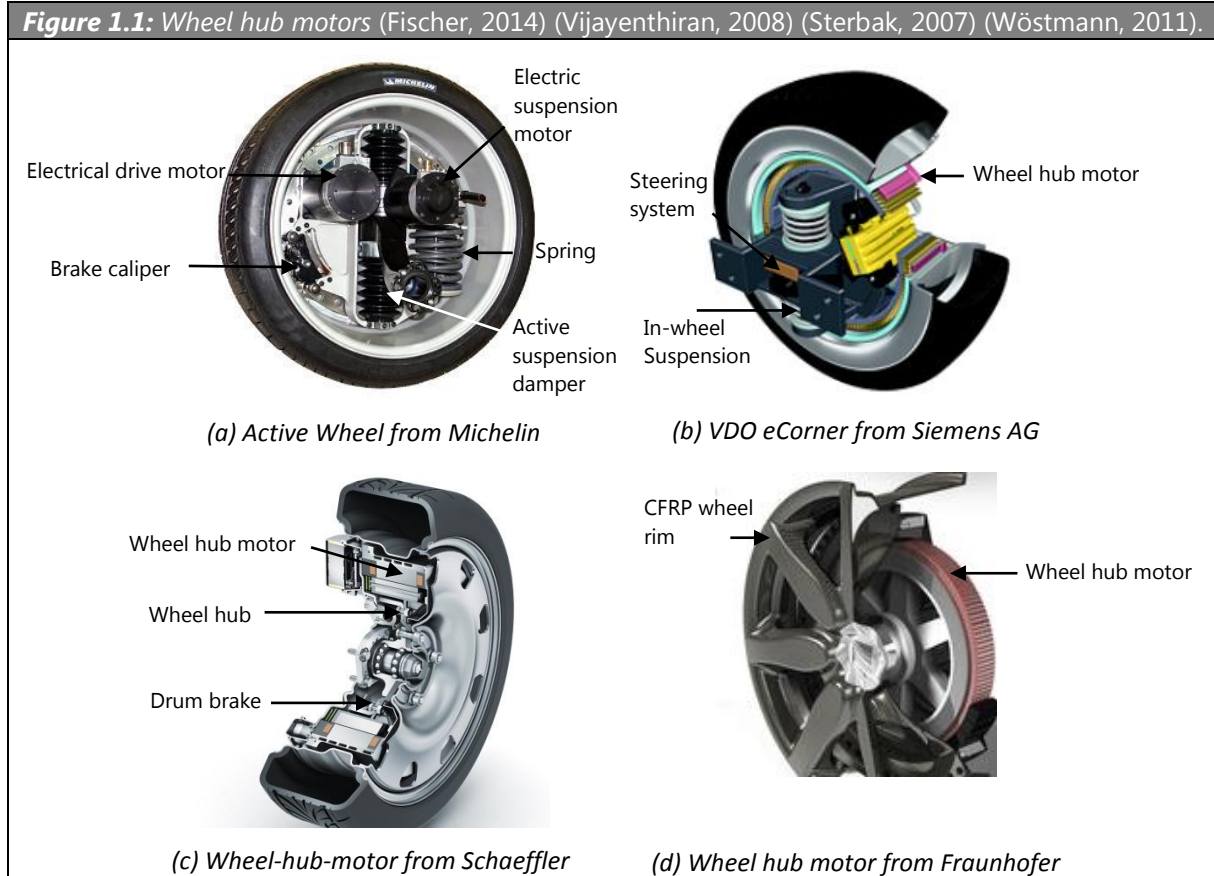
The optimization of power-to-mass and torque-to-mass ratios of motors for EVs makes it possible to integrate the electric motors into suspensions. The German literature usually classifies these electric motors into wheel hub motors and wheel-close motors according to the structure and position of the electric motors (Heißing, et al., 2013). The wheel hub motors have two typical configurations: with inner or outer rotor. The internal rotor rotates the motor shaft which is then fastened to the wheel hub, e.g. the wheel hub motor from Schaeffler in year 2014 (Fischer, 2014) (see Figure 1.1 (c)). The external rotor rotates the motor housing which must be attached to the wheel rim, e.g. the wheel hub motor from Protean (Protean Electric Ltd, 2016). By these wheel-hub motors, the rotor rotates with the same speed as the wheel. However, there are still electric motors by which the rotor is connected to the wheel hub through a gear system, e.g. the electric motor from Michelin Active Wheel (Heißing & Ersoy, 2007) and the electric motor from Schaeffler in year 2018 (Harkort, et al., 2018). In this dissertation, they are all classified to in-wheel motors.

The wheel-close motors refer to the electric motors that are located close to the wheel. With rigid and semi-rigid axles or single-link wheel suspensions, the electric motor can be fastened directly to the wheel carrier (see Figure 1.3). Since the tight space

conditions this concept is only suitable for smaller electric motors with low power. If the electric motor becomes too large and heavy, it must be attached to the body (see Figure 1.4). A special configuration or structure should be considered, due to the short distance between the motor shaft and the wheel hub. It is not possible to install a side shaft because the necessary bending angles would be too large.

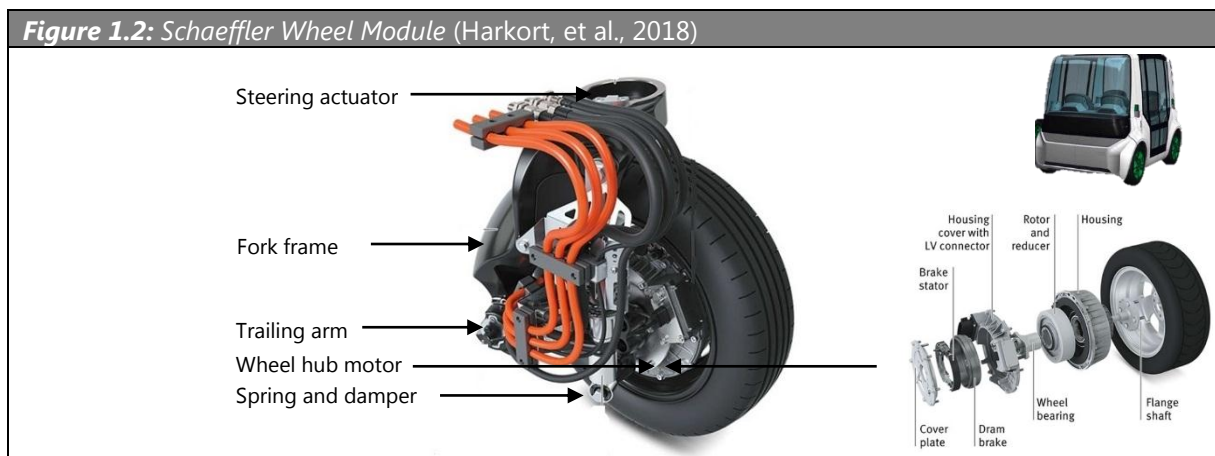
1.2.1 Drive systems integrated into wheels (In-wheel motor)

As high transmission efficiency from drive system to wheels, numerous researches have been launched in the area of in-wheel drive system. The drive system could include a high-speed electric motor with a set of reduction gear or only a wheel hub motor. Wheel hub motor is a combination of the wheel hub and the electric motor. Their features are introduced by the examples in Figure 1.1. The Michelin Active Wheel (see Figure 1.1 (a)) applies the in-wheel drive motor with reduction gears, in which the power of the electric motor is transferred to the wheel hub through a reduction gearing set (covered by the shell) and moreover an active suspension system (consisting of a coil spring and active damper) are also integrated into the wheel (Vijayenthiran, 2008). In this design the power and torque of this electric motor are limited by narrow design space. Instead of the small drive motor the VDO eCorner from Siemens in Figure 1.1 (b) installs a wheel hub motor as propulsion motor and meanwhile an active steering system is also compactly integrated into the wheel. These two designs are high-level functional integration (Sterbak, 2007). However, there is still no open data to illustrate and evidence the performance of the active in-wheel suspensions. Obviously, the complex designs make the wheels a high engineering challenge in the system robustness and stability. Wheels are easily-worn and sensitive components that are exposed to harsh environments, which cause both designs high maintenance difficulty and application cost. Schaeffler and Fraunhofer Institute both have engaged in the development of the wheel hub motor (see Figure 1.1 (c) and Figure 1.1 (d) respectively), but the suspension systems are deployed independently out of the wheel. Schaeffler design incorporates the rotor and drum brake to the wheel hub.



They also evaluated the application of their wheel hub motor system on the basis of FORD Fiesta. By a series of road testing they obtained the conclusion that the handling could be kept at the same level as the original series production car through adjustment of spring-damper system and drive dynamics control system (Eckert, et al., 2018) (Fischer, 2014). In order to reduce the increment of unsprung mass caused by the in-wheel motor, Fraunhofer Institute developed a carbon-fiber-reinforced polymer (CFRP) wheel rim (Wöstmann, 2011). The detailed operative principles of above designs are described in the references (Fischer, 2014) (Vijayenthiran, 2008) (Sterbak, 2007) (Wöstmann, 2011). These designs free up space beneath the hood and reduce the total mass of the drive and chassis systems, which give more possibilities for automotive design. However, the increased unsprung mass deteriorates the dynamic performance of vehicles to a certain extent (Jungmann, 2006). German automotive Original Equipment Manufacturers (OEM) have not applied this kind of suspensions with wheel hub motor in series vehicle productions until the current dissertation (Gombert, November 2007).

On the basis of wheel hub motors Schaeffler developed further the E-mobility solution. For example, a wheel module (see Figure 1.2) for urban vehicle concept in which all four wheels can be driven and steered independently of each other incorporates a wheel hub motor, suspension, steering system and fork frame (Harkort, et al., 2018). The wheel hub motor utilizes a permanently excited synchronous machine (continuous output of 13 kW and temporary peak output of 25 kW) and a three-stage planetary gear with a gear ratio of 3.35. The fork frame connected with a steering actuator can realize the whole wheel steering to 45°.

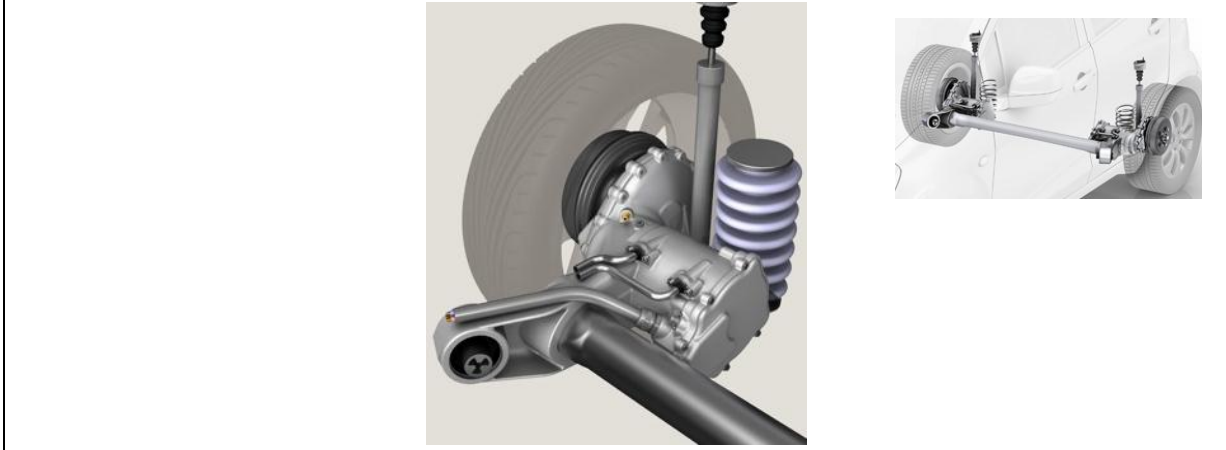


1.2.2 Drive systems integrated into arms (Wheel-close motor)

Integrating the drive system to suspensions arms is a way to diminish the negative effect of the increased unsprung mass. When the motor is installed to the suspension arm, its mass is partially distributed on the vehicle body and the rest on the wheel. In addition, the design integrating the drive system to suspensions arms can free more design space, which is traditionally occupied by drive systems, and at the same time generates less increase of the unsprung mass.

The model of the electric twist beam in Figure 1.3 is a concept from ZF Friedrichshafen AG (ZF) used in small cars or mini cars. In this concept, two electric motors with each 40 KW power are combined to the longitudinal arms of the twist beam axle separately (Buchmeier, 2014). The motor shell is made of aluminum material which is used to minimize the increment of the unsprung mass.

Figure 1.3: Electric Twist Beam (eTB) from ZF AG (Buchmeier, 2014)

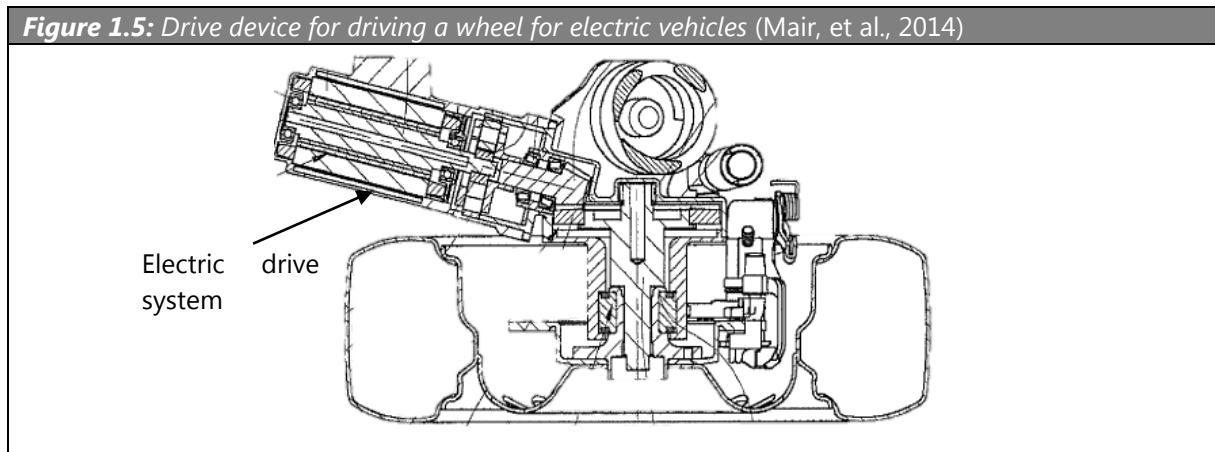
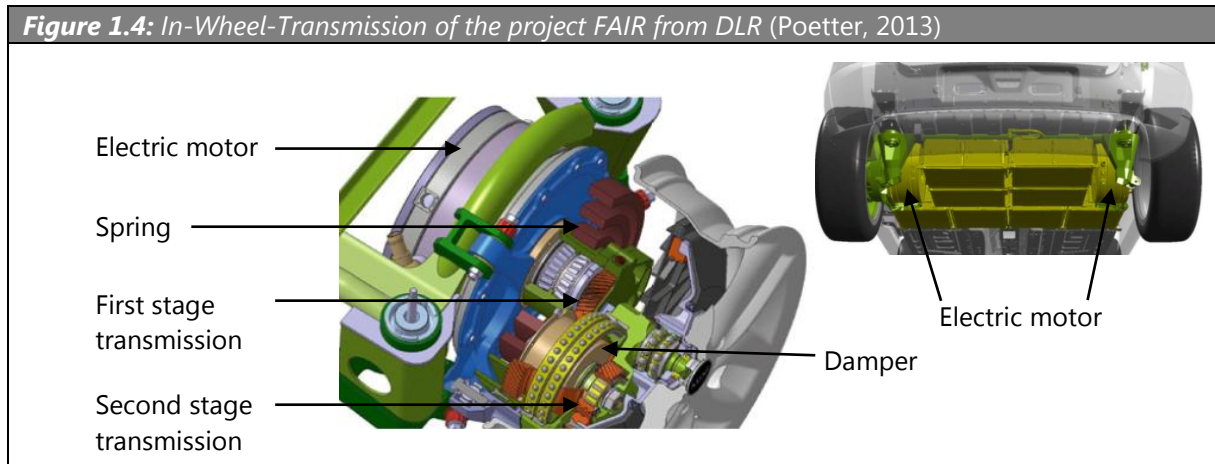


In a cooperative research project, FAIR (Fahrwerk/Antrieb-Integration ins Rad), conducted by the German Aerospace Center (DLR) and BMW, a concept with an in-wheel-transmission (see Figure 1.4) carries out the functions of suspension and transmission (Poetter, 2013). In this concept, the transmission housing defines the wheel alignment. The rotational damper and spiral-wound spring in rotational axes absorb the shock as the wheel bumps and rebounds. This structure enables an installation of the motors close to or in the wheel. It leads to a high gains in installation space with low unsprung masses despite the choice of scalable input torques, and improves the crash safety of the high-voltage battery between the wheels (Pruckner, et al., March 2014).

In Figure 1.5, the electric drive system functions simultaneously as the longitudinal arm of a suspension. The power from the drive system is transferred to the wheels through a planetary gear and a bevel gear. The utilization of this structure is possible for suspensions which possess longitudinal arms, such as twist beam suspensions, suspensions with longitudinal link arms, central link suspension or semi-trailing link suspension (Mair, et al., 2014).

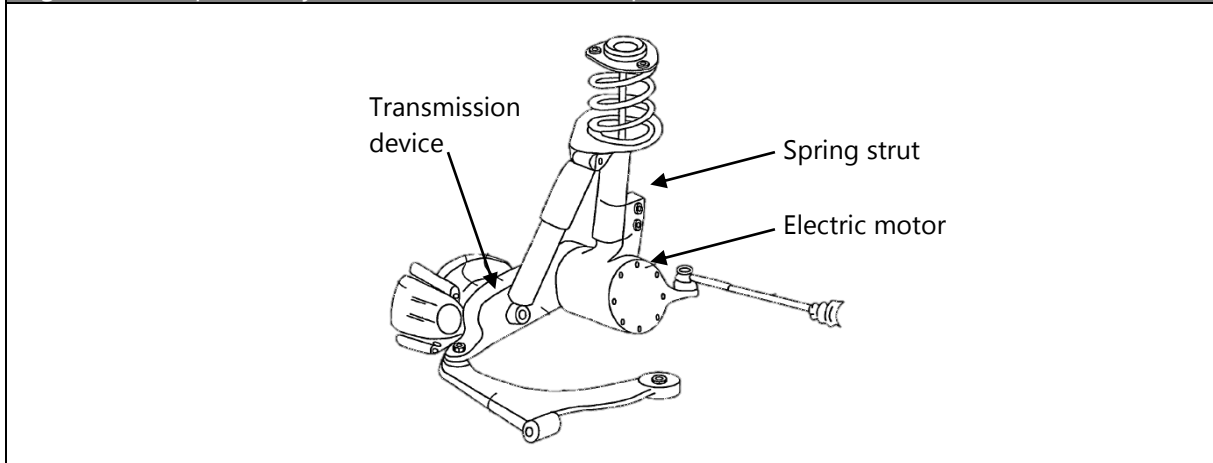
Figure 1.6 shows a suspension that combines an electric motor into the longitudinal arm. The power from the motor is transferred to the wheel through a transmission device. The shell of the electric motor supporting the spring strut is part of the suspension which transfers the loads from the road surface to the vehicle body. It takes

over the role of the longitudinal arm of the suspension together with the shell of the transmission device (Kurata, 2008).



Besides these studies, a number of investigations on suspensions integrated with electric motors are also conducted by researchers from China. For example, kinematics simulation was carried out for a suspension with a belt transmission device whose housing performs as the longitudinal arm of the suspension (Chen, et al., 2013); a double trailing arm suspension integrated with chain transmission device was designed and studied (Xue, 2009).

Figure 1.6: Suspension system for electric vehicles in patent US 7413203 B2 (Kurata, 2008)



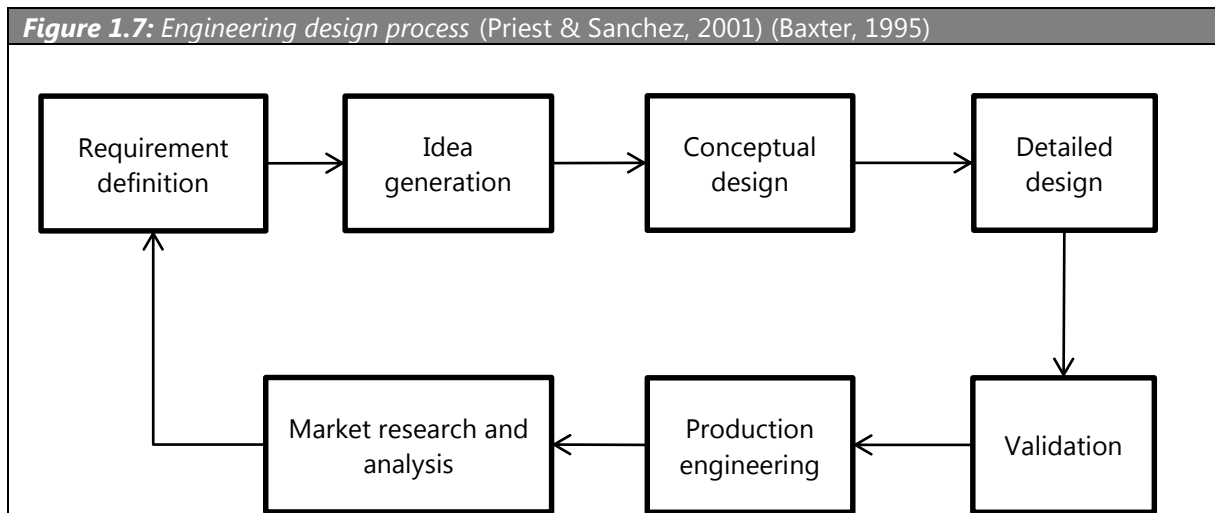
1.3 Overview of design theories and models

1.3.1 Development process

The development of new suspensions in the automotive industry is essentially a process of new product development (NPD) involving business and engineering activities (Zhang, 2006). Increasing global competition compels automotive manufacturers to streamline the NPD process in order to meet the needs of different markets and segments timely. Because of high dependence on technology and engineering, reducing product design and development (D&D) time in engineering process poses a great factor for this target.

The basic process of NPD principle can be illustrated by the flowchart in Figure 1.7 (Priest & Sanchez, 2001) (Baxter, 1995). This flowchart consists of two processes: the engineering process (from idea generation to production engineering) and the marketing process (from market research and analysis to requirement definition). Idea generation for NPD can be inspired by various factors, such as market requirements, brainstorming, morphological charts, products of competitors, revolutions of relevant technology, and solutions to analog problems. After the initial inspiration unfeasible ideas should be eliminated. In the conceptual design stage, inspired ideas should be conceptualized according to specific product requirements. The concepts should be evaluated depending on specified criteria, such as product functions, marketing, cost or other related factors. The purpose of this stage is to form and evaluate the feasible

concepts, in order to make a final decision by identifying the most appropriate solution. The detailed design aims to provide a complete description of the product with respect to material, reliability, durability, manufacture and other items. In the validation stage a prototype of the product is tested on component, subsystem and whole vehicle levels. The problems, which need to be solved in the production stage, are related to volume production, communication with suppliers, and improvement of productivity.



1.3.2 Design model und theories

Engineering design is different from artistic design which is more inspired from intuition, feeling or incentive. A lot of experts' references are required to an optimum design. NPD needs to deal with a large number of variables. Engineering design is a systematic intelligent generation and evaluation of object specifications which satisfy specified form and functional requirements (Dym, 1994). Designers must rely on their own experience and expertise to generate and evaluate concepts in lack of quantitative information in the conceptual design phase (Jin, et al., 2005). In the initial stage, modelling and simulating all the concepts using Computer Aided Design (CAD) is time-consuming and unrealistic. With industry development, a number of design approaches have been developed to assist designers in generating innovative product concepts and identifying appropriate product concepts (Magrab, et al., 2009). Main publications on design models and theories are collected in chronological order with summary of individual efforts and achievements in reference (Pahl, et al., 2007). But

when considering their fundamental principles, these models do not differ significantly from each other. To avoid confusion, five elementary categories of design models are classified according to their focal points: algorithmic models, strategic models, tactical models, operative models and models of reasoning (Geis & Birkhofer, 2010). In order to take advantage of these models to accomplish complex designs and evaluation, engineering design theories are reviewed briefly as follows.

VDI 2221 guideline

The VDI 2221 (English translation: systematic approach to the design of technical systems and products) has been developed by German VDI (Verein Deutscher Ingenieure, English translation: German Association of Engineers) community comprising a wide range of experienced designers from industry and education. It defines a generic approach to the design of technical systems and products, which includes seven basic working steps iterating forwards and backwards between previous and following stages (see Figure 1.8) (VDI-Guideline 2221, 1993). It defines the tasks of each phase and the relevant methods could be used in this phase to complete these tasks. This guideline works as a fundamental framework for designers and engineers to develop new products in a wide field of application in German-speaking lands (Jänsch & Birkhofer, 2006). The design process is generally structured, which permits designers to specify their detailed design procedure in according with practical conditions. This guideline can be regarded as a generic procedure model of product design, and practical design can be flexibly assigned along the procedure structure proposed by the stages of design process in this guideline. It can also be considered as a prescriptive approach to product design, because the general development procedures and working steps in each phase have been prescript in the application of this guideline. In this approach the procedure concept governs the product designing.

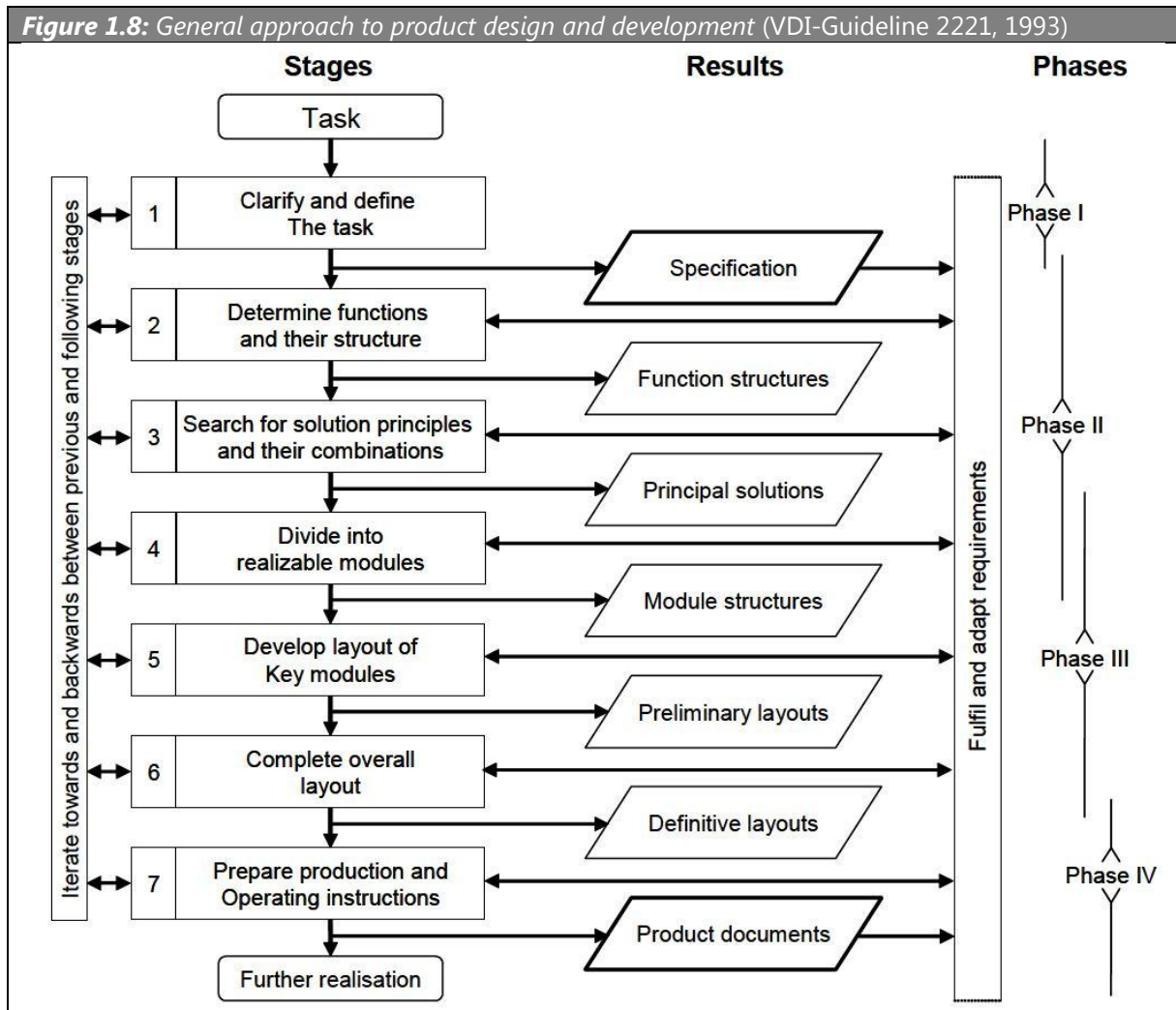
Axiomatic design

The Axiomatic Design, developed by Suh Nam Pyo, introduces a systematic approach for the product design (Suh, 1990), which is completely different from the VDI

procedure model. This design method considers designing from perspective of mathematics, by applying matrix equation to describe designing structure. In this approach designs are considered to consist of customer needs, functional requirements, design parameters, and process variables. The design process proceeds in a more abstract form as a continuous interplay among the above four domains. The transformation of functional requirements into design parameters is formalized by the design matrix. The design can be evaluated according to Axioms introduced in AD method. This approach focuses on the attribute of design and expressing the transformation of attributes in a mathematic algorithm. The matrix attributes and Axioms govern the designing. The application difficulty of axiomatic design is to decompose appropriate functional requirements and coupled design parameters in a complex product design.

Design structure matrix

Design structure matrix (DSM) is an effective tool to analyze the interaction relations among system elements (Steward, 1981). Through mapping the information flow of product components or project developing process, the inter-relationships in systems can be investigated. Thereby the DSM provides important guidance to the new product development and project management. However, this method is inadequate in innovative design and has been commonly applied in the analysis of the existing systems. DSM and AD are integrated by Tang (Tang, et al., 2008), DSM is mainly applied to analyze the interaction of existing products; AD method has more advantages for guiding the designer to find appropriate parameters that meet the requirements of functions.



Concept-knowledge (C-K) design theory

C-K theory, introduced by Hatchuel in 1996 (Hatchuel, 1996), was recognized as a unified design theory describing creative reasoning and process in engineering design. This theory is based on a formal distinction between two interdependent spaces: the space of concepts (C) and the space of knowledge (K). Design reasoning is defined as logic of expansion processes between C and K with different structures and logics. As such, it provides a rigorous and unified formal framework to generate innovative concepts. The interplay and expansion between unknown objects and existing knowledge improve our understanding of innovative design. However, this theory does not explain specific interaction between the functions and design parameters.

Theory of inventive problem solving (TRIZ)

TRIZ, proposed by Altshuller in the 1950s (Sushkov, et al., 1995), is a method intended for application in problem-solving and system analysis. This method solves inventive problems based on the study of existing analogue problems and solutions (Gadd, 2011). According to TRIZ, an inventive situation might be identified to contradictions (one of the basic TRIZ concepts). On the study of invention patterns in the global patent literatures, 40 inventive principles and a contradiction matrix are developed to help engineers to find the existing analogue contradictions and further innovative solutions. The inventive process can be structured as: firstly define the specific problem to contradictory elements; then find the analog contradictory elements in the existing problems-solutions using the 40 inventive principles or contradiction matrix; at last through thinking the solutions, develop the specific solution.

1.3.3 Comparison of design methods

These methods have their own respective advantages and disadvantages. Their characteristics are summarized in the Table 1.1. The VDI 2221 guideline offers a generic approach to design and is strong in the proscribed procedure, which can help designers to assign the design strategy. The AD provides a method from a matrix standpoint to decompose a design by matrix equation; it supports designers from the mathematical aspect to perceive physical attributes in designing and the relationships among design functions and parameters, moreover the Axioms help the designers to evaluate designs and make decisions. This AD method can be applied to new concept design and extended design study on the basis of existing design matrix equation. The DSM provides an approach to describe the interaction among the design parameters, which is suitable in design improvement and project management. The C-K design method is an approach in focus on the concepts and knowledge, which can help in reasoning of designers. The TRIZ is a strong tool for inventive problem solving for engineers.

<i>Table 1.1: Characteristics of design methods</i>		
	Advantages	Disadvantages
VDI 2221 guideline	<ul style="list-style-type: none"> • Prescribed design process • Procedure model 	<ul style="list-style-type: none"> • Lack of model to express design itself • Lack of model to express the transformation among requirement, function and parameters
AD method	<ul style="list-style-type: none"> • Mathematical formalization of designing • Matrix description of transformation from functions into design parameters • Design axioms as decision criteria 	<ul style="list-style-type: none"> • Decomposition of complex designing • Abstract design process
Design structure matrix	<ul style="list-style-type: none"> • Analysis the interaction relations among systems elements 	<ul style="list-style-type: none"> • Less effective in innovative design applied in the existing systems
C-K design theory	<ul style="list-style-type: none"> • Rigorous and unified formal framework • creative reasoning 	<ul style="list-style-type: none"> • Lack of specific interaction between the functions and design parameters • No know-how for concept evaluation
TRIZ	<ul style="list-style-type: none"> • Inventive problem solving 	<ul style="list-style-type: none"> • Product modelling.

1.4 Research statement

The engineering target of this thesis is to generate and investigate the suspension concepts with integrated electric motors by novel conceptual design approach.

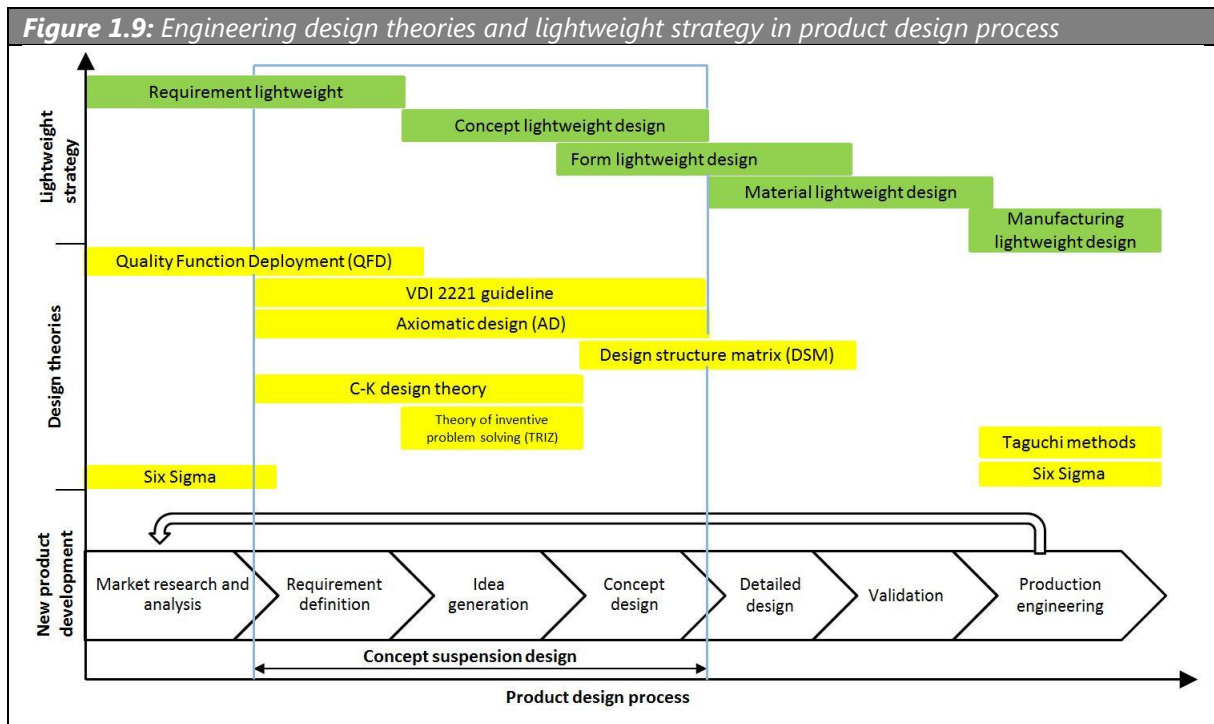
Integrating the functions of two complex products in conceptual design phase intensively depends on designer knowledge and experience, and the insufficient information in this phase raises even more design and decision-making difficulties. Therefore, it is hard to enable the new product concept to perform the integrated functions as expectation without appearing undesired properties.

At current, the lightweight design must be considered in this novel suspension design. In practical engineering, a lightweight strategy considering requirements, concept, form, material and manufacture involves throughout the entire product development process (Friedrich, 2013) (Henning & Moeller, 2010). As shown in Figure 1.9 in the product design process, the concept suspension design is primarily involved in requirement definition, idea generation and conceptual design phases. In this figure,

the commonly used engineering design theories are enumerated corresponding to the new product design process, and meanwhile the lightweight strategy are also likewise arranged along to the design process. Corresponding behavior and actions are necessary on each level. This picture gives the main design theories in a certain design phase with regards to lightweight design; for example, in the concept design phase, the VDI 2221 guideline, AD method, DSM and so on could be applied, and meanwhile the concept lightweight design and form lightweight design should also be taken into account. These methods mentioned above have potential to be utilized to functional integration for concept lightweight design, with which the generation and evaluation for new suspension concepts become more effective and reasonable.

Considering change of design conditions caused by the integrated electric motor, a new suspension structure combining drive units should be designed. In traditional way, structural design of suspensions is performed by means of trial and error or iterative shape optimization. These traditional ways are time-consuming and do not change the initial structural solutions. Form optimization on the basis of traditional suspension structures has less potential, because it does not change the topology of the suspension structures which are already deeply exploited. Increased utilization of computer-aided engineering (CAE) effectively speeds up the process from idea generation to detailed design by simplifying the establishment of concepts, as well as reducing design iteration steps and optimization time of a product. Structural optimization methods can be used to find a preliminary structural topology that meets predefined criteria through calculating material properties of each discretized part of the design domain (Lee, et al., 2007) (Bendsoe, 1989). Structure optimization methods are typically used to solve linear problems with small displacement in vehicle structure lightweight design. The suspension structure development must take into account not only the mechanical strength but also the axle kinematic and compliance, which makes the suspension structure development more complex than a mechanical problem. In order to apply structural optimization methods to find an appropriate suspension

configuration, the structure large displacement and geometry non-linearity have to be considered.



The suspension system is strongly related to the vehicle ride dynamics, i.e. ride comfort and safety. The effect of the concept suspension on the vehicle ride dynamics should be investigated. In the conceptual design phase, a fast response analytical model oriented to the new suspension concept is necessary to improve the design efficiency and shorten the design time.

Research subject of this dissertation is suspensions with integrated electric motors into arms. The objectives of this study are defined as follows:

- Objective 1: Explore a product design approach for functional integration with respect to suspensions and electric motors in the conceptual design phase (chapter 3 and chapter 4).
- Objective 2: Develop a structure design approach to suspension conception considering drive units on the basis of structural optimization method (chapter 7).
- Objective 3: Develop an analytical model of ride dynamics oriented to the concept suspension (chapter 8).

- Objective 4: Develop a feasible suspension concept using the above methods.

1.5 Outline

The outline of the thesis is illustrated in Figure 1.10. The present thesis describes a design methodology for a new design of suspension concepts with integrated electric motor. This design methodology includes a new conceptual design approach to integrating the function of the two systems based on the axiomatic design, a topological design approach for the design of the concept suspension, and an analytical rear-axle vehicle dynamic model for the concept vehicle with the concept suspension.

The high level of functional integration leads to a set of complex requirements to the design concept. Moreover, the undesirable potential conflicts among functions increase design complexity. This requires a systematic approach for the conceptual design, evaluation and design arrangement, which is developed on the basis of the axiomatic design presented in chapter 3.

This approach for functional integration is applied to the design of the concept suspension with integrated electric motors. The elements in the design matrix of the selected suspension concept are rearranged into parameter groups along its diagonal. Consequently, the positions of the groups along the diagonal are used to determine the design sequence of the suspension parameters according to the Axiomatic Design method. This process is interpreted in the chapter 4.

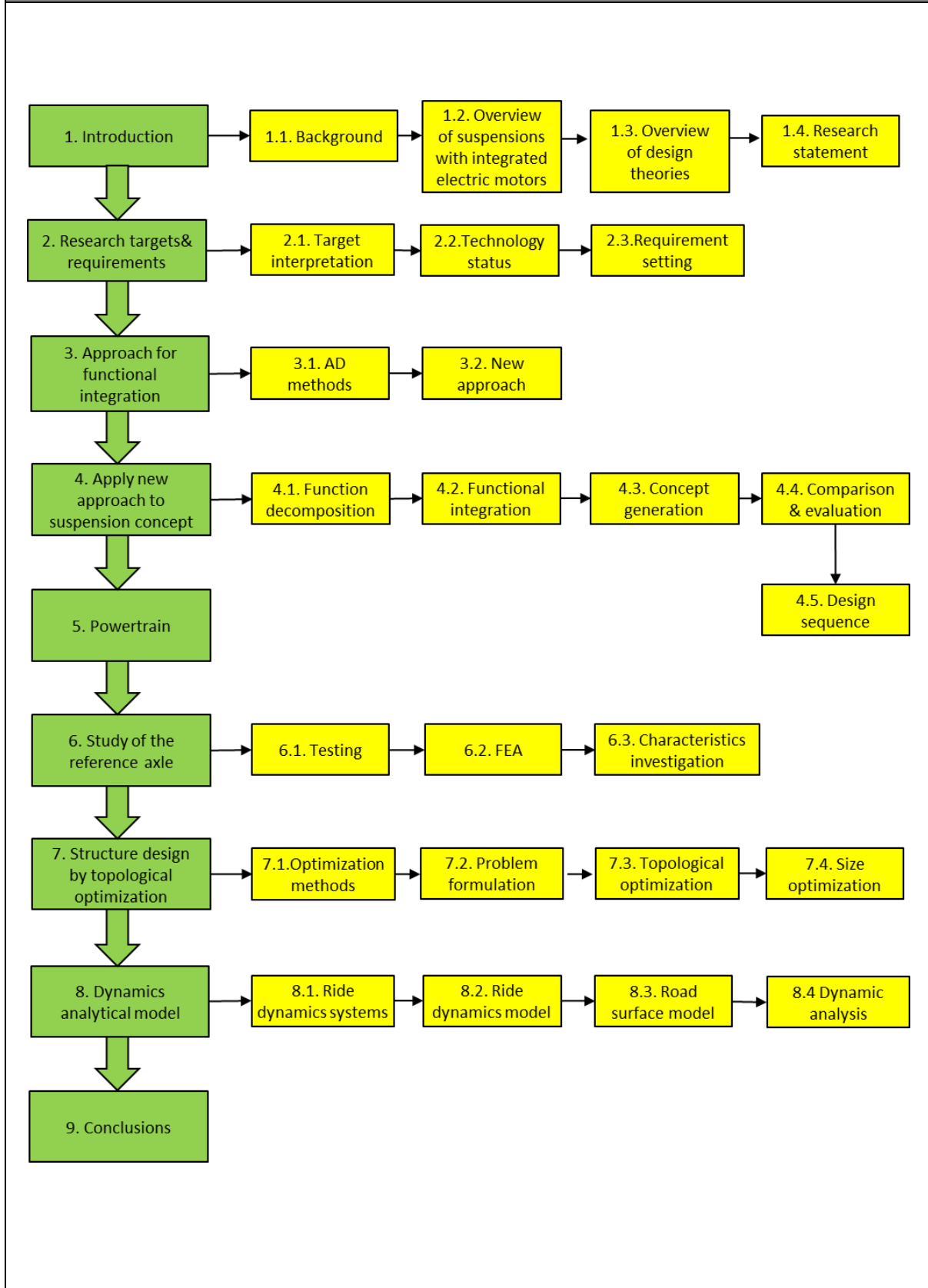
In chapter 5, the basic parameters of the drive system are calculated in this section.

In chapter 6, the K&C characteristics of a reference suspension are investigated through the testing and FEM simulation method.

A novel topological design approach is introduced in chapter 7. On the basis of this approach, a topological structure for the lightweight suspension is firstly achieved. Furthermore, based on this topology, specified cross sections of suspension links are

calculated through size optimization. This concept with a lower mass performs better K&C characteristics than the reference twist beam structure.

The analytical models of the concept suspension and reference suspension are built in chapter 8. By using analytical models, the ride comfort of the target car with the concept suspension is compared with the benchmark car equipped with a reference suspension.

Figure 1.10: Outline of thesis

2 Research target interpretation and requirement setting

In this chapter, the research objectives are further explained. The technology status of traditional suspension and electric motors are separately introduced. In the early design phase, general requirements of the concept suspension based on the target car are given in a certain scope.

2.1 Research target interpretation

2.1.1 Functional integration in the conceptual design phase

The functional integration of individual products in one product is one of lightweight design principles to realize system lightweight in conceptual design phase (Friedrich, 2013) (Gaertner, et al., 2015). Functional integration of two products refers to the realization of the independent functions of two products in one product, while maintaining the independence of these functions, i.e. the functions are not in conflict with each other in one product. Functional integration in mechanical design means to fulfill further functions by one component without significantly increasing manufacturing requirements (Koller, 1998), which can realize creative design and lightweight design (Ziebart, 2012) (Klein, 2009). It is an effective engineering way to achieve cost reduction, space saving or system mass reduction (Gaertner, et al., 2015) (Gumpinger & Krause, 2008), for example, sandwich structures for automotive application (Kopp, et al., 2009) and a metallic casting A-pillar in the front body structure (Beeh, et al., 2013). In this thesis a systematic approach for functional integration of products should be designed for assisting conceptual design of new suspensions with integrated electric motors. This approach should include the definition of design requirements, design parameters and their relationships; most importantly, this approach should consider the functionality of the new product to ensure they can be holistically evaluated and sequentially developed.

2.1.2 Structural design approach oriented to the concept suspension

In the design of vehicle suspensions, there are requirements for mechanical and K&C characteristics. But it is difficult to directly generate a configuration which meets both the mechanical and K&C requirements in the initial design phase. The traditional design approach is based on an iterative process wherein the mechanical and K&C characteristics are addressed in iterative steps to meet their requirements (Heißing & Ersoy, 2007). The traditional design strategy, depending on engineer experience, struggles to take all the requirements into account in the initial design phase simultaneously. For example, in the design of a traditional twist beam axle, it firstly defines the initial hardpoints by applying the model data abstracted from existing twist beam axles, and subsequently defines dimensional parameters of the components to satisfy stiffness and further strength requirements (Linning, et al., 2009) (Lee & Yang, 2013). This is the typical conversion design, which does not change the topology of the initial design, and therefore makes it difficult to obtain an optimal result, because other potential competing topologies are not considered. In the concept phase, developing a structure design approach which takes all the technical requirements of suspension linkage into account and subsequently using this approach to complete suspension structure design can avoid iterative steps in the design process between mechanical property, K&C requirements and structure mass.

The important parameters of suspension K&C characteristics are introduced as follows. Kinematics is the study of motion geometry (Beer, et al., 1987). Compliance is the structural elastic deformation of the applied load. The suspension K&C characteristics have significant influence on the vehicle handling stability and ride comfort (Chen, et al., 2012) (Beggs, 1983).

- Toe angle: The toe angle is between the longitudinal axis of vehicles and the line of intersection of the wheel plane and the road surface. When the forward part of the wheel plane turns inwards, the angle is positive (toe-in) and vice versa is

negative angle (toe-out). The toe angle and the changes play an important role in the vehicle understeer property (Zandbergen, 2004).

- Camber angle: The camber angle is the inclination between the wheel center plane and the vertical direction. The angle is defined as positive when the inclination is outwards from the vertical axis. Positive camber makes the car agiler on steering and on driving because of lower rolling resistance and reductions on the wear of tires. On the other hand, negative camber improves the car handling stability under lateral force (Reimpell & Betzler, 2005).
- Wheel track: the wheel track is the distance between the left and right wheel-road contact patches on the same axle.

The kinematic characteristics are introduced as follows:

- Kinematic characteristics refer to the change of wheel alignment angles and displacements of wheel centers in lateral and longitudinal directions with the wheel travel. In order to lower tire wear and rolling resistance, during the car driving toe angle and camber angle change should be minimized. In order to cause understeer tendency in cornering, the outside wheel of the rear axle should tend to toe-in, while the inner rebounding wheel should tend to toe-out (Gillespie, 1992). The camber change under jounce is desirable to be negative, because in cornering the outside wheels that carry more load than inside wheels with negative camber can improve the wheel lateral grip. Wheel lateral displacement as the wheel travels vertically causes the rolling tires to slip that leads to additional lateral force, which at the meantime deteriorates vehicle stability (Reimpell, et al., 2001).

The compliance characteristics are explained as follows:

- Lateral compliance characteristics are the change of toe, camber and lateral wheel center displacements under lateral force at the tire and road contact patch. To achieve understeer effect under lateral force, the toe angle of outside

wheel of the rear axle should have a toe-in tendency and the inside wheel should have a toe-out tendency. The camber change and lateral displacement under lateral force should be as small as possible.

- Longitudinal compliance characteristics are the change of toe, longitudinal wheel center displacements under longitudinal force at the tire and road contact patch. They are related the vehicle longitudinal dynamics. Toe-in effect contributes to braking stability. Longitudinal wheel center displacement should be as small as possible under longitudinal force.

2.1.3 Analytical model for ride dynamics

A study of automotive product design and development from University of Michigan points out that most influential technology criteria for chassis and suspensions currently are vehicle performance and safety (Kota, et al., 1998). Suspension systems, which transmit the forces between the vehicle body and road, play a significant role in determining vehicle ride dynamics (Torrance, 2009).

The ride dynamics is an important aspect for evaluation of vehicle comfort and driving safety. Vehicle comfort is essentially subjective perception of vehicle occupants. Vehicle body vibration is the main influential factor of the passenger's feeling (Heißing & Ersoy, 2007). On the other hand, load fluctuation between the wheels and roads plays in the drive performance of vehicles. The ride quality of this vehicle vibrational system are determined by the sprung stiffness, damping ratio, unsprung mass, sprung mass and the wheel rate and meanwhile it is influenced by other suspension parameters such as axle geometries and stiffness of anti-roll bars. For the concept suspension, because the electric motor is integrated into the suspension axle, the excitation of this system is from external road undulation and engine oscillation. In the conceptual design phase, we need to develop a computationally efficient engineering tool taking account of all the involved parameters.

Generally, there are four engineering ways to Noise Vibration Harshness (NVH, defined in VDI report Nr.186 (Hieronimus, 1990)) modelling and simulation. The characteristics of these modelling methods are summarized in Table 2.1 according to the references (Zeller, 2009) (Griffin, 1990) (Iliev, 2011). The selection of appropriate simulation methods for vehicle ride dynamics should take into account of problem complexity and model extensibility (Zeller, 2009). The analytical model can be applied to directly investigate dynamic characteristics of the vibration system for uncomplicated problems, whose advantage is suitable for a wide frequency range. The multi-body simulation (MBS) can be established for more complicated NVH problems. Since multi-body system consists of rigid or elastic bodies (Schindler, 2013), it is typically used in NVH simulation in low frequency. The finite element method (FEM) is applied in relative higher frequency area. It provides exact simulation results, but the computing time is longer and modelling process is more complex. For even higher frequency above 500 Hz the method of statistical energy analysis (SEA) can be used.

NVH methods	Advantage	Disadvantage
Analytical model (0~set Hz)	<ul style="list-style-type: none"> Better reflecting the mathematical nature of NVH systems 	<ul style="list-style-type: none"> Difficult for complicated problems
MBS (0~30 Hz)	<ul style="list-style-type: none"> Application for complicated NVH problems 	<ul style="list-style-type: none"> Low frequency; Modelling more complex
FEM (30-200 Hz)	<ul style="list-style-type: none"> Application for complicated NVH problems; High accuracy 	<ul style="list-style-type: none"> Complex modelling Long computing time; Hard for model extensibility
SEA (>500)	<ul style="list-style-type: none"> Application in very high frequency 	<ul style="list-style-type: none"> Low accuracy

The vehicle ride dynamics excited by road are mainly related with suspension systems in the frequency 0-20 Hz (Mitschke & Wallentowitz, 2004). The direct way to improve the vehicle ride dynamics is the tuning of the spring rate and shock absorber damping, i.e. on one hand to reduce the body vibration amplitude to increase the ride comfort, on the other hand to suppress the dynamic load fluctuation on the wheels to improve

safety (Heißing & Ersoy, 2007). Therefore, it is beneficial for the ride dynamics analysis to build an analytical model for the concept suspension.

2.2 Technology status

As the new concept suspension is integrated of two primary systems, i.e. the suspension system and the electric motor system, it is necessary to overview the technology status of traditional suspensions and electric motors. Section 2.2.1 gives an overview of suspension configurations mostly used in current passenger cars and their application trends. Section 2.2.2 summarizes different types of electric motors and statistical data about power-to-mass and torque-to-mass ratios of electric motors used for EVs.

2.2.1 Traditional suspension systems





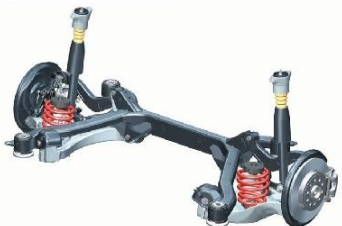
Classifications of vehicle suspensions




Various configurations of suspensions were designed in the technology progress of automotive. These configurations and their characteristics have been introduced in a lot of publications (Heißing & Ersoy, 2007) (Reimpell & Betzler, 2005) (Reimpell, et al., 2001). In this dissertation, the main configurations with application examples are briefly summarized in Table 2.2. These collected configurations for front and rear axles act as potential variants of functional integration with electric motors in section 4.3.

Trend of suspension application

Market segments of passenger cars are defined in the reference (Commission of the European Communities, 1999). The application status and trends of different suspension configurations in car market segments are summarized in Figure 2.1. The McPherson struts and double wishbone suspensions are classical configuration used in front axles (Reimpell, et al., 2001). McPherson suspensions are used in a wide range of vehicle segments not only in mini cars such as Mitsubishi i-MiEV but also in sport cars like Porsche 997 (Overholser, 2006). However, in order to bring more handling and stability, luxury cars previously applying McPherson suspensions turn to use double

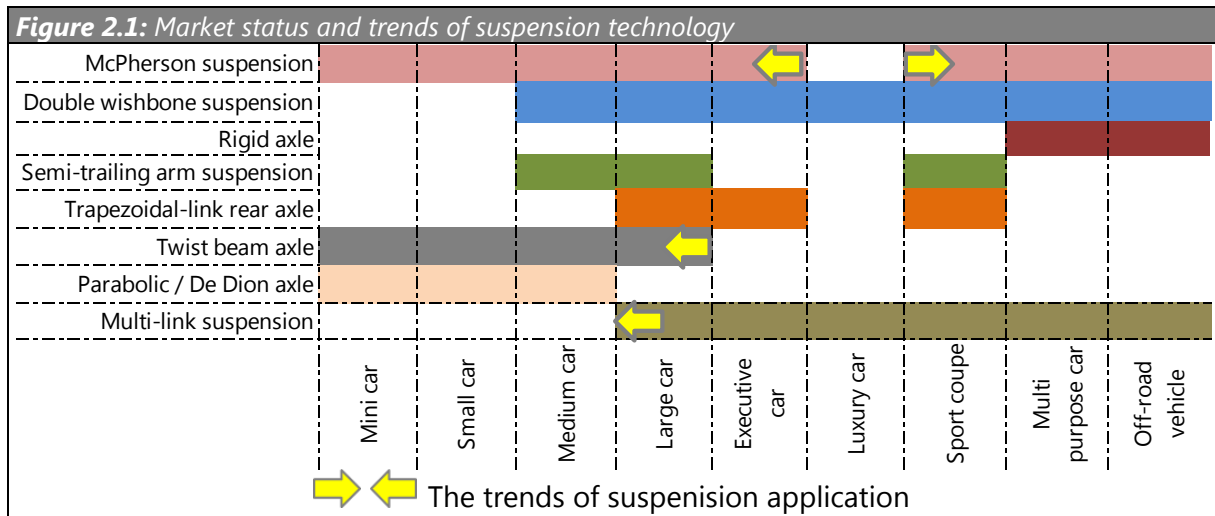
Table 2.2: Suspension classification and characteristics

	Configurations	Advantages	Disadvantages
McPherson suspension	<p><i>McPherson-strut of Honda Pilot</i> (Torrance, 2009)</p> 	<ol style="list-style-type: none"> 1. Low cost and lightweight 2. Low volume requirement 3. Low unsprung mass 	<ol style="list-style-type: none"> 1. Bad noise and vibration isolation 2. Camber changes with wheel vertical motion
Double wishbone suspension	<p><i>Double-wishbone front axle of BMW x6</i> (BMW AG, 2013)</p> 	<ol style="list-style-type: none"> 1. Large design freedom 2. High lateral stiffness 3. Good ride and handling 	<ol style="list-style-type: none"> 1. Large package volume 2. High cost 3. Additional subframe handling
Rigid suspension	<p><i>Rear axle of Ford Mustang</i> (Phillips, 2004)</p> 	<ol style="list-style-type: none"> 1. Robustness 2. Large load capacity 3. Off-road capability 	<ol style="list-style-type: none"> 1. High unsprung mass 2. The motion of one wheel affects the other wheel
Semi-trailing arm suspension	<p><i>Rear axle of VW Sharan/Ford Galaxy</i> (Volkswagen AG, 1996)</p> 	<ol style="list-style-type: none"> 1. Independent wheels 2. Adjustable kinematics 3. Good compromise between trailing link and swing axle 	<ol style="list-style-type: none"> 1. Large camber changes 2. Toe out under lateral force 3. Bad cornering performance
Trapezoidal-link rear suspension	<p><i>Rear axle of Audi A4</i> (Audi AG, 2011)</p> 	<ol style="list-style-type: none"> 1. Minimal toe change 2. Good longitudinal resistance 3. Flat and space-saving package 	<ol style="list-style-type: none"> 1. High cost and complexity 2. Additional subframe

Twist beam suspension	<p>Rear axle of VW GOLF VII (Volkswagen AG, 2013)</p> 	<ol style="list-style-type: none"> 1. Simple structure/assembly 2. Small volume 3. Minimal mass added to each wheel 4. Minimal track width changes 	<ol style="list-style-type: none"> 1. Low lateral stiffness 2. Not suitable for high axle loads 3. Over steer tendency
Parabolic axle / De Dion suspension	<p>Rear axle of Mercedes B Class (Daimler AG, 2005)</p> 	<ol style="list-style-type: none"> 1. Good anti-roll control 2. More space between two wheels 3. Fixed camber on axle rebound 	<ol style="list-style-type: none"> 1. Worse off-road capacity, higher cost and complexity than rigid axle 2. Wheels not independent
Multi-link suspension	<p>Rear axle of Golf V (Volkswagen AG, 2019)</p> 	<ol style="list-style-type: none"> 1. K&C adjustable 2. Minimal unsprung mass 3. An even force distribution 4. Very good ride and handling 	<ol style="list-style-type: none"> 1. High space requirements 2. Expensive and complex 3. Additional subframe

wishbone suspension such as BMW 7 series (Reimpell & Betzler, 2005). Double wishbone suspensions are mainly applied in the car with high requirement of comfort and dynamic from medium to large cars. Semi-trailing suspension is an old and abandoned configuration that can be found in BMW E30 and BMW Z3 (Bowen, 2013). Multi-link suspensions are widely used due to multi-faceted advantages, however considering its high cost and complexity they are equipped mostly only limited in large cars, sport coupe, luxury cars and off-road vehicles because of their requirement on high drive performance (Reimpell, et al., 2001). The twist beam axles are extensively used as non-driven rear axles that can be found usually in economic cars (mini, small and medium cars) like VW GOLF VII (Volkswagen AG, 2013) and even in large cars for example VW Passat B5 and Audi A6 (1997 version) (HeiBing & Ersoy, 2007). Parabolic axles were developed by Daimler AG, which were used in Mercedes A and B class

(Daimler AG, 2005). De-Dion axles can be found in mini cars like Smart Fortwo (Daimler AG, 2019).



2.2.2 Electric motors used for EVs

The requirements of electric motors used for EVs are different from those for industry. Besides high power density and outstanding efficiency they are also required to have high torque at low rotational speed for vehicle acceleration and wide speed range for highway driving (Chan & Chau, 2001). Table 2.3 summarizes the types of electric motors used in EVs and their characteristics can be found in reference (Chan & Chau, 2001) (Rahman, et al., August, 2000) (Wallentowitz & Freialdenhoven, 2011) (Xue, et al., 2008). Among them the permanent magnet synchronous motor (PMSM) and induction motor (IM) are the most selected motors in EV drive system. PMSM has high efficiency and power density. Features of the IM are robustness and low maintenance.

The weights of the electric motors for EVs have dramatically reduced in recent years. A group of power-to-mass and torque-to-mass ratio data about current EV motors is collected in Figure 2.2 and Figure 2.3. They are: axial flux motors like YASA motors (YASA Motors, 2014) and EMRAX motor (EMRAX d.o.o., 2014); permanent magnet synchronous motors like BMW i3 electric motor (Pudenz, 29. Juli 2013), AMK DT5-26-10-POW (Brand, 2012), HVH series electric motors (BorgWarner Inc., 2016) and the electric motor for second generation Toyota Prius (Kiyota & Chiba, 2012); induction motors like Raser Symetron P2 motors (Ogando, 2005), TESLA Roadster (Grabianowski,

2006) and ACP AC series motors (AC Propulsion, 2013); the switched reluctance motor for the third generation Toyota Prius; and Hi-Pa Drive HPD40 Brushless DC wheel hub motor (Protean Electric, 2010). These charts indicate lightweight electric motors for EVs can achieve a high power-to-mass and torque-to-mass ratios. They have great potential to be integrated into the suspension axle without dramatic increase of the axle mass and meanwhile meet the drive requirements of EVs.

	Advantages	Disadvantages
Axial flux machine	1. Inferior axial length	1. Additional axial forces support
Permanent magnet synchronous motor	1. High efficiency and power density 2. Compact structure	1. Complex and costly compared to IM
Induction motor	1. Low maintenance and higher speed 2. Robust 3. Low manufacturing cost	1. High reactive power demand for magnetization 2. Power loss in the rotor 3. Narrow air gap required
Switched reluctance motors	1. Low cost 2. Good performance characteristics for EV propulsion	1. Noise problem 2. Torque undulation
Direct current (DC) machine	1. Robust 2. Easy to control 3. High torque at low speed	1. Commutators and brushings need careful maintenance

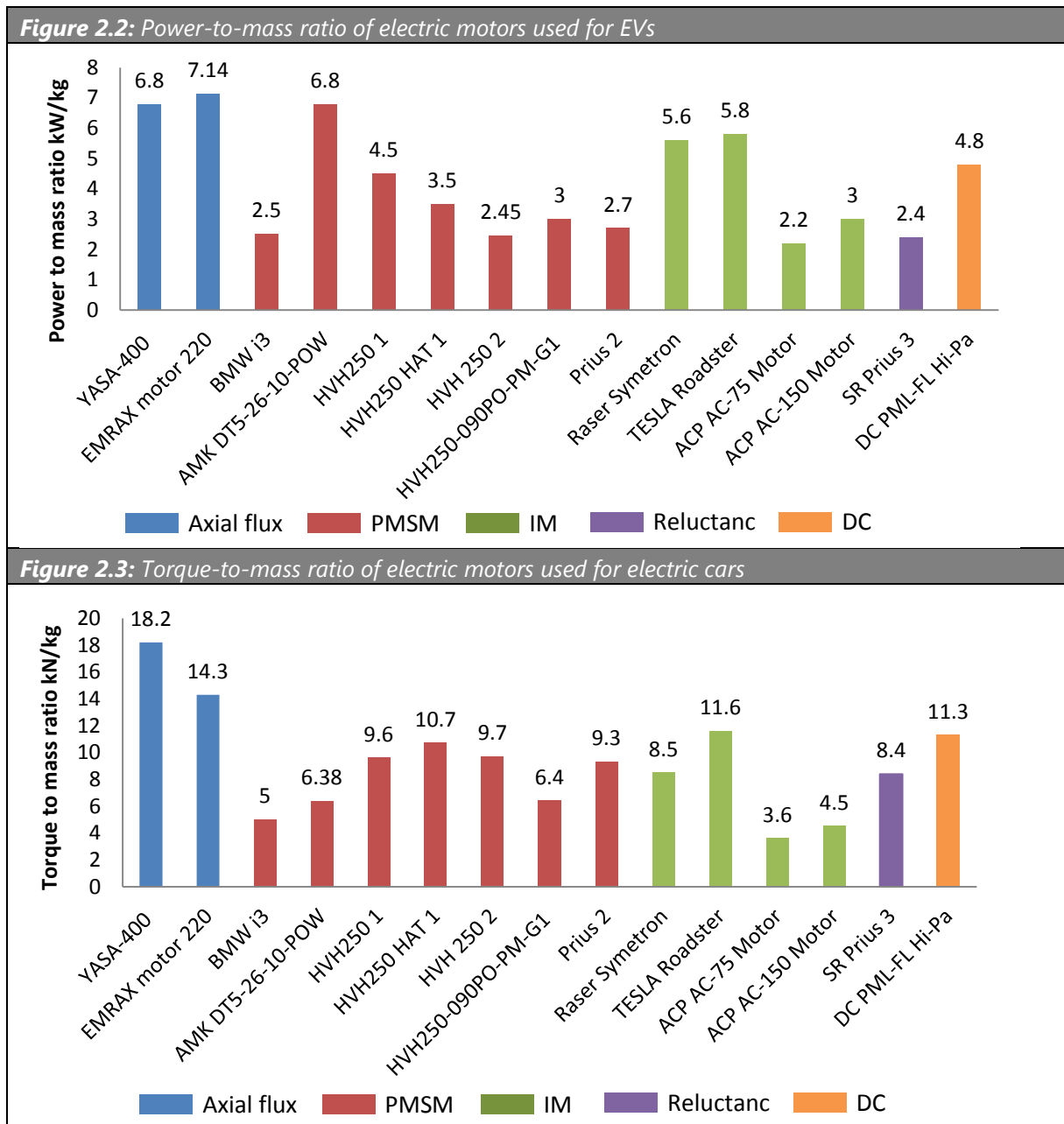
2.3 Requirements setting

The performance of the suspension concept is directly reflected in the performance of the target vehicle. Considering the fundamental application object of the design methodology interpreted in this thesis is a concept suspension for passenger cars, the specifications of the target vehicle are defined firstly.

2.3.1 Specification of the target car

The target vehicle specifications are set on the basis of the statistical data of EVs in the same market segment and a benchmark car (Volkswagen Polo Trendline with 44 kW

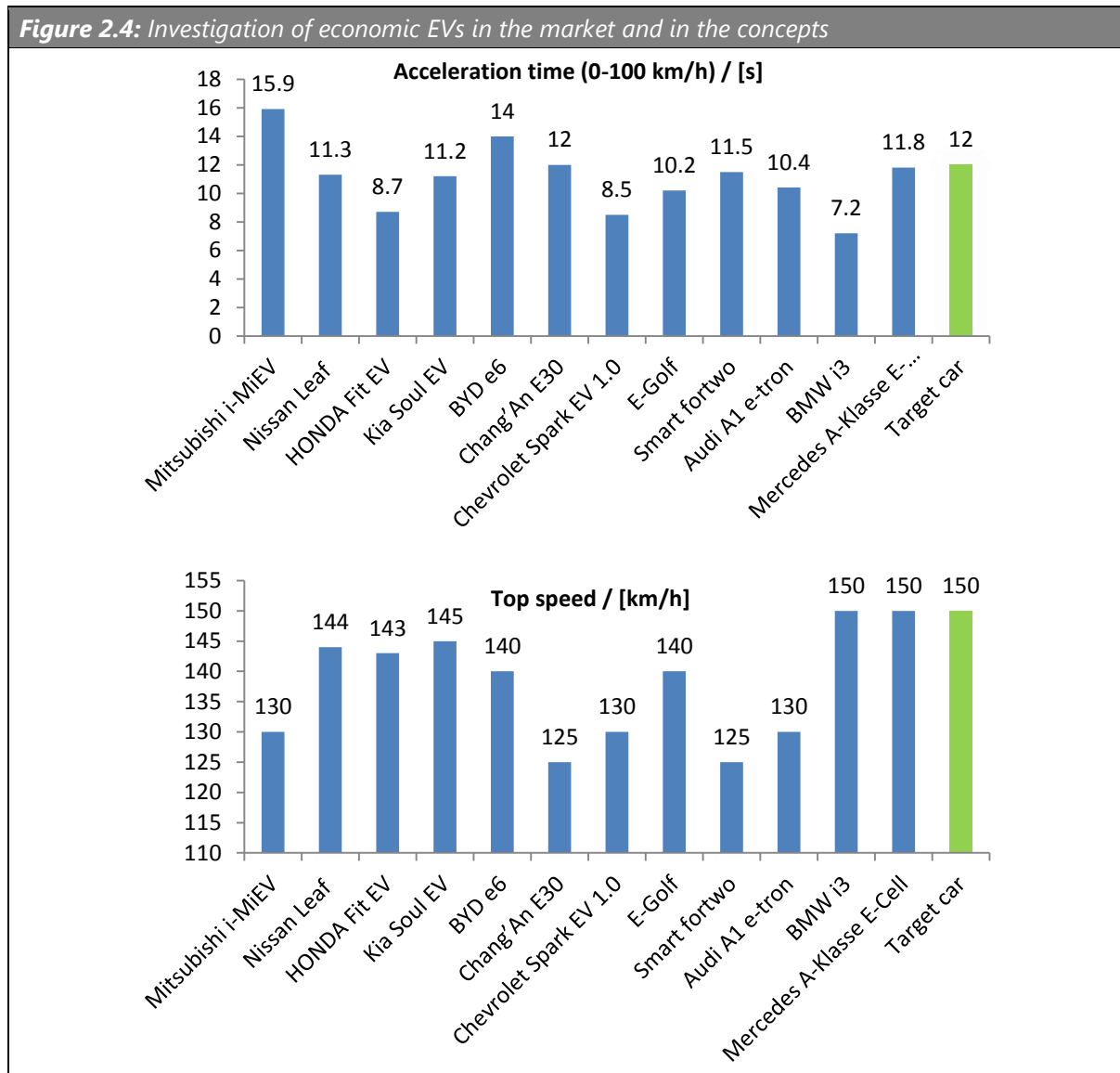
gasoline engines). The requirements of the concept suspension are established in accordance with the specification of the target vehicle.



The target car

Suspensions are strongly related to the target vehicle orientation in market segments. The target car in this thesis orients to the economic cars (i.e., the segments of mini, small or medium cars). According to engineering design process (see Figure 1.7), the specifications of the target vehicle should be defined considering the market and

customer needs which are approached in this work through the statistical data of the EVs in the same segment (see appendix A).



The required acceleration time and top speed of the target car are set by green columns according to an investigation of the economic EVs (see Figure 2.4). The EVs are selected from the mini, small and medium segments respectively. Mitsubishi i-MiEV, Nissan Leaf and HONDA Fit EV of Japanese automakers were introduced to the market in 2010, 2010 and 2013, respectively (Ecomento.de, 2019) (Czajka, 2014) (Sessions, 2013); Kia Soul EV, whose sales began from 2014, is a compact EV from Korea (Branke, 2014). BYD e6 and ChangAn E30 from China were released to the market in 2010 and 2011 separately (Falk, 2011) (Luan, 2012). The new Chevrolet Spark EV from USA was

introduced to the market in 2014 (Anon., 2013) (Anon., 2014). E-Golf (Czajka, 2014), smart fortwo (Mercedes-Benz USA, LLC, 2014), Audi A1 e-tron (Maydell, 2012), BMW i3 (BMW AG, 2014) and Mercedes A-Class E-Cell (Maydell, 2011) represent the EVs from Germany. HONDA Fit EV and Chevrolet Spark EV have a short acceleration time but their ranges are only 130 km with almost equal energy capacity to other EVs (Sessions, 2013) (Anon., 2013) (Anon., 2014). Taking account of technical data of the above reference cars, acceleration time 12 s from 0 to 100 km/h and top speed 150 km/h are the appropriate basic requirements for the target car.

The specifications on target vehicle dimensions and weights are defined on the basis of technique data of the benchmark car (Winterkorn & König, 2001). The defined parameters of the target car are listed in Table 2.4.

Table 2.4: Parameters of target car			
Target car	Parameters	Target car	Parameters
Market segment	Small cars	Wheel base	2.47 m
Wheel type	185/60 R15	Wheel track	1.456 m
Vehicle mass m_v	1050 kg	Mass distribution i	50:50
Acceleration	12 s (0-100 km/h)	Top speed	150 km/h
Cross sectional area	2 m ²	Drag coefficient	0.3
Rolling resistance	$f_R = f_{R0} + f_{R1} \left(\frac{v}{100 \text{ km/h}} \right) + f_{R4} \left(\frac{v}{100 \text{ km/h}} \right)^4$ (Mitschke & Wallentowitz, 2004) where, $f_{R0} = 0.008$, $f_{R1} = 0.0013$, and $f_{R4} = 0.0003$		
Wheel radius	301.5 mm	Unsprung mass m_1	< 40 kg
vehicular coordinate system	ISO standard 4130: 1978 (ISO 4130: 1978, 1978) (see Appendix B)		

2.3.2 Preliminary requirements for the suspension concept

Because the development of the electric motor is not the focus of this thesis, the electric motor specifications are not detailed in the early design phase. However, the power and torque of the electric motors must meet the requirements on the target vehicle acceleration and top speed. The design volume for the electric motor is constrained by the tight surrounding space, so the motor size should be appropriate

to the space without interference in the motions of suspension components. The mass of electric motors should not dramatically bring up the unsprung mass coordinated with vehicle dynamic performance. The preliminary requirements of the suspension are generally defined in terms of the K&C characteristics, ride comfort and safety. The specific requirements are set according to the investigation of a benchmark suspension, which is elaborated in the fifth chapter.

Table 2.5: Preliminary K&C requirements		
Geometries under empty load state		
Toe	<ul style="list-style-type: none"> Rear wheel drive: front axle: 0 to + 30'; rear axle: -20' to + 20' Front wheel drive: front axle: -30' to + 20'; rear axle: -20' to + 20' 	
Camber	<ul style="list-style-type: none"> Front wheel: 0° to 1° 20', rear wheel: -1° 30' ± 20' 	
Roll center	<ul style="list-style-type: none"> According to reference suspension 	
Straight line driving		Cornering
Wheel travel / mm	<ul style="list-style-type: none"> Compression: 60 to 100 Extension: -70 to -120 	<ul style="list-style-type: none"> Compression: 60 to 100 Extension: -70 to -120
Toe	<ul style="list-style-type: none"> Keep toe-in, nearly constant 	<ul style="list-style-type: none"> Rear axle: <ul style="list-style-type: none"> Outer wheel: toe-in tendency; Inner wheel: toe-out tendency Outer wheel: keeps negative
Camber	<ul style="list-style-type: none"> To negative (jounce) 	
Acceleration		Braking
Toe	<ul style="list-style-type: none"> Keep toe-in 	<ul style="list-style-type: none"> Keep toe-in
Camber	<ul style="list-style-type: none"> As small as possible 	<ul style="list-style-type: none"> As small as possible
Wheel center	<ul style="list-style-type: none"> As small as possible 	<ul style="list-style-type: none"> As small as possible

K&C characteristics

Vehicle handling is directly influenced by the K&C characteristics of suspensions. The K&C characteristics should be optimized in the suspension design to realize the car straight driving without steering inputs, understeer tendency in cornering, steady drive tendency under lateral forces and so on. In the early design phase, an appropriate vehicle handling is guaranteed through the definition of K&C. Desired K&C characteristics for the concept suspension are given in Table 2.5, which are investigated in the literatures (Heißing & Ersoy, 2007) (Henker, 1993). The desired characteristics

include a group of static geometrical parameters and desired motion tendencies in four driving maneuvers, straight line driving, cornering acceleration and braking. The specific K&C requirements for the concept suspension are given depending on the reference suspension in chapter 6 after the suspension configuration is determined, because the K&C attributes of different suspension configurations (see Table 2.2) perform significant deviations.

Ride comfort and safety

Ride comfort can be expressed by the objective measures. The vibrational response of vehicle body, which depends on frequency, provides an objective description of ride comfort (Reimpell & Betzler, 2005). The vibrations of the concept suspensions are generated from not only the interaction of wheels and road undulation but also the excitation of electric motors. The spring and damper are most important components to isolate disturbance from the wheels to the vehicle body. The target vehicle, which is equipped with the new concept suspension, should have equivalent or better vibrational responses when driving on road surfaces as the benchmark car, i.e., smaller vibration amplitudes of the vehicle body than the benchmark car. The vibrational responses of the benchmark car are simulated in chapter 8 after parameters related to the ride comfort of benchmark car are studied.

Suspension systems should ensure the wheels being in contact with the road all the time while driving (Heißing & Ersoy, 2007). The dynamic loads at wheels are decisive parameters to statistically calculate the possibility for loss of contact between tires and road surface. It is used to compare the ride safety of the concept suspension and the benchmark suspension. Ride safety related to wheel load fluctuation is primarily influenced by unsprung mass, springs and dampers. The ride safety associated with roll stability is affected by the anti-roll bar. The hard anti-roll bar reduces the body roll risk. However, it deteriorates the ride comfort in a certain degree (Mitschke & Wallentowitz, 2004). The concept suspension system should at least ensure the target vehicle equivalent ride safety to the benchmark car with reference to wheel load fluctuation.

Meanwhile, the ride safety with respect of roll stability should be at least maintained through matching anti-roll bars without severe deterioration of the ride comfort.

3 A concept design approach based on Axiomatic Design for functional integration

This chapter proposes an approach to formulate the process of functional integration by matrix equations on the basis of axiomatic design (AD) method. This approach is elaborated with an example with 3×3 matrices.

The general approach to design complex mechanical systems is: firstly decomposing a complex design problem into manageable sub-problems, then solving the less complex sub-problems, at last synthesizing the sub-solutions to the overall design problem (Li, 2006). This decomposition-solving process commonly involves multiple-levels, from systems to components, in which corresponding problems and solutions are collected and explored, and further design concepts are generated.

Because the mapping from physical parameters to functions is implicit, the development process of functional integration strongly depends on designer knowledge and experience. The challenge to achieve functional integration is to enable the new concept the integrated functions without appearing undesired properties. However, the design process for functional integration can be assisted by using appropriate engineering design methods to ensure the product functionality.

When generating a concept by integrating the functions of two independent systems, the arising impact on the system functions must be taken into account. A certain number of new interactions among functions and parameters of original systems could emerge in the new concept. As obscuration of these relationships, they are often neglected by designers. In evaluation of new concepts, the impact of these interactions on functions should also be considered.

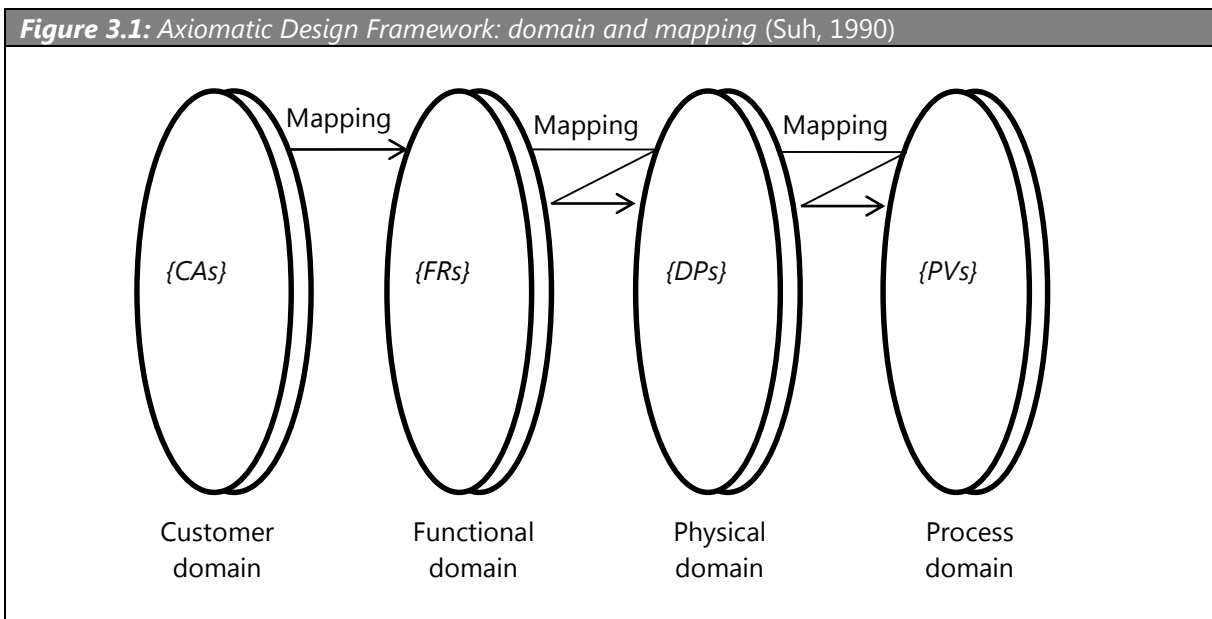
The functional integration and AD method can be complementarily and cooperatively applied together to a specific design object. Concept generation through the integration of functions can be explicitly expressed with the help of the AD method. Thus, a new approach for functional integration based on the AD method is proposed,

in which the implicit relationships between functions and parameters are able to be expressed by the design matrix in the design process for functional integration.

3.1 AD method

Key concepts of the AD method

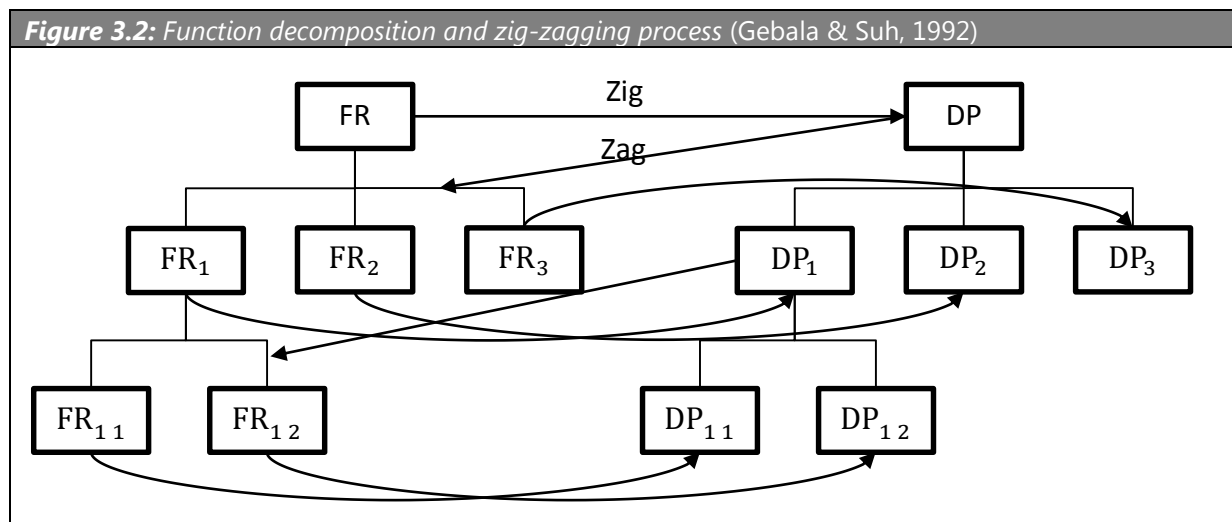
The AD method introduces a systematic framework for conceptual design and the evaluation of products or systems that helps the designer to formalize and structure the design process based on its fundamental Axioms (Suh, 1990) (Suh, 2001).



In axiomatic design, the design world is divided into four domains, namely the customer domain (CAs), functional domains (FRs), physical design domains (DPs) and process domains (PVs), as shown in Figure 3.1. Functional requirements (FRs) make up a set consisting of the minimum independent requirements that completely satisfies the functional needs of the product. Design parameters make up a set defined as the key variables that characterizes the physical entity of the product.

Elements in each domain are classified and divided in different levels into a top-down order to form a hierarchy tree. In each level of design hierarchy, relationships mapping of elements between domains are built by designers from left to right and top to down. In the functional and physical domains, the design process follows a zig-zagging pattern between FRs and DPs in decomposing a design problem (see Figure 3.2)

(Gebala & Suh, 1992). At a given level of design hierarchy, the specified FRs in functional domain must map to certain design parameters with a design solution in physical domain, which is called a "zig" process; after the mapping, the selected DPs draw the FRs of next lower level, which is called a "zag" process. Repeating the loop as above, the design is further specified, and the FRs and DPs are decomposed and mapped. The decomposition and mapping process proceed from a high level of general definition to a low level with detailed elements. The definition of FRs and DPs and the selection of the best alternative follow two basic axioms, which are given by Suh (Suh, 1990) (Suh, 2001).



Axiom 1: Independence Axiom- Maintain the independence of all functional requirements

Axiom 2: Information Axiom- Minimize the information content of the design

The independence axiom means for the optimal design the corresponding DP of a specific FR can be adjusted without influencing other FRs. The information axiom can be understood that the design with minimum information content which satisfies independence axiom is the best design among the candidate concepts. The two design axioms provide the basic principles for the analysis and decision-making in the conceptual design stage (Suh, 1990). They provide the objective criteria for identifying acceptable solutions and for selecting the optimal solution among the candidate designs.

The interplay of FRs and DPs can be written by the mathematic formula (3-1) (Suh, 2001).

$$\{FRs\} = [A]\{DPs\} \quad (3-1)$$

$$[A] = \begin{bmatrix} A_{11} & A_{12} & \cdots & A_{1n} \\ A_{21} & A_{22} & \cdots & A_{2n} \\ \vdots & \vdots & \ddots & \vdots \\ A_{m1} & A_{m2} & \cdots & A_{mn} \end{bmatrix}$$

Where $[A]$ is the design matrix (DM) denoting the effect of DPs on FRs. A design with the diagonal DM, called uncoupled design, means the relationships among FRs and DPs of the design meet the Independence Axiom, because the entry of a DP individually affects the entry of an FR. A design with triangular DM is called a decoupled design, which means the DPs must be adjusted by a certain order (top-down and left-right) to meet the FRs. When the design matrix is a full matrix, the design is a coupled design, with which it is difficult to satisfy the FRs independently. This design is considered as a poor design, which should be modified or abandoned.

The application of the AD method in suspension design

There are already a number of related works applying AD method for suspension design. In these works, the AD method was applied for assessment of existing designs or as a tool to assist innovative designs.

Bae compared the McPherson, double wishbone and multilink suspensions on the basis of AD theory and applied this theory to suspension kinematic design (Bae, et al., 2002). Kim analyzed effects of suspension hardpoint positions on ride comfort and suspension kinematics using axiomatic design, and proposed a sequential design of global coordinates of suspension hardpoints to improve ride comfort (Kim, et al., 2007). Bae applied the AD method to generate a design matrix among kinematic functions and hardpoint positions of McPherson suspensions and subsequently decoupled the DM by combining the Independence Axiom and suspension knowledge (Bae, et al., 2003). Deo and Suh proposed a six-bar suspension concept to remove the coupling of suspensions and steering systems on the basis of AD method (Deo & Suh, 2004).

Furthermore, Deo analyzed the coupled design element of traditional suspensions with the help of axiomatic design, and designed a control system for a novel customizable suspension by which the suspension stiffness and ride height were decoupled (Deo & Suh, 2004).

3.2 Approach interpretation and illustration with an example of 3×3 matrices

3.2.1 Approach interpretation

The AD method provides a systematic design program for conceptual design and furthermore two objective axioms to evaluate the design. Based on the theory of the AD method, a design approach is proposed to formulate the process of functional integration by matrix equations. The functionalities of new concepts are able to be specifically and explicitly evaluated.

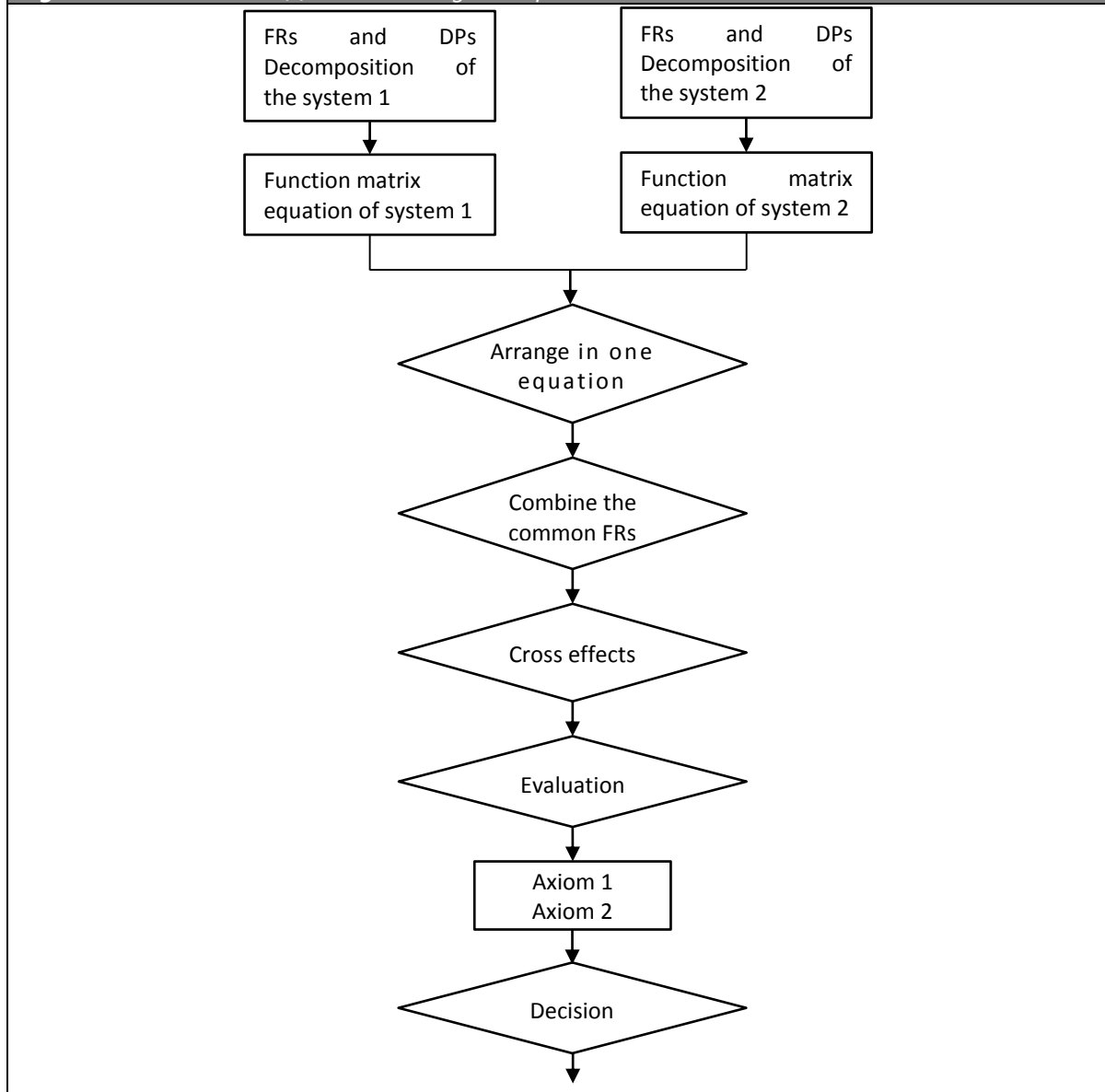
The approach for functional integration is illustrated in Figure 3.3. The prerequisite of the combination is that the systems to be combined have common *FRs*, which makes them possible to integrate from the perspective of functions. In the meanwhile, from the point of view of physical synthesis the corresponding *DPs* should be able to be combined.

In order to clearly indicate the function and parameter relationships, at first the separated systems should be decomposed to *FRs* and *DPs* independently until the design level with the common *FRs*. Then, the DM i.e. the mapping from the *FRs* to the *DPs* should be investigated by means of literature review, expert consulting, team working or some advance design models, with which the design hierarchy of each system is written as the matrix equation.

Subsequently, the matrix equations of the independent subsystems are going to be arranged in one matrix equation which represents the combined system. In the arrangement the subsystem DMs are located along the diagonal of the combined DM. The common *FRs* and corresponding *DPs* are combined in a unified *FR* and *DP*,

respectively. Unknown elements appear on the off diagonal of the new DM, which represent the cross effects of one system on the other system. The unknown element should be defined in order to probe the influence of the combination on the system functions.

Figure 3.3: Framework of functional integration process based on AD



The obtained design matrix can be evaluated by the two axioms of the AD method i.e. the Independence Axiom and the Information Axiom. There may be multiple candidate designs with the same DM in the given hierarchy levels, which are sometimes very difficult to compare in the early stage of conceptual design. The comparison can still be carried out by the DM of next levels, the quantity of the information content or

taking account of the non-functional criteria. The selected concept is further developed by the engineers. With the development of more details, the design matrix equation of the new concept can be further decomposed to the next levels. The matrix equation functions as the guidance throughout the product developing process.

3.2.2 Approach illustration with an example of 3 × 3 matrices

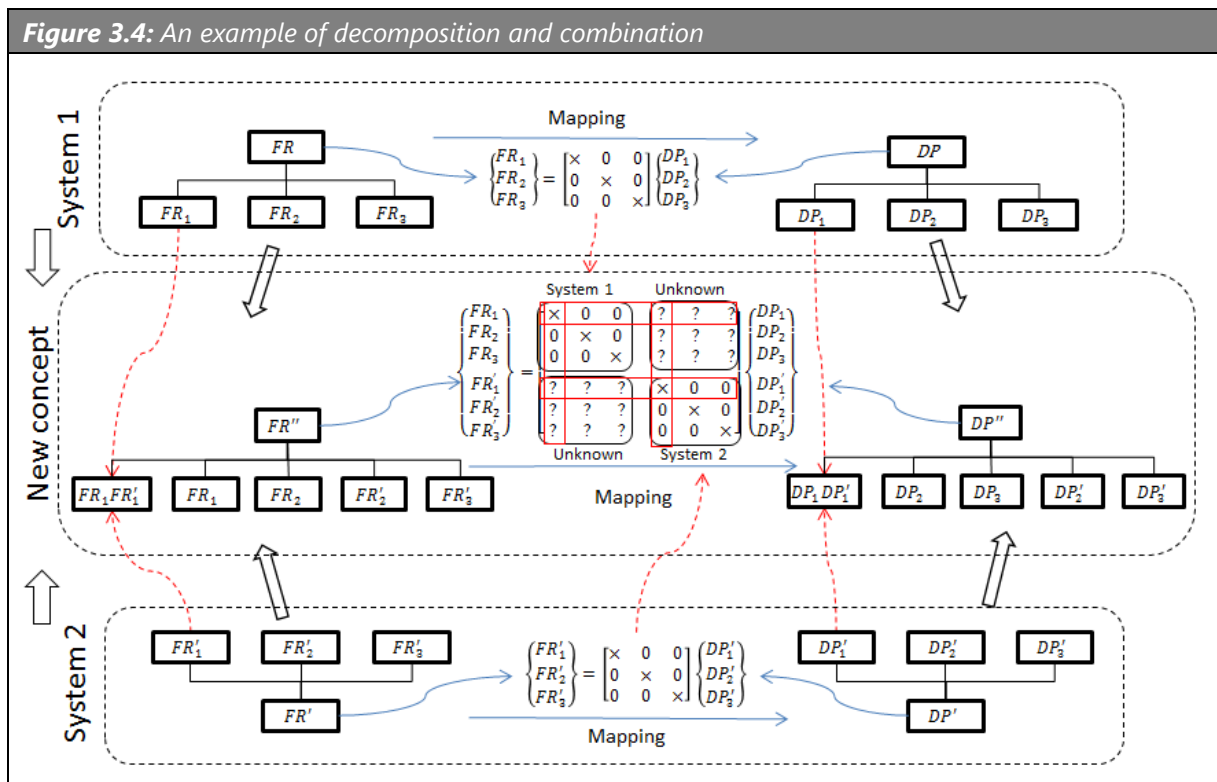
The process is interpreted by an example with the equations of 3 × 3 matrices.

Decomposition and combination

In the illustration in Figure 3.4, system 1 is assumed as an uncoupled design described with the 3 × 3 matrix.

$$\begin{Bmatrix} FR_1 \\ FR_2 \\ FR_3 \end{Bmatrix} = \begin{bmatrix} \times & 0 & 0 \\ 0 & \times & 0 \\ 0 & 0 & \times \end{bmatrix} \begin{Bmatrix} DP_1 \\ DP_2 \\ DP_3 \end{Bmatrix} \quad (3-2)$$

In this DM, the effect of *DPs* on *FRs* is represented as ×(strong) or 0 (weak). The symbols × are not simply placeholders. They are associated with the solution principles.



System 2 is assumed as an uncoupled design described by the following equation:

$$\begin{Bmatrix} FR'_1 \\ FR'_2 \\ FR'_3 \end{Bmatrix} = \begin{bmatrix} \times & 0 & 0 \\ 0 & \times & 0 \\ 0 & 0 & \times \end{bmatrix} \begin{Bmatrix} DP'_1 \\ DP'_2 \\ DP'_3 \end{Bmatrix} \quad (3-3)$$

Assuming that FR_1 and FR'_1 represent common functions of the two systems, the two equations are arranged in the unified equation (3-4). Thus, with the combination of system 1 and system 2, their function matrices and parameter matrices are integrated together that represent the FRs and DPs of the new design concept, respectively. In the new DM, the design matrix of the system 1 is arranged in the left top block, and the design matrix of the system 2 is arranged in the right bottom block. In this process, new unknown elements appear in the off-diagonal of the new combined matrix. They are the cross effects of the DPs of one system on the FRs of the other system. The cross effects determine the compatibility of the two systems in the new combined concept. The functional integration should combine the common FRs and corresponding DPs in the design equation and figure out the unknown elements of the DM. First of all, the matrix elements in the red rectangular frames related to the common FRs and corresponding DPs should be combined.

$$\begin{Bmatrix} FR_1 \\ FR_2 \\ FR_3 \\ FR'_1 \\ FR'_2 \\ FR'_3 \end{Bmatrix} = \begin{array}{c} \begin{array}{ccc|ccc} & P_1 & & P_2 & & \\ \hline \times & 0 & 0 & ? & ? & ? \\ 0 & \times & 0 & ? & ? & ? \\ 0 & 0 & \times & ? & ? & ? \\ \hline ? & ? & ? & \times & 0 & 0 \\ ? & ? & ? & 0 & \times & 0 \\ ? & ? & ? & 0 & 0 & \times \end{array} \\ P_3 \quad P_4 \end{array} \begin{Bmatrix} DP_1 \\ DP_2 \\ DP_3 \\ DP'_1 \\ DP'_2 \\ DP'_3 \end{Bmatrix} \quad (3-4)$$

Integration

Taking into account of the rows in the two red horizontal rectangles of the DM in equation (3-4), because DP_1 and DP'_1 have effect on the FR_1 and FR'_1 in their own systems respectively and FR_1 and FR'_1 are the same functions, after combination the DP''_1 has an effect on the FR''_1 . The cross effects of other DPs on the common FR''_1 are considered. DP_2 and DP_3 in system 1 have no effect on FR_1 , so they have no effect on FR'_1 . DP'_2 and DP'_3 likewise have no effect on FR_1 .

The matrix elements in the two red vertical rectangles in equation (3-4) represent the effects of the DPs to be combined on the FRs . The combined DP_1'' possesses the attribute of DP_1 and DP_1' . If one of DP_1 and DP_1' has an effect on a certain FR , the DP_1'' has an effect on this FR . Only if both DPs have no effect on the FR , the combined DP must have no effect on this FR .

Thus the elements representing the common FRs are known (see equation (3-5)); they can be integrated as long as the combination of DP_1 and DP_1' is feasible in the physical domain. The other unknown elements of blocks P_2 and P_3 that describe cross effect are still not able to be defined before the design is specified.

$$\begin{Bmatrix} FR_1 \\ FR_2 \\ FR_3 \\ FR'_1 \\ FR'_2 \\ FR'_3 \end{Bmatrix} = \begin{bmatrix} \times & 0 & 0 & \times & 0 & 0 \\ 0 & \times & 0 & ? & ? & ? \\ 0 & 0 & \times & ? & ? & ? \\ \times & 0 & 0 & \times & 0 & 0 \\ ? & ? & ? & 0 & \times & 0 \\ ? & ? & ? & 0 & 0 & \times \end{bmatrix} \begin{Bmatrix} DP_1 \\ DP_2 \\ DP_3 \\ DP'_1 \\ DP'_2 \\ DP'_3 \end{Bmatrix} \quad (3-5)$$

Assuming DP_1 and DP_1' are available to be combined in physical domain, the DM of the above equation can be combined and rearranged to be the DM of the equation (3-6). However, without specific information it is impossible to determine whether this DP_1 has effect on FR'_2 and FR'_3 , the effects of the combined DP_1'' on the FR'_2, FR'_3, FR_2 and FR_3 are temporarily defined as unknown.

$$\begin{Bmatrix} FR''_1 \\ FR_2 \\ FR_3 \\ FR'_2 \\ FR'_3 \end{Bmatrix} = \begin{bmatrix} \times & 0 & 0 & 0 & 0 \\ ? & \times & 0 & ? & ? \\ ? & 0 & \times & ? & ? \\ ? & ? & ? & \times & 0 \\ ? & ? & ? & 0 & \times \end{bmatrix} \begin{Bmatrix} DP''_1 \\ DP_2 \\ DP_3 \\ DP'_2 \\ DP'_3 \end{Bmatrix} \quad (3-6)$$

The integration of the common FRs of two independent systems can be interpreted by three cases: case 1 is the functional integration of two uncoupled systems illustrated above; in case 2, there are one uncoupled system and one decoupled system of which one FR to be combined is impacted by two DPs ; and case 3 explains another situation, i.e. one decoupled system and one uncoupled system. The interpretation of case 2 and 3 are presented in the appendix D.

The principles for combining the common *FRs* and corresponding *DPs* of the two matrices are as follows:

1. In defining the rows which represent the common functions, the cross effects of the *DPs* on the common function of the other system are the same as the effects on this function of their own system.
2. In defining the columns which represent the cross effects of the *DPs* to be combined on all *FRs*, one of the *DPs* has an effect on a certain *FR*, the combined *DP* has an effect on this *FR*.

Evaluation

From the equation (3-6), it can be known that the elements representing cross effects between systems determine the form of a new design. After the unknown elements of the new combined design equation are defined, the new concept can be evaluated depending on the axioms of AD, i.e. Independence Axiom and Information Axiom.

If the DM of the new system can be expressed as a diagonal matrix, it means the new system is an uncoupled design; if the DM is expressed as a triangular matrix, for example as the form of equation (3-7), the combination is a decoupled design, which must follow a design sequence to decouple the design.

$$\begin{Bmatrix} FR_1'' \\ FR_2 \\ FR_3 \\ FR_2' \\ FR_3' \end{Bmatrix} = \begin{bmatrix} \times & 0 & 0 & 0 & 0 \\ 0 & \times & 0 & 0 & 0 \\ \times & 0 & \times & 0 & 0 \\ 0 & \times & 0 & \times & 0 \\ \times & 0 & 0 & 0 & \times \end{bmatrix} \begin{Bmatrix} DP_1'' \\ DP_2 \\ DP_3 \\ DP_2' \\ DP_3' \end{Bmatrix} \quad (3-7)$$

If the DM of the design equation (3-6) was defined as the form of DM for example in (3-8), neither triangular nor diagonal matrix, it means the new system is a coupled design, which is very hard to be solved.

$$\begin{Bmatrix} R_1'' \\ FR_2 \\ FR_3 \\ FR_2' \\ FR_3' \end{Bmatrix} = \begin{bmatrix} \times & 0 & 0 & 0 & 0 \\ 0 & \times & 0 & \times & 0 \\ \times & 0 & \times & 0 & 0 \\ 0 & \times & 0 & \times & 0 \\ \times & 0 & 0 & 0 & \times \end{bmatrix} \begin{Bmatrix} DP_1'' \\ DP_2 \\ DP_3 \\ DP_2' \\ DP_3' \end{Bmatrix} \quad (3-8)$$

When multiple candidate designs need to be compared, it can be conducted by comparing their DMs. According to the Independence Axiom, the uncoupled design is the best; the uncoupled design is better than the coupled design. When multiple designs are found from Axiom 1, theoretically the best one can be chosen based on Axiom 2. However, real application of Axiom 2 in the starting of the conceptual design can be very difficult, because Axiom 2 is related to robust design and the information content is usually quantified by the probability of success (Park, 2007). In this case the decision can be made with the full consideration of the constraints like compatibility, manufacturability, cost, time, safety, etc.

Analyses of DM

The new design equation of the combined system can be used to guide the further design. The design elements of the matrix can be rearranged and regrouped, as far as possible to form a diagonal matrix with the element groups. An example of the regrouped DM derived from the equation (3-7) is shown in equation (3-9). The element groups essentially represent the subsystems with related functions.

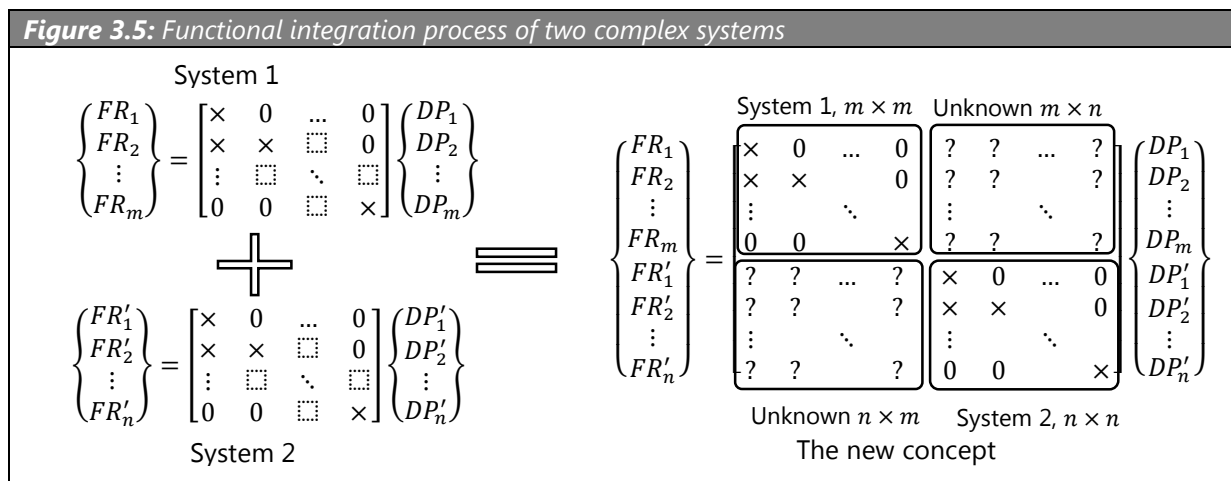
$$\begin{Bmatrix} FR_1'' \\ FR_3 \\ FR_3' \\ FR_2 \\ FR_2' \end{Bmatrix} = \begin{bmatrix} \boxed{\begin{matrix} \times & 0 & 0 \\ \times & \times & 0 \\ \times & 0 & \times \end{matrix}} & \begin{matrix} 0 & 0 \\ 0 & 0 \\ 0 & 0 \end{matrix} \\ \begin{matrix} 0 & 0 & 0 \\ 0 & 0 & 0 \end{matrix} & \boxed{\begin{matrix} \times & 0 \\ \times & \times \end{matrix}} \end{bmatrix} \begin{Bmatrix} DP_1'' \\ DP_3 \\ DP_3' \\ DP_2 \\ DP_2' \end{Bmatrix} \begin{matrix} \text{Subsystem 1} \\ \text{Subsystem 2} \end{matrix} \quad (3-9)$$

Group 1
Group 2

The elements related with functions are rearranged into two groups; correspondingly the design parameters are regrouped into two subsystems. In mathematics, to determine the elements in the lower triangular matrix, one should follow the order from top to down and left to right. The two subsystems are independent, so they can be determined independently regardless the design sequence. The design parameters

(or the range of the design parameters) in the subsystem can be determined on a top-down sequence, for example the sequence of subsystem 1 is: $DP_1'' \rightarrow DP_3 \rightarrow DP_3'$.

This functional integration process described by design equations can be extended to the combination of two complex systems. In Figure 3.5, equation 1 represents the system with m functions; equation 2 represents the system with n functions; the new design equation expresses the new concept by integrating system 1 and system 2. In the DM, the element groups in the diagonal are system 1 and system 2. The other new appeared two groups in the off-diagonal are unknown elements representing the cross effects of the DPs of one system on the FRs of the other system. The steps to combine the common FRs , evaluate and analyze the design matrix are the same as the above interpretation of the 3×3 matrix equations.



In general, the approach to functional integration by matrix equations can be summarized as follows:

1. Decompose the two independent systems to matrix design equations according to the principle of AD method;
2. Write the matrix equations in one unified design equation. Arrange the DMs of the independent systems along the main diagonal of the new DM; additional unknown elements appear in the off-diagonal of the new DM;

3. Combine the common *FRs* and corresponding *DPs* of the two systems; define these unknown elements regarding the cross effects of one system on the other system on the basis of specific concept properties;
4. Evaluate the DM of new concepts according to the axioms of the AD method.

4 Concept design of suspensions with integrated electric motors using the proposed approach

In this chapter the proposed approach is applied for the generation and evaluation of new suspension concepts with integrated electric motors into suspension arms. The work in this chapter is carried out in the following steps:

- 1) Decompose electric motors and conventional suspensions generally to design matrix equations independently: decompose the two systems to FRs and DPs; build the mapping between the FRs and DPs of each system, separately. Indicate the relationship between the FRs and DPs by DMs.
- 2) Generate new concepts by combining the electric motor into conventional suspension parts which have common functions; combine the design equations of electric motors and suspensions in a general design equation for the new concepts, and then integrate their common *FRs* and corresponding *DPs* and partially figure out the unknown elements.
- 3) Define the remaining unknown elements according to the specific concepts; accomplish the design equation of each concept.
- 4) Compare and evaluate the design equations of new concepts according to the AD method; select the suspension concept for the target vehicle.

The parent FR of the target concept can be briefly stated as follows:

Parent *FR*: Provide a suspension with electric motors integrated into arms

This *FR* has not only the function of normal suspensions FR_s but also the function of drive systems FR_m to propel the car.

FR_s : Functions of suspensions

FR_m : Functions of drive systems

This concept in the physical domain consists of two systems:

DP_s : Suspensions

DP_m : Drive system

They can be written in one equation as follows:

$$\begin{Bmatrix} FR_m \\ FR_s \end{Bmatrix} = \begin{bmatrix} \times & ? \\ ? & \times \end{bmatrix} \begin{Bmatrix} DP_m \\ DP_s \end{Bmatrix} \quad (4-1)$$

These unknown elements in this equation should be figured out to accomplish the design matrix equation of each generated design concept and subsequently to evaluate the DM of each concept on the basis of AD.

4.1 Functional decomposition of the electric motor and suspension

The function decomposition of the two independent systems follows the top-down principle (see Figure 3.2). Electric motors and suspensions are respectively decomposed into three levels in functional domain and physical domain, i.e. system level, subsystem level and parameter level.

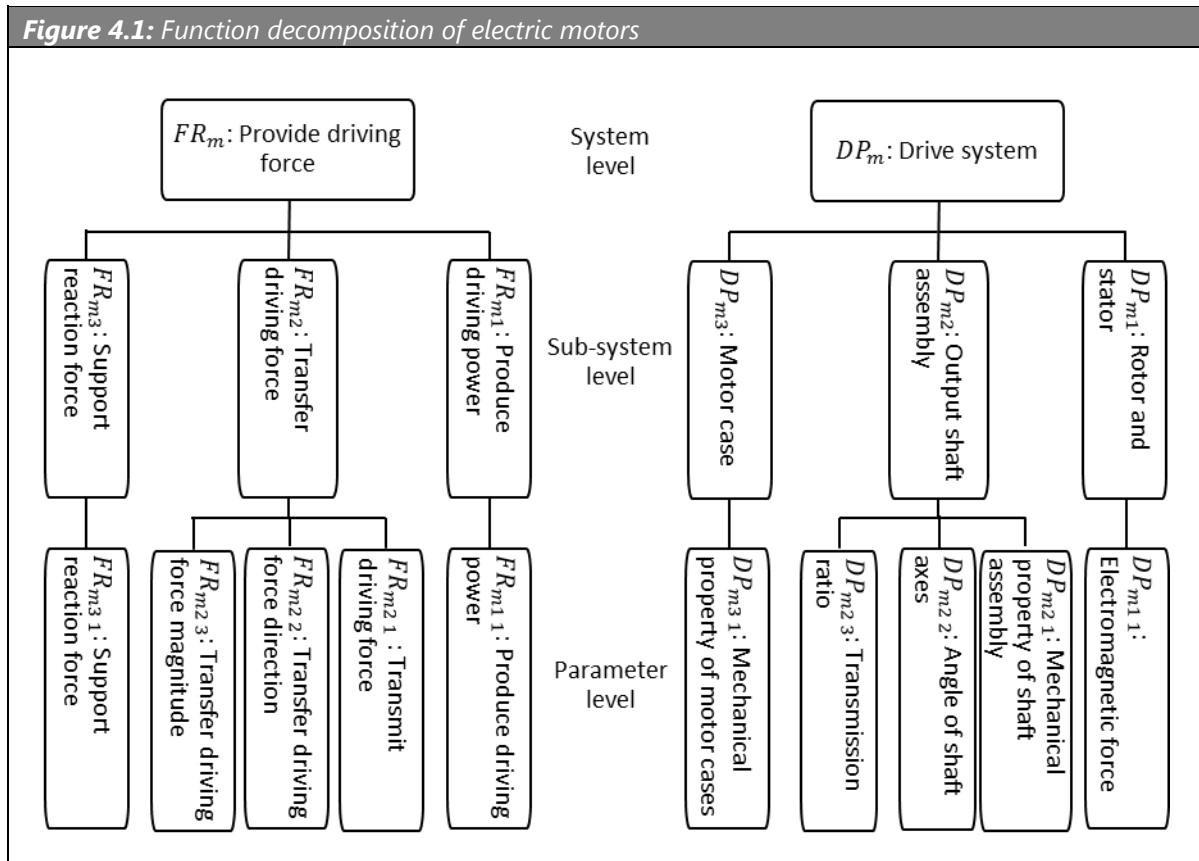
4.1.1 Function decomposition of electric motors

The electric motor as a driving system has the primary function to provide driving force for the whole vehicle. In the subsystem level, it has three main functions: produce driving power, transfer driving force and support reaction force. In the physical domain, the driving force is produced by the interaction of the electromagnetic force between the rotor and stator in electric motors; the power and torque are transferred through an output shaft assembly to the wheel, including output shafts, joints or transmission gears, which cause also reaction force; the reaction force is carried by the motor case that also support the rotor and stator.

In further decomposition of the subsystem, as the functions of electric motors as a drive unit is relatively simple, the FR_{m1} and FR_{m3} are kept in the parameter level. Transferring the driving force from electric motors to wheels should meet not only force continuity but also the required force direction and force magnitude. They are strongly related to the mechanical property of shaft assembly, intersection angle of

transfer shaft and transmission ratios. The angle of transfer shafts and transmission ratios have also impact on reaction force.

As previous mentioned, by means of literature review, expert consulting and team collaboration, the functional decomposition of electric motors corresponding to DPs may be stated as follows:



The design equation of electric motors is written as follows:

$$\begin{Bmatrix} FR_{m11} \\ FR_{m21} \\ FR_{m22} \\ FR_{m23} \\ FR_{m31} \end{Bmatrix} = \begin{bmatrix} \times & 0 & 0 & 0 & 0 \\ \times & \times & 0 & 0 & 0 \\ 0 & 0 & \times & 0 & 0 \\ 0 & 0 & 0 & \times & 0 \\ \times & \times & \times & \times & \times \end{bmatrix} \begin{Bmatrix} DP_{m11} \\ DP_{m21} \\ DP_{m22} \\ DP_{m23} \\ DP_{m31} \end{Bmatrix} \quad (4-2)$$

4.1.2 Function decomposition of suspensions

FRs in subsystem level

Suspension functions are decomposed into four primary functions in the subsystem level on the basis of vehicle function requirements as follows (Heißing & Ersoy, 2007) (Reimpell & Betzler, 2005):

FR_{s1} : Meet required DOFs

FR_{s2} : Transmit the mechanical force between roads and vehicle bodies

FR_{s3} : Ensure ride comfort

FR_{s4} : Maintain driving stability

Suspensions must allow the wheels certain required degree of freedoms (DOFs). For example, to match the road terrain suspension systems must enable the wheels to jounce and rebound relative to the vehicle body in direction z-axis of the vehicle coordination (see Figure B.1 in Appendix B); moreover, front suspensions should provide the wheel rotational DOF when steering. The vehicle body should be supported on suspensions and therefore suspensions must be able to transmit the force between roads and vehicle bodies. Suspensions should isolate passengers or cargos from severe vibrations induced from roads, in other words they have the function to ensure ride comfort. As a mechanical structure that supports the vehicle body and fixes the wheels, the suspension system must have the ability to maintain the vehicle stability. For example, while driving in straight line vehicles should keep the driving direction and must be able to align to the driving direction against small steering disturbances; while turning, the vehicle must be able to accurately follow the steering angle to ensure that the vehicle can turn as the driver wish.

DPs in subsystem level

In suspension system the metal parts are connected through different types of rubber bushings. They have a certain amount of movements because of rubber elasticity that

allow suspension parts to move under meeting kinematic requirements. The DP_{s1} is defined as: bushings.

The function transmitting the mechanical force is carried by suspensions links and springs. The longitudinal and lateral forces on wheels are supported by the links of suspensions; while the vertical forces are exerted on the vehicle body through the springs. The DP_{s2} is defined as: suspension links and springs.

In the suspension, shock absorbers are used to control suspension oscillation and dissipate the mechanical energy caused by vibration. The noise from roads is briefly isolated by the damping of rubber bushings due to its viscoelasticity. As the rubber bushing has already been defined as the DP_{s1} , the DP_{s3} is defined as: dampers.

These requirements of driving stability are directly related to wheels and vehicle body attitudes, for example wheel alignments to keep driving direction in straight line and inclination of vehicle body in cornering. The roll stiffness of vehicle bodies is determined by the coil spring stiffness and anti-roll bar stiffness. As the coil spring is defined as DP_{s2} , the DP_{s4} is defined as: wheel assembly and anti-roll bars.

Above all, the DPs corresponding to the FRs of suspension in subsystem level are:

DP_{s1} : Bushings

DP_{s2} : Suspension links and springs

DP_{s3} : Dampers

DP_{s4} : Wheel assembly and anti-roll bars

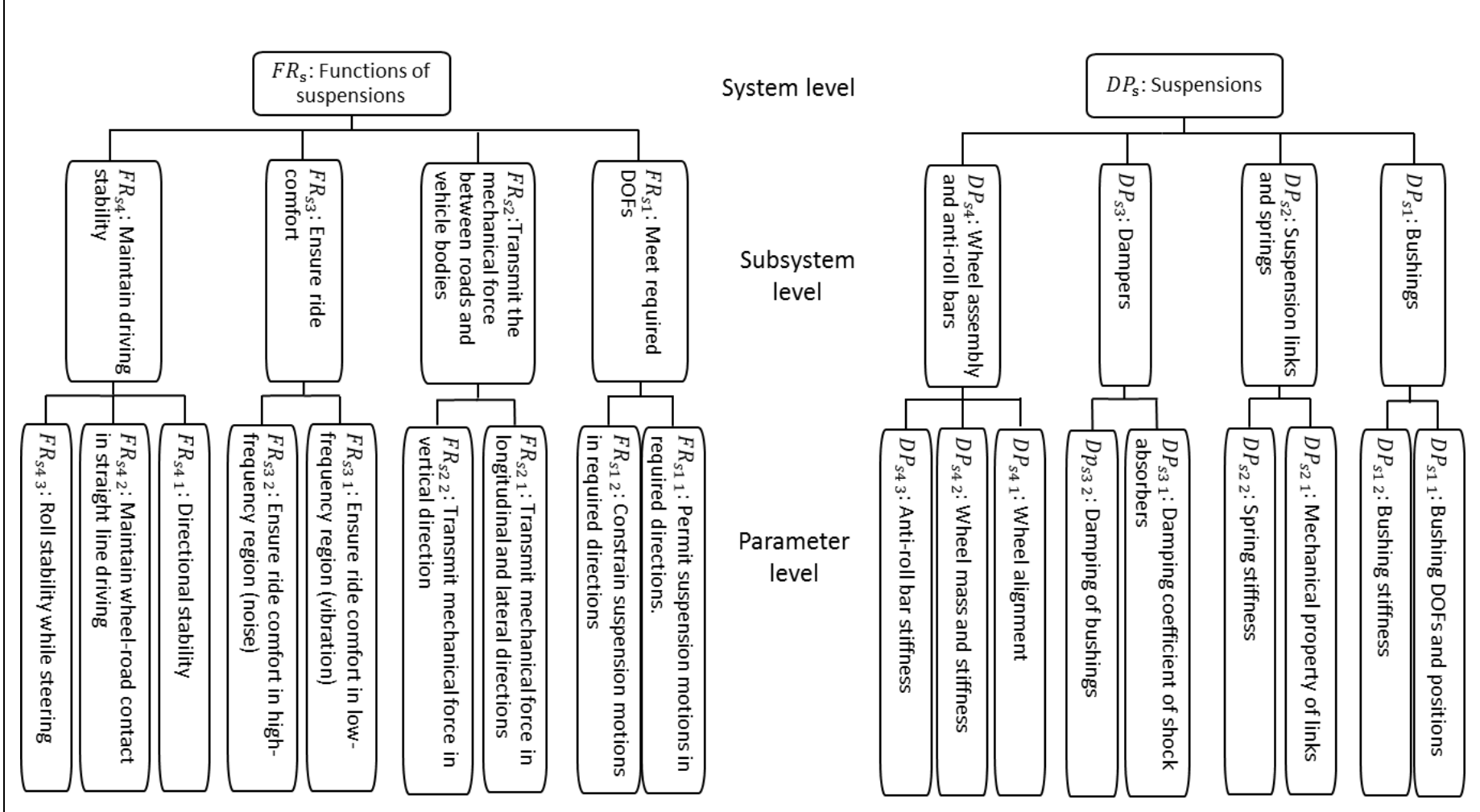
FRs and DPs in parameter level

The DPs in the sub-system level are further specified in the physical parameter level. The function decompositions of suspensions are stated in the Figure 4.2. In this level, the physical parameters are dominant factors of the corresponding sub-function.

For FR_{s1} , the allowed suspension motions $FR_{s1\ 1}$ are realized by the bushing own DOFs and their positions ($DP_{s1\ 1}$), and on the other side the limited motions $FR_{s1\ 2}$ are constrained by the bushing stiffness ($DP_{s1\ 2}$).

FR_{s2} is divided into two parts according the force direction: for $FR_{s2\ 1}$ the load the loads in longitudinal and lateral directions are carried by mechanical property of links ($DP_{s2\ 1}$); for $FR_{s2\ 2}$ the loads in vertical direction are normally carried $DP_{s2\ 1}$ and spring stiffness ($DP_{s2\ 2}$). Bushings are parts connecting suspension links, so $DP_{s1\ 2}$ has also

Figure 4.2: Function decomposition of suspensions

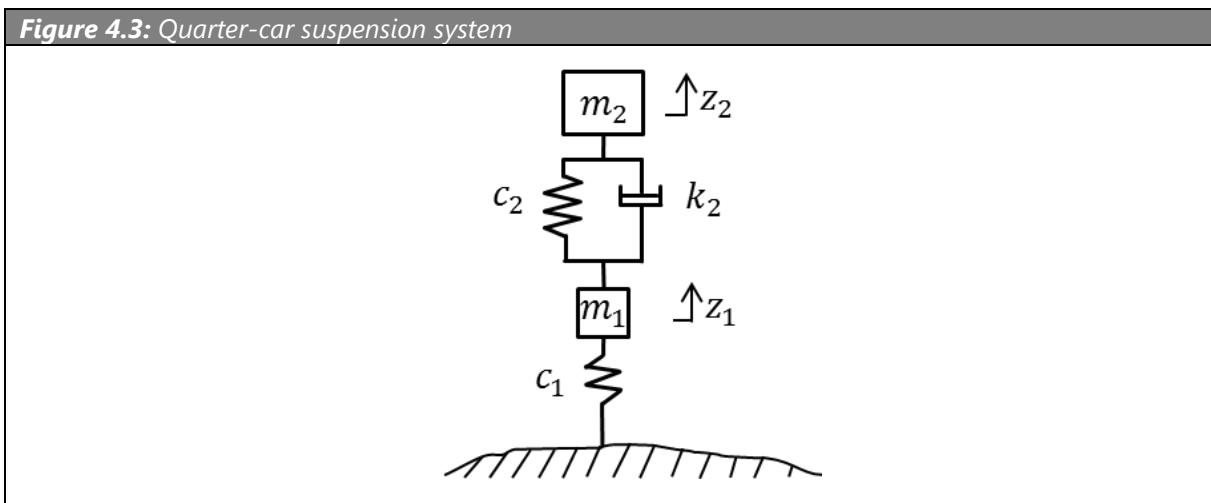


influence on $FR_{s2\ 1}$ and $FR_{s2\ 2}$.

FR_{s3} is decomposed into $FR_{s3\ 1}$ low frequency region and $FR_{s3\ 2}$ high frequency region according the vibrational frequency.

For $FR_{s3\ 1}$, suspensions can be treated as a mass-spring-damper system. A schematic diagram of a quarter-vehicle suspension system is shown in Figure 4.3. In this diagram m_2 denotes the sprung mass; m_1 represents the unsprung mass which consists of wheel mass ($DP_{s4\ 2}$) and the equivalent mass of suspension links related to $DP_{s1\ 1}$ and $DP_{s2\ 1}$; k_2 is the damping coefficient of suspensions ($DP_{s3\ 1}$); c_2 and c_1 are the spring stiffness of suspensions and stiffness of wheels, respectively; z_2 is the displacement of the sprung mass; and z_1 is the displacement of the unsprung mass. In addition, the anti-roll bar stiffness ($DP_{s4\ 3}$) has an effect on the roll acceleration of the vehicle body that could be illustrated by a transfer function between roll acceleration and roll excitation in the reference (Iliev, 2011), but the effect is not as strong as that by the spring and damper. In above parameters, $DP_{s2\ 2}$ and $DP_{s3\ 1}$ are the dominant factors of the $FR_{s3\ 1}$, while $DP_{s1\ 1}$, $DP_{s2\ 1}$, $DP_{s4\ 2}$ and $DP_{s4\ 3}$ have a certain effect but less than dominant factors on $FR_{3\ 1}$. In order to distinguish the DPs that is not the determining parameter of a function but cannot be ignored, the notation " \otimes " is introduced to the DM .

Figure 4.3: Quarter-car suspension system



For $FR_{s3\ 2}$, the $DP_{s1\ 2}$ and the damping of bushings ($DP_{s3\ 2}$) have the function of high frequency vibration isolation.

For FR_{s4} , driving stability is decomposed into three FRs: directional stability $FR_{s4\ 1}$, tire-road contact in straight-line driving $FR_{s4\ 2}$ and roll stability while steering $FR_{s4\ 3}$.

For $FR_{s4\ 1}$, the drive directional stability is determined by steering and suspension systems. The wheel alignments ($DP_{s4\ 1}$) and K&C characteristics of suspensions associated with $DP_{s1\ 1}$ and $DP_{s1\ 2}$ are significant parameters to maintain driving direction and cornering accuracy while steering.

For $FR_{s4\ 2}$, force between wheel-road contact can also be derived from the mass-spring-mass system in Figure 4.3. In contrast to $FR_{s3\ 1}$, the $DP_{s3\ 1}$ $DP_{s3\ 1}$ and $DP_{s4\ 2}$ have strong effect on this contact force but the effect of the $DP_{s4\ 3}$ is insignificant.

For $FR_{s4\ 3}$, vehicle body roll stiffness is determined by the spring stiffness, damping rate of shock absorbers and stiffness of anti-roll bars.

As mentioned above, with the addition of expert consulting and group discussion, the design equation of suspensions can be written as follows:

$$\begin{Bmatrix} FR_{s1\ 1} \\ FR_{s1\ 2} \\ FR_{s2\ 1} \\ FR_{s2\ 2} \\ FR_{s3\ 1} \\ FR_{s3\ 2} \\ FR_{s4\ 1} \\ FR_{s4\ 2} \\ FR_{s4\ 3} \end{Bmatrix} = \begin{bmatrix} \times & 0 & 0 & 0 & 0 & 0 & 0 & 0 & 0 \\ 0 & \times & 0 & 0 & 0 & 0 & 0 & 0 & 0 \\ 0 & \times & \times & 0 & 0 & 0 & 0 & 0 & 0 \\ 0 & \times & \times & \times & 0 & 0 & 0 & 0 & 0 \\ \otimes & 0 & \otimes & \times & \times & 0 & 0 & \otimes & \otimes \\ 0 & \times & 0 & 0 & 0 & \times & 0 & 0 & 0 \\ \times & \times & 0 & 0 & 0 & 0 & \times & 0 & 0 \\ \otimes & 0 & \otimes & \times & \times & 0 & 0 & \times & 0 \\ 0 & 0 & 0 & \times & \times & 0 & 0 & 0 & \times \end{bmatrix} \begin{Bmatrix} DP_{s1\ 1} \\ DP_{s1\ 2} \\ DP_{s2\ 1} \\ DP_{s2\ 2} \\ DP_{s3\ 1} \\ DP_{s3\ 2} \\ DP_{s4\ 1} \\ DP_{s4\ 2} \\ DP_{s4\ 3} \end{Bmatrix} \quad (4-3)$$

4.2 Functional integration

4.2.1 Common functions

Using the proposed functional integration approach, the prerequisites of functional integration between electric motors and suspensions are that there should be common functions in the functional domain and in parallel the possibility to combine these corresponding design parameters in the physical domain. Considering $FR_{m2\ 1}$ and $FR_{m3\ 1}$ of electric motors have the common function as $FR_{s2\ 1}$ and $FR_{s2\ 2}$ of

suspensions, i.e. transmitting mechanical force, they have the possibility to be combined. However, the $DP_{s2\ 1}$ has large deformations with the movement of wheels in vertical direction and meanwhile driving shaft assembly is a rotational object in transmitting force, which makes them impossible to combine with DPs of electric motors with aspect to kinematics. Suspension links and electric motors have no large deformation, which provide them possibility to be combined in physical domain. Considering the mass and volume of electric motors have been considerably reduced under the application of new materials and improvement of power density, which enables the possibility to combine the two components, for example the chosen electric motor (see Appendix C). Its diameter and length are about 110 mm and 320 mm, respectively, which does not occupy too much space of suspensions. The motor power and torque coupled with an appropriate transmission ratio satisfy the requirements of the vehicle acceleration and top speed (see chapter 5).

4.2.2 Functional integration based on design equation

According to the equation of functional integration (3-5), the design equation of the electric motor (4-2) and suspension (4-3) can be combined in a new design equation (4-4). The unknown blocks P_2 and P_3 are cross effects of two systems to each other. The rows in the horizontal boxes represent the effect of each DP on the common FR i.e. $FR_{m3\ 1}$ of electric motors and $FR_{s2\ 1}$ of suspensions. The columns in the vertical rectangular boxes represent the impacts of $DP_{m3\ 1}$ of electric motors and $DP_{s2\ 1}$ of suspensions to all FR s.

$$\begin{matrix}
 \left. \begin{matrix} FR_{m1\ 1} \\ FR_{m2\ 1} \\ FR_{m2\ 2} \\ FR_{m2\ 3} \\ FR_{m3\ 1} \\ FR_{s1\ 1} \\ FR_{s1\ 2} \\ FR_{s2\ 1} \\ FR_{s2\ 2} \\ FR_{s3\ 1} \\ FR_{s3\ 2} \\ FR_{s4\ 1} \\ FR_{s4\ 2} \\ FR_{s4\ 3} \end{matrix} \right\} = &
 \begin{matrix}
 P_1 & P_2 \\
 \left[\begin{array}{cccc|cccccccc}
 \times & 0 & 0 & 0 & 0 & ? & ? & ? & ? & ? & ? & ? & ? & ? \\
 \times & \times & 0 & 0 & 0 & ? & ? & ? & ? & ? & ? & ? & ? & ? \\
 0 & 0 & \times & 0 & 0 & ? & ? & ? & ? & ? & ? & ? & ? & ? \\
 0 & 0 & 0 & \times & 0 & ? & ? & ? & ? & ? & ? & ? & ? & ? \\
 \times & 0 & \times & \times & \times & ? & ? & ? & ? & ? & ? & ? & ? & ? \\
 \hline
 ? & ? & ? & ? & ? & \times & 0 & 0 & 0 & 0 & 0 & 0 & 0 & 0 \\
 ? & ? & ? & ? & ? & 0 & \times & 0 & 0 & 0 & 0 & 0 & 0 & 0 \\
 ? & ? & ? & ? & ? & 0 & \times & \times & 0 & 0 & 0 & 0 & 0 & 0 \\
 ? & ? & ? & ? & ? & 0 & \times & \times & \times & 0 & 0 & 0 & 0 & 0 \\
 ? & ? & ? & ? & ? & \otimes & 0 & \otimes & \times & \times & 0 & 0 & \otimes & \otimes \\
 ? & ? & ? & ? & ? & 0 & \times & 0 & 0 & 0 & \times & 0 & 0 & 0 \\
 ? & ? & ? & ? & ? & \times & \times & 0 & 0 & 0 & 0 & \times & 0 & 0 \\
 ? & ? & ? & ? & ? & \otimes & 0 & \otimes & \times & \times & 0 & 0 & \times & 0 \\
 ? & ? & ? & ? & ? & 0 & 0 & 0 & \times & \times & 0 & 0 & 0 & \times
 \end{array} \right] &
 \left. \begin{matrix} DP_{m1\ 1} \\ DP_{m2\ 1} \\ DP_{m2\ 2} \\ DP_{m2\ 3} \\ DP_{m3\ 1} \\ DP_{s1\ 1} \\ DP_{s1\ 2} \\ DP_{s2\ 1} \\ DP_{s2\ 2} \\ DP_{s3\ 1} \\ DP_{s3\ 2} \\ DP_{s4\ 1} \\ DP_{s4\ 2} \\ DP_{s4\ 3} \end{matrix} \right\}
 \end{matrix} \quad (4-4)
 \end{matrix}$$

At first, the matrix elements in the red horizontal and vertical rectangular boxes of the equation (4-4) are defined by applying the principle of combining the common functions of the two matrices which is summarized in section 3.2. The result is given in equation (4-5).

$$\begin{matrix}
 \left. \begin{matrix} FR_{m1\ 1} \\ FR_{m2\ 1} \\ FR_{m2\ 2} \\ FR_{m2\ 3} \\ FR_{m3\ 1} \\ FR_{s1\ 1} \\ FR_{s1\ 2} \\ FR_{s2\ 1} \\ FR_{s2\ 2} \\ FR_{s3\ 1} \\ FR_{s3\ 2} \\ FR_{s4\ 1} \\ FR_{s4\ 2} \\ FR_{s4\ 3} \end{matrix} \right\} = &
 \begin{matrix}
 P_1 & P_2 \\
 \left[\begin{array}{cccc|cccccccc}
 \times & 0 & 0 & 0 & 0 & ? & ? & ? & ? & ? & ? & ? & ? & ? \\
 \times & \times & 0 & 0 & 0 & ? & ? & ? & ? & ? & ? & ? & ? & ? \\
 0 & 0 & \times & 0 & 0 & ? & ? & ? & ? & ? & ? & ? & ? & ? \\
 0 & 0 & 0 & \times & 0 & ? & ? & ? & ? & ? & ? & ? & ? & ? \\
 \times & 0 & \times & \times & \times & 0 & \times & \times & 0 & 0 & 0 & 0 & 0 & 0 \\
 \hline
 ? & ? & ? & ? & ? & \times & 0 & 0 & 0 & 0 & 0 & 0 & 0 & 0 \\
 ? & ? & ? & ? & ? & 0 & \times & 0 & 0 & 0 & 0 & 0 & 0 & 0 \\
 \times & 0 & \times & \times & \times & 0 & \times & \times & 0 & 0 & 0 & 0 & 0 & 0 \\
 ? & ? & ? & ? & \times & 0 & \times & \times & \times & 0 & 0 & 0 & 0 & 0 \\
 ? & ? & ? & ? & \otimes & \otimes & 0 & \otimes & \times & \times & 0 & 0 & \otimes & \otimes \\
 ? & ? & ? & ? & ? & 0 & \times & 0 & 0 & 0 & \times & 0 & 0 & 0 \\
 ? & ? & ? & ? & ? & \times & \times & 0 & 0 & 0 & 0 & \times & 0 & 0 \\
 ? & ? & ? & ? & \otimes & \otimes & 0 & \otimes & \times & \times & 0 & 0 & \times & 0 \\
 ? & ? & ? & ? & ? & 0 & 0 & 0 & \times & \times & 0 & 0 & 0 & \times
 \end{array} \right] &
 \left. \begin{matrix} DP_{m1\ 1} \\ DP_{m2\ 1} \\ DP_{m2\ 2} \\ DP_{m2\ 3} \\ DP_{m3\ 1} \\ DP_{s1\ 1} \\ DP_{s1\ 2} \\ DP_{s2\ 1} \\ DP_{s2\ 2} \\ DP_{s3\ 1} \\ DP_{s3\ 2} \\ DP_{s4\ 1} \\ DP_{s4\ 2} \\ DP_{s4\ 3} \end{matrix} \right\}
 \end{matrix} \quad (4-5)
 \end{matrix}$$

The unknown elements in the DM of this equation are defined individually. They are determined according to the interview with suspension engineers and the relevant technical documentation.

The first row in P_2 :

- The driving power is only determined by the electromagnetic of the rotor and stator, but the dimension of the rotor and stator is limited by design space of suspensions that depends on the configurations, so $DM_{1\ 6}$ is defined as "?". Other DPs of suspensions have no effect on $FR_{m1\ 1}$. The elements from $DM_{1\ 7}$ to $DM_{1\ 14}$ are defined as "0".

The second row in P_2 :

- The driving force from the electric motor is transmitted by the shaft and gears, the arrangement of which depends on the design space of suspensions. $DM_{2\ 6}$ is defined as "?". Other DPs of suspensions have no effect on $FR_{m2\ 1}$, so the elements from $DM_{2\ 7}$ to $DM_{2\ 14}$ are defined as "0".

The third row in P_2 :

- In the third row, the driving force direction is determined by the driving shaft axis and the driving shafts are supported on bearings, which make the transferring of the driving force free from the interference of suspension motions but the design space is still limited, so $DM_{3\ 6}$ is defined as "?" and elements from $DM_{3\ 7}$ to $DM_{3\ 14}$ are defined as "0".

The fourth row in P_2 :

- In the fourth row, the transmission ratio is determined by the configuration of transmissions which is limited by the space of suspensions. Therefore, $DM_{4\ 6}$ is defined as "?" and elements from $DM_{4\ 7}$ to $DM_{4\ 14}$ are defined as "0".

Validation of the fifth row in P_2 :

- Reaction force inside of the electric motor is supported by the mechanical property of motor cases. After combination with suspension links, the motor case is a part of suspension links, so reaction force is also supported by

suspension links and bushings. $DM_{5\ 7}$ and $DM_{5\ 8}$ are defined as "×" and other elements in this row is defined as "0".

The first column in P_3 :

- When electric motors are fixed into suspension arms, electromagnetic force generated by motor rotors and stators has strong effect on the mechanical equilibrium of the suspension arm, so $DM_{8\ 1}$ and $DM_{9\ 1}$ are defined as "×".
- The unsprung mass increase and new mechanical equilibrium caused by electric motors deteriorates the ride comfort in low frequency region. The vibration and noise generated by the rotor and stators worsen the suspensions NVH, so $DM_{10\ 1}$ and $DM_{11\ 1}$ are defined as "×".
- Other elements in the DM are kept "?", they should be defined according to the specific configuration of each suspension.

The second column, third column and fourth column in P_3 :

- The form of the shaft assembly has influence on the mechanical equilibrium of the combined suspension arms, e.g. the distribution of shaft supporting bearings has influence on application point of reaction of transmission force on the combined suspension arms, so $DM_{8\ 2}$ and $DM_{9\ 2}$ are defined as "×". The operating angle of shaft axes and transmission ratio have influence on the directions and magnitude of reaction of transmission force respectively, so $DM_{8\ 3}$, $DM_{9\ 3}$, $DM_{8\ 4}$ and $DM_{9\ 4}$ are defined as "×".
- As the reaction of transmission force and the mass of transmissions both influence the ride comfort in low frequency region, $DM_{10\ 2}$, $DM_{10\ 3}$ and $DM_{10\ 4}$ are defined as "×".
- The shaft assembly has less effect on the body roll while steering, so $DM_{14\ 2}$, $DM_{14\ 3}$ and $DM_{14\ 4}$ are defined as "0".
- Other elements in the DM are kept "?", and they will be defined according to the configuration of suspensions.

Validation of the fifth column in P_3 :

- $DM_{65} = "?"$: the influence of DP_{m31} on FR_{s11} depends on the configuration of each suspension;
- $DM_{75} = "0"$: DP_{m31} has no effect on FR_{s12} ;
- $DM_{85} = "x"$: DP_{m31} as a part of the suspension arm carries the function FR_{s21} after combination;
- $DM_{95} = "x"$: DP_{m31} as a part of the suspension arm carries the function FR_{s22} ;
- $DM_{105} = "\otimes"$: unsprung mass increased by DP_{m31} has a certain influence on FR_{s31} but not strong;
- $DM_{115} = "0"$: DP_{m31} has no effect on FR_{s32} ;
- $DM_{125} = "0"$: DP_{m31} has no effect on FR_{s41} ;
- $DM_{135} = "\otimes"$: DP_{m31} has a certain influence effect on FR_{s42} ;
- $DM_{145} = "0"$: DP_{m31} has no effect on FR_{s43} .

With above analysis, the equation (4-5) can be written as the following equation (4-6)

$$\begin{pmatrix} FR_{m11} \\ FR_{m21} \\ FR_{m22} \\ FR_{m23} \\ FR_{m31} \\ FR_{s11} \\ FR_{s12} \\ FR_{s21} \\ FR_{s22} \\ FR_{s31} \\ FR_{s32} \\ FR_{s41} \\ FR_{s42} \\ FR_{s43} \end{pmatrix} = \begin{pmatrix} \times & 0 & 0 & 0 & 0 & ? & 0 & 0 & 0 & 0 & 0 & 0 & 0 & 0 \\ \times & \times & 0 & 0 & 0 & ? & 0 & 0 & 0 & 0 & 0 & 0 & 0 & 0 \\ 0 & 0 & \times & 0 & 0 & ? & 0 & 0 & 0 & 0 & 0 & 0 & 0 & 0 \\ 0 & 0 & 0 & \times & 0 & ? & 0 & 0 & 0 & 0 & 0 & 0 & 0 & 0 \\ \times & \times & \times & \times & \times & 0 & \times & \times & 0 & 0 & 0 & 0 & 0 & 0 \\ ? & ? & ? & ? & ? & \times & 0 & 0 & 0 & 0 & 0 & 0 & 0 & 0 \\ ? & ? & ? & ? & 0 & 0 & \times & 0 & 0 & 0 & 0 & 0 & 0 & 0 \\ \times & \times & \times & \times & \times & 0 & \times & \times & 0 & 0 & 0 & 0 & 0 & 0 \\ \times & \times & \times & \times & \otimes & \otimes & 0 & \otimes & \times & \times & 0 & 0 & \otimes & \otimes \\ \times & ? & ? & ? & 0 & 0 & \times & 0 & 0 & 0 & \times & 0 & 0 & 0 \\ ? & ? & ? & ? & 0 & \times & \times & 0 & 0 & 0 & 0 & \times & 0 & 0 \\ ? & ? & ? & ? & \otimes & \otimes & 0 & \otimes & \times & \times & 0 & 0 & \times & 0 \\ 0 & 0 & 0 & 0 & 0 & 0 & 0 & 0 & \times & \times & 0 & 0 & 0 & \times \end{pmatrix} \begin{pmatrix} DP_{m11} \\ DP_{m21} \\ DP_{m22} \\ DP_{m23} \\ DP_{m31} \\ DP_{s11} \\ DP_{s12} \\ DP_{s21} \\ DP_{s22} \\ DP_{s31} \\ DP_{s32} \\ DP_{s41} \\ DP_{s42} \\ DP_{s43} \end{pmatrix} \quad (4-6)$$

After combining the common FR s and the corresponding DP s, the equation can be written as the equation (4-7).

$$\begin{pmatrix} FR_{m1\ 1} \\ FR_{m2\ 1} \\ FR_{m2\ 2} \\ FR_{m2\ 3} \\ FR_{s1\ 1} \\ FR_{s1\ 2} \\ FR_{ms2\ 1} \\ FR_{s2\ 2} \\ FR_{s3\ 1} \\ FR_{s3\ 2} \\ FR_{s4\ 1} \\ FR_{s4\ 2} \\ FR_{s4\ 3} \end{pmatrix} = \begin{bmatrix} \times & 0 & 0 & 0 & ? & 0 & 0 & 0 & 0 & 0 & 0 & 0 & 0 \\ \times & \times & 0 & 0 & ? & 0 & 0 & 0 & 0 & 0 & 0 & 0 & 0 \\ 0 & 0 & \times & 0 & ? & 0 & 0 & 0 & 0 & 0 & 0 & 0 & 0 \\ 0 & 0 & 0 & \times & ? & 0 & 0 & 0 & 0 & 0 & 0 & 0 & 0 \\ ? & ? & ? & ? & \times & 0 & ? & 0 & 0 & 0 & 0 & 0 & 0 \\ ? & ? & ? & ? & 0 & \times & 0 & 0 & 0 & 0 & 0 & 0 & 0 \\ \times & \times & \times & \times & 0 & \times & \times & 0 & 0 & 0 & 0 & 0 & 0 \\ \times & \times & \times & \times & 0 & \times & \times & \times & 0 & 0 & 0 & 0 & 0 \\ \times & \times & \times & \times & \otimes & 0 & \otimes & \times & \times & 0 & 0 & \otimes & \otimes \\ \times & ? & ? & ? & 0 & \times & 0 & 0 & 0 & \times & 0 & 0 & 0 \\ ? & ? & ? & ? & \times & \times & 0 & 0 & 0 & 0 & \times & 0 & 0 \\ ? & ? & ? & ? & \otimes & 0 & \otimes & \times & \times & 0 & 0 & \times & 0 \\ 0 & 0 & 0 & 0 & 0 & 0 & 0 & \times & \times & 0 & 0 & 0 & \times \end{bmatrix} \begin{pmatrix} DP_{m1\ 1} \\ DP_{m2\ 1} \\ DP_{m2\ 2} \\ DP_{m2\ 3} \\ DP_{s1\ 1} \\ DP_{s1\ 2} \\ DP_{ms2\ 1} \\ DP_{s2\ 2} \\ DP_{s3\ 1} \\ DP_{s3\ 2} \\ DP_{s4\ 1} \\ DP_{s4\ 2} \\ DP_{s4\ 3} \end{pmatrix} \quad (4-7)$$

in which, FR_{ms21} represents the function to transmit load from wheels and electric motors; DP_{ms21} means mechanical property of combined structure of the suspension links and motor case. The definition of elements with symbol "?" depends on following specified motor combined configurations of suspensions and electric motors.

4.3 Concept generation based on design equation

The possible concepts are generated on the basis of these traditional suspensions (see Table 2.2) through combining the suspension arm with the electric motor. The combinations are listed in Table 4.1, in which the traditional suspensions are selected from the suspensions used by small and medium cars. The functionality of all the new generated concepts can be investigated on the basis of equation (4-7). With the purpose of ascertaining the unknown relationships in the DM of each concept, suspensions listed in Table 4.1 are conceptualized and analyzed depending on their design equations, respectively. The cross effects in each concept are discussed.

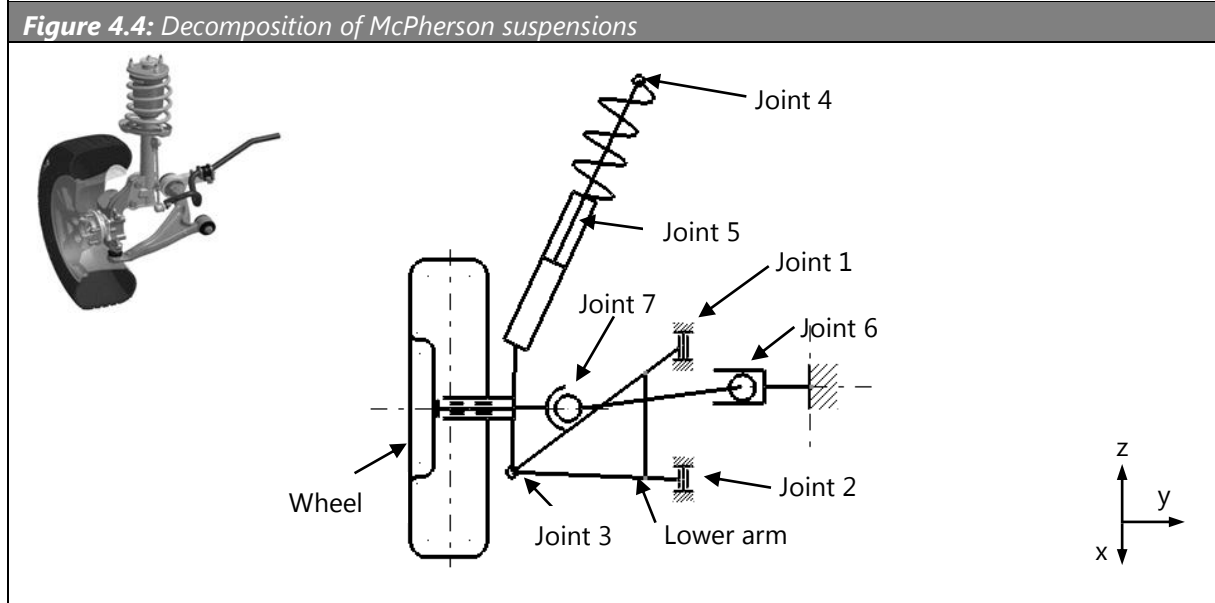
Table 4.1: New concepts generated by integrating common functions of suspension links and electric motors

Suspension	Arm or link to be integrated	Possible concepts
McPherson suspensions	Lower control arm	Concept 1
Double wishbone suspensions	Lower wishbone	Concept 2
	Upper wishbone	Concept 3
Trapezoidal-link rear suspension	Trapezoidal-link	Concept 4
	Lateral arm	Concept 5
Twist beam suspensions	Longitudinal arm	Concept 6
	Center beam	Concept 7
	De-Dion tube	Concept 8
De-Dion rear suspension	Watt link	Concept 9
	Longitudinal link	Concept 10
Multilink suspensions with a longitudinal arm	Lateral link	Concept 11

4.3.1 Conception based on McPherson suspensions

Concept 1: Concept generation with lower control arms

McPherson suspensions combined with the steering system are used for front-wheel-drive cars (shown in Figure 4.4). The bushings of McPherson suspensions include revolute joint 1, revolute joint 2, spherical joint 3, spherical joint 4 and cylindrical joint 5 (see Figure 4.4).



Motions of McPherson suspensions in required directions are:

$FR_{s1\ 1}$: Permit suspension motions in required directions

- $FR_{s1\ 1\ 1}$: Permit the steering motion around the king-pin axis
- $FR_{s1\ 1\ 2}$: Permit relative motion to the vehicle body in z-direction

$FR_{s1\ 2}$: Constrain suspension motions in required directions

- $FR_{s1\ 2\ 1}$: Constrain suspension motion in x-direction
- $FR_{s1\ 2\ 2}$: Constrain suspension motion in y-direction

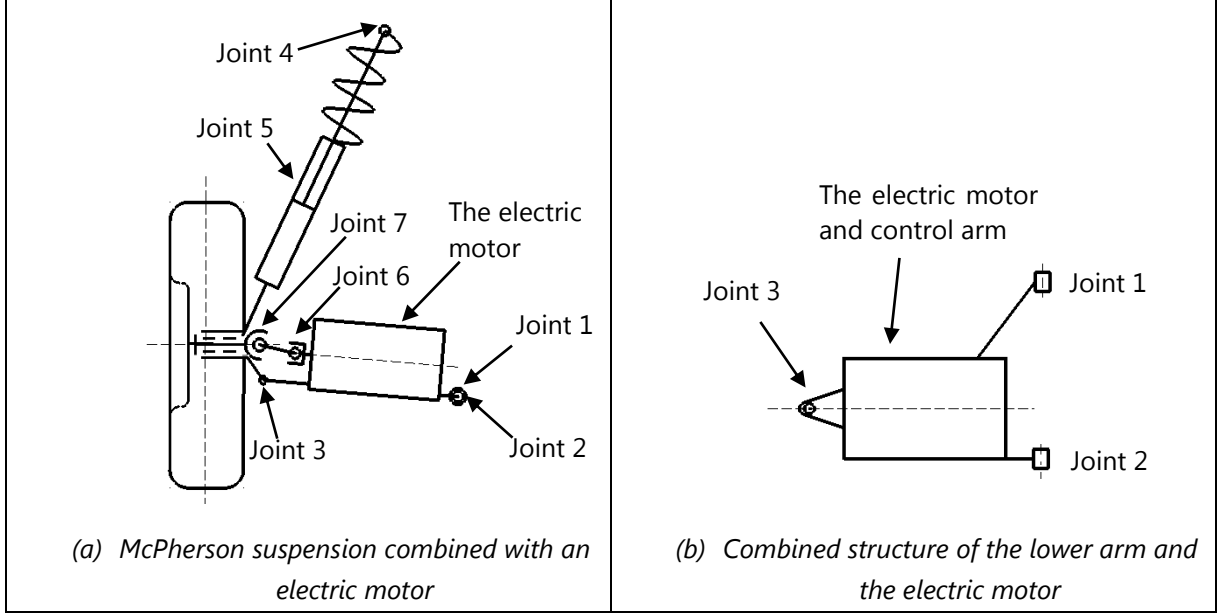
To accommodate these movements, the constant velocity (CV) driveshaft with joint 6 and joint 7 is used in the traditional suspension system to permit the driveshaft to be angled in any direction around the wheel centerline and allow the changes in axial length of the driveshaft. The DM related to motions and joints can be concluded as follows.

	joint 1	joint 2	joint 3	joint 4	joint 5	joint 6	joint 7
$FR_{s1\ 1\ 1}$	0	0	×	×	0	⊗	⊗
$FR_{s1\ 1\ 2}$	×	×	×	0	×	⊗	⊗
$FR_{s1\ 2\ 1}$	×	×	×	⊗	⊗	0	0
$FR_{s1\ 2\ 2}$	×	×	×	⊗	⊗	0	0

The combined structure of the lower arm and the electric motor is shown in the Figure 4.5 (a). In terms of the functions of suspensions, the motor system should not interfere with the kinematics of the suspension and vice versa. The combined electric motor with the output shaft assembly should possess the following DOFs:

- Allow length change in axial direction with suspension motion in z-direction,
- Angle in any direction around the wheel centerline

For $FR_{s1\ 1}$, the revolute joint 1 and joint 2 as well as the spherical joint 3 are kept in the combination in order to meet the basic kinematic requirements of McPherson suspensions (see Figure 4.5 (b)), i.e. steering and suspension travels. However, the compact space between the wheel and the electric motor makes it very hard to deploy the CV joints and the driveshaft. The dimensions of $DP_{m1\ 1}$, $DP_{m2\ 1}$, $DP_{m2\ 2}$, $DP_{m2\ 3}$ and $DP_{ms2\ 1}$ have strong influence on the bushing positions that further influence the $FR_{s1\ 1}$.

Figure 4.5: Concept 1 by combining the McPherson suspension with an electric motor

For $FR_{s1\ 2}$, the joint 1 and joint 2 have the capacity to ensure lateral compliance of suspensions under lateral and longitudinal loads. The loads caused by $DP_{m1\ 1}$, $DP_{m2\ 1}$, $DP_{m2\ 2}$ and $DP_{m2\ 3}$ have strong effect on suspension compliance.

The design equation about $FR_{s1\ 1}$, $FR_{s1\ 2}$ and $FR_{ms2\ 1}$ can be written as equation (4-8):

$$\begin{Bmatrix} FR_{m1\ 1} \\ FR_{m2\ 1} \\ FR_{m2\ 2} \\ FR_{m2\ 3} \\ FR_{s1\ 1} \\ FR_{s1\ 2} \\ FR_{ms2\ 1} \end{Bmatrix} = \begin{bmatrix} \times & 0 & 0 & 0 & 0 & 0 & 0 \\ \times & \times & 0 & 0 & 0 & 0 & 0 \\ 0 & 0 & \times & 0 & 0 & 0 & 0 \\ 0 & 0 & 0 & \times & 0 & 0 & 0 \\ \times & \times & \times & \times & \times & 0 & \times \\ \times & \times & \times & \times & 0 & \times & 0 \\ \times & \times & \times & \times & 0 & \times & \times \end{bmatrix} \begin{Bmatrix} DP_{m1\ 1} \\ DP_{m2\ 1} \\ DP_{m2\ 2} \\ DP_{m2\ 3} \\ DP_{s1\ 1} \\ DP_{s1\ 2} \\ DP_{ms2\ 1} \end{Bmatrix} \quad (4-8)$$

where, $DP_{s1\ 1}$ = DOFs and positions of {bushing 1, bushing 2, bushing 3 and bushing 4}; $DP_{s1\ 2}$ = stiffness of {bushing 1, bushing 2, and bushing 3 and bushing 4}; $DP_{m2\ 1}$ = mechanical property of shaft assembly including joint 6 and joint 7.

For $FR_{s3\ 2}$, design equation about $FR_{s3\ 2}$ is written as equation (4-9). Because the bushing 1 is sensitive for vehicle comfort to the disturbance from lower control arms, $DP_{m1\ 1}$, $DP_{m2\ 1}$, $DP_{m2\ 2}$, and $DP_{m2\ 3}$ has strong influence on vehicle comfort not only in low frequency but also in high frequency region when combined into suspension arms.

$$\begin{Bmatrix} FR_{m1\ 1} \\ FR_{m2\ 1} \\ FR_{m2\ 2} \\ FR_{m2\ 3} \\ FR_{s3\ 2} \end{Bmatrix} = \begin{bmatrix} \times & 0 & 0 & 0 & 0 \\ \times & \times & 0 & 0 & 0 \\ 0 & 0 & \times & 0 & 0 \\ 0 & 0 & 0 & \times & 0 \\ \times & \times & \times & \times & \times \end{bmatrix} \begin{Bmatrix} DP_{m1\ 1} \\ DP_{m2\ 1} \\ DP_{m2\ 2} \\ DP_{m2\ 3} \\ DP_{s3\ 2} \end{Bmatrix} \quad (4-9)$$

For $FR_{s4\ 1}$ and $FR_{s4\ 2}$, design equation (4-10) about $FR_{s4\ 1}$ and $FR_{s4\ 2}$ is written as follows. Because joint 3 is positioning point of a king-pin axis, the disturbance to this point causes influence on keeping driving direction and steering precision. The increased unprung mass and load caused by $DP_{m1\ 1}$, $DP_{m2\ 1}$, $DP_{m2\ 2}$, and $DP_{m2\ 3}$ have strong effect on wheel vertical load i.e. $FR_{s4\ 2}$.

$$\begin{Bmatrix} F_{m1\ 1} \\ FR_{m2\ 1} \\ FR_{m2\ 2} \\ FR_{m2\ 3} \\ FR_{s4\ 1} \\ FR_{s4\ 2} \end{Bmatrix} = \begin{bmatrix} \times & 0 & 0 & 0 & 0 & 0 \\ \times & \times & 0 & 0 & 0 & 0 \\ 0 & 0 & \times & 0 & 0 & 0 \\ 0 & 0 & 0 & \times & 0 & 0 \\ \times & \times & \times & \times & \times & 0 \\ \times & \times & \times & \times & 0 & \times \end{bmatrix} \begin{Bmatrix} DP_{m1\ 1} \\ DP_{m2\ 1} \\ DP_{m2\ 2} \\ DP_{m2\ 3} \\ DP_{s4\ 1} \\ DP_{s4\ 2} \end{Bmatrix} \quad (4-10)$$

Based on equation (4-8), equation (4-9) and equation (4-10), the design equation of concept 1 is developed to the equation (4-11).

$$\begin{Bmatrix} FR_{m1\ 1} \\ FR_{m2\ 1} \\ FR_{m2\ 2} \\ FR_{m2\ 3} \\ FR_{s1\ 1} \\ FR_{s1\ 2} \\ FR_{ms2\ 1} \\ FR_{s2\ 2} \\ FR_{s3\ 1} \\ FR_{s3\ 2} \\ FR_{s4\ 1} \\ FR_{s4\ 2} \\ FR_{s4\ 3} \end{Bmatrix} = \begin{bmatrix} \times & 0 & 0 & 0 & 0 & 0 & 0 & 0 & 0 & 0 & 0 & 0 & 0 \\ \times & \times & 0 & 0 & 0 & 0 & 0 & 0 & 0 & 0 & 0 & 0 & 0 \\ 0 & 0 & \times & 0 & 0 & 0 & 0 & 0 & 0 & 0 & 0 & 0 & 0 \\ 0 & 0 & 0 & \times & 0 & 0 & 0 & 0 & 0 & 0 & 0 & 0 & 0 \\ \times & \times & \times & \times & \times & 0 & \times & 0 & 0 & 0 & 0 & 0 & 0 \\ \times & \times & \times & \times & 0 & \times & 0 & 0 & 0 & 0 & 0 & 0 & 0 \\ \times & \times & \times & \times & 0 & \times & \times & 0 & 0 & 0 & 0 & 0 & 0 \\ \times & \times & \times & \times & \otimes & 0 & \otimes & \times & \times & 0 & 0 & \otimes & \otimes \\ \times & \times & \times & \times & 0 & \times & 0 & 0 & 0 & \times & 0 & 0 & 0 \\ \times & \times & \times & \times & \otimes & 0 & \otimes & \times & \times & 0 & 0 & \times & 0 \\ 0 & 0 & 0 & 0 & 0 & 0 & 0 & \times & \times & 0 & 0 & 0 & \times \end{bmatrix} \begin{Bmatrix} DP_{m1\ 1} \\ DP_{m2\ 1} \\ DP_{m2\ 2} \\ DP_{m2\ 3} \\ DP_{s1\ 1} \\ DP_{s1\ 2} \\ DP_{ms2\ 1} \\ DP_{s2\ 2} \\ DP_{s3\ 1} \\ DP_{s3\ 2} \\ DP_{s4\ 1} \\ DP_{s4\ 2} \\ DP_{s4\ 3} \end{Bmatrix} \quad (4-11)$$

4.3.2 Conception based on double wishbone suspensions

Concept 2: Concept generation with lower wishbones

Double wishbone suspensions with the steering system using for front-wheel-drive cars (shown in Figure 4.6) consist of two wishbone arms, one toe link, one driveshaft and the joints.

Motions of double wishbone suspensions in required directions are the same as McPherson suspensions. The effect of the joints related to suspension motions is concluded in Table 4.3.

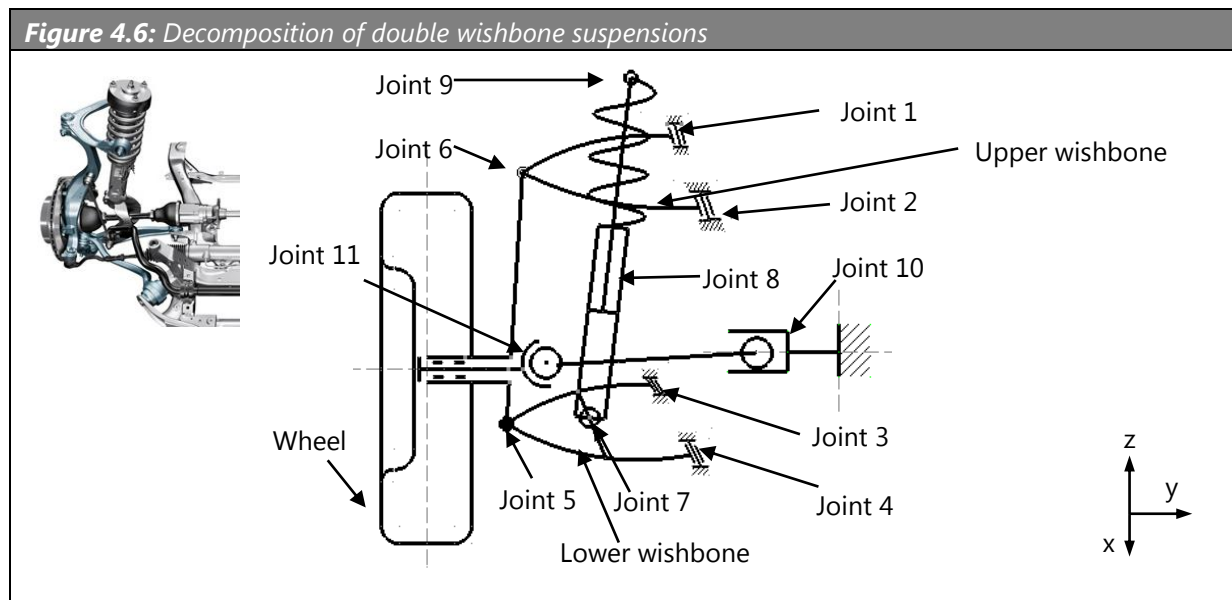


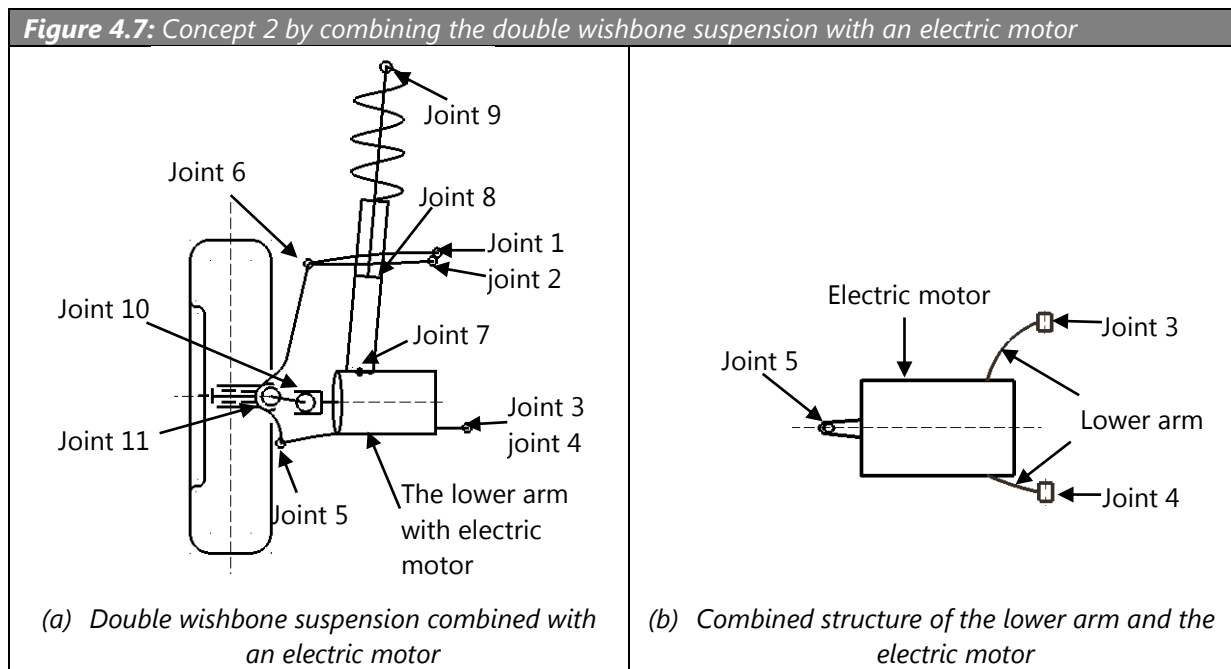
Table 4.3: Effects of joints on required motions of double wishbone suspensions

Joints	J 1	J 2	J 3	J 4	J 5	J 6	J 7	J 8	J 9	J 10	J 11
$FR_{s1\ 1\ 1}$	0	0	0	0	×	×	0	0	0	⊗	⊗
$FR_{s1\ 1\ 2}$	×	×	×	×	×	×	⊗	×	0	⊗	⊗
$FR_{s1\ 2\ 1}$	×	×	×	×	×	×	0	0	0	0	0
$FR_{s1\ 2\ 2}$	×	×	×	×	×	×	0	0	0	0	0

The concept to integrate an electric motor to a double wishbone suspension is designed in the same way as that of the McPherson suspension. The lower wishbone combined with the electric motor is illustrated in Figure 4.7. The drive shaft is shortened in contrast to the traditional one. The motor case is a part of the wishbone, supporting

the reaction force from the wheel. The suspension strut may be set on the motor case, so as to take advantage of the space and further integrate the components. Between the wheel and the electric motor, a pair of CV joints is applied to adapt the movement of the wheel. They also guarantee the rotational speed of the output side constantly the same as that of the input side.

For FR_{s11} , the influence of DP_{m11} , DP_{m21} , DP_{m22} , DP_{m23} and DP_{ms21} on FR_{s11} is the same as the concept 1.



For FR_{s12} , in double wishbone suspensions the design parameter constraining suspension motions is not only bushings of lower control arms but also the bushings of the upper wishbone. Therefore, the influence of DP_{m11} , DP_{m21} , DP_{m22} and DP_{m23} on FR_{s12} in concept 2 is relatively less than that in concept 1. The design equation about FR_{s11} and FR_{s12} is written in equation (4-12).

$$\begin{Bmatrix} FR_{m11} \\ FR_{m21} \\ FR_{m22} \\ FR_{m23} \\ FR_{s11} \\ FR_{s12} \\ FR_{ms21} \end{Bmatrix} = \begin{bmatrix} \times & 0 & 0 & 0 & 0 & 0 & 0 \\ \times & \times & 0 & 0 & 0 & 0 & 0 \\ 0 & 0 & \times & 0 & 0 & 0 & 0 \\ 0 & 0 & 0 & \times & 0 & 0 & 0 \\ \times & \times & \times & \times & \times & 0 & \times \\ \otimes & \otimes & \otimes & \otimes & 0 & \times & 0 \\ \times & \times & \times & \times & 0 & \times & \times \end{bmatrix} \begin{Bmatrix} DP_{m11} \\ DP_{m21} \\ DP_{m22} \\ DP_{m23} \\ DP_{s11} \\ DP_{s12} \\ DP_{ms21} \end{Bmatrix} \quad (4-12)$$

where, $DP_{s1\ 1}$ = DOFs and positions of {bushing 1, bushing 2, bushing 3, bushing 4, bushing 5 and bushing 6}; $DP_{s1\ 2}$ = stiffness of {bushing 1, bushing 2, bushing 3, bushing 4, bushing 5 and bushing 6}; $DP_{m2\ 1}$ = mechanical property of shaft assembly including joint 10 and joint 11.

For $FR_{s3\ 2}$, $FR_{s4\ 1}$ and $FR_{s4\ 2}$, since the principle of this lower control arm combined with electric motors is similar as in concept 1, the influence of $DP_{m1\ 1}$, $DP_{m2\ 1}$, $DP_{m2\ 2}$ and $DP_{m2\ 3}$ on these three FRs is the same as in concept 1.

As discussed above, the design equation of this concept is developed as follows.

$$\begin{pmatrix} F_{m1\ 1} \\ FR_{m2\ 1} \\ FR_{m2\ 2} \\ FR_{m2\ 3} \\ FR_{s1\ 1} \\ FR_{s1\ 2} \\ FR_{ms2\ 1} \\ FR_{s2\ 2} \\ FR_{s3\ 1} \\ FR_{s3\ 2} \\ FR_{s4\ 1} \\ FR_{s4\ 2} \\ FR_{s4\ 3} \end{pmatrix} = \begin{bmatrix} \times & 0 & 0 & 0 & 0 & 0 & 0 & 0 & 0 & 0 & 0 & 0 & 0 \\ \times & \times & 0 & 0 & 0 & 0 & 0 & 0 & 0 & 0 & 0 & 0 & 0 \\ 0 & 0 & \times & 0 & 0 & 0 & 0 & 0 & 0 & 0 & 0 & 0 & 0 \\ 0 & 0 & 0 & \times & 0 & 0 & 0 & 0 & 0 & 0 & 0 & 0 & 0 \\ \times & \times & \times & \times & \times & 0 & \times & 0 & 0 & 0 & 0 & 0 & 0 \\ \otimes & \otimes & \otimes & \otimes & 0 & \times & 0 & 0 & 0 & 0 & 0 & 0 & 0 \\ \times & \times & \times & \times & 0 & \times & \times & 0 & 0 & 0 & 0 & 0 & 0 \\ \times & \times & \times & \times & 0 & \times & \times & \times & 0 & 0 & 0 & 0 & 0 \\ \times & \times & \times & \times & \otimes & 0 & \otimes & \times & \times & 0 & 0 & \otimes & \otimes \\ \times & \times & \times & \times & 0 & \times & 0 & 0 & 0 & \times & 0 & 0 & 0 \\ \times & \times & \times & \times & \times & \times & 0 & 0 & 0 & 0 & \times & 0 & 0 \\ \times & \times & \times & \times & \otimes & 0 & \otimes & \times & \times & 0 & 0 & \times & 0 \\ 0 & 0 & 0 & 0 & 0 & 0 & 0 & \times & \times & 0 & 0 & 0 & \times \end{bmatrix} \begin{pmatrix} DP_{m1\ 1} \\ DP_{m2\ 1} \\ DP_{m2\ 2} \\ DP_{m2\ 3} \\ DP_{s1\ 1} \\ DP_{s1\ 2} \\ DP_{ms2\ 1} \\ DP_{s2\ 2} \\ DP_{s3\ 1} \\ DP_{s3\ 2} \\ DP_{s4\ 1} \\ DP_{s4\ 2} \\ DP_{s4\ 3} \end{pmatrix} \quad (4-13)$$

Concept 3: Concept generation with upper wishbones

Considering the long vertical distance from joint 6 to joint 11, this concept requires a large transmission angle on joint 10 and joint 11. This makes it very difficult for $DP_{m3\ 1}$ and $DP_{m3\ 2}$ of concept 3 to avoid interference under the motion of the suspension. The narrow space of upper control arm limits the feasibility of combining electric motors. Therefore, concept 3 is not feasible in practice.

4.3.3 Conception based on trapezoidal-link suspensions

Concept 4: Concept generation with trapezoidal links

The trapezoidal-link rear suspension used in rear drive axles consists of three arms, one drive shaft, rubber bushings, a spring and a damper separately deployed (see Figure

4.8). The rubber bushings have revolute joint 1, revolute joint 2, revolute joint 3, revolute joint 4, revolute joint 5, revolute joint 6, revolute joint 7, revolute joint 8 and revolute joint 9 according to the specific positions.

The trapezoidal-link suspension for rear-wheel-drive cars possesses no steering function. Motions of trapezoidal-link suspensions in required directions are:

$FR_{s1\ 1}$: Permit suspension motions in required directions

- $FR_{s1\ 1\ 1}$: Permit relative motion to the vehicle body in z-direction

$FR_{s1\ 2}$: Constrain suspension motions in required directions

- $FR_{1\ 2\ 1}$: Constrain suspension motion in x-direction
- $FR_{s1\ 2\ 2}$: Constrain suspension motion in y-direction

The DM for motions of the trapezoidal-link rear suspensions is expressed in the Table 4.4.

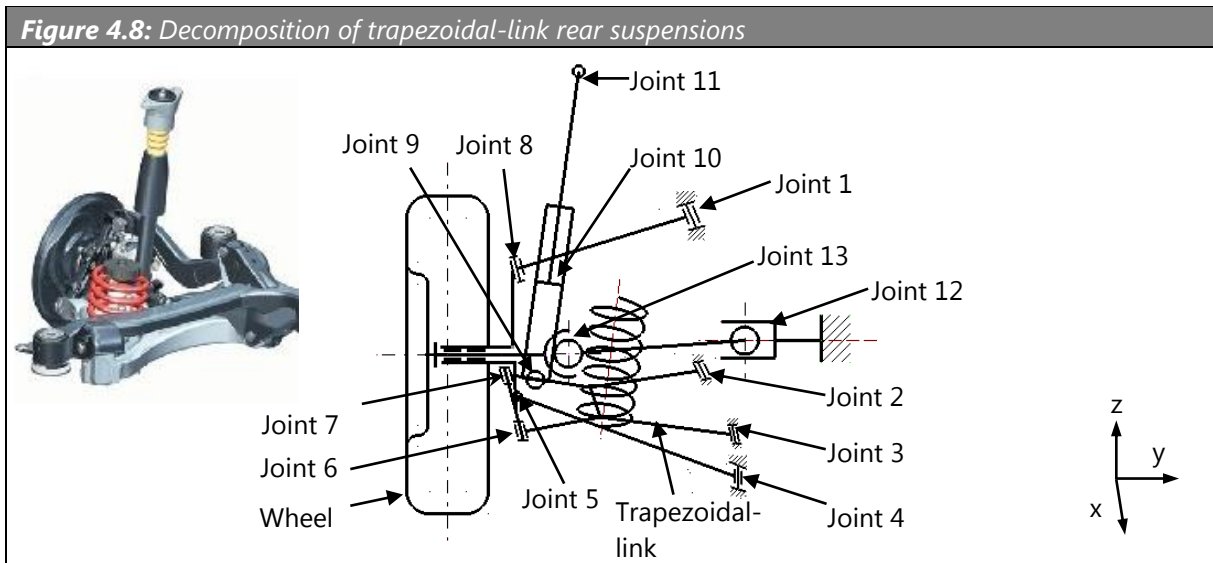


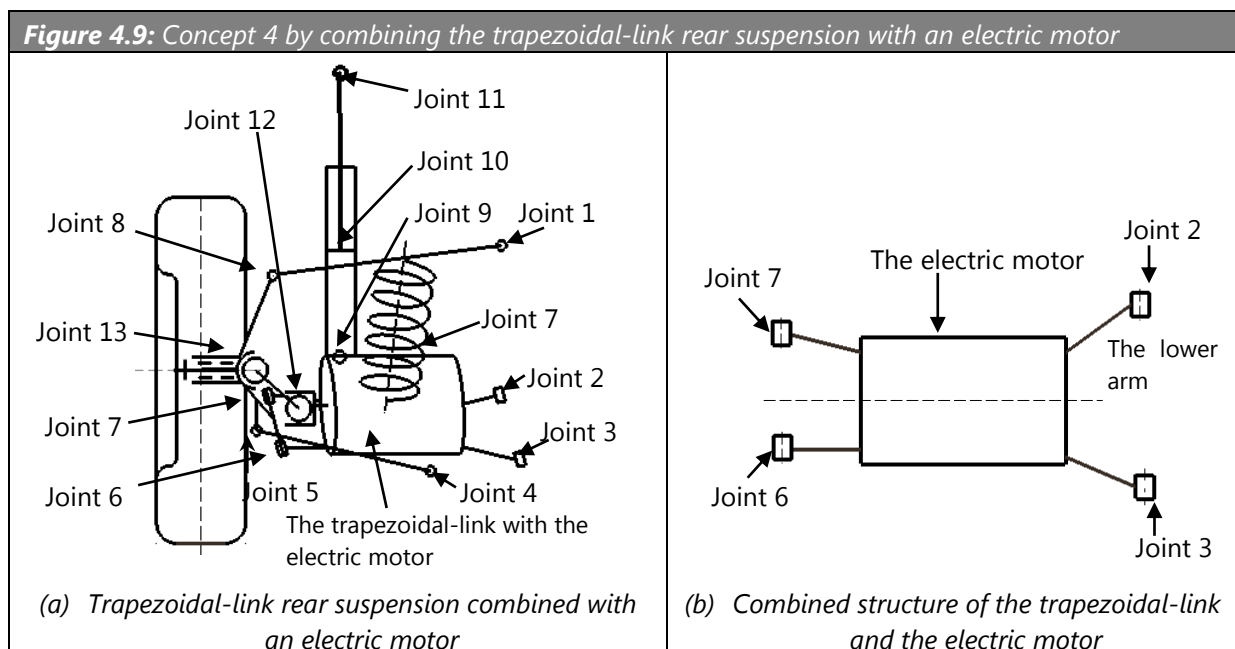
Table 4.4: Effects of joints on required motions of trapezoidal-link rear suspensions

Joints	J 1	J 2	J 3	J 4	J 5	J 6	J 7	J 8	J 9	J 12	J 13
$FR_{s1\ 1\ 1}$	x	x	x	x	x	x	x	x	x	⊗	⊗
$FR_{s1\ 2\ 1}$	x	x	x	x	x	0	x	x	0	0	0
$FR_{s1\ 2\ 2}$	x	x	x	x	x	x	x	x	0	0	0

The new concept is generated based on the trapezoidal-link suspension in the Figure 4.9 (a). In this concept, the trapezoidal link is combined with an electric motor (see Figure 4.9(b)) and the motor case is a part of the trapezoidal link.

For $FR_{s1\ 1}$ and $FR_{s1\ 2}$, a pair of CV joints is required for the basic suspension kinematic. Because of the tight space and complex structure, the combination of electric motors may carry strong influence on bushing position. The trapezoidal link is important to constrain suspension motions in lateral and longitudinal direction, so the reaction force of $DP_{m1\ 1}$, $DP_{m2\ 1}$, $DP_{m2\ 2}$ and $DP_{m2\ 3}$ on the trapezoidal link has a certain influence on $FR_{s1\ 2}$ in concept 4.

The design equation relating to $FR_{s1\ 1}$ and $FR_{s1\ 2}$ is expressed by equation (4-14), in which $DP_{s1\ 1}$ = DOFs and positions of {bushing 1, bushing 2, bushing 3, bushing 4, bushing 5, bushing 6, bushing 7, bushing 8 and bushing 9}; $DP_{s1\ 2}$ = stiffness of {bushing 1, bushing 2, bushing 3, bushing 4, bushing 5, bushing 6, bushing 7, bushing 8 and bushing 9}; $DP_{m2\ 1}$ = mechanical property of shaft assembly incorporating joint 12 and joint 13.



$$\begin{Bmatrix} FR_{m1\ 1} \\ FR_{m2\ 1} \\ FR_{m2\ 2} \\ FR_{m2\ 3} \\ FR_{s1\ 1} \\ FR_{s1\ 2} \\ FR_{ms2\ 1} \end{Bmatrix} = \begin{bmatrix} \times & 0 & 0 & 0 & 0 & 0 & 0 \\ \times & \times & 0 & 0 & 0 & 0 & 0 \\ 0 & 0 & \times & 0 & 0 & 0 & 0 \\ 0 & 0 & 0 & \times & 0 & 0 & 0 \\ \times & \times & \times & \times & \times & 0 & \times \\ \otimes & \otimes & \otimes & \otimes & 0 & \times & 0 \\ \times & \times & \times & \times & 0 & \times & \times \end{bmatrix} \begin{Bmatrix} DP_{m1\ 1} \\ DP_{m2\ 1} \\ DP_{m2\ 2} \\ DP_{m2\ 3} \\ DP_{s1\ 1} \\ DP_{s1\ 2} \\ DP_{ms2\ 1} \end{Bmatrix} \quad (4-14)$$

For $FR_{s3\ 2}$, the noise caused by $DP_{m1\ 1}$, $DP_{m2\ 1}$, $DP_{m2\ 2}$ and $DP_{m2\ 3}$ is transferred to vehicle body through bushing 2 and bushing 3, so the design equation is written as follows.

$$\begin{Bmatrix} FR_{m1\ 1} \\ FR_{m2\ 1} \\ FR_{m2\ 2} \\ FR_{m2\ 3} \\ FR_{s3\ 2} \end{Bmatrix} = \begin{bmatrix} \times & 0 & 0 & 0 & 0 \\ \times & \times & 0 & 0 & 0 \\ 0 & 0 & \times & 0 & 0 \\ 0 & 0 & 0 & \times & 0 \\ \times & \times & \times & \times & \times \end{bmatrix} \begin{Bmatrix} DP_{m1\ 1} \\ DP_{m2\ 1} \\ DP_{m2\ 2} \\ DP_{m2\ 3} \\ DP_{s3\ 2} \end{Bmatrix} \quad (4-15)$$

For $FR_{s4\ 1}$ and $FR_{s4\ 2}$, unlike the front-wheel drive suspension, trapezoidal-link rear suspension has no steering function, so the reaction load acting on the trapezoidal link from electric motors has no strong influence on steering direction. However, bushing stiffness of trapezoidal-links causes a toe-in effect when braking (Glaser & Schweizer, 2007) which has effect on braking direction, so the reaction load has certain of influence on the drive direction when braking. The unsprung mass increase and reaction force from electric motors have strong influence on wheel vertical fluctuation i.e. $FR_{s4\ 2}$. The design equation for these two functions is stated in equation (4-16).

$$\begin{Bmatrix} FR_{m1\ 1} \\ FR_{m2\ 1} \\ FR_{m2\ 2} \\ FR_{m2\ 3} \\ FR_{s4\ 1} \\ FR_{s4\ 2} \end{Bmatrix} = \begin{bmatrix} \times & 0 & 0 & 0 & 0 & 0 \\ \times & \times & 0 & 0 & 0 & 0 \\ 0 & 0 & \times & 0 & 0 & 0 \\ 0 & 0 & 0 & \times & 0 & 0 \\ \otimes & \otimes & \otimes & \otimes & \times & 0 \\ \times & \times & \times & \times & 0 & \times \end{bmatrix} \begin{Bmatrix} DP_{m1\ 1} \\ DP_{m2\ 1} \\ DP_{m2\ 2} \\ DP_{m2\ 3} \\ DP_{s4\ 1} \\ DP_{s4\ 2} \end{Bmatrix} \quad (4-16)$$

As discussed above, the design equation of this concept is written as follows.

$$\begin{Bmatrix} FR_{m1\ 1} \\ FR_{m2\ 1} \\ FR_{m2\ 2} \\ FR_{m2\ 3} \\ FR_{s1\ 1} \\ FR_{s1\ 2} \\ FR_{ms2\ 1} \\ FR_{s2\ 2} \\ FR_{s3\ 1} \\ FR_{s3\ 2} \\ FR_{s4\ 1} \\ FR_{s4\ 2} \\ FR_{s4\ 3} \end{Bmatrix} = \begin{bmatrix} \times & 0 & 0 & 0 & 0 & 0 & 0 & 0 & 0 & 0 & 0 & 0 & 0 \\ \times & \times & 0 & 0 & 0 & 0 & 0 & 0 & 0 & 0 & 0 & 0 & 0 \\ 0 & 0 & \times & 0 & 0 & 0 & 0 & 0 & 0 & 0 & 0 & 0 & 0 \\ 0 & 0 & 0 & \times & 0 & 0 & 0 & 0 & 0 & 0 & 0 & 0 & 0 \\ \times & \times & \times & \times & \times & 0 & \times & 0 & 0 & 0 & 0 & 0 & 0 \\ \otimes & \otimes & \otimes & \otimes & 0 & \times & 0 & 0 & 0 & 0 & 0 & 0 & 0 \\ \times & \times & \times & \times & 0 & \times & \times & 0 & 0 & 0 & 0 & 0 & 0 \\ \times & \times & \times & \times & 0 & \times & \times & \times & 0 & 0 & 0 & 0 & 0 \\ \times & \times & \times & \times & \otimes & 0 & \otimes & \times & \times & 0 & 0 & \otimes & \otimes \\ \times & \times & \times & \times & 0 & \times & 0 & 0 & 0 & \times & 0 & 0 & 0 \\ \otimes & \otimes & \otimes & \otimes & \times & \times & 0 & 0 & 0 & 0 & \times & 0 & 0 \\ \times & \times & \times & \times & \otimes & 0 & \otimes & \times & \times & 0 & 0 & \times & 0 \\ 0 & 0 & 0 & 0 & 0 & 0 & 0 & \times & \times & 0 & 0 & 0 & \times \end{bmatrix} \begin{Bmatrix} DP_{m1\ 1} \\ DP_{m2\ 1} \\ DP_{m2\ 2} \\ DP_{m2\ 3} \\ DP_{s1\ 1} \\ DP_{s1\ 2} \\ DP_{ms2\ 1} \\ DP_{s2\ 2} \\ DP_{s3\ 1} \\ DP_{s3\ 2} \\ DP_{s4\ 1} \\ DP_{s4\ 2} \\ DP_{s4\ 3} \end{Bmatrix} \quad (4-17)$$

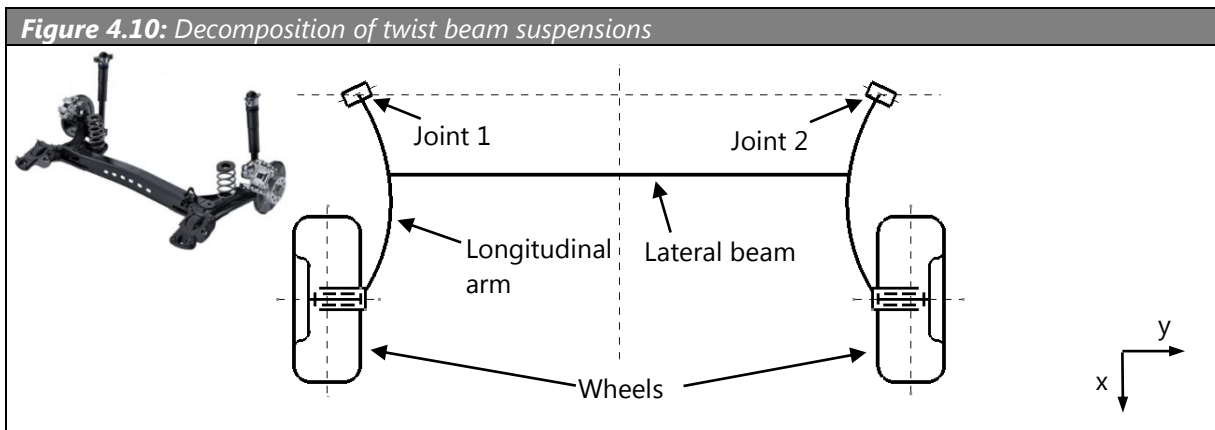
Concept 5: Concept generation with lateral links

If the electric motor is combined with the lateral link, the reaction force of the electric motor in the combined structure is supported by two revolute joints. They are difficult to fix the electric motor. Compared to concept 4, concept 5 is not an available design. Accordingly, it is not further discussed.

4.3.4 **Conception based on twist beam suspensions**

Concept 6: Concept generation with longitudinal arms

As shown in Figure 4.10, the twist beam axle is connected to the vehicle body with two revolute joints, and on the other side the axle is rigidly installed to the wheel hubs through longitudinal arms by bolts.



The twist beam axle works as neither driven axle nor steering axle, and therefore the required DOFs in FR_{s1} that are carried by DP_{s11} and DP_{s12} can be stated in the following way:

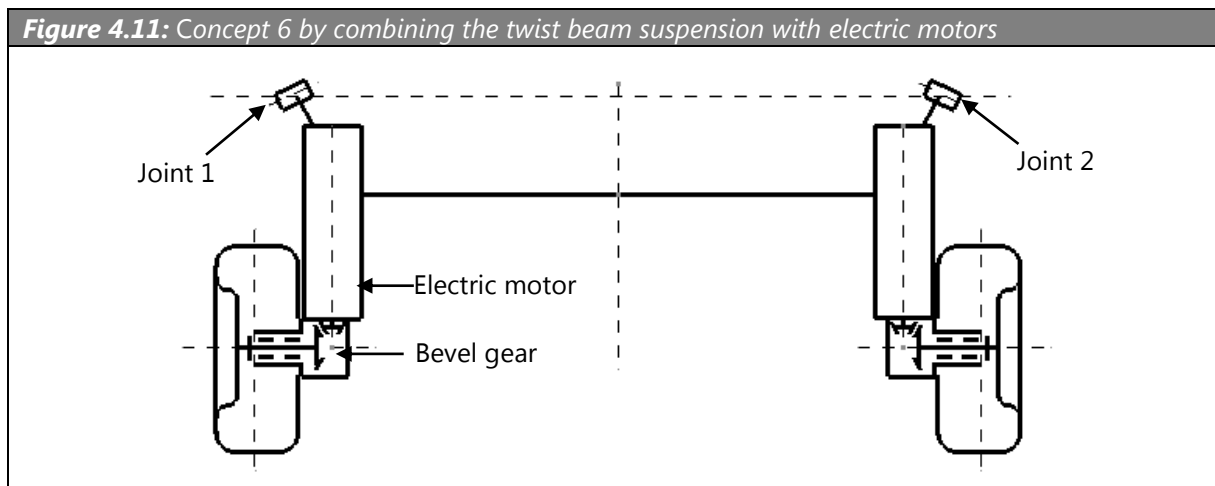
FR_{s11} : Permit suspension motions in required directions

- FR_{s111} : Permit relative motion to the vehicle body in z-direction

FR_{s12} : Constrain suspension motions in required directions

- FR_{s121} : Constrain suspension motion in x-direction
- FR_{s122} : Constrain suspension motion in y-direction

The new concept based on the twist beam axle is illustrated by Figure 4.11, in which the electric motor is combined into the longitudinal arm of the twist beam axle. On the front side of the arm, bushing 1 and bushing 2 are aligned to meet the required DOFs; on the rear side, the combined arm is fixed with the wheel hub rigidly through the gear case. Bevel gears are used in the power transmission from electric motors to wheels. The road load acts on the wheel body, besides through springs and dampers, successively through wheels, wheel hubs, gear case, motor cases and bushings.



For FR_{s11} and FR_{s12} , the DOFs of bushing 1 and bushing 2 are kept and the combination of electric motors and gear set in each side has only a certain influence on the bushing positions because of adequate free space of twist beam suspensions. Because the combined electric motor is partly connected on the center beam partly, the load from DP_{m11} , DP_{m21} , DP_{m22} and DP_{m23} on longitudinal arms has only a

certain influence on bushing stiffness. The design matrix relating to $FR_{s1\ 1}$ and $FR_{s1\ 2}$ is expressed in the equation (4-18).

$$\begin{pmatrix} FR_{m1\ 1} \\ FR_{m2\ 1} \\ FR_{m2\ 2} \\ FR_{m2\ 3} \\ FR_{s1\ 1} \\ FR_{s1\ 2} \\ FR_{ms2\ 1} \end{pmatrix} = \begin{bmatrix} \times & 0 & 0 & 0 & 0 & 0 & 0 \\ \times & \times & 0 & 0 & 0 & 0 & 0 \\ 0 & 0 & \times & 0 & 0 & 0 & 0 \\ 0 & 0 & 0 & \times & 0 & 0 & 0 \\ \otimes & \otimes & \otimes & \otimes & \times & 0 & \otimes \\ \otimes & \otimes & \otimes & \otimes & 0 & \times & 0 \\ \times & \times & \times & \times & 0 & \times & \times \end{bmatrix} \begin{pmatrix} DP_{m1\ 1} \\ DP_{m2\ 1} \\ DP_{m2\ 2} \\ DP_{m2\ 3} \\ DP_{s1\ 1} \\ DP_{s1\ 2} \\ DP_{ms2\ 1} \end{pmatrix} \quad (4-18)$$

For $FR_{s3\ 2}$ the noise caused by $DP_{m1\ 1}$, $DP_{m2\ 1}$, $DP_{m2\ 2}$ and $DP_{m2\ 3}$ is transferred to vehicle body through bushings, springs and dampers, so the design equation is written as follows.

$$\begin{pmatrix} FR_{m1\ 1} \\ FR_{m2\ 1} \\ FR_{m2\ 2} \\ FR_{m2\ 3} \\ FR_{s3\ 2} \end{pmatrix} = \begin{bmatrix} \times & 0 & 0 & 0 & 0 \\ \times & \times & 0 & 0 & 0 \\ 0 & 0 & \times & 0 & 0 \\ 0 & 0 & 0 & \times & 0 \\ \times & \times & \times & \times & \times \end{bmatrix} \begin{pmatrix} DP_{m1\ 1} \\ DP_{m2\ 1} \\ DP_{m2\ 2} \\ DP_{m2\ 3} \\ DP_{s3\ 2} \end{pmatrix} \quad (4-19)$$

For $FR_{s4\ 1}$ and $FR_{s4\ 2}$, the alignment angles of twist beam suspension are fixed. They do not change with axle kinematic motions. The reaction load of $DP_{m1\ 1}$, $DP_{m2\ 1}$, $DP_{m2\ 2}$ and $DP_{m2\ 3}$ may result in small toe angle change in acceleration and braking and it may also cause slight over steering because of axle compliance performance, but these influence is not strong and moreover can be restrained through adjusting axle mechanical property. Like above concept, the unsprung mass increase and reaction force from electric motors have strong influence on wheel vertical fluctuation i.e. $FR_{s4\ 2}$. The design equation for these two FR s is written as equation (4-20).

$$\begin{pmatrix} FR_{m1\ 1} \\ FR_{m2\ 1} \\ FR_{m2\ 2} \\ FR_{m2\ 3} \\ FR_{s4\ 1} \\ FR_{s4\ 2} \end{pmatrix} = \begin{bmatrix} \times & 0 & 0 & 0 & 0 & 0 \\ \times & \times & 0 & 0 & 0 & 0 \\ 0 & 0 & \times & 0 & 0 & 0 \\ 0 & 0 & 0 & \times & 0 & 0 \\ \otimes & \otimes & \otimes & \otimes & \times & 0 \\ \times & \times & \times & \times & 0 & \times \end{bmatrix} \begin{pmatrix} DP_{m1\ 1} \\ DP_{m2\ 1} \\ DP_{m2\ 2} \\ DP_{m2\ 3} \\ DP_{s4\ 1} \\ DP_{s4\ 2} \end{pmatrix} \quad (4-20)$$

To sum up the above discussion about this concept, its design equation is written as follows.

$$\begin{pmatrix} FR_{m1\ 1} \\ FR_{m2\ 1} \\ FR_{m2\ 2} \\ FR_{m2\ 3} \\ \\ FR_{s1\ 1} \\ FR_{s1\ 2} \\ FR_{ms2\ 1} \\ FR_{s2\ 2} \\ FR_{s3\ 1} \\ FR_{s3\ 2} \\ FR_{s4\ 1} \\ FR_{s4\ 2} \\ FR_{s4\ 3} \end{pmatrix} = \begin{bmatrix} \times & 0 & 0 & 0 & 0 & 0 & 0 & 0 & 0 & 0 & 0 & 0 & 0 & 0 \\ \times & \times & 0 & 0 & 0 & 0 & 0 & 0 & 0 & 0 & 0 & 0 & 0 & 0 \\ 0 & 0 & \times & 0 & 0 & 0 & 0 & 0 & 0 & 0 & 0 & 0 & 0 & 0 \\ 0 & 0 & 0 & \times & 0 & 0 & 0 & 0 & 0 & 0 & 0 & 0 & 0 & 0 \\ \\ \otimes & \otimes & \otimes & \otimes & \times & 0 & \otimes & 0 & 0 & 0 & 0 & 0 & 0 & 0 \\ \otimes & \otimes & \otimes & \otimes & 0 & \times & 0 & 0 & 0 & 0 & 0 & 0 & 0 & 0 \\ \times & \times & \times & \times & 0 & \times & \times & 0 & 0 & 0 & 0 & 0 & 0 & 0 \\ \times & \times & \times & \times & 0 & \times & \times & \times & 0 & 0 & 0 & 0 & 0 & 0 \\ \times & \times & \times & \times & \otimes & 0 & \otimes & \times & \times & 0 & 0 & \otimes & \otimes & 0 \\ \times & \times & \times & \times & 0 & \times & 0 & 0 & 0 & \times & 0 & 0 & 0 & 0 \\ \otimes & \otimes & \otimes & \otimes & \times & \times & 0 & 0 & 0 & 0 & \times & 0 & 0 & 0 \\ \times & \times & \times & \times & \otimes & 0 & \otimes & \times & \times & 0 & 0 & \times & 0 & 0 \\ 0 & 0 & 0 & 0 & 0 & 0 & 0 & \times & \times & 0 & 0 & 0 & \times & 0 \end{bmatrix} \begin{pmatrix} DP_{m1\ 1} \\ DP_{m2\ 1} \\ DP_{m2\ 2} \\ DP_{m2\ 3} \\ \\ DP_{s1\ 1} \\ DP_{s1\ 2} \\ DP_{ms2\ 1} \\ DP_{s2\ 2} \\ DP_{s3\ 1} \\ DP_{s3\ 2} \\ DP_{s4\ 1} \\ DP_{s4\ 2} \\ DP_{s4\ 3} \end{pmatrix} \quad (4-21)$$

Concept 7: Concept generation with center beams

The concept combining the electric motor into the center beam of the twist beam axle has to confront more difficulties than concept 6. For the following reasons, the concept 7 is not further considered.

1. The distance between the lateral beam and wheel center is large, so it is hard to set up the transmission device. The gear as transmission of a large diameter is too heavy. The chain as transmission is too unstable to transfer high load.
2. The lateral beam of the twist beam axle must have certain torsion stiffness. The cast motor case has no such material property.

4.3.5 **Conception based on De-Dion suspensions**

Concept 8: Concept generation with De-Dion tubes

De-Dion rear suspensions are featured with the De-Dion tube, which connects the left and right wheels. In order to be compatible with surrounding parts in space, the De Dion tube could be arranged forward or backward depending on the design requirements. This suspension can be used as driven and non-driven axles, e.g. Mercedes B-Class applies the De-Dion axle as non-driven axle. This tube is connected to the vehicle body with a joint in the middle (see Figure 4.12). The lateral force is

supported by the Watt link, Panhard rod (e.g. Mitsubishi i-MiEV) or lateral links (e.g. Smart Fortwo).

The required DOFs of De-Dion suspensions are stated as follows:

FR_{s11} : Permit suspension motions in required directions

- FR_{s111} : Permit relative motion to the vehicle body in z-direction

FR_{s12} : Constrain suspension motions in required directions

- FR_{s121} : Constrain suspension motion in x-direction
- FR_{122} : Constrain suspension motion in y-direction

As the special structure, FR_{s11} is realized by DOFs and positions of bushing 1, bushing 2, bushing 3 and joint 4; FR_{s12} is realized by stiffness of bushing 1, bushing 2 and bushing 3 as well as the watt-link.

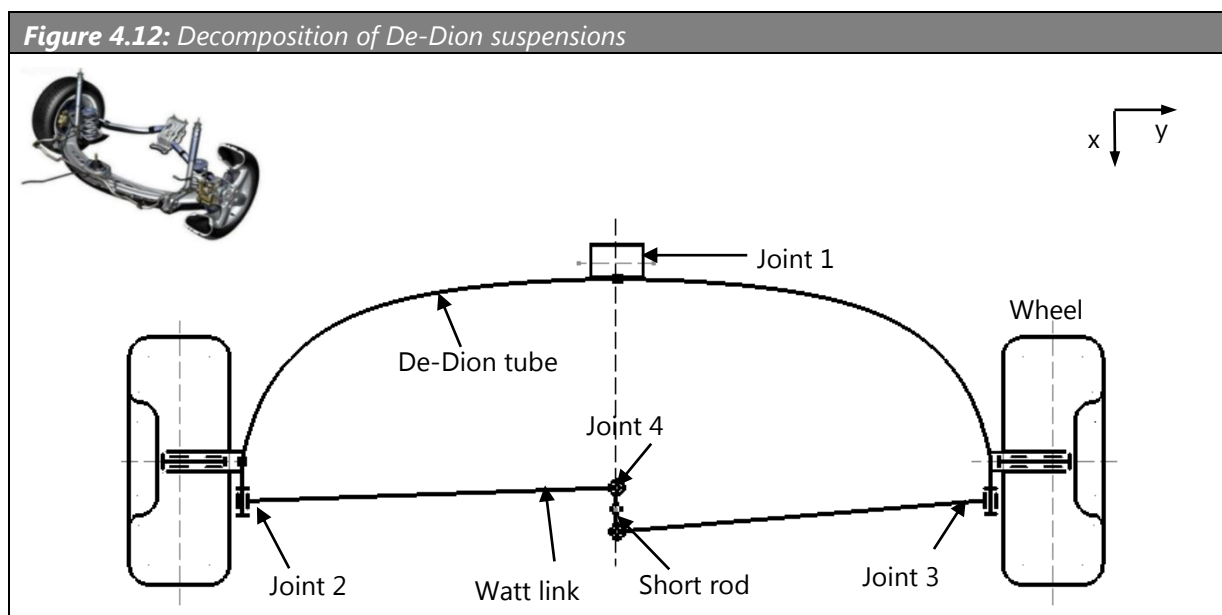
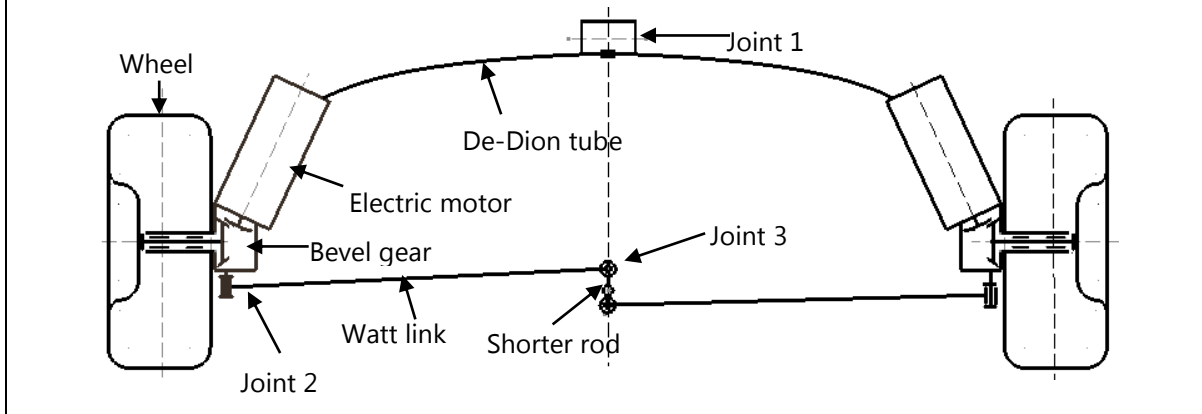


Figure 4.13 illustrates the concept 8, in which the electric motor is integrated into the De-Dion tube. The motor case guides and supports the suspension as a part of the De-Dion tube. The bevel gears are used as the transmission device instead of shafts with CV joints. The watt link is still used to support the lateral force.

Figure 4.13: Concept 8 by combining the De-Dion axle with electric motors



For $FR_{s1\ 1}$ and $FR_{s1\ 2}$, the combination of electric motors brings a certain influence on bushing positions. The De-Dion tube is connected to the vehicle body only through bushing 1, so the reaction force from electric motors have strong influence on $FR_{s1\ 2}$. The design equation is written as equation (4-22).

$$\begin{Bmatrix} FR_{m1\ 1} \\ FR_{m2\ 1} \\ FR_{m2\ 2} \\ FR_{m2\ 3} \\ FR_{s1\ 1} \\ FR_{s1\ 2} \\ FR_{ms2\ 1} \end{Bmatrix} = \begin{bmatrix} \times & 0 & 0 & 0 & 0 & 0 & 0 \\ \times & \times & 0 & 0 & 0 & 0 & 0 \\ 0 & 0 & \times & 0 & 0 & 0 & 0 \\ 0 & 0 & 0 & \times & 0 & 0 & 0 \\ \otimes & \otimes & \otimes & \otimes & \times & 0 & \otimes \\ \otimes & \otimes & \otimes & \otimes & 0 & \times & 0 \\ \times & \times & \times & \times & 0 & \times & \times \end{bmatrix} \begin{Bmatrix} DP_{m1\ 1} \\ DP_{m2\ 1} \\ DP_{m2\ 2} \\ DP_{m2\ 3} \\ DP_{s1\ 1} \\ DP_{s1\ 2} \\ DP_{ms2\ 1} \end{Bmatrix} \quad (4-22)$$

For $FR_{s3\ 2}$, the noise caused by $DP_{m1\ 1}$, $DP_{m2\ 1}$, $DP_{m2\ 2}$ and $DP_{m2\ 3}$ is transferred to vehicle body directly through bushing 1, springs and dampers, so the design equation is written as follows.

$$\begin{Bmatrix} FR_{m1\ 1} \\ FR_{m2\ 1} \\ FR_{m2\ 2} \\ FR_{m2\ 3} \\ FR_{s3\ 2} \end{Bmatrix} = \begin{bmatrix} \times & 0 & 0 & 0 & 0 \\ \times & \times & 0 & 0 & 0 \\ 0 & 0 & \times & 0 & 0 \\ 0 & 0 & 0 & \times & 0 \\ \times & \times & \times & \times & \times \end{bmatrix} \begin{Bmatrix} DP_{m1\ 1} \\ DP_{m2\ 1} \\ DP_{m2\ 2} \\ DP_{m2\ 3} \\ DP_{s3\ 2} \end{Bmatrix} \quad (4-23)$$

For $FR_{s4\ 1}$ and $FR_{s4\ 2}$, the reaction force of $DP_{m1\ 1}$, $DP_{m2\ 1}$, $DP_{m2\ 2}$ and $DP_{m2\ 3}$ can cause the De-Dion axle fluctuation and the reaction force can also lead to more tendency of over-steering. They have strong influence on $FR_{s4\ 1}$. The combination of electric motors causes increase of unsprung mass and vertical load. It has strong influence on $FR_{s4\ 2}$. The design equation for these two FR s is written as follows.

$$\begin{Bmatrix} FR_{m1\ 1} \\ FR_{m2\ 1} \\ FR_{m2\ 2} \\ FR_{m2\ 3} \\ FR_{s4\ 1} \\ FR_{s4\ 2} \end{Bmatrix} = \begin{bmatrix} \times & 0 & 0 & 0 & 0 & 0 \\ \times & \times & 0 & 0 & 0 & 0 \\ 0 & 0 & \times & 0 & 0 & 0 \\ 0 & 0 & 0 & \times & 0 & 0 \\ \times & \times & \times & \times & \times & 0 \\ \times & \times & \times & \times & 0 & \times \end{bmatrix} \begin{Bmatrix} DP_{m1\ 1} \\ DP_{m2\ 1} \\ DP_{m2\ 2} \\ DP_{m2\ 3} \\ DP_{s4\ 1} \\ DP_{s4\ 2} \end{Bmatrix} \quad (4-24)$$

As above discussion on concept 8, this design equation is written as follows.

$$\begin{Bmatrix} FR_{m1\ 1} \\ FR_{m2\ 1} \\ FR_{m2\ 2} \\ FR_{m2\ 3} \\ FR_{s1\ 1} \\ FR_{s1\ 2} \\ FR_{ms2\ 1} \\ FR_{s2\ 2} \\ FR_{s3\ 1} \\ FR_{s3\ 2} \\ FR_{s4\ 1} \\ FR_{s4\ 2} \\ FR_{s4\ 3} \end{Bmatrix} = \begin{bmatrix} \times & 0 & 0 & 0 & 0 & 0 & 0 & 0 & 0 & 0 & 0 & 0 & 0 \\ \times & \times & 0 & 0 & 0 & 0 & 0 & 0 & 0 & 0 & 0 & 0 & 0 \\ 0 & 0 & \times & 0 & 0 & 0 & 0 & 0 & 0 & 0 & 0 & 0 & 0 \\ 0 & 0 & 0 & \times & 0 & 0 & 0 & 0 & 0 & 0 & 0 & 0 & 0 \\ \otimes & \otimes & \otimes & \otimes & \times & 0 & \otimes & 0 & 0 & 0 & 0 & 0 & 0 \\ \times & \times & \times & \times & 0 & \times & 0 & 0 & 0 & 0 & 0 & 0 & 0 \\ \times & \times & \times & \times & 0 & \times & \times & 0 & 0 & 0 & 0 & 0 & 0 \\ \times & \times & \times & \times & \otimes & 0 & \otimes & \times & \times & 0 & 0 & \otimes & \otimes \\ \times & \times & \times & \times & 0 & \times & 0 & 0 & 0 & \times & 0 & 0 & 0 \\ \times & \times & \times & \times & \times & \times & 0 & 0 & 0 & 0 & \times & 0 & 0 \\ \times & \times & \times & \times & \otimes & 0 & \otimes & \times & \times & 0 & 0 & \times & 0 \\ 0 & 0 & 0 & 0 & 0 & 0 & 0 & \times & \times & 0 & 0 & 0 & \times \end{bmatrix} \begin{Bmatrix} DP_{m1\ 1} \\ DP_{m2\ 1} \\ DP_{m2\ 2} \\ DP_{m2\ 3} \\ DP_{s1\ 1} \\ DP_{s1\ 2} \\ DP_{ms2\ 1} \\ DP_{s2\ 2} \\ DP_{s3\ 1} \\ DP_{s3\ 2} \\ DP_{s4\ 1} \\ DP_{s4\ 2} \\ DP_{s4\ 3} \end{Bmatrix} \quad (4-25)$$

Concept 9: Concept generation with watt links

The combination with the watt link has the same problem as concept 5. The long rod of the watt link is fixed at the outer endpoint by joint 2 and at the inner endpoint to the short rod which rotates around its center point. In this structure, joint 2 and joint 3 cannot fix the electric motor stably because of the reaction force to the driving force of the electric motor. The concept 9 is therefore abandoned.

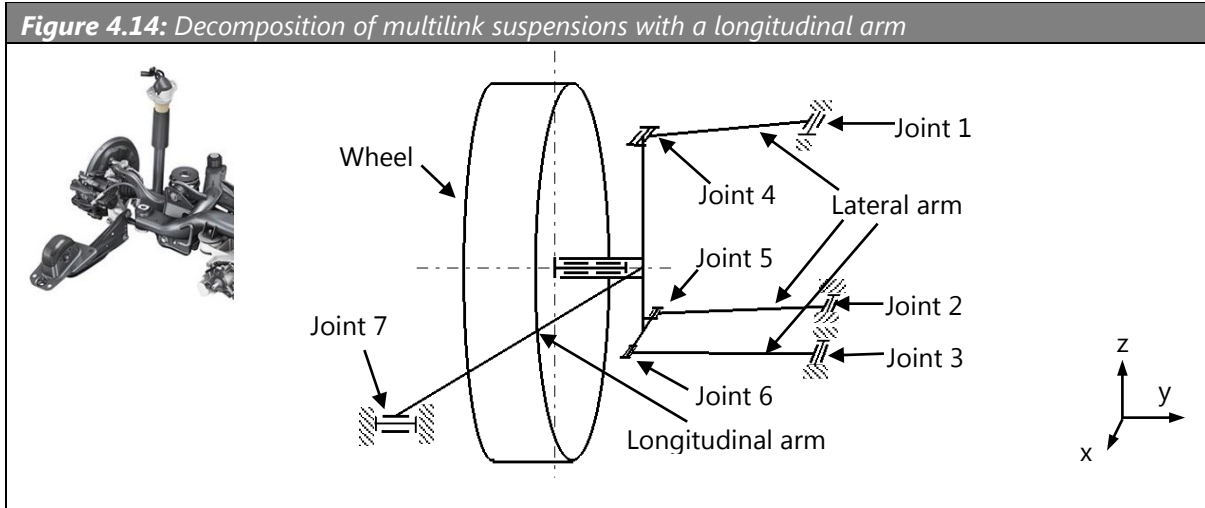
4.3.6 Conception based on multilink suspensions with one longitudinal arm

Concept 10: Concept generation with longitudinal arms

The multilink suspension with a longitudinal arm rigidly attached to the wheel carrier and three lateral arms is a widely used type of suspensions (see Figure 4.14), for example the rear axle of the Ford Focus (Ford Motor Company, 2015) and Mercedes-Benz CLA-Class (Daimler AG, 2013). The longitudinal control arm is typically a blade form. The transverse elastic properties of the blade arm and the mounting bushings

allow it to accommodate change of the wheel track with suspension travels, form a toe-in effect under braking, and lead to understeer tendency when cornering.

This suspension is generally applied as a rear non-driven suspension, and therefore the joints of this suspension need to be compatible with the vertical motion of wheels.



The required DOFs of this kind of suspensions are stated as follows:

$FR_{1\ 1}$: Permit suspension motions in required directions

- $FR_{s1\ 1\ 1}$: Permit relative motion to the vehicle body in z-direction

$FR_{s1\ 2\ 2}$: Constrain suspension motions in required directions

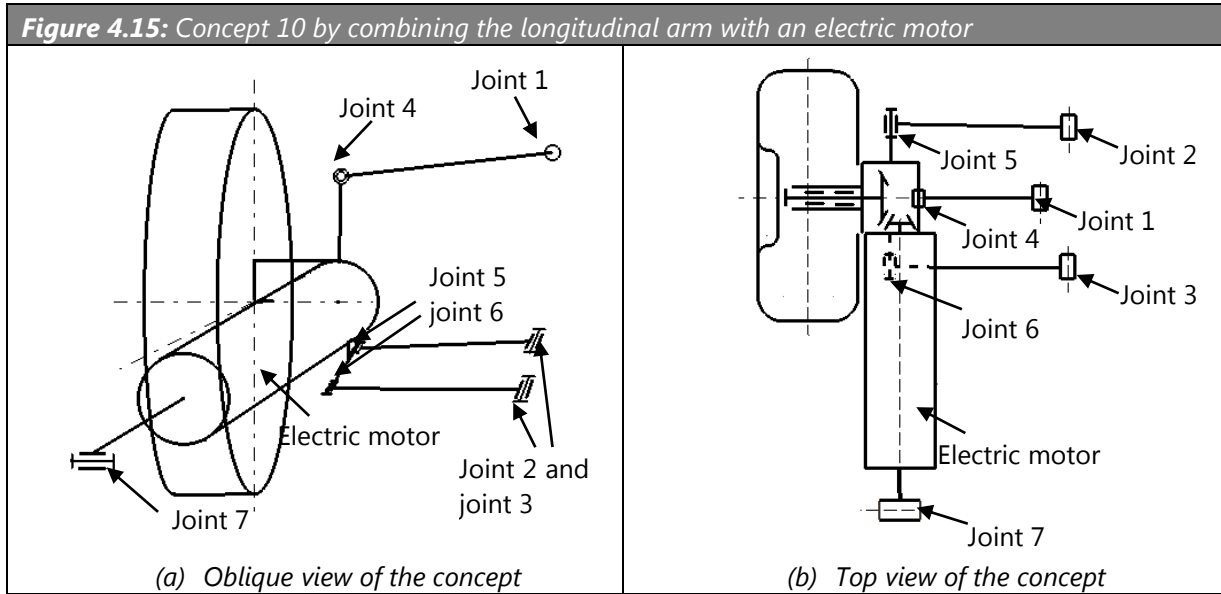
- $FR_{s1\ 2\ 1}$: Constrain suspension motion in x-direction
- $FR_{s1\ 2\ 2}$: Constrain suspension motion in y-direction

The DM for the motions of this kind of suspensions is stated in Table 4.5.

Joints	J1	J2	J3	J4	J5	J6	J7
$FR_{s1\ 1\ 1}$	×	×	×	×	×	×	×
$FR_{s1\ 2\ 1}$	×	×	×	×	×	×	×
$FR_{s1\ 2\ 2}$	×	×	×	×	×	×	0

The concept 10 is illustrated by Figure 4.15, in which the longitudinal arm integrates with the electric motor. The motor case works not only as the longitudinal arm but also as the wheel carrier. The wheel alignment is still determined by the lateral arms,

because the combined trailing beam is transversely rigid. The elasticity of bushing 7 is applied to accommodate changes of the wheel track with the wheel bounce.



For $FR_{s1\ 1}$ and $FR_{s1\ 2}$, as discussed above, the complex mechanical properties of the combined trailing arm may result in strong influence on suspension kinematics and the combined structure geometry must cause a certain change in bushing positions. The reaction force against the driven system may change lateral and transverse load conditions of the whole suspension dramatically, so they have strong influence on bushing stiffness. The design equation is written as equation (4-26).

$$\begin{Bmatrix} FR_{m1\ 1} \\ FR_{m2\ 1} \\ FR_{m2\ 2} \\ FR_{m2\ 3} \\ FR_{s1\ 1} \\ FR_{s1\ 2} \\ FR_{ms2\ 1} \end{Bmatrix} = \begin{bmatrix} \times & 0 & 0 & 0 & 0 & 0 & 0 \\ \times & \times & 0 & 0 & 0 & 0 & 0 \\ 0 & 0 & \times & 0 & 0 & 0 & 0 \\ 0 & 0 & 0 & \times & 0 & 0 & 0 \\ \times & \times & \times & \times & \times & 0 & \times \\ \times & \times & \times & \times & 0 & \times & 0 \\ \times & \times & \times & \times & 0 & \times & \times \end{bmatrix} \begin{Bmatrix} DP_{m1\ 1} \\ DP_{m2\ 1} \\ DP_{m2\ 2} \\ DP_{m2\ 3} \\ DP_{s1\ 1} \\ DP_{s1\ 2} \\ DP_{ms2\ 1} \end{Bmatrix} \quad (4-26)$$

For $FR_{s3\ 2}$, the noise caused by $DP_{m1\ 1}$, $DP_{m2\ 1}$, $DP_{m2\ 2}$ and $DP_{m2\ 3}$ is transferred to vehicle body through bushings, springs and dampers, so the design equation is written as follows.

$$\begin{Bmatrix} FR_{m1\ 1} \\ FR_{m2\ 1} \\ FR_{m2\ 2} \\ FR_{m2\ 3} \\ FR_{s3\ 2} \end{Bmatrix} = \begin{bmatrix} \times & 0 & 0 & 0 & 0 \\ \times & \times & 0 & 0 & 0 \\ 0 & 0 & \times & 0 & 0 \\ 0 & 0 & 0 & \times & 0 \\ \times & \times & \times & \times & \times \end{bmatrix} \begin{Bmatrix} DP_{m1\ 1} \\ DP_{m2\ 1} \\ DP_{m2\ 2} \\ DP_{m2\ 3} \\ DP_{s3\ 2} \end{Bmatrix} \quad (4-27)$$

For $FR_{s4\ 1}$ and $FR_{s4\ 2}$ the rigid trailing arm in this suspension leads toe-out effect under braking and oversteering tendency under cornering, and therefore $DP_{m1\ 1}$, $DP_{m2\ 1}$, $DP_{m2\ 2}$ and $DP_{m2\ 3}$ have a certain influence on driving direction. As above concepts, the increased unsprung mass and reaction force caused by combination have strong influence on vertical dynamics. The design equation is written as equation

$$\begin{Bmatrix} FR_{m1\ 1} \\ FR_{m2\ 1} \\ FR_{m2\ 2} \\ FR_{m2\ 3} \\ FR_{s4\ 1} \\ FR_{s4\ 2} \end{Bmatrix} = \begin{bmatrix} \times & 0 & 0 & 0 & 0 & 0 \\ \times & \times & 0 & 0 & 0 & 0 \\ 0 & 0 & \times & 0 & 0 & 0 \\ 0 & 0 & 0 & \times & 0 & 0 \\ \otimes & \otimes & \otimes & \otimes & \times & 0 \\ \times & \times & \times & \times & 0 & \times \end{bmatrix} \begin{Bmatrix} DP_{m1\ 1} \\ DP_{m2\ 1} \\ DP_{m2\ 2} \\ DP_{m2\ 3} \\ DP_{s1\ 1} \\ DP_{s1\ 2} \end{Bmatrix} \quad (4-28)$$

As above discussion, the design equation of this concept is written as follows.

$$\begin{Bmatrix} F_{m1\ 1} \\ FR_{m2\ 1} \\ FR_{m2\ 2} \\ FR_{m2\ 3} \\ FR_{s1\ 1} \\ FR_{s1\ 2} \\ FR_{ms2\ 1} \\ FR_{s2\ 2} \\ FR_{s3\ 1} \\ FR_{s3\ 2} \\ FR_{s4\ 1} \\ FR_{s4\ 2} \\ FR_{s4\ 3} \end{Bmatrix} = \begin{bmatrix} \times & 0 & 0 & 0 & 0 & 0 & 0 & 0 & 0 & 0 & 0 & 0 & 0 \\ \times & \times & 0 & 0 & 0 & 0 & 0 & 0 & 0 & 0 & 0 & 0 & 0 \\ 0 & 0 & \times & 0 & 0 & 0 & 0 & 0 & 0 & 0 & 0 & 0 & 0 \\ 0 & 0 & 0 & \times & 0 & 0 & 0 & 0 & 0 & 0 & 0 & 0 & 0 \\ \times & \times & \times & \times & \times & 0 & \times & 0 & 0 & 0 & 0 & 0 & 0 \\ \times & \times & \times & \times & 0 & \times & 0 & 0 & 0 & 0 & 0 & 0 & 0 \\ \times & \times & \times & \times & 0 & \times & \times & 0 & 0 & 0 & 0 & 0 & 0 \\ \times & \times & \times & \times & 0 & \times & \times & \times & 0 & 0 & 0 & 0 & 0 \\ \times & \times & \times & \times & \otimes & 0 & \otimes & \times & \times & 0 & 0 & \otimes & \otimes \\ \times & \times & \times & \times & 0 & \times & 0 & 0 & 0 & \times & 0 & 0 & 0 \\ \otimes & \otimes & \otimes & \otimes & \times & \times & 0 & 0 & 0 & 0 & \times & 0 & 0 \\ \times & \times & \times & \times & \otimes & 0 & \otimes & \times & \times & 0 & 0 & \times & 0 \\ 0 & 0 & 0 & 0 & 0 & 0 & 0 & \times & \times & 0 & 0 & 0 & \times \end{bmatrix} \begin{Bmatrix} DP_{m1\ 1} \\ DP_{m2\ 1} \\ DP_{m2\ 2} \\ DP_{m2\ 3} \\ DP_{s1\ 1} \\ DP_{s1\ 2} \\ DP_{ms2\ 1} \\ DP_{s2\ 2} \\ DP_{s3\ 1} \\ DP_{s3\ 2} \\ DP_{s4\ 1} \\ DP_{s4\ 2} \\ DP_{s4\ 3} \end{Bmatrix} \quad (4-29)$$

Concept 11: Concept generation with lateral arms

Compared with concept 10, the lateral arm with combined electric motor alone is difficult to support the reaction force from the electric motor, since each of the lateral beams is connected only by two revolute joints. In contrast, the longitudinal beam in concept 10 is rigidly connected with the wheel carrier which is fixed with the wheel hub

on one side and with three lateral beams on the other side, so the suspension of concept 10 can accommodate the electric motor stably. Accordingly, concept 11 is not taken into account further.

4.4 Comparison and evaluation

The feasibility of all the concepts is concluded in Table 4.6. The concepts with strong feasibility are selected out for further evaluation. The infeasible concepts are abandoned to diminish effort of evaluation.

Reference conventional suspensions	Possible Concepts	Feasibility
McPherson suspension	Concept 1	feasible
Double wishbone suspension	Concept 2	feasible
	Concept 3	not feasible
Trapezoidal-link rear suspension	Concept 4	feasible
	Concept 5	not feasible
Twist beam suspension	Concept 6	feasible
	Concept 7	not feasible
De-Dion rear suspension	Concept 8	feasible
	Concept 9	not feasible
Rear suspension with one longitudinal arm	Concept 10	feasible
	Concept 11	not feasible

Apart from the infeasible concepts there are 6 feasible concepts. The feasibility of the concepts can be studied by comparison of the DMs. In the DM of each concept, the element group P_1 and P_4 (see equation (4-4)) represent the mappings of the FRs and DPs respective inside the electric motor system and suspension system, while P_2 and group P_3 represent cross effect between the two subsystems. Since comparisons of P_1 and P_4 among the concepts essentially refers to the comparison subsystem itself, the comparison of the integration feasibility should be among the cross effect design elements P_2 and P_3 . It is assumed that the external conditions and the combined

electric motors in each concept were the same, in order to improve efficiency furthermore, the comparison focuses on the cross effect in design equations.

Comparing the design equations, the cross effect of $DP_{m1\ 1}$, $DP_{m2\ 1}$, $DP_{m2\ 2}$, $DP_{m2\ 3}$ and $DP_{ms2\ 1}$ on the new suspension concepts is scored in Table 4.7. In scoring, the symbol "⊗" in the *DM* equals to score 1; "×" equals to score 2 and "0" equals to score 0. The scoring field means the sum of cross effect on the corresponding *FRs* of each concept. From Table 4.7, it can be known combination of electric motors in concept 6 brings to minimal influence on the basic suspension functions. Compared to other concepts, concept 6 has more space to arrange electric motors, and the electric motor has no strong influence on required suspension DOFs. The noise from the electric motor and transmission cannot be avoided, however all concepts have this influence inevitably. With respect to drive stability, in concept 6 the reaction force from electric motors has nearly no influence on vehicle steering angle and no essential change of axle basic K&C property. For the suspension vertical dynamics, all the concepts lead to unsprung mass increase, which must be taken into consideration in concept development subsequently.

Table 4.7: Integration feasibility comparison - Cross effects of $DP_{m1\ 1}$, $DP_{m2\ 1}$, $DP_{m2\ 2}$, $DP_{m2\ 3}$ and $DP_{ms2\ 1}$ on new suspension concepts

	Concept 1	Concept 2	Concept 4	Concept 6	Concept 8	Concept 10
$FR_{s1\ 1}$	10	10	10	5	5	10
$FR_{s1\ 2}$	8	4	4	4	8	8
$FR_{s3\ 2}$	8	8	8	8	8	8
$FR_{s4\ 1}$	8	8	4	4	8	4
$FR_{s4\ 2}$	9	9	9	9	9	9
Total cross effect	43	39	35	30	38	39

To comprehensively evaluate suspension concepts for the target vehicle, not only functional feasibility but also other essential aspects should be taken into account, for example: cost, lightweight degree, development difficulty and so on, which are intensively involved in project and product assessment. Since in this phase the

characteristics of the concepts in these aspects are unable to be exactly investigated. Objective criteria of these aspects are inappropriate to specify in detailed value range before the characteristics can be investigated. The involved criteria are collected and normalized in a team of professional suspension and lightweight design (see Figure 4.16). Weighting factors are used to represent different importance of the evaluation criteria. Pair comparison way is applied to distinguish relative weighting of criteria. In comparison, "2" means the criterion on the row is more important than the one on the column; "1" represents the pair have equivalent weighting; and "0" means the criterion on the row has less important than the one on the column. In the rightmost column of the table, nominal weighting factors of each evaluation criterion are calculated.

Each of these concepts is scored by scales in five levels from "1" to "5" under every evaluation criterion, respectively:

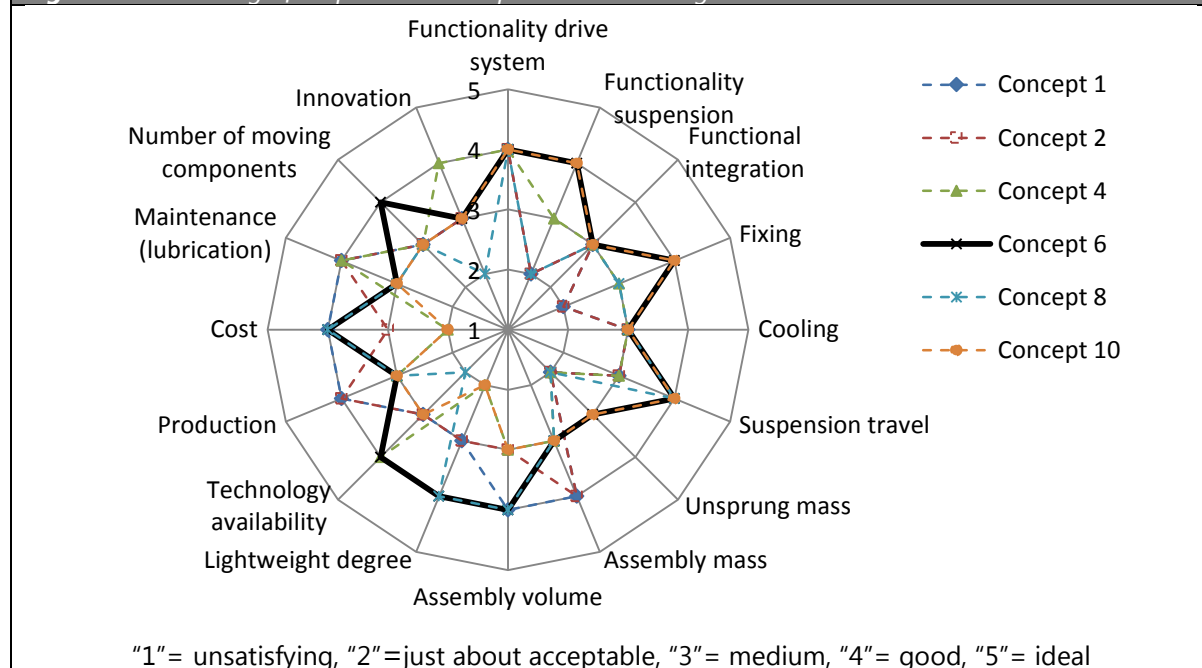
- "1"= unsatisfying: the concept performs worse than an acceptable level, and it would have significant shortcomings in this aspect;
- "2"= just about acceptable: slightly negative, this concept performs worse than average level but can still be accepted in the design;
- "3"= medium: the concept has neither distinct negative nor distinct positive properties that would be a average level in this aspect;
- "4"= good: the concept properties would have significant advantage in this aspect but still have space to be further improved;
- "5"= ideal: the concept properties would have perfect performance in this aspect and there is no necessity of further improvement.

Ratings based on criteria were conducted by team discussions and results of concepts are illustrated in the radar chart of Figure 4.17. From this chart it is shown that the concept 6 has no major disadvantage. It possesses full functionalities of drive system and suspension system. In comparison to other concepts, concept 6 has high lightweight degree and small assembly volume, which are suitable for a lightweight electric vehicle.

Figure 4.16: Nominal weighting factor of design criteria

	Functionality drive system	Functionality suspension	Fixing	Cooling	Suspension travel	Unsprung mass	Assembly mass	Assembly volume	Lightweight degree	Functional integration	Technology availability	Production	Cost	Maintenance (lubrication)	Number of moving components	Innovation	Sum	Nominal Weighting factor
Functionality drive system		1	2	2	2	2	1	2	1	1	1	2	2	2	2	1	24	0,100
Functionality suspension	1		2	2	2	2	1	2	1	1	1	2	2	2	2	1	24	0,100
Fixing	0	0		0	1	0	0	1	0	0	0	1	1	1	1	0	6	0,025
Cooling	0	0	1		2	1	0	2	0	0	0	2	2	2	2	0	14	0,059
Suspension travel	0	0	1	0		0	0	1	0	0	0	1	0	1	2	0	6	0,025
Unsprung mass	0	0	2	1	2		0	1	0	1	0	2	2	2	2	0	15	0,063
Assembly mass	1	1	2	2	2	2		2	0	1	0	2	2	2	2	1	22	0,092
Assembly volume	0	0	1	0	1	1	0		0	0	0	2	1	2	2	0	10	0,042
Lightweight degree	1	1	2	2	2	2	2	2		2	0	2	2	2	2	2	26	0,109
Functional integration	1	1	2	2	2	1	1	2	0		0	0	0	0	0	1	13	0,054
Technology availability	1	1	2	2	2	2	2	2	2	2		2	2	2	2	2	28	0,117
Production	0	0	1	0	1	0	0	0	0	2	0		0	1	2	0	7	0,029
Cost	0	0	1	0	2	0	0	1	0	2	0	2		2	2	0	12	0,050
Maintenance (lubrication)	0	0	1	0	1	0	0	0	0	2	0	1	0		2	0	7	0,029
Number of moving components	0	0	1	0	0	0	0	0	0	2	0	0	0			0	3	0,013
Innovation	1	1	2	2	2	2	1	2	0	1	0	2	2	2	2		22	0,092
																	239	1

Figure 4.17: Scoring of suspension concepts based on design criteria



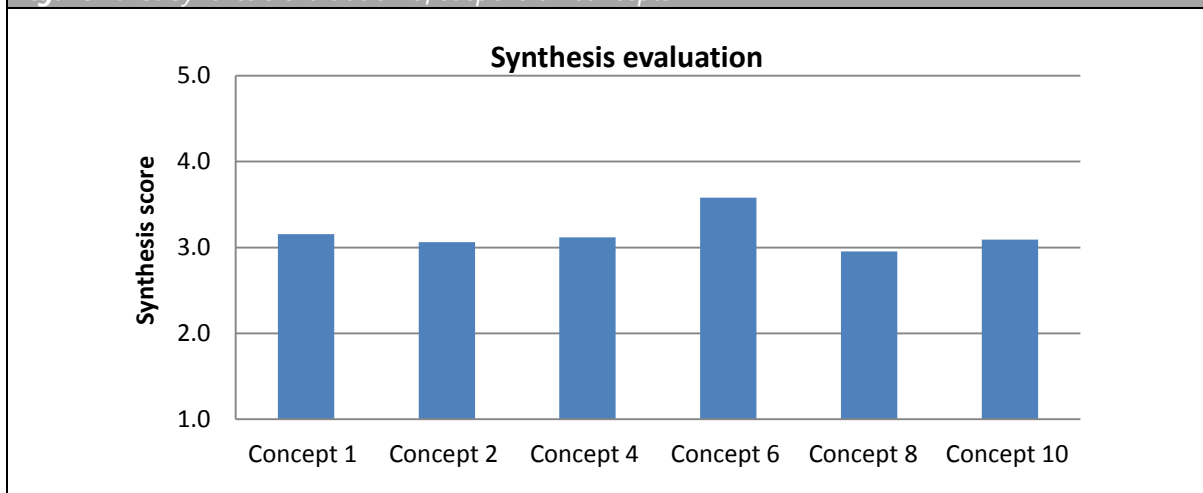
However, each concept has also distinguishing features derived from their adopted suspension configurations, these concepts are evaluated in synthesis perspectives by the following formula.

$$\text{Synthesis score}_j = \sum_i \text{score}_{ij} \cdot \text{nominal weighting factor}_{ij} \quad (4-30)$$

where, j is the design concept and i is the design criterion of each concept. On the basis of the scoring of design concepts on each criterion in Figure 4.17 and the nominal weighting factors in Figure 4.16, synthesis evaluation are depicted in Figure 4.18. The synthesis evaluation result shows that concept 6 is suitable for the further development considering the multiple aspects listed in Figure 4.16.

As a result of above integration feasibility and evaluation, concept 6 is chosen as the initial concept for further development. It needs to declare that a drive device combining the electric motors with the suspension longitudinal arm was patented by the company ZF (see reference (Mair, et al., 2014)); the innovative point of the thesis is the systematic methodology for the conceptual design and development more than the concept of this drive device.

Figure 4.18: Synthesis evaluation of suspension concepts



4.5 Design sequence on the basis of DM

To specify the mapping between *FRs* and *DPs*, the design equation (4-21) of concept 6 (see Figure 4.11) is further developed into the equation (4-31). In each row of the DM corresponding to the specified FR, the adjustable elements are denoted with the checkmark "√". The nonadjustable design parameters in a specified row are treated as the necessary conditions for the corresponding function.

$$\begin{pmatrix} FR_{m1\ 1} \\ FR_{m2\ 1} \\ FR_{m2\ 2} \\ FR_{m2\ 3} \\ FR_{s1\ 1} \\ FR_{s1\ 2} \\ FR_{ms2\ 1} \\ FR_{s2\ 2} \\ FR_{s3\ 1} \\ FR_{s3\ 2} \\ FR_{s4\ 1} \\ FR_{s4\ 2} \\ FR_{s4\ 3} \end{pmatrix} = \begin{bmatrix} \times^{\sqrt{}} & 0 & 0 & 0 & 0 & 0 & 0 & 0 & 0 & 0 & 0 & 0 & 0 \\ \times & \times^{\sqrt{}} & 0 & 0 & 0 & 0 & 0 & 0 & 0 & 0 & 0 & 0 & 0 \\ 0 & 0 & \times^{\sqrt{}} & 0 & 0 & 0 & 0 & 0 & 0 & 0 & 0 & 0 & 0 \\ 0 & 0 & 0 & \times^{\sqrt{}} & 0 & 0 & 0 & 0 & 0 & 0 & 0 & 0 & 0 \\ \otimes & \otimes & \otimes & \otimes & \times^{\sqrt{}} & 0 & \otimes & 0 & 0 & 0 & 0 & 0 & 0 \\ \otimes & \otimes & \otimes & \otimes & 0 & \times^{\sqrt{}} & 0 & 0 & 0 & 0 & 0 & 0 & 0 \\ \times & \times & \times & \times & 0 & \times & \times^{\sqrt{}} & 0 & 0 & 0 & 0 & 0 & 0 \\ \times & \times & \times & \times & 0 & \times & \times & \times^{\sqrt{}} & 0 & 0 & 0 & 0 & 0 \\ \times & \times & \times & \times & \otimes & 0 & \otimes & \times^{\sqrt{}} & \times^{\sqrt{}} & 0 & 0 & \otimes & \otimes \\ \times & \times & \times & \times & 0 & \times^{\sqrt{}} & 0 & 0 & 0 & \times^{\sqrt{}} & 0 & 0 & 0 \\ \otimes & \otimes & \otimes & \otimes & \times^{\sqrt{}} & \times^{\sqrt{}} & 0 & 0 & 0 & 0 & \times^{\sqrt{}} & 0 & 0 \\ \times & \times & \times & \times & \otimes & 0 & \times & \times^{\sqrt{}} & \times^{\sqrt{}} & 0 & 0 & \times^{\sqrt{}} & 0 \\ 0 & 0 & 0 & 0 & 0 & 0 & 0 & \times & \times & 0 & 0 & 0 & \times^{\sqrt{}} \end{bmatrix} \begin{pmatrix} DP_{m1\ 1} \\ DP_{m2\ 1} \\ DP_{m2\ 2} \\ DP_{m2\ 3} \\ DP_{s1\ 1} \\ DP_{s1\ 2} \\ DP_{ms2\ 1} \\ DP_{s2\ 2} \\ DP_{s3\ 1} \\ DP_{s3\ 2} \\ DP_{s4\ 1} \\ DP_{s4\ 2} \\ DP_{s4\ 3} \end{pmatrix} \quad (4-31)$$

The matrix equation is rearranged so as to coordinate the relevant design parameters. The elements representing the adjustable parameters are arranged along the diagonal of the DM (see equation (4-32)) to form design groups. The groups are lower triangular matrices. The definition of the design sequence is in the way of top-down and left-right referring to the distribution of the groups in the DM.

The design sequence is defined as Group 1 → Group 2 → Group 3 → Group 4 along the diagonal of DM of equation (4-32). The elements indicated by symbol "√" in the DM mean these *DPs* are adjustable for the *FRs*.

Group 1: This group is investigated at first; since the characteristics of the $DP_{m1\ 1}$, $FR_{m2\ 1}$, $FR_{m2\ 2}$ and $FR_{m2\ 3}$ have strong influence on the suspension performance, they should be determined before design of the suspension parameters. In this group, the $DP_{m1\ 1}$ must firstly be determined according to the $FR_{m1\ 1}$; then the $FR_{m2\ 1}$, $FR_{m2\ 2}$ and $FR_{m2\ 3}$ are designed according to the transmission requirements under condition of $FR_{m1\ 1}$. The designs of the motor and transmission device are not the main content in this thesis. The key parameters $DP_{m1\ 1}$, $DP_{m2\ 1}$, $DP_{m2\ 2}$ and $DP_{m2\ 3}$ are generally calculated depending on the requirements of the target vehicle.

$$\begin{pmatrix} FR_{m1\ 1} \\ FR_{m2\ 1} \\ FR_{m2\ 2} \\ FR_{m2\ 3} \\ FR_{s1\ 1} \\ FR_{s1\ 2} \\ FR_{s3\ 2} \\ FR_{s4\ 1} \\ FR_{ms2\ 1} \\ FR_{s2\ 2} \\ FR_{s3\ 1} \\ FR_{s4\ 3} \\ FR_{s4\ 2} \end{pmatrix} = \begin{pmatrix} \times^{\sqrt{}} & 0 & 0 & 0 \\ \times & \times^{\sqrt{}} & 0 & 0 \\ 0 & 0 & \times^{\sqrt{}} & 0 \\ 0 & 0 & 0 & \times^{\sqrt{}} \\ \otimes & \otimes & \otimes & \otimes \\ \otimes & \otimes & \otimes & \otimes \\ \times & \times & \times & \times \\ \otimes & \otimes & \otimes & \otimes \\ \times & \times & \times & \times \\ \times & \times & \times & \times \\ \times & \times & \times & \times \\ 0 & 0 & 0 & 0 \\ \times & \times & \times & \times \end{pmatrix} \begin{pmatrix} 0 & 0 & 0 & 0 & 0 & 0 & 0 & 0 & 0 \\ 0 & 0 & 0 & 0 & 0 & 0 & 0 & 0 & 0 \\ 0 & 0 & 0 & 0 & 0 & 0 & 0 & 0 & 0 \\ 0 & 0 & 0 & 0 & 0 & 0 & 0 & 0 & 0 \\ \times^{\sqrt{}} & 0 & \otimes & 0 & 0 & 0 & 0 & 0 & 0 \\ 0 & \times^{\sqrt{}} & 0 & 0 & 0 & 0 & 0 & 0 & 0 \\ 0 & \times^{\sqrt{}} & \times^{\sqrt{}} & 0 & 0 & 0 & 0 & 0 & 0 \\ \times^{\sqrt{}} & \times^{\sqrt{}} & 0 & \times^{\sqrt{}} & 0 & 0 & 0 & 0 & 0 \\ 0 & \times & 0 & 0 & \times^{\sqrt{}} & 0 & 0 & 0 & 0 \\ 0 & \times & 0 & 0 & \times & \times^{\sqrt{}} & 0 & 0 & 0 \\ \otimes & 0 & 0 & 0 & \otimes & \times^{\sqrt{}} & \times^{\sqrt{}} & \otimes & \otimes \\ 0 & 0 & 0 & 0 & 0 & \times & \times & \times^{\sqrt{}} & 0 \\ \otimes & 0 & 0 & 0 & \times & \times^{\sqrt{}} & \times^{\sqrt{}} & 0 & \times^{\sqrt{}} \end{pmatrix} \begin{pmatrix} DP_{m1\ 1} \\ DP_{m2\ 1} \\ DP_{m2\ 2} \\ DP_{m2\ 3} \\ DP_{s1\ 1} \\ DP_{s1\ 2} \\ DP_{s3\ 2} \\ DP_{s4\ 1} \\ DP_{ms2\ 1} \\ DP_{s2\ 2} \\ DP_{s3\ 1} \\ DP_{s4\ 3} \\ DP_{s4\ 2} \end{pmatrix} \quad (4-32)$$

Group 1
Group 2
Group 3
Group 4

Group 2: In this group, the bushing DOFs and positions $DP_{s1\ 1}$, bushing stiffness $DP_{s1\ 2}$, bushing damping $DP_{s3\ 2}$ and wheel alignments $DP_{s4\ 1}$ should be designed. Among these parameters, $DP_{s1\ 1}$ are the most basic element which should be defined at first. The definition should consider dimension of the combined electric motor. The $DP_{s1\ 1}$ with $DP_{s1\ 2}$ determine the change of the $DP_{s4\ 1}$ under driving loads, which strongly relates to the K&C characteristics of the suspension. The $FR_{s3\ 2}$ primarily depends on $DP_{s1\ 2}$ and $DP_{s3\ 2}$. Therefore $DP_{s3\ 2}$ should also be defined in this group. In this thesis, the concept suspension uses the same bushing parameters of the reference suspension.

Group 3: When key parameters of the drive unit and hardpoints are defined, the suspension structure can be designed under the load conditions. In this dissertation, a topological design approach for suspension structure considering K&C performance is developed. Through this approach the DPs of group 2 and group 3 are taken into account simultaneously, which is demonstrated in chapter 7.

Group 4: $FR_{s2\ 2}$, $FR_{s3\ 1}$, $FR_{s4\ 3}$ and $FR_{s4\ 2}$ can be treated as suspension vertical dynamics. The DPs of this group are intensively related to suspension vertical dynamics. Besides, it can be known that $DP_{m1\ 1}$, $DP_{m2\ 1}$, $DP_{m2\ 2}$, $DP_{m2\ 3}$, $DP_{s1\ 1}$, $DP_{s1\ 2}$ and $DP_{ms2\ 1}$ are also involved in the design of these parameters. $DP_{s4\ 3}$ is usually applied to intensify the roll stiffness of the vehicle and it is tuned, subsequent to the design of $DP_{s2\ 2}$ and

$DP_{s3\ 1}$. Besides the influence on $FR_{s4\ 2}$ and $DP_{s4\ 3}$, the $DP_{s4\ 2}$ and $DP_{s4\ 3}$ also affect the design of $FR_{s3\ 1}$ and consequently they should be defined with comprehensive consideration of their effect on $FR_{s3\ 1}$, $FR_{s4\ 2}$ and $FR_{s4\ 3}$. Regarding above mentioned reasons, the $FR_{s2\ 2}$, $FR_{s3\ 1}$, $FR_{s4\ 3}$ and $FR_{s4\ 2}$ in group 4 are designed by a mathematical method which is interpreted in chapter 8.

5 Power and torque requirement of the powertrain

The parameters of the powertrain in the group 1 of equation (4-32) are calculated in this chapter. Since the development of the electric motor is not the research focus of this thesis, this calculation is only to define the power and torque requirements of the electric motor. A CATIA model of the powertrain is built to provide basic geometric and mechanical parameters of the powertrain for subsequent development of the concept suspension. The performance requirements of the target vehicle on top speed and acceleration are determined by the characteristics of the powertrain. The wheel power and torque requirements are calculated at first.

Drive resistance

When a vehicle drives on the road, the wheel driving force of the vehicle $F_{Req,wheel}$ is equal to the running resistance F_T , which consists of rolling resistance F_R , aerodynamic resistance F_A , gradient resistance F_G and acceleration resistance F_I . This force balance can be expressed by equation (5-1) (Braess & Seiffert, 2013).

$$F_{Req,wheel} = F_T = F_R + F_A + F_G + F_I \quad (5-1)$$

Assuming that the vehicle drives on a dry road surface along straight line, the rolling resistance F_R can be expressed as follows:

$$F_R = m_v \cdot g \cdot f_R \quad (5-2)$$

where, f_R is the coefficient of rolling resistance which can be numerically approximated as polynomial related to the vehicle speed v :

$$f_R = f_{R0} + f_{R1} \left(\frac{v}{100 \text{ km/h}} \right) + f_{R4} \left(\frac{v}{100 \text{ km/h}} \right)^4 \quad (5-3)$$

referencing to the experimental data recorded in the literature (Mitschke & Wallentowitz, 2004), $f_{R0} = 0.008$, $f_{R1} = 0.0013$, and $f_{R4} = 0.0003$.

The aerodynamic resistance causes significant resistance on the body especially when high speed driving. It can be estimated by equation (5-4).

$$F_A = \frac{1}{2} \cdot \rho_A \cdot A \cdot c_w \cdot v^2 \quad (5-4)$$

where c_w is the drag coefficient, A is a projected frontal area of the vehicle, and ρ_A is air density which is $\rho_A = 1.225 \text{ kg/m}^3$ under standard atmospheric pressure and room temperature. In this thesis, a commonly used value for the parameter c_w is selected: $c_w = 0.3$ (Braess & Seiffert, 2013); frontal area of the target vehicle is set as $A = 2 \text{ m}^2$.

The gradient resistance F_G is given by the following equation:

$$F_G = m_v \cdot g \cdot \sin \beta \quad (5-5)$$

where, β is the road grade angle.

Acceleration resistance is also called inertial resistance which consists of two different parts: the angular inertia of the rotating parts of the powertrain and the linear inertia of the running vehicle.

$$F_I = m_v \cdot \lambda \cdot a \quad (5-6)$$

where, a is vehicle acceleration and λ is mass factor which compensates for the apparent increase in vehicle mass due to the rotating mass. The value of mass factor λ is usually set as 1.1 according to reference (Husain, 2010).

Top speed

To calculate the power required for the maximum speed 150 km/h, the target vehicle is assumed to drive on level ground, i.e., the grade angle β is 0. The driving force on the vehicle in this case is equivalent to the drag force and acceleration a of the vehicle is 0. The equation (5-1) can be written as follows.

$$F_{Req,wheel} = F_T = m_v \cdot g \cdot f_R + \frac{1}{2} \cdot \rho_A \cdot A \cdot c_w \cdot v_{max}^2 \quad (5-7)$$

The force $F_{Req,wheel}$ required for the top vehicle speed can be solved by this equation. Then the corresponding required power is equal to the product of the required force and the top speed.

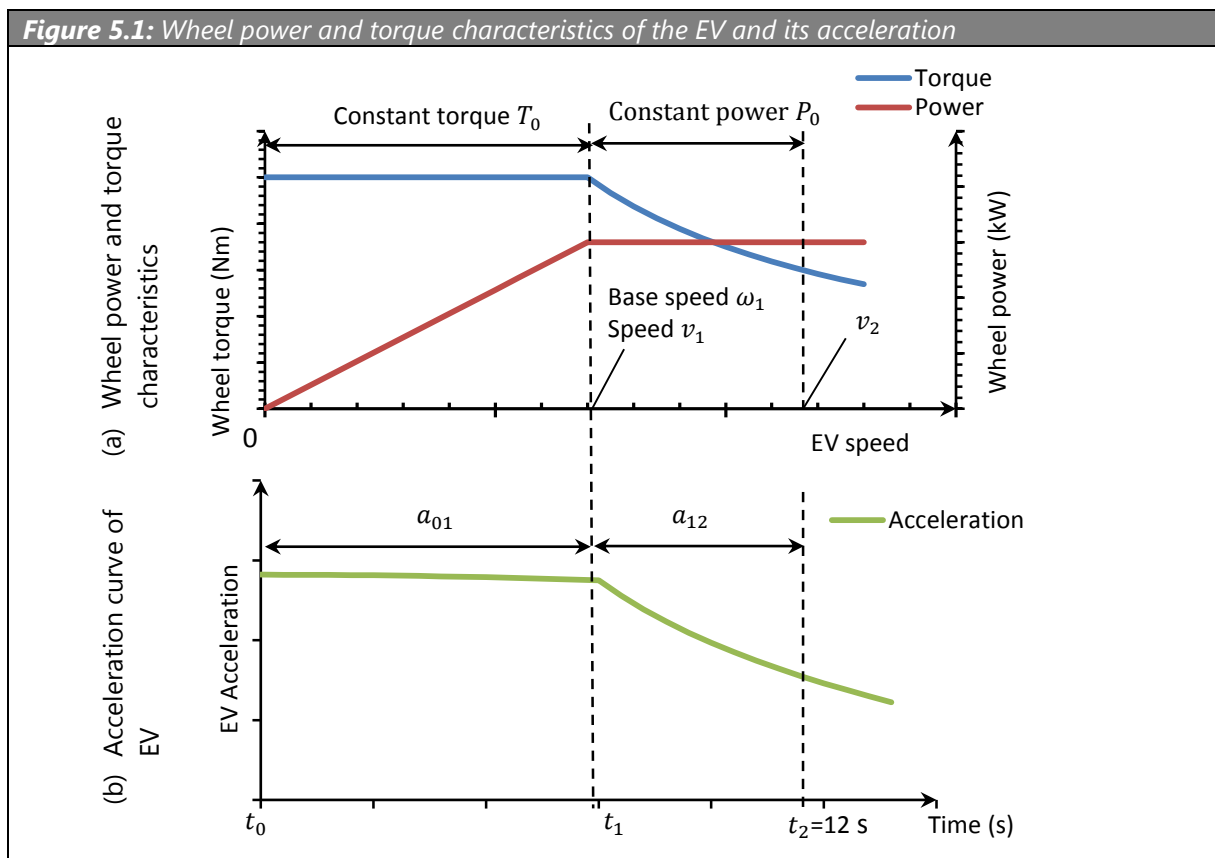
$$P_{Req,wheel} = F_{Req,wheel} \cdot v_{max} \quad (5-8)$$

When the known data are applied to these two equations, the minimum required traction force can be obtained $F_{Req,wheel} = 814 \text{ N}$; while the wheel torque is equal to the product of the traction force and the wheel radius r : $T_{Req,wheel} = F_{Req,wheel} \cdot r$, the

torque required for the top vehicle speed is $T_{Req,wheel} = 245 \text{ Nm}$ at the wheels. The power required for the vehicle is $P_{Req,wheel} = 33.9 \text{ kW}$.

Acceleration

Generally, typical power and torque speed curves of electric motor operating characteristics can be divided into two regions, constant torque region and constant power region (Hughes & Drury, 2013). Similarly, when the EV is maximally accelerated only by electric motors, the characteristics of wheel power and torque can be illustrated by the curves in Figure 5.1, ignoring power transmission loss. In the constant torque region, the E-powertrain outputs the constant torque T_0 up to the E-motor base speed ω_1 . After exceeding the base speed ω_1 of E-motor, the powertrain provides the drive wheels constant power P_0 and the wheel torque decrease inversely with speed.



The vehicle acceleration a is the derivative of velocity v .

$$a = \frac{dv}{dt} \quad (5-9)$$

Accordingly, the acceleration time t can be calculated by integral of speed v . The a_{01} is vehicle acceleration in the constant-torque region, while the a_{12} is vehicle acceleration in the constant power region.

$$t_2 - t_0 = \int_{v_0}^{v_2} \frac{1}{a} dv = \int_{v_0}^{v_1} \frac{1}{a_{01}} dv + \int_{v_1}^{v_2} \frac{1}{a_{12}} dv \quad (5-10)$$

Assuming there is no gradient resistance on a flat ground, the drag force F_I can be solved as follows according to the equation (5-1):

$$F_I = F_T - F_R - F_A \quad (5-11)$$

In constant torque region, drag force F_T can be calculated in point t_1 : $F_T = P_0/v_1$; in constant power, $F_T = P_0/v$. Consequently, the acceleration equation $a = F_I/(m \cdot \lambda)$ can be calculated as follows:

$$a_{01} = \frac{\frac{P_0}{v_1} - (G \cdot f_R + \frac{\rho_A}{2} \cdot c \cdot A \cdot v^2)}{m_v \cdot \lambda} \quad (5-12)$$

and

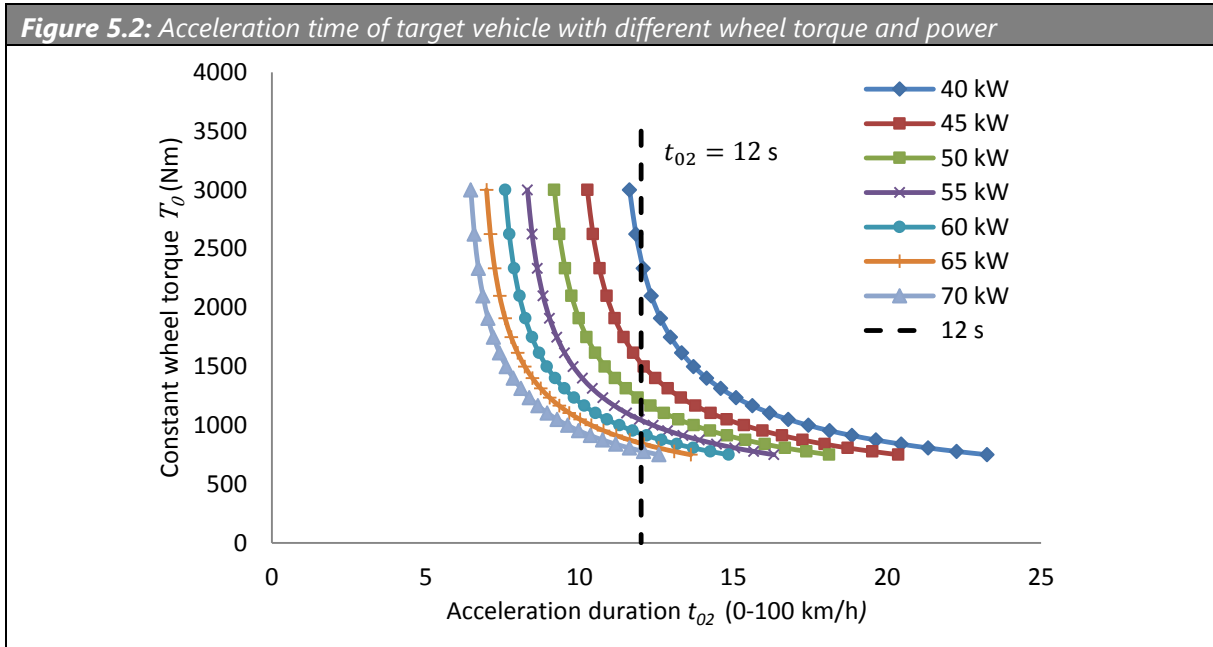
$$a_{12} = \frac{\frac{P_0}{v} - (G \cdot f_R + \frac{\rho_A}{2} \cdot c \cdot A \cdot v^2)}{m_v \cdot \lambda} \quad (5-13)$$

Combining equations (5-12) and (5-13) into equation (5-10) the equation (5-14) is obtained, which can be used to calculate the acceleration time.

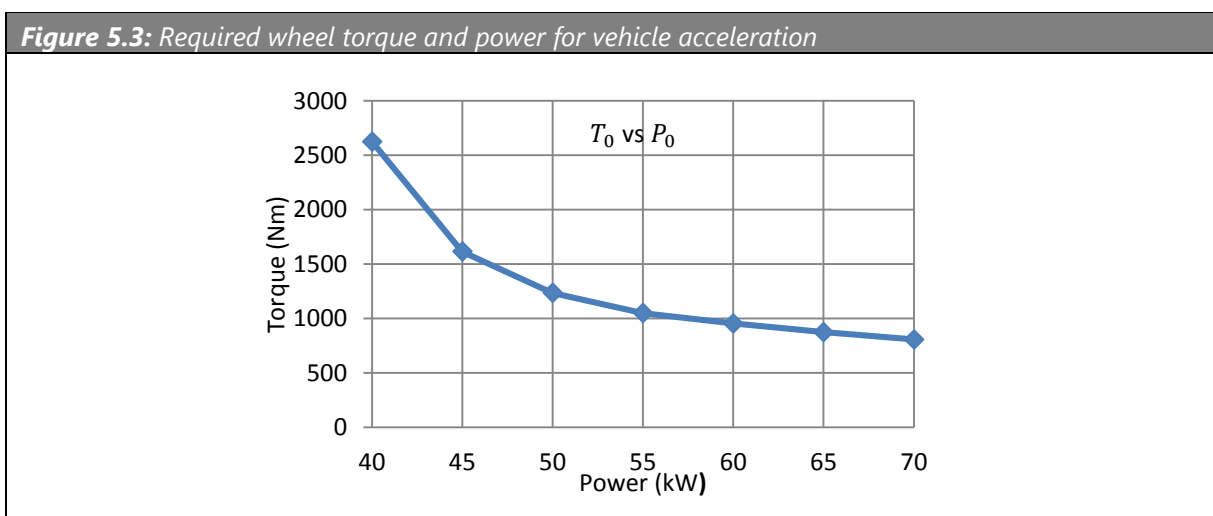
$$\begin{aligned} t_{02} &= t_{01} + t_{12} \\ &= \int_0^{v_1} \frac{m_v \cdot \lambda}{\frac{P_0}{v_1} - (G \cdot f_R + \frac{\rho_A}{2} \cdot c \cdot A \cdot v^2)} dv \\ &\quad + \int_{v_1}^{28} \frac{m_v \cdot \lambda}{\frac{P_0}{v} - (G \cdot f_R + \frac{\rho_A}{2} \cdot c \cdot A \cdot v^2)} dv \end{aligned} \quad (5-14)$$

By tuning the base speed, i.e., vehicle speed v_1 from 0 to 27.8 m/s (0 – 100 km/h) under each specific wheel power P_0 from 40 kW to 70 kW, a group of wheel torque T_0 to acceleration time t_{02} curves can be obtained (see Figure 6.2). Once P_0 and T_0 are specified, the acceleration time t_{02} from 0 to 100 km/h can be determined. The numerical calculation is performed with variables P_0 and v_1 in Matlab. The P_0 is set from 40 kW to 70 kW with an increment of 5 kW. The v_1 is set from 1 to 28 m/s with

an increment of 1 m/s , indicated in the curves. The points on the left side of the dash line $t_{02} = 12$ s means the acceleration duration is less than 12 s, otherwise on the right sides they fail the requirement.



By connecting the intersection points of the dashed line $t_{02} = 12$ and wheel torque-power curves of Figure 5.2, a boundary curve is plotted in Figure 5.3. The wheel torque and power pairs located on the upper area of this curve can meet the vehicle acceleration requirement; on the contrary, these data below this curve cannot satisfy the vehicle acceleration requirement.



The requirements of the powertrain (dual E-motors) are given in Table 5.1, which are converted from wheel torque and power by using equation (5-15). The electric motor

each mated with a gearbox of fixed ratio $i_g = 9.36$ is chosen for the powertrain. Transmission efficiency η_t is initially defined to be 95%. The rated power and torque of the powertrain should be able to meet the requirement of the vehicle top speed and the maximum power and torque should fulfill the requirement for acceleration time. The top speed requires the rated power of the powertrain $P_N \geq 35.7 \text{ kW}$, the rated torque of the powertrain $T_N \geq 27.5 \text{ Nm}$ and the rated rotation $n_N \geq 12350 \text{ r/min}$. From Figure 5.3 it is observed that the torque requirement can be reduced by appropriately increasing the motor power. However, around $P_0 = 70 \text{ kW}$ the downward trend has slowed down very significantly. In order to reduce the torque requirement and simultaneously to avoid excessive requirement on motor power, $T_{max} \geq 90.8 \text{ Nm}$ and $P_{max} \geq 73.7 \text{ kW}$ are set as the powertrain requirements; the powertrain can keep output of maximum torque or maximum power until $n_0 \geq 8228 \text{ r/min}$ and this maximum torque should last up to $t_1 \geq 11 \text{ s}$.

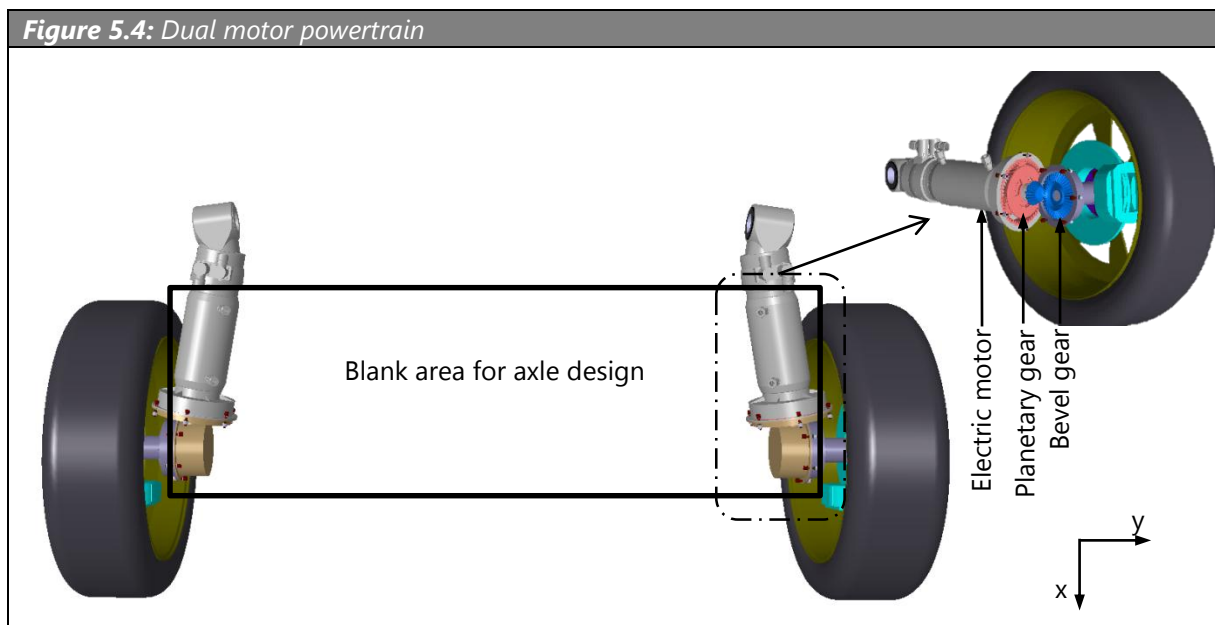
$$\begin{cases} n_{motor} = n_{wheel} \cdot i_g \\ T_{motor} = \frac{T_{wheel}}{i_g \cdot \eta_t} \\ P_{motor} = P_{wheel} / \eta_t \end{cases} \quad (5-15)$$

Vehicle Performance	Wheel			Powertrain		
	Rotational speed	Torque	Power	Rotational speed	Torque	Power
Top speed: $v_{max} = 150 \text{ km/h}$	1319 r/min	245 Nm	33.9 kW	n_N $\geq 12350 \text{ r/min}$	T_N $\geq 27.5 \text{ Nm}$	P_N $\geq 35.7 \text{ kW}$
Acceleration: $t_{02} \leq 12 \text{ s};$ 0~100 km/h	0~879 r/min	$\geq 807 \text{ Nm}$	$\geq 70 \text{ kW}$	n_0 $\geq 8228 \text{ r/min}$	T_{max} $\geq 90.8 \text{ Nm}$	P_{max} $\geq 73.7 \text{ kW}$

The electric motor attached in appendix C is selected as the basic for matching the powertrain. From the power and torque speed curves it can be found that such dual electric motors can generate rated torque T_N of 30 Nm and the rated power P_N of 38 kW by $n = 12350 \text{ r/min}$ that can meet the requirement of the vehicle top speed.

The single motor can reach 52 kW maximum power and 51.3 Nm maximum torque. Consequently, the powertrain of dual electric motors can generate 104 kW maximum power and 960.3 Nm maximum torque; and the maximum torque can continue up to $n_0 = 8228 \text{ r/min}$. Although the duration t_1 of maximum torque is not given in the technical data, it should be designed to $t_1 \geq 11 \text{ s}$ in matching the powertrain.

The mechanical powertrain concept is designed using the software CATIA (see Figure 5.4). The blank area between two electric motors is the design space for the subsequent axle design. The gear transmission consists of a set of planetary gears and a pair of bevel gears with the respective ratio of 3.12: 1 and 3: 1.

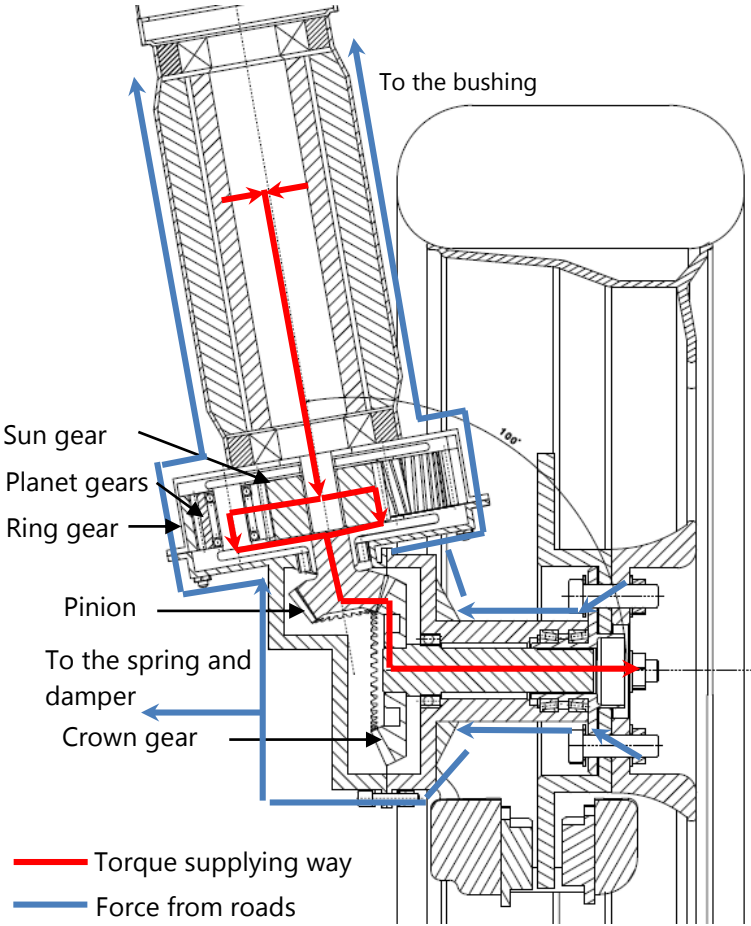
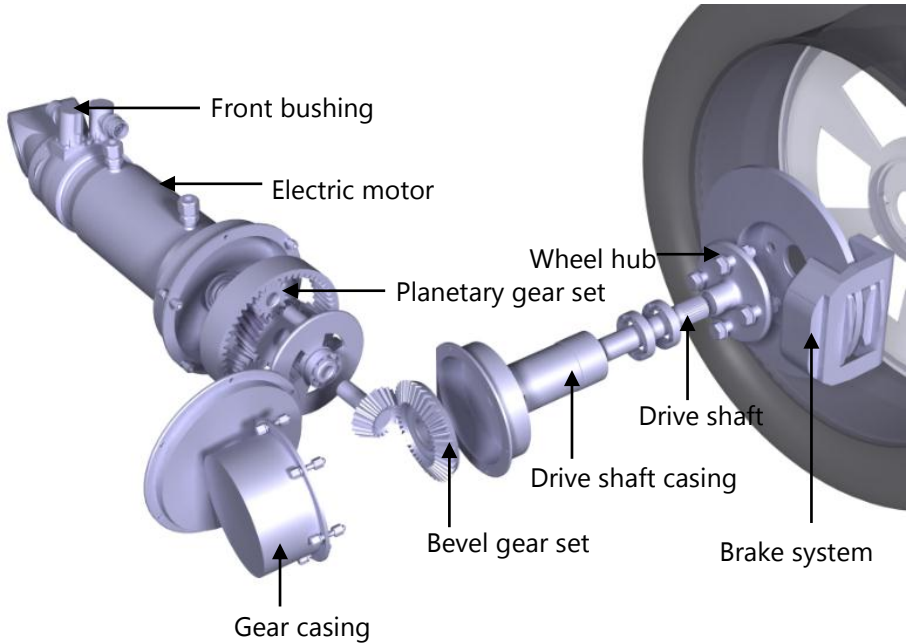


The concept structure of single drive unit is given in Figure 5.5 on the basis of the selected motor and the references (Müller & Ponick, 2005) (Vogt, 1996). As above mentioned the purpose of this structure is to provide reference parameter for the design of the concept suspension. The motor power is supplied to the wheel through planetary gear system, bevel gears, drive shaft and wheel hub successively. The reaction forces from the road are supported by the drive shaft casing, gear casing and electric motor casing. The Figure 5.5 of the next page shows the way in which the motor torque is supplied to the wheel by the red line and the force from the road by the blue line.

The above simplified calculation is applied to provide general parameters for the concept design. The following items should be considered in the detail design:

- The limitations out of de-rating of the subsystems: battery management system, inverter, stator and so on
- Efficiency map of the drivetrain
- Slip limit of the wheel

Figure 5.5: Drive unit construction



6 Investigation of the reference twist beam axle

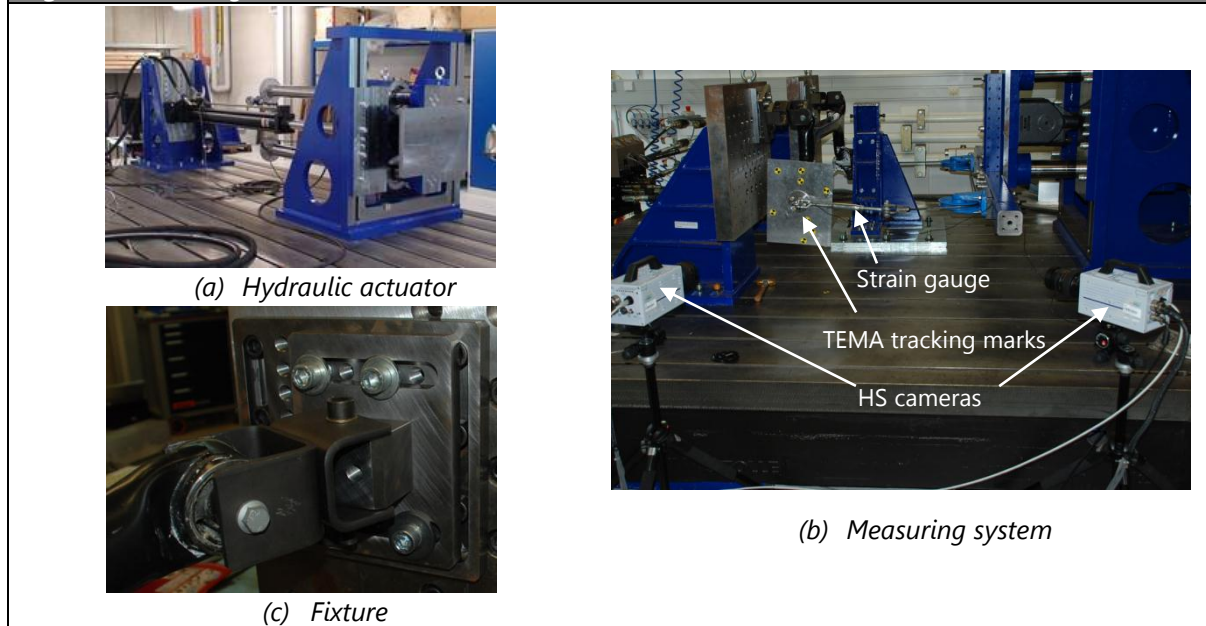
The twist beam axle of the benchmark car i.e. Volkswagen Polo is the reference suspension. The target of this chapter is to investigate the K&C characteristics of the twist beam which are set as the baseline of the new concept suspension.

The K&C characteristics of the reference suspension are investigated through experimental and simulated methods. K&C characteristics are tested by test rigs based on MTS hydraulic actuators in section 6.1. In order to obtain the complete K&C characteristics, a FEM model of this reference suspension is built in section 6.2. In order to validate the FEM model, the simulated results are compared with the experimental results in section 6.3. After the validation, K&C analysis of the reference twist beam is performed in section 6.4 by FEM ignoring the influence of rubber bushings.

6.1 Investigation of the reference rear axle by the test bench

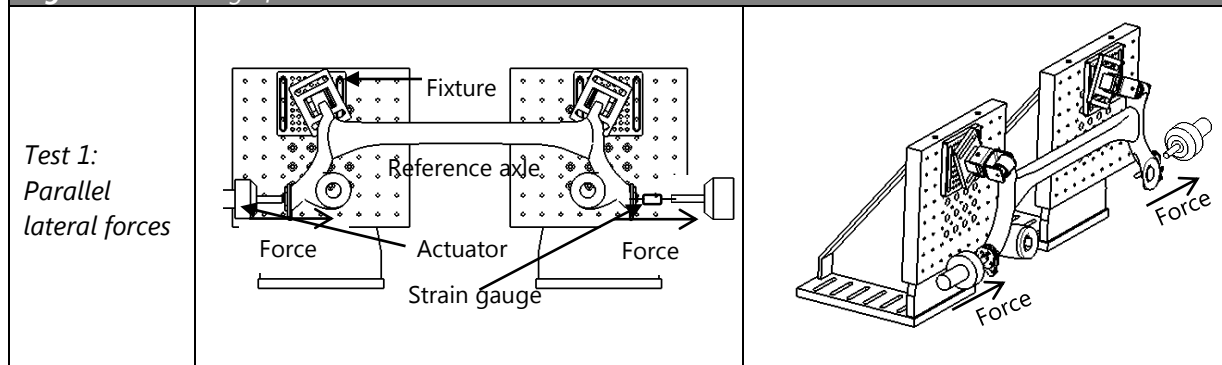
6.1.1 Test rig

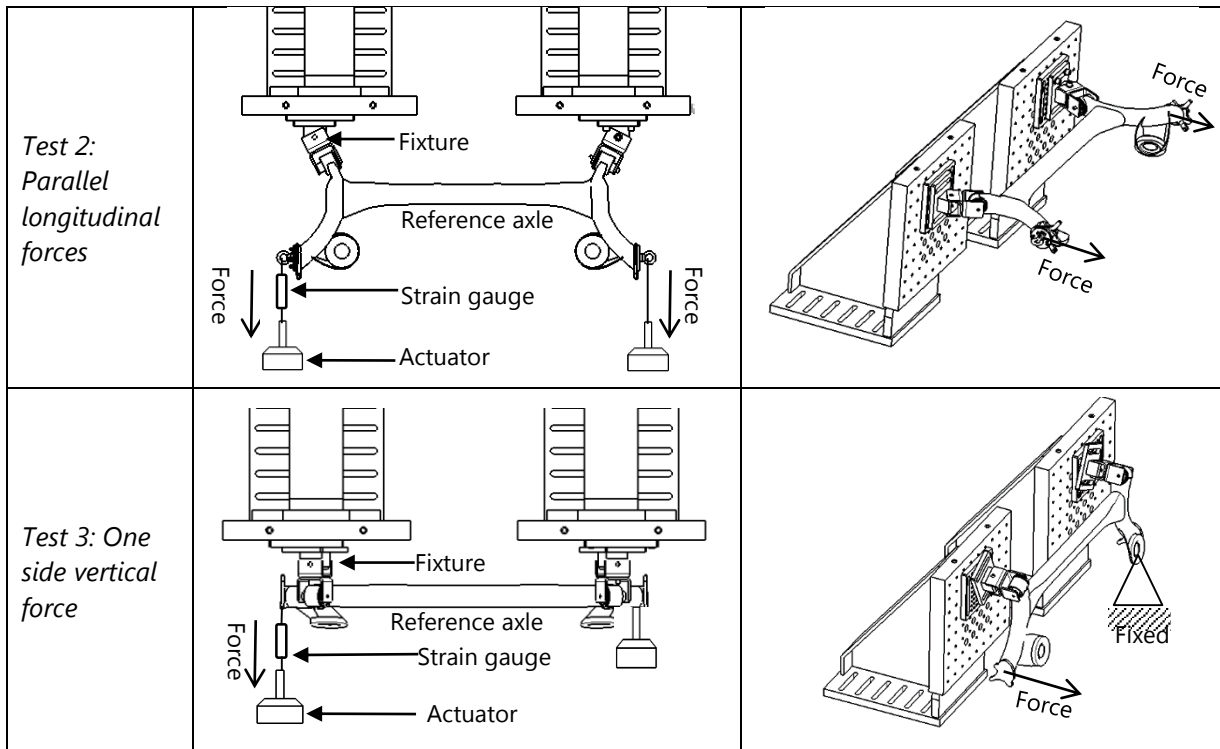
The test rig consists of load actuators, measuring system and fixtures (Figure 6.1 (a), (b), (c)). MTS hydraulic actuators are used as Load generators, which produce quasi-static pulling or pushing force in this test. In order to avoid the deviation caused by the friction force in the cylinder. The strain gauge is used to test the force on the axle. Wheel center displacements and wheel alignment parameters are recorded by the TEMA point tracking system which uses the high-speed camera (HS camera) to record the motion of tracking points. For the purpose of measuring the changing of wheel alignments, two high speed cameras are applied to simultaneously record the movement of target points which are quadrant target markers pasted on a metal plate. This metal plate is attached to the wheel plate tightly. The 3D motion of this wheel plate can be recorded. The fixtures on both sides are free to rotate and translate, which assures the connection of the twist beam axle to the test rig the same as to the car body.

Figure 6.1: Test rig for the reference twist beam axle

6.1.2 Testing cases

The tests are performed in quasi-static mode with a frequency of 0.002 Hz. Considering conditions of the test equipment and the test purpose, the following three cases in Figure 6.2 are carried out. The case 1 aims to investigate the longitudinal compliance characteristics of the axle. The case 2 is to the torsion stiffness and kinematic characteristics. The purpose of case 3 is to test the lateral compliance characteristics of the axle.

Figure 6.2: Testing of the twist beam axle



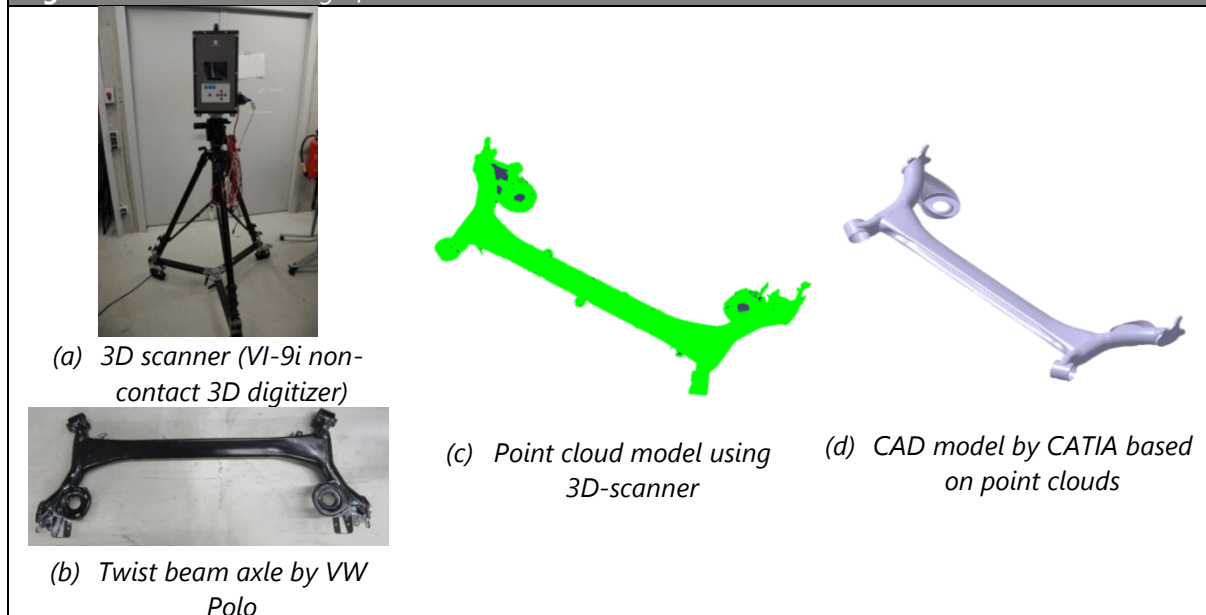
6.2 FEM model of the twist beam axle

K&C characteristics of twist beam axles are principally dependent on the geometries and material properties.

6.2.1 CAD model

The modelling process of the rear twist beam axle is presented in Figure 6.3.

Figure 6.3: CAD modelling of the twist beam axle



In order to ensure the geometric accuracy of the model, the 3D-Scanner (VI-9i non-contact 3D digitizer) is applied to capture the geometric information of the twist beam axle. The accuracy of this scanner reaches to ± 0.2 mm with a middle lens (Konica Minolta Sensing Inc, 2004-2006). The data collected by the scanner are the form of point clouds. They are trimmed into small pieces in CATIA. The positions of the points on the trimmed sections can be picked up. The digital model of the twist beam axle is rebuilt on the basis of the picked points.

6.2.2 FEM modelling

Rubber bushings are used as connecting elements of chassis components. The bushings used in the twist beam axle are shown in Figure 6.4, which consists of two concentric plastic sleeves and a rubber component. The complete properties of rubber material are manifold and complex, for example hyperelasticity, viscoelasticity, Mullins Effect and so on. Generally, the selection of the material models and the quality of the material identification is decisive to the accuracy of the FE simulation for rubber material. In this work at the early design phase the investigation focuses on the static K&C characteristics. The most related property of rubber material to the static K&C is hyperelasticity. A material, of which the stress can be defined by a strain energy function W , is termed as hyperelastic material (Ogden, 1997) which is described in modern FE-program by Hyperelastic material models, commonly using Neo-Hookean and Mooney-Rivlin solids (Engelmann, 2013) (Bormann, 2005). The expressions of these two material models are as follows (Altidis & Warner, 2005), respectively.

$$W = C_{10}(I_1 - 3) \quad (6-1)$$

and

$$W = C_{10}(I_1 - 3) + C_{01}(I_2 - 3) \quad (6-2)$$

where, I_1 and I_2 are the first and second invariant of the right Cauchy-Green deformation tensor, and C_{10} and C_{01} are material constants which can be automatically generated in LS-DYNA after inputting material test results. In order to simplify the material test process, material constants can also be obtained from an empirical

formula with shear modulus G (MPa) and Shore A hardness H of applied rubber material (Bormann, 2005) (Kunz & Studer, 2006).

$$G_{ShA}(H) \approx e^{a(H-H_0)} \text{ MPa with } a = 0.05; H_0 = 53 \quad (6-3)$$

The relationship of Young's modulus E and shear Modulus G is as follows.

$$E = 2(1 + \nu) \cdot G \quad (6-4)$$

where, ν is Poisson's ratio. The Modulus E derived from above formulas matches quite well (Bormann, 2005) with the analytical descriptions (Tobisch, 1981), among the hardness of $H = 50 - 80$ ShA.

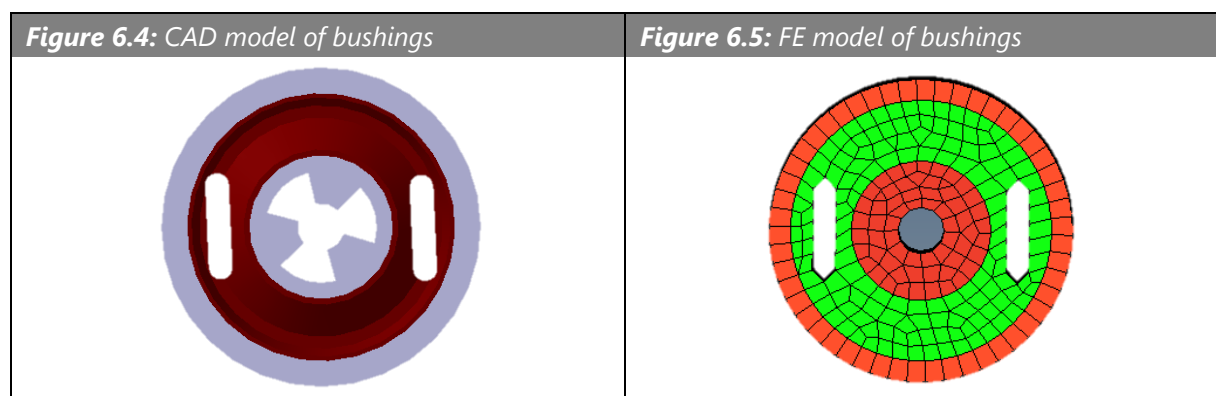
Further, the E -Modulus can be written by material constants, for Neo-Hookean solid,

$$E = 6 \cdot C_{10} \quad (6-5)$$

For Mooney-Rivlin solid,

$$E = 6 \cdot (C_{10} + C_{01}) \quad (6-6)$$

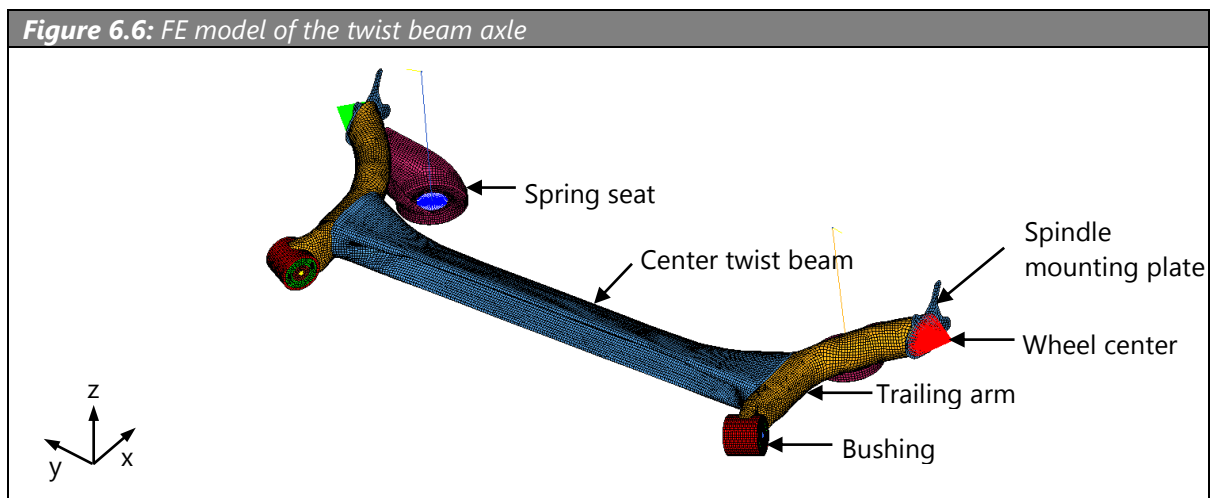
Although both of above solid models do not meet high precise demand of calculation, the deviation to testing result is still acceptable in linear area when material deformation is small and Neo-Hookean is a simple way to describe rubber material according to the literature (Bormann, 2005). Therefore, this Neo-Hookean model was chosen to simulate the rubber bushing.



With two kidney-shaped holes between these sleeves, this structure leads to the bushing's different stiffness in radial directions so as to further influence the K&C characteristics. The FEM model of the twist beam axle is meshed in software Altair HyperMesh on the basis of the CATIA model. Bushings are discretized with hexahedral

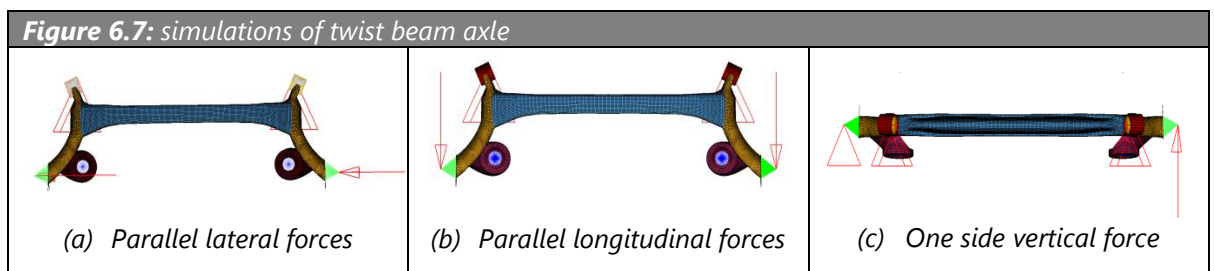
elements (see Figure 6.5). The Shore hardness of the rubber compound in twist beam axle is 63 ShA (Engelmann, 2013). The rubber material property is simulated based on the formulas (6-1) to (6-6).

The other parts of the twist beam axle are discretized into amount of 29912 shell elements with specified thickness in different parts (see Figure 6.6). The lateral beam of the twist beam axle is an important part to perform torsion function and support lateral force. The minimal element size of the beam part is 5 mm. The joints of the twist beam axle with the vehicle body are simulated by the revolute joints.

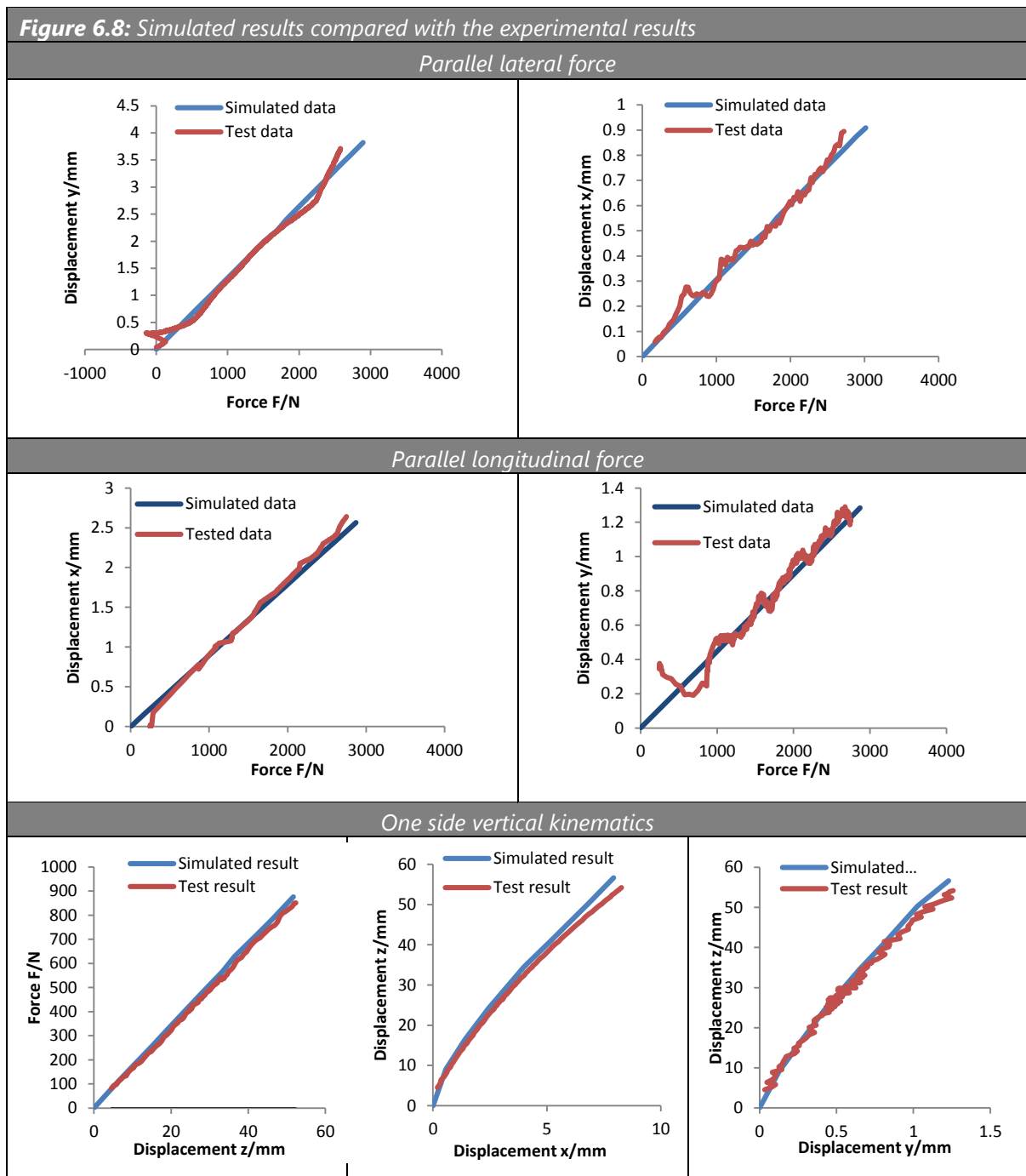


6.3 Model validation

The simulations of the twist beam axle are carried out with the same load cases as the testing (see Figure 6.7). The simulations are carried out by LS-DYNA with implicit solver, of which the force is defined by load curves with simulation time of 110 seconds, because explicit solver in LS-DYNA is to solve problems in particularly high speed domain, e.g., crash or explosion.



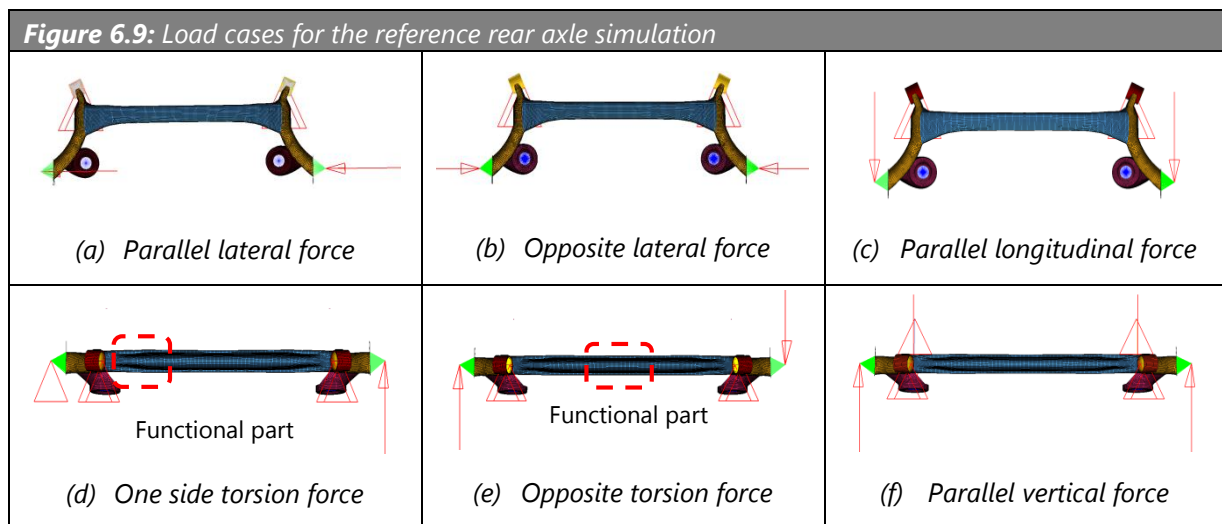
The simulated results are described by blue curves in Figure 6.8, and the corresponding results from the experiments are presented using red curves. In these graphs, the simulated results are compared with the test results. In the subfigure of one side vertical kinematics, three group parameters obtained from simulation and test are compared. The left curves are the torsion stiffness with one vertical force on the single side wheel center; the middle curves and the right curves are the longitudinal and lateral displacements of the wheel center in the wheel vertical travel.



In the subfigures of parallel longitudinal forces and parallel lateral forces, the displacements of the wheel center along the force direction are compared. The displacements of the wheel center with the compliance in the orthogonal direction to the force are also compared. From the comparisons, the quasi-static simulation results show good agreement with the experimental results.

6.4 K&C analysis of reference twist beam axle

The purpose of the FEM analysis in this section is to investigate the K&C and mechanical characteristics of the twist beam suspension. The analysis results are used as the baseline for the design of concept suspension.



Different load cases in accordance with the working cases of vehicles are applied at the wheel centers, which are aimed to simulate the K&C response of the twist beam axle under real operations. Load case 1 with two parallel lateral forces acting at the left and right wheel centers (Figure 6.9 (a)) relates to the operation case when the car subjects to the lateral force like cornering; when the car drives on uneven road the wheels on the two sides may sustain opposite lateral forces, it corresponds to the load case 2 (Figure 6.9 (b)); the load case 3 (Figure 6.9 (c)) simulates the longitudinal loads when the car is braking; the load case 4 (Figure 6.9 (d)) with one side vertical force simulates the situation when the wheel on single side rolls over a bump, of which the functional part for the torsional stiffness is the transitional part of the beam close to the fixed side. The load case 5 (Figure 6.9 (e)) with opposite vertical forces on the wheel centers

simulates the case when the car is transiently steering, of which the functional area for torsion stiffness is in the middle of the lateral beam; the load case 6 (Figure 6.9 (f)) with parallel vertical force simulates the loads on the axle while the wheels parallel bump.

The parameters obtained through the FEM simulation of suspension are listed in Table 6.1. For the load case with lateral force, the lateral compliance means the lateral displacement of the wheel center relative to the lateral force; the lateral force steer means the toe angle change relative to the lateral force; the lateral force camber means the camber angle change relative to the lateral force; and likewise for the load case of longitudinal force. For the load case with twist force, the roll steer and roll camber mean the toe and camber change relative to the vehicle roll. For the load case with parallel bump, the ride steer and ride camber mean the toe and camber change relative to the wheel bump.

Table 6.1: Important K&C parameters for twist beam axles

Load case	Parameters			
Lateral force	Lateral compliance	Lateral force steer	Lateral force camber	
Longitudinal force	Longitudinal compliance	Longitudinal force steer	Longitudinal force camber	
Twist	Twist stiffness	Roll steer	Roll camber	Wheel track
Parallel bump	Ride stiffness	Ride steer	Ride camber	Wheel track

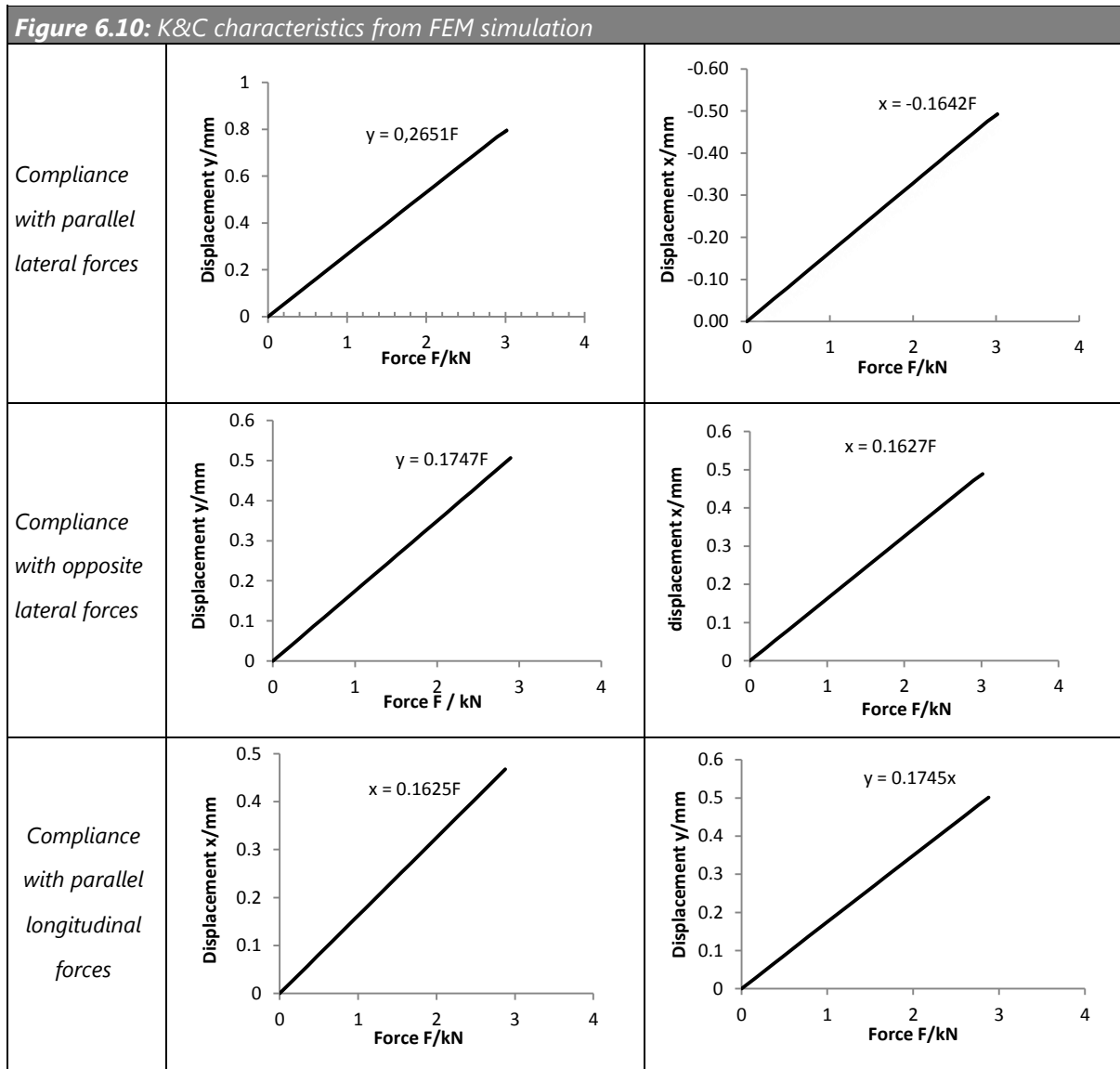
Ignoring the shift of the vehicle gravity center, the maximum lateral and braking force on the rear axle is

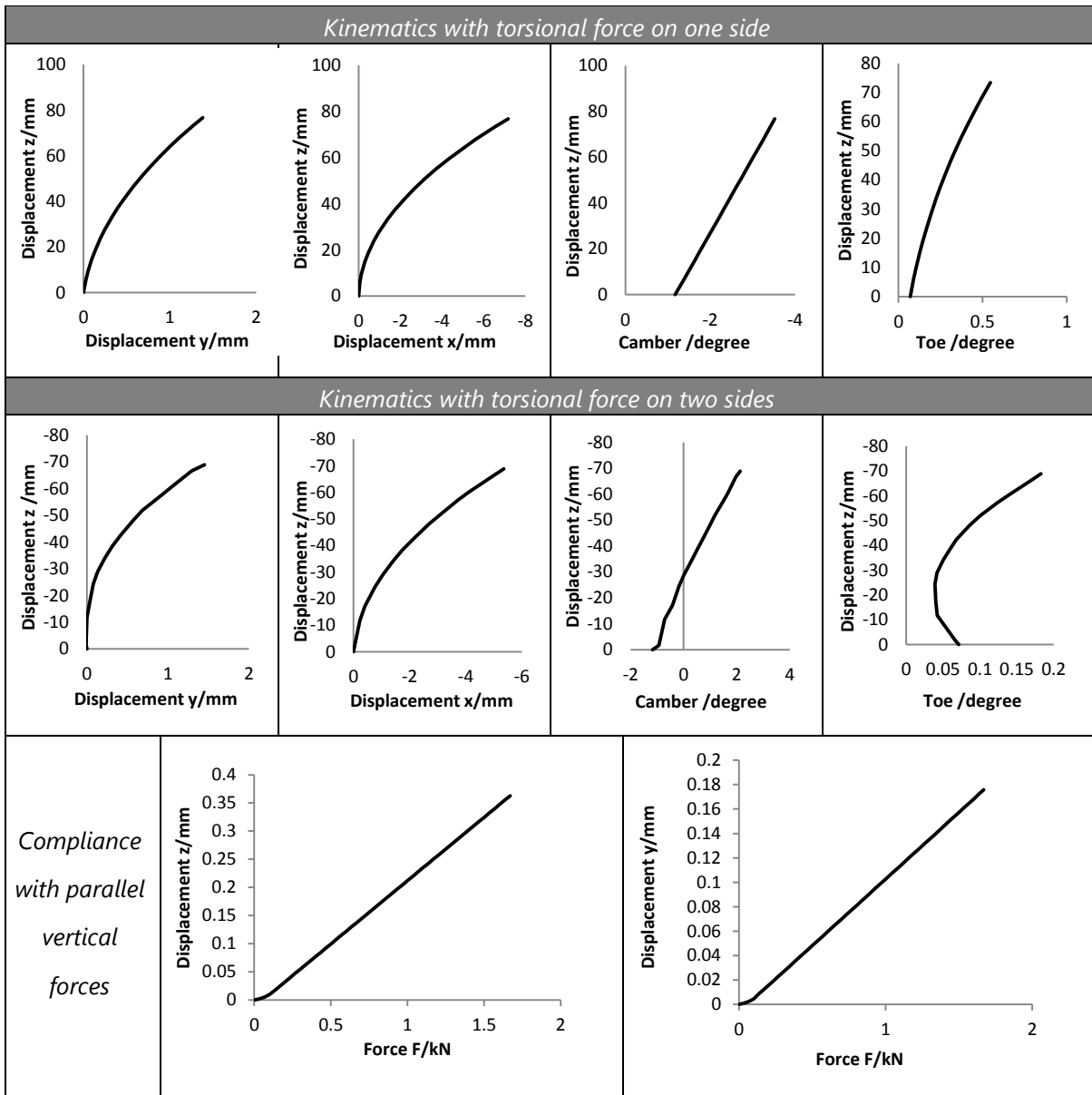
$$F = m_v \cdot g \cdot \frac{1}{i + 1} \cdot \mu_R \cdot c \quad (6-7)$$

where, i is the vehicle mass front and rear distribution, for the reference vehicle $i = 62:38$ (Eckstein, et al., 2011); μ_R is the frictional coefficient between tires and road; $c = 1.5$ is a safety coefficient. As a result, the compliance lateral and longitudinal force is defined as 3000 N. The twist force is defined according to the torsional capability of the center twist beam. For the twist beam axle, when the wheel center is raised up 75 mm along the z axis, the axle reaches the torsional limit. In the parallel bump, the

displacement of the wheel center along the z axis is $\pm 85 \text{ mm}$ from the equilibrium position.

The simulation results of the twist beam axle are present in Figure 6.10 in the form of curves. The data are measured at wheel center on the left side of Figure 6.9 (a) (b) (c) and on the right side of Figure 6.9 (d) (e) (f).





7 Structure optimization design considering K&C performance and geometric non-linearity

Structure optimization can be classified into size, shape and topology optimization (Yamada, et al., 2010). The optimizations of suspension components based on the topological method have been conducted in a number of papers (Lee, et al., 2007) (Altair Engineering Inc., April, 2009), but these component optimizations did not need to consider the K&C performance and geometric non-linearity. The structural optimization has already been applied to optimize the size and shape of existing twist beam axles (Steel Market Development Institute, 2013). However, only the component stiffness was considered and, moreover, size optimization and shape optimization did not change the structure topology. The K&C performance had to be achieved using subsequent backward structural modification. As in the optimization approaches mentioned in the above literatures, the mechanical requirements can be satisfied by the usual linear topological optimization. The compliance characteristics of a suspension are small displacements, and therefore optimization involving compliance characteristics can be performed using the linear method. The kinematics characteristics are the suspension parameters with large displacements. Optimization with respect to large displacements should be treated as a geometric non-linear problem.

The functionality of rear suspensions with integrated drive units is complicated, which makes the structural design of these suspensions more complex. As such, it is necessary in the concept phase to analyze the load conditions and to develop a design approach based on the structural topological optimization method with design constraints on the suspension K&C characteristics and the mechanical properties considering the geometric non-linearity, by which the optimized material distribution can be obtained and the design iteration process between the concept and prototype can be simplified.

In this chapter, a design approach based on structure optimization is proposed for the structure design of the concept suspension. At first, a topological structure with

required characteristics is obtained on the basis of topological optimization result. Then, on the basis of the topological structure, tubes are chosen as the suspension links to demonstrate the functionality of this structure. Further, size optimizations are carried out to optimize the thickness of the suspension links and then two suspension structures made of tubes satisfying the K&C requirements with a reduced mass are designed. By this topological and size optimization, the K&C requirements are taken into account in the structure optimization. In the optimization, six load cases are applied to simulate the different load situations acting on the suspensions. The optimizing situations relating to kinematic requirements are solved by the Equivalent Static Load Method (ESL) (Lee & Park, 2012).

7.1 Structure optimization methods

The structure topological optimization method addresses the issue of laying out material in an optimal manner. Based on different algorithms, the topological methods can be principally classified into three types, i.e. evolutionary methods, shape-gradient based methods and material distribution methods (Calvel & Mongeau, 2007) (Chiandussi, et al., 2004). The evolutionary methods calculate the optimal results through removing the unnecessary elements where the stress tensor is low (Yang, et al., 1999). Shape-gradient methods solve the optimization on the basis of the sensitivity of the objective function according to the displacement of the frontier of the domain (Sokolowski & Zolesio, 1992). The material distribution methods that lay out material on a design grid are the mostly used methods which have been applied in a variety of design problems. The material distribution methods subdivide into three categories: the discrete optimization method, the homogenization method and the density method (Calvel & Mongeau, 2007). The density method, also called Solid Isotropic Material with Penalization (SIMP), is based on the analysis of isotropic material. Because of the simplicity of the theory and numerical implementation, it is widely employed in commercial software systems, e.g. OptiStruct and GENESIS (Lee & Park, 2012).

Structure optimization in this chapter aims to find a suspension structure with minimal mass while meeting the mechanical requirements and K&C requirements of the suspension. On the basis of the SIMP, optimization can be generally expressed as.

$$\begin{aligned}
 &\text{find} && \mathbf{e} \in \mathbf{Z} && (7-1) \\
 &\text{to} && \min_{\mathbf{e} \in \mathbf{Z}} f_{obj}(\mathbf{e}) && \mathbf{e}_l \leq \mathbf{e} \leq \mathbf{e}_u \\
 &\text{s.t.} && h_i(\mathbf{e}) = 0, i \in E \\
 &&& g_i(\mathbf{e}) \leq 0, i \in I
 \end{aligned}$$

where, \mathbf{Z} is the scope of the design variable, $\mathbf{e} \in \mathbf{Z}$ is the design variable vector, f_{obj} is the objective function i.e. minimal mass in this work, $h_i(\mathbf{e}) = 0$ are the equilibrium equations, g_i are the constraint functions i.e. the mechanical and K&C requirements in this work, I and E are finite index sets, i is the number and s.t. means subject to.

Linear static response structural optimization has been developed very well by using linear static response analysis. However, it is difficult and expensive (high computational capacity and time consuming) for conventional optimization with respect to the nonlinearities or the dynamic effects. As the finite element analysis considering the non-linearities or the dynamic effects has also been developed quite well, solving non-linear response structural optimization by using ESLs has been proposed. This method has been implemented for the optimization problem with various responses: the linear dynamic response, the non-linear static response and the non-linear dynamic response. The structural optimization case of suspensions with a non-linear geometry considering the kinematic characteristics can be treated as a problem with a non-linear static response.

7.2 Proposed approach

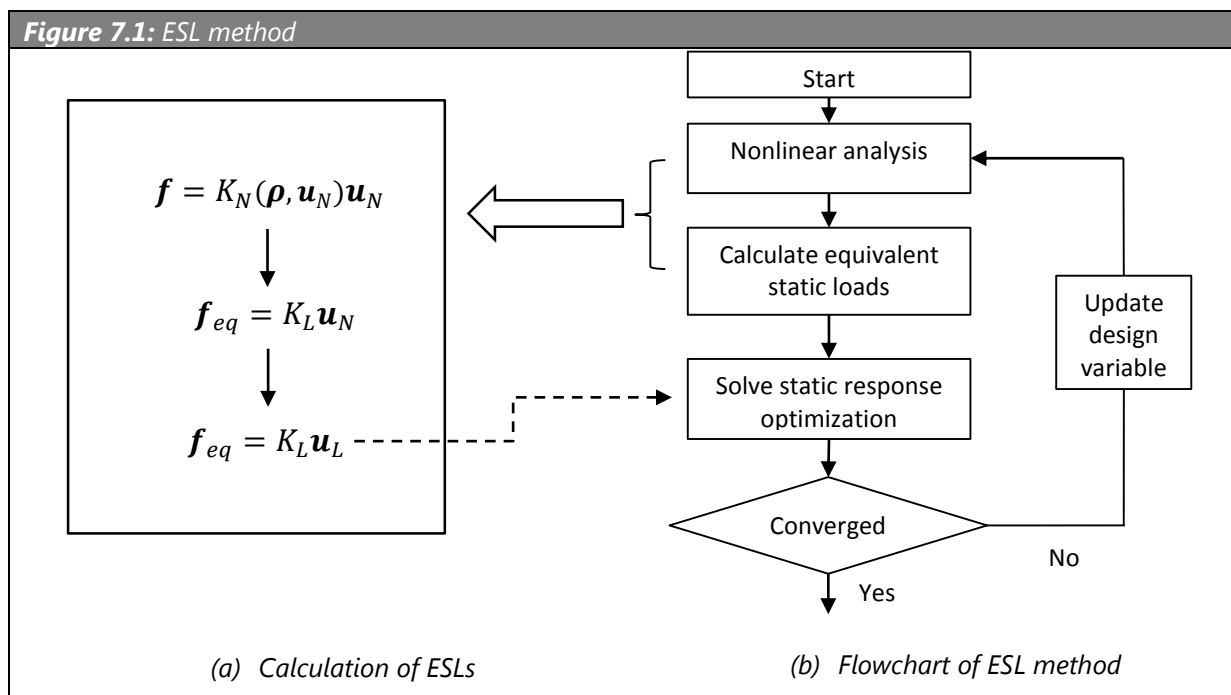
The optimization cases can be defined according to the required K&C characteristics. However, for suspension kinematics the geometric nonlinearity should be taken into account.

7.2.1 Geometric non-linearity

The geometric non-linearity includes the non-linearities in kinematic quantities such as the strain-displacement relationships. The geometric non-linearity is characterized as large displacements, strains and rotations (Wriggers, 2008). The ESL method illustrated in Figure 7.1 is one of the non-linear methods for non-linear response optimization (Park, 2014). In finite element method, the equilibrium equation of a structure with static non-linear response is

$$\mathbf{f} = K_N(\boldsymbol{\rho}, \mathbf{u}_N)\mathbf{u}_N \quad (7-2)$$

where K_N is the non-linear stiffness matrix, \mathbf{u}_N is the non-linear nodal displacement vector, \mathbf{f} is the external force vector and the subscript "N" means the values from non-linear static analysis.



The ESLs are defined as

$$\mathbf{f}_{eq} = K_L \mathbf{u}_N \quad (7-3)$$

where, the subscript "L" indicates the values from linear analysis. The ESLs are obtained by multiplication of the linear stiffness matrix and the non-linear nodal displacement vector from equation (7-2). \mathbf{f}_{eq} is the vector of the equivalent static nodal forces. If the ESLs are used as external forces in the equation of linear static response analysis, then

$$\mathbf{f}_{eq} = \mathbf{K}_L \mathbf{u}_L \quad (7-4)$$

Thus, non-linear optimization can be treated as the linear static optimization. If the results of the linear optimization do not converge, a new updated variable is assigned to the non-linear analysis, and then a new optimization loop is performed. The design variable for topology optimization is element density vector (Altair Engineering Inc., April, 2009).

For suspension kinematics, relationships between the load and wheel center displacements as well as wheel alignment angles are non-linear and structural large displacements are involved with the wheel travel. To solve this non-linear problem, the geometry changes as the structure deformations must be taken into account in formulating the constitutive and equilibrium equations. Under the load case related to suspension kinematics, geometric non-linear optimization methods must be applied. The structure optimization problem for load cases associated with suspension kinematics characteristics can be expressed by the equation (7-5) based on the SIMP. The objective of the optimization is defined to find a density distribution, with which the mass is minimized. The equilibrium equation is based on ESL method. The responses are the related parameters of suspension kinematics i.e. the wheel travel displacement, the wheel center lateral displacement, the camber angle change and the toe angle change.

$$\text{Find} \quad \boldsymbol{\rho} \in \mathbf{Z} \quad (7-5)$$

$$\text{to} \quad \min_{\boldsymbol{\rho} \in \mathbf{Z}} \sum_{i=1}^{n_{el}} \rho_i v_i; \quad 0 \leq \rho_i \leq 1, i = 1, \dots, n_{el}$$

$$\text{s.t.} \quad h: \quad \mathbf{f} = \mathbf{K}_N(\boldsymbol{\rho}, \mathbf{u}_N) \mathbf{u}_N \quad (\text{equilibrium equation})$$

$$g: \quad \Delta z_l \leq g_1(\boldsymbol{\rho}, \mathbf{u}_{z,N}) \leq \Delta z_w,$$

$$\Delta y_l \leq g_2(\boldsymbol{\rho}, \mathbf{u}_{y,N}) \leq \Delta y_u,$$

$$\theta_l^{camber} \leq g_3(\boldsymbol{\rho}, \mathbf{u}_N) \leq \theta_u^{camber},$$

$$\theta_l^{toe} \leq g_4(\boldsymbol{\rho}, \mathbf{u}_N) \leq \theta_u^{toe}$$

In this equation, n_{el} is the number of elements of the domain, ρ_i is the continuous densities of the i^{th} element $0 \leq \rho_i \leq 1$, v_i is the volume of the i^{th} element, \mathbf{K}_N means the non-linear stiffness matrix which is related to element density vector $\boldsymbol{\rho}$ and structure deformation vector \mathbf{u} , the subscript u and l mean the upper and lower limitations of the structure responses under the loads.

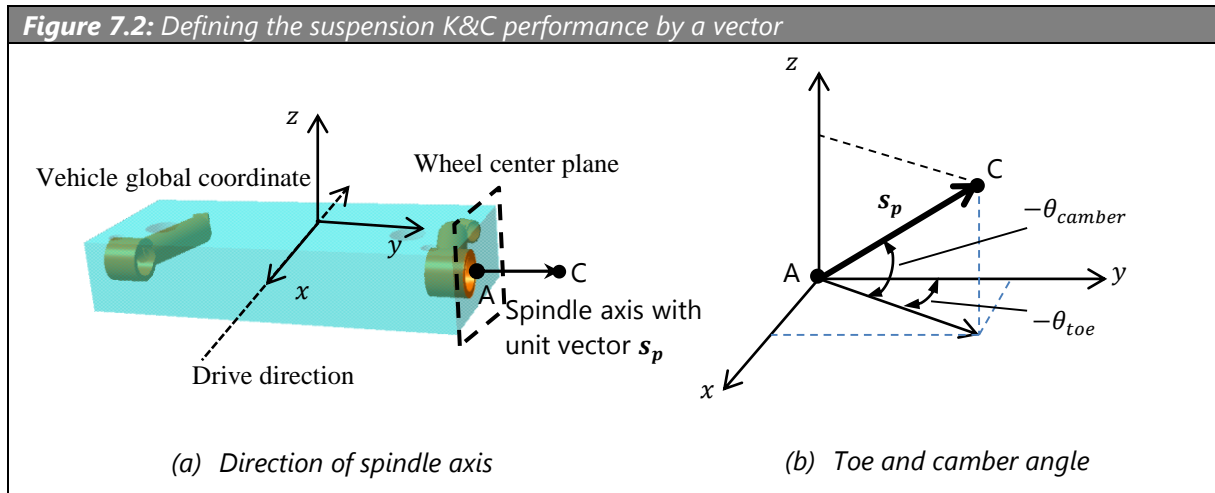
For suspension compliance, because the structural deformation is small under the loads, the load case related to suspension compliance can be solved by linear optimization method. In the optimization case related to suspension compliance, the wheel center displacements in longitudinal and lateral directions are used to describe the compliance characteristics. The optimization problem related to suspension compliance characteristics is described by the following linear equation based on the SIMP.

$$\begin{aligned}
 &\text{Find} && \boldsymbol{\rho} \in \mathbf{Z} && (7-6) \\
 &\text{to} && \min_{\boldsymbol{\rho} \in \mathbf{Z}} \sum_{i=1}^{n_{el}} \rho_i v_i; && 0 \leq \rho_i \leq 1, i = 1, \dots, n_{el} \\
 &\text{s.t.} && h: && \mathbf{K}_L(\boldsymbol{\rho})\mathbf{u} = \mathbf{f} \\
 &&& g: && \Delta x_l \leq g_1(\boldsymbol{\rho}, \mathbf{u}_x) \leq \Delta x_u, \\
 &&& && \Delta y_l \leq g_2(\boldsymbol{\rho}, \mathbf{u}_y) \leq \Delta y_u
 \end{aligned}$$

7.2.2 Wheel alignment vectors

The commercially available software suffers from limitations of applicability, i.e. the camber and toe angle changes are difficult to define directly; currently this software can address problems with only constraints or objectives on responses in the mass, the volume, the compliance, the eigenvalues, the displacement at a node or a weighted combination of these functions. Furthermore, the large displacements of the suspension in the load case for kinematics increase the difficulty of optimization. However, the camber and toe angles can be defined by introducing a local vector \mathbf{s}_p perpendicular to the plane (Figure 7.2 (a)) attached to the wheel (Mun, et al., 2010).

Therefore, the wheel alignment angles can be constrained by wheel aligning vectors which are generated by node positions and the displacements on the wheel centres.



The vector is located on the wheel center. It can be expressed by the components s_x, s_y, s_z along the global coordinate axes x, y, z , respectively.

$$\mathbf{s}_p = [s_x, s_y, s_z] \quad (7-7)$$

The toe angle θ_{toe} and camber angle θ_{camber} shown in Figure 7.2 (b) can be expressed as follows.

$$\sin(-\theta_{camber}) = \frac{|s_z|}{\sqrt{s_x^2 + s_y^2 + s_z^2}} \quad (7-8)$$

$$\tan(-\theta_{toe}) = \frac{s_x}{s_y} \quad (7-9)$$

In practice, the vector \mathbf{s}_p is defined by the node A (x_A, y_A, z_A) on the wheel center and a reference node C (x_C, y_C, z_C) along the vector direction. Thus, the vector can be written as follows.

$$\mathbf{s}_p = \overline{CA} = [x_A - x_C, y_A - y_C, z_A - z_C] \quad (7-10)$$

Correspondingly the camber and toe angles on each wheel can be defined by the coordinates of the two nodes.

$$\sin(-\theta_{camber}) = \frac{|z_A - z_C|}{\sqrt{(x_A - x_C)^2 + (y_A - y_C)^2 + (z_A - z_C)^2}} \quad (7-11)$$

$$\tan(-\theta_{toe}) = \frac{x_A - x_C}{y_A - y_C} \quad (7-12)$$

7.3 Application to topological optimization of a concept suspension

The powertrain is shown in Figure 5.4. This concept needs a suspension linkage to support the lateral and longitudinal loads from the road to satisfy the K&C characteristics.

7.3.1 Load cases

When the car drives on the road, the loads on the concept suspension arise from not only the road but also the drive unit. The loads from the drive unit incorporate the reaction torque from the electric motor and bearing reaction forces from the transmission, which act on the suspension in each load case. The loads from the road are dependent on the vehicle work situations. The optimization cases should consider the different suspension work situations. 6 load cases are considered according to the vehicle work situations (see Figure 6.9).

Case 1, parallel lateral forces acting on the wheel centers.

Case 2, opposite lateral forces acting on the wheel centers.

Case 3, parallel longitudinal forces acting on the wheel centers.

Case 4, one side fixed and one side vertical force on the wheel centers.

Case 5, opposite vertical forces on the wheel centers.

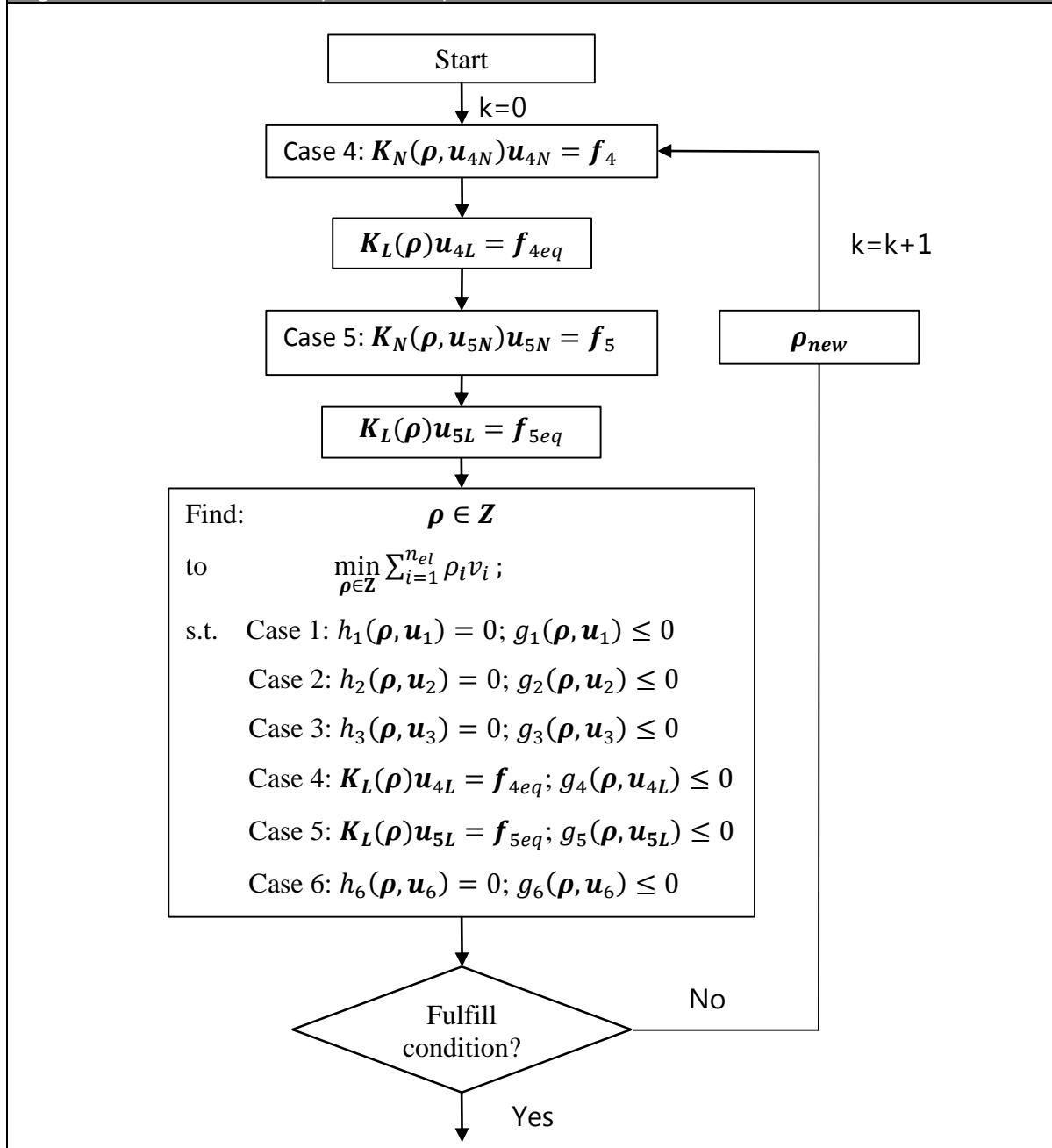
Case 6, parallel vertical forces acting on the wheel centers.

The loads from the road and the loads from the drive unit are applied simultaneously in the optimization cases.

7.3.2 Optimization procedure

The cases 1, case 2 and case 3 are associated with suspension compliance. Thus, optimizations for these three cases are solved by the linear method.

Figure 7.3: Flowchart of the optimization procedure



Optimizations in load cases 4 and case 5 associated with suspension kinematics involve large displacements. In these cases, the relations between loads and displacements are non-linear, which makes the optimization have to consider the geometric non-linear problem. The case 6 is equivalent to optimization case with small displacements by constraining the z-DOF of the spring base. If the suspension K&C analysis is considered to be a quasi-static process, optimization is treated as an implicit static problem. The

procedure for solving this problem using ESL method is illustrated in the flowchart in Figure 7.3.

The steps for the whole process are as follows:

Step 1. Set the initial design variables, the parameters and the jump-out conditions (the cycle number $k=0$; the design variables $\boldsymbol{\rho}^k = \boldsymbol{\rho}^0$; the jump-out condition). The most commonly used jump-out condition is when optimization converges. For application in this section, in order to see the result of the subsequent optimization loops after convergence, the maximum number of inner and outer loops of 10 is applied as the jump-out condition.

Step 2. Perform non-linear static analysis with $\boldsymbol{\rho}^k$ in case 4 and case 5, and calculate ESLs $\mathbf{K}_L(\boldsymbol{\rho})\mathbf{u}_{4L} = \mathbf{f}_{4eq}$ and $\mathbf{K}_L(\boldsymbol{\rho})\mathbf{u}_{5L} = \mathbf{f}_{5eq}$, respectively

Step 3. Perform linear static response structural optimization with ESLs.

Step 4. If the jump-out condition is fulfilled, terminate the process; otherwise, update the design variable (element density vector $\boldsymbol{\rho}_{new}$) and go to Step 2.

7.3.3 Mathematical model

The topological optimization problem based on the SIMP considering the 6 load cases can be mathematically stated as follows.

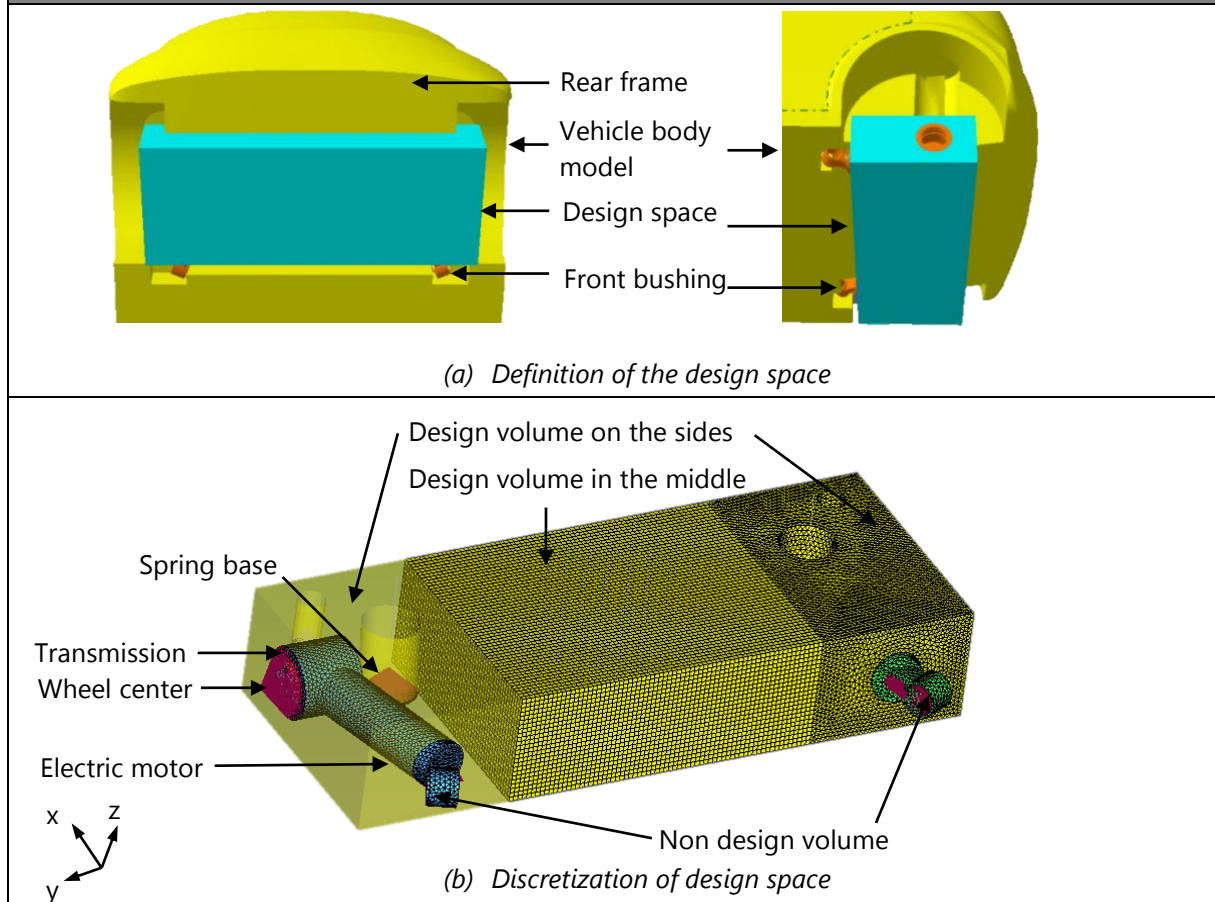
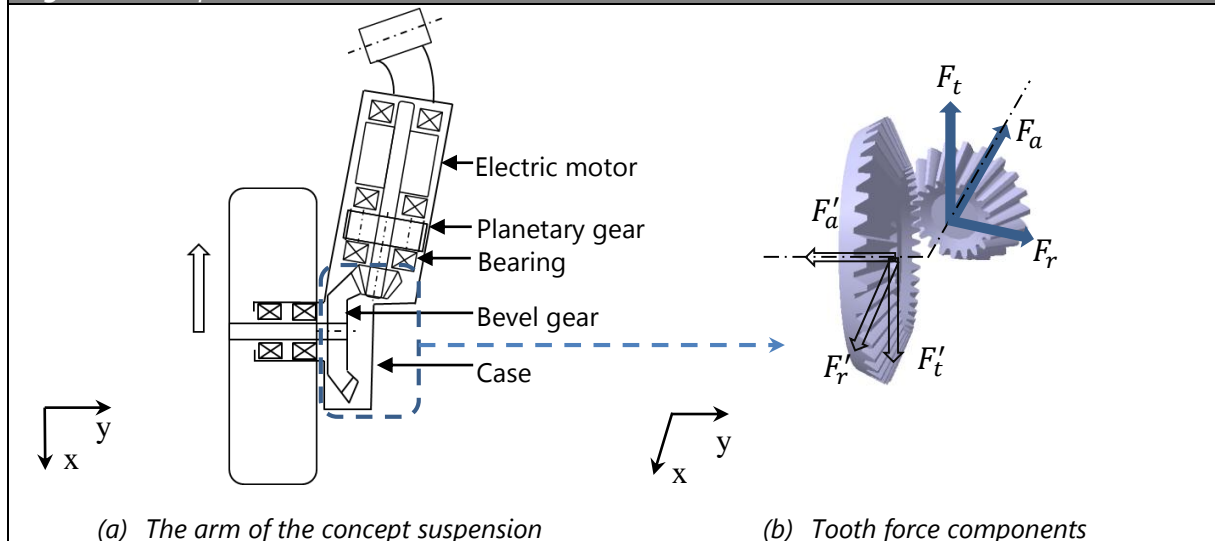
$$\begin{aligned}
 &\text{Find} && \boldsymbol{\rho} \in \mathbf{Z} && (7-13) \\
 &\text{to} && \min_{\boldsymbol{\rho} \in \mathbf{Z}} \sum_{i=1}^{n_{el}} \rho_i v_i; && 0 \leq \rho_i \leq 1, i = 1, \dots, n_{el} \\
 &\text{s.t.} && \text{case 1: } h_1: && \mathbf{K}_L(\boldsymbol{\rho})\mathbf{u}_1 = \mathbf{f}_1 \\
 &&& && g_1: \Delta x_{1l} \leq g_{1,1}(\boldsymbol{\rho}, \mathbf{u}_{1x}) \leq \Delta x_{1u}, \\
 &&& && \Delta y_{1l} \leq g_{1,2}(\boldsymbol{\rho}, \mathbf{u}_{1y}) \leq \Delta y_{1u} \\
 &&& \text{case 2: } h_2: && \mathbf{K}_L(\boldsymbol{\rho})\mathbf{u}_2 = \mathbf{f}_2 \\
 &&& && g_2: \Delta x_{2l} \leq g_{2,1}(\boldsymbol{\rho}, \mathbf{u}_{2x}) \leq \Delta x_{2u}, \\
 &&& && \Delta y_{2l} \leq g_{2,2}(\boldsymbol{\rho}, \mathbf{u}_{2y}) \leq \Delta y_{2u} \\
 &&& \text{case 3: } h_3: && \mathbf{K}_L(\boldsymbol{\rho})\mathbf{u}_3 = \mathbf{f}_3
 \end{aligned}$$

$$\begin{aligned}
g_3: \quad & \Delta x_{3l} \leq g_{3,1}(\boldsymbol{\rho}, \mathbf{u}_{3x}) \leq \Delta x_{3u}, \\
& \Delta y_{3l} \leq g_{3,2}(\boldsymbol{\rho}, \mathbf{u}_{3y}) \leq \Delta y_{3u} \\
\text{case 4: } \quad & h_4: \quad \mathbf{K}_L(\boldsymbol{\rho})\mathbf{u}_{4L} = \mathbf{f}_{4eq} \text{ (geometric non – linearity)} \\
g_4: \quad & \Delta z_{4l} \leq g_{4,1}(\boldsymbol{\rho}, \mathbf{u}_{4zL}) \leq \Delta z_{4u}, \\
& \Delta y_{4l} \leq g_{4,2}(\boldsymbol{\rho}, \mathbf{u}_{4yL}) \leq \Delta y_{4u}, \\
& \sin(-\theta_{camber}^{4u}) \leq g_{4,3}(\boldsymbol{\rho}, \mathbf{u}_{4L}) \leq \sin(-\theta_{camber}^{4l}), \\
& \tan(-\theta_{toe}^{4u}) \leq g_{4,4}(\boldsymbol{\rho}, \mathbf{u}_{4L}) \leq \tan(-\theta_{toe}^{4l}) \\
\text{case 5: } \quad & h_5: \quad \mathbf{K}_L(\boldsymbol{\rho})\mathbf{u}_{5L} = \mathbf{f}_{5eq} \text{ (geometric non – linearity)} \\
g_5: \quad & \Delta z_{5l} \leq g_{5,1}(\boldsymbol{\rho}, \mathbf{u}_{5zL}) \leq \Delta z_{5u}, \\
& \Delta y_{5l} \leq g_{5,2}(\boldsymbol{\rho}, \mathbf{u}_{5yL}) \leq \Delta y_{5u}, \\
& \sin(-\theta_{camber}^{5u}) \leq g_{5,3}(\boldsymbol{\rho}, \mathbf{u}_{5L}) \leq \sin(-\theta_{camber}^{5l}), \\
& \tan(-\theta_{toe}^{5u}) \leq g_{5,4}(\boldsymbol{\rho}, \mathbf{u}_{5L}) \leq \tan(-\theta_{toe}^{5l}) \\
\text{case 6: } \quad & h_6: \quad \mathbf{K}_L(\boldsymbol{\rho})\mathbf{u}_6 = \mathbf{f}_6 \\
g_6: \quad & \Delta z_{6l} \leq g_{6,1}(\boldsymbol{\rho}, \mathbf{u}_{6z}) \leq \Delta z_{6u}, \\
& \Delta y_{6l} \leq g_{6,2}(\boldsymbol{\rho}, \mathbf{u}_{6y}) \leq \Delta y_{6u}
\end{aligned}$$

7.3.4 Implementation with full constraints

These above functions are implicit and therefore need to use the finite-element method to solve the problem. This problem is solved with the commercial engineering software ALTAIR/OptiStruct which provides solution for structural design and optimization. The definitions of these optimization simulations are presented, and the results are discussed in this following.

The structural topological optimization problem can be generally stated as the definitions of the design variables, the responses, the constraints and the optimization objectives (Kranzeder, 2013). When the design variables and optimization objectives are specified in the initial stage, the precise definitions of the responses and the constraints meeting actual situations are the major determinant of structural topological optimization. In these simulations, 22MnB5 steel quenched in water was defined with the following properties: Young's modulus 210 000 MPa; Poisson's ratio 0.3; density 7830 kg/m³; yield strength 1000 MPa (Rautaruukki Corporation, 2014).

Figure 7.4: Topological design space**Figure 7.5:** Suspension arm combined with the electric motor

Design space: The available space for the conceptual axle is illustrated in Figure 7.4. The volumes for the bearings, the electric motor and the transmission assembly are kept in the non-design domain. The other volume is kept as the design volume of topological optimization. The whole design volume is meshed into 10 mm size. The volume in the

middle is discretized with 84 865 hexahedral elements, and the sides of the design volume are discretized with 593 765 tetrahedral elements (see Figure 7.4 (b)).

Material model: The model used for the material is the Johnson–Cook elastic–plastic material model.

Design objective: The objective of this topological optimization is to find a density distribution for which the mass is minimized. When it is considered that just one material is used in the design, the objective function is defined as minimal volume fraction.

Design variable: The element density in the design space is defined as the design variable.

Maximum number of inner and outer loops: The maximum number of inner and outer loops is 10.

Boundary conditions: The loads from the drive unit are the reaction-torques arising from the electric motor and the bearing reaction forces arising in the gear meshing process. A schematic diagram of the structure of the suspension arm combined with the drive units is shown in Figure 7.5 (a), and the reaction force on the bearings generated by the meshing of the bevel gears is illustrated in Figure 7.5 (b)) (Beitz & Grote, 2000).

The rotational DOF about axial axis of the front bushing (see Figure 7.5) is set free and the other five DOFs in each load case are constrained. In addition, the spring bases are constrained by the z displacements in load cases 1, 2, 3 and 6. The values of forces applied in each case are defined according to the analysis of the reference suspension (see Table 7.1).

<i>Table 7.1: Definition of loading conditions</i>			
No.	Loading ways	Left side	Right side
Each case	Reaction torque on electric motors along axis of electric motor, clockwise torque is positive from the rear view	$50 N \cdot m$ (clockwise)	$-50 N \cdot m$ (counter clockwise)
Each case	Bearing reaction forces at the centers of the bevel gears with directions	$F_t = 5000 N$ $F_a = 676 N$ $F_r = 1690 N$	$F_t = 5000 N$ $F_r = -676 N$ $F_a = 1690 N$
Load case 1	Parallel force at wheel centers along x-axis	$-3000 N$	$-3000 N$
Load case 2	Opposite force at wheel centers along x-axis	$3000 N$	$-3000 N$
Load case 3	Parallel force at wheel centers along y-axis	$3000 N$	$3000 N$
Load case 4	One side along z-axis, the other side fixed	$2500 N$	fixed
Load case 5	Opposite force at wheel centers along z-axis	$-1800 N$	$1800 N$
Load case 6	Parallel force at wheel centers along z-axis	$1670 N$	$1670 N$

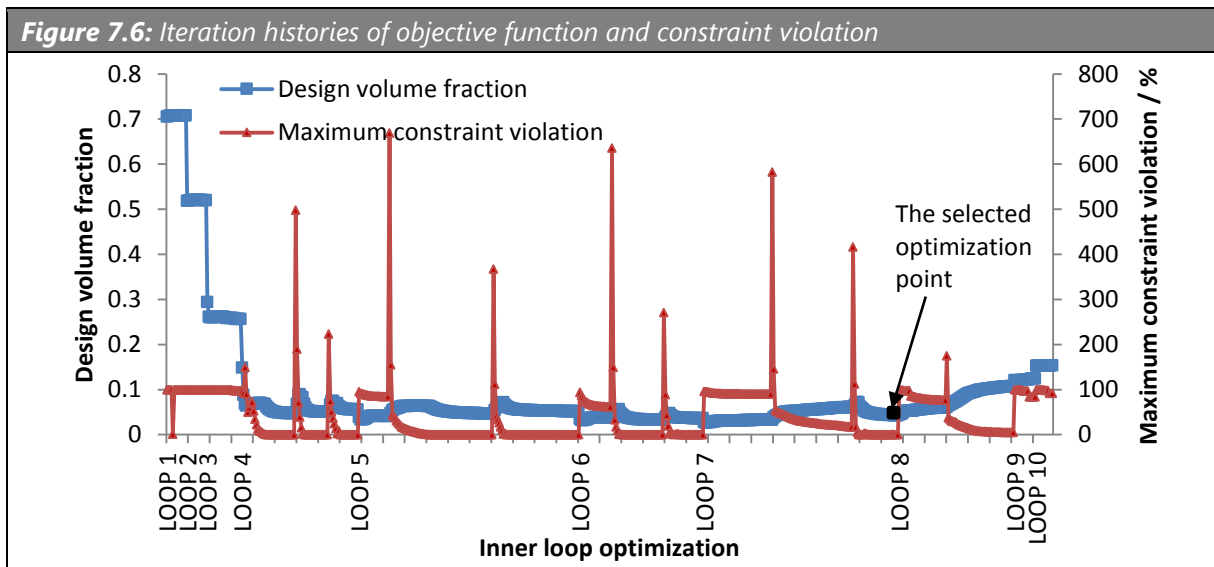
Constraints: According to Table 7.2, the constraints are defined on the responses for each load case, which is derived from test results of a reference suspension.

Interpretation of results: The implicit static geometric non-linear solver is chosen for optimization. For optimization, the software OptiStruct solves the non-linear problem by the ESL method (Altair Engineering Inc., 2014). The iteration histories of the objective function (the design volume fraction) and constraint violation are presented by the curve with full squares and by the curve with full triangles respectively in Figure 7.6. From this Figure it can be seen that the whole optimization last 10 inner and outer loops. One loop is one optimization procedure. In loops 4, 5, 6 and 7, all the constraints are satisfied, and stable converged results are achieved in these computation loops. In the last optimization step of loop 7, the lowest design volume fracture is obtained which satisfies the constraints. In loop 8, the design volume fracture increased and at least one constraint is violated. According to the output file, the constraints on the x -direction displacement of the measured nodal in subcase 4 are violated by 4.6%. It can be observed that the constraint violation of the first iteration in a new Loop results in nearly a 100% violated value, because in the new Loop the design variable is updated

and the corresponding stiffness matrix is changed on the basis of the new design variable, which lead to a new ESL for the new inner-loop optimization. This point is indicated in the optimization history.

Table 7.2: Definition of the constraints for the optimization

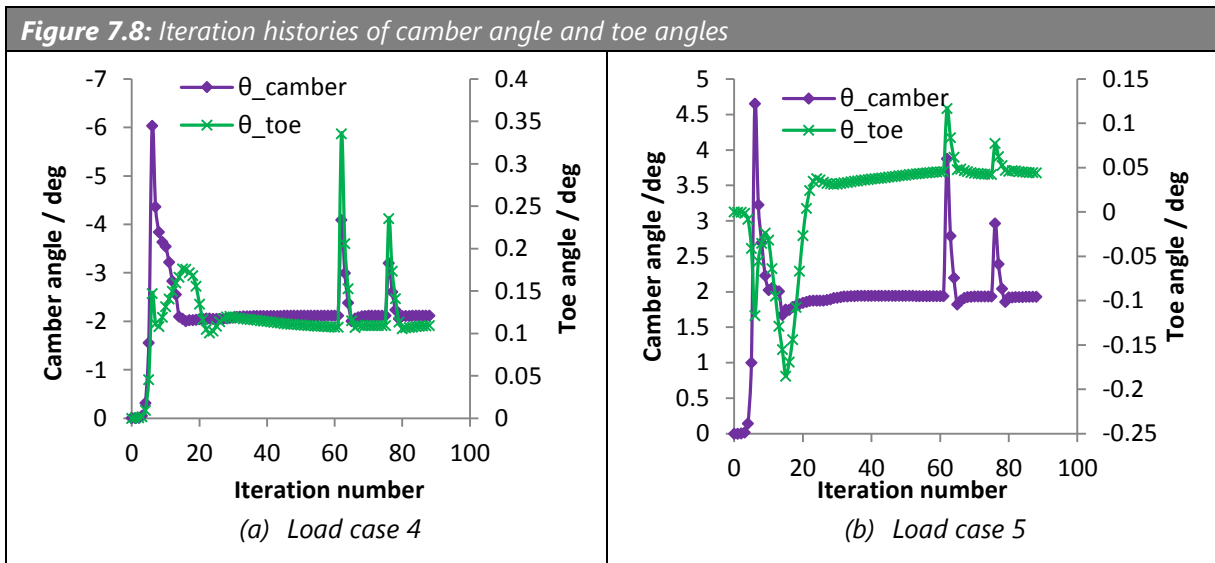
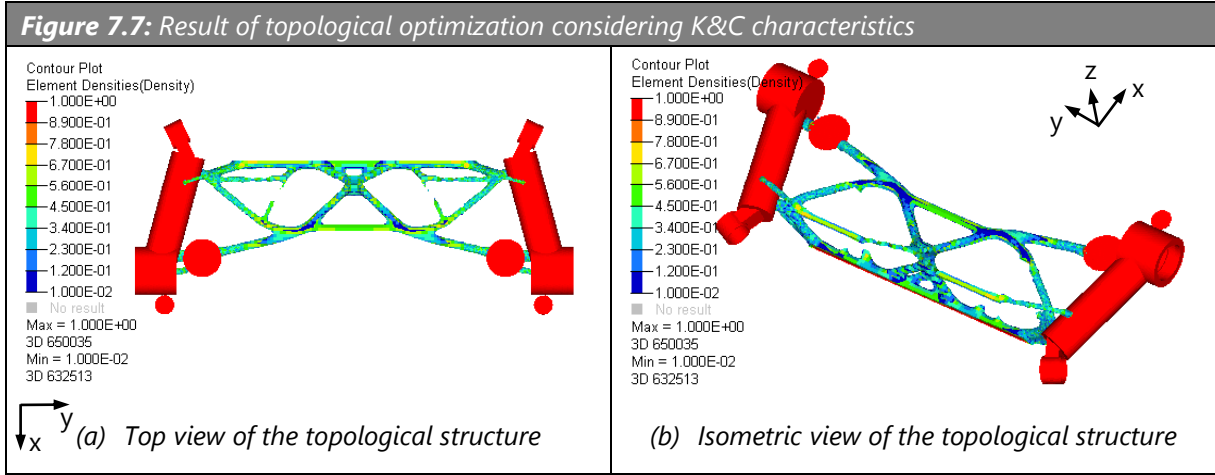
Load cases	Constraints	
Case 1	$0 \leq \Delta x \leq 0.5 \text{ mm}$	$-0.81 \text{ mm} \leq \Delta y \leq 0$
Case 2	$-0.47 \text{ mm} \leq \Delta x \leq 0$	$0 \leq \Delta y \leq 0.51 \text{ mm}$
Case 3	$0 \leq \Delta x \leq 0.48 \text{ mm}$	$0 \leq \Delta y \leq 0.5 \text{ mm}$
Case 4	$65 \text{ mm} \leq \Delta z \leq 78 \text{ mm}$ $-1.38 \text{ mm} \leq \Delta y \leq 0$	$0 \leq \sin(-\theta_{\text{camber}}) \leq 0.061$ $0 \leq \tan(-\theta_{\text{toe}}) \leq 0.0101$
Case 5	$-70 \leq \Delta z \leq -60 \text{ mm}$ $-1.45 \text{ mm} \leq \Delta y \leq 0$	$0 \leq \sin(-\theta_{\text{camber}}) \leq 0.037$ $0 \leq \tan(-\theta_{\text{toe}}) \leq 0.00319$
Case 6	$0 \leq \Delta z \leq 0.38 \text{ mm}$	$0 \leq \Delta y \leq 0.18 \text{ mm}$



The optimized structural layout indicated in the iteration history of loop 7 is shown in Figure 7.7. It can be seen that the implemented method leads to identification of a structural topology which is quite well defined.

The optimal structural configuration satisfies the K&C requirements. The iteration histories of the camber angle and the toe angle of loop 7 in load case 4 and load case 5 are presented in Figure 7.8. The wheel alignment angles in the constrained load cases are not over the boundaries. The camber angle θ_{camber} and the toe angle θ_{toe} in the

last iteration step are -2.119° and 0.109° in load case 4 and -1.929° and 0.044° in load case 5. These indicate that the suspension structure based on this topological structure can satisfy the K&C requirements.



7.3.5 Implementation without kinematic constraints

In order to identify the influence of kinematic constraints on the optimization result, topological optimization by contrast without kinematic constraints is carried out. This optimization is performed for the load cases related to suspension compliance and is formulated as (7-14). The problem does not have to consider the geometric nonlinearity, because the compliance characteristics are not associated with large displacements. Static linear optimization is implemented.

$$\begin{aligned}
 & \text{Find} && \in \mathbf{Z} && (7-14) \\
 & \text{to} && \min_{\rho \in \mathbf{Z}} \sum_{i=1}^{n_{el}} \rho_i v_i; && 0 \leq \rho_i \leq 1, i = 1, \dots, n_{el} \\
 & \text{s.t.} && \text{case 1: } h_1: \mathbf{K}_L(\boldsymbol{\rho})\mathbf{u}_1 = \mathbf{f}_1 \\
 & && g_1: 0 \leq g_{11}(\mathbf{u}_{1x}) \leq 0.5 \text{ mm}, \\
 & && \quad \quad -0.81 \text{ mm} \leq g_{12}(\mathbf{u}_{1y}) \leq 0 \\
 & && \text{case 2: } h_2: \mathbf{K}_L(\boldsymbol{\rho})\mathbf{u}_2 = \mathbf{f}_2 \\
 & && g_2: -0.47 \text{ mm} \leq g_{21}(\mathbf{u}_{2x}) \leq 0, \\
 & && \quad \quad 0 \leq g_{22}(\mathbf{u}_{2y}) \leq 0.51 \text{ mm} \\
 & && \text{case 3: } h_3: \mathbf{K}_L(\boldsymbol{\rho})\mathbf{u}_3 = \mathbf{f}_3 \\
 & && g_3: 0 \leq g_{31}(\mathbf{u}_{3x}) \leq 0.48 \text{ mm}, \\
 & && \quad \quad 0 \leq g_{32}(\mathbf{u}_{3y}) \leq 0.5 \text{ mm} \\
 & && \text{case 4: } h_4: \mathbf{K}_L(\boldsymbol{\rho})\mathbf{u}_4 = \mathbf{f}_4 \\
 & && g_4: 0 \leq g_{41}(\mathbf{u}_{4z}) \leq 0.38 \text{ mm}, \\
 & && \quad \quad 0 \leq g_{42}(\mathbf{u}_{4y}) \leq 0.18 \text{ mm}
 \end{aligned}$$

The result is shown in Figure 7.9 which proposes a structure with a cross beam connecting the bodies of the drive units and a lateral beam connecting the rear of the drive units. The structure meets the stiffness requirements; however, because of the lateral beam the structure apparently does not meet the kinematics requirements. The camber angles and toe angles in these two optimization results are presented in Table 7.3. In load case 4, the camber angle reaches 8.624° , which is 147% over the boundary 3.497° ; in load case 5, the camber angle reaches 3.170° , which is 49% over the boundary 2.120° . These results indicate that the suspension structure depending on this topological structure does not satisfy the K&C requirements.

7.4 Implementation of size optimizations

The topological optimization result is interpreted into tube structures with different thicknesses as shown in the Figure 7.10. The size optimization is applied to obtain an optimum dimension on the basic of the design topology.

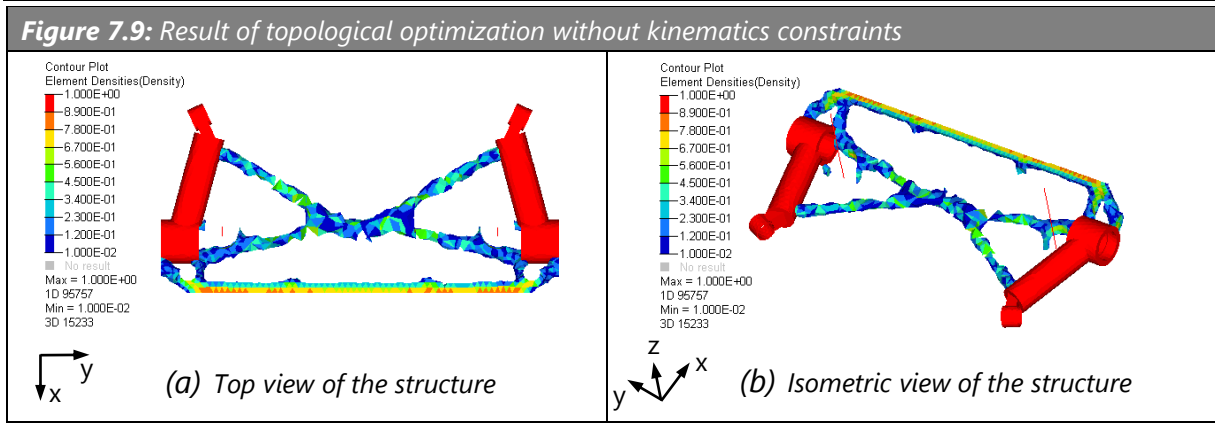


Table 7.3: Definition of the constraints for the optimization

	Case 4		Case 5	
	Camber angle	Toe angle	Camber angle	Toe angle
Limitation	-3.497°	0.579°	2.120°	0.183°
Definition 1	-2.119°	0.109°	1.929°	0.044°
Definition 2	-8.624°	0.333°	3.170°	0.157°

7.4.1 Problem formulation

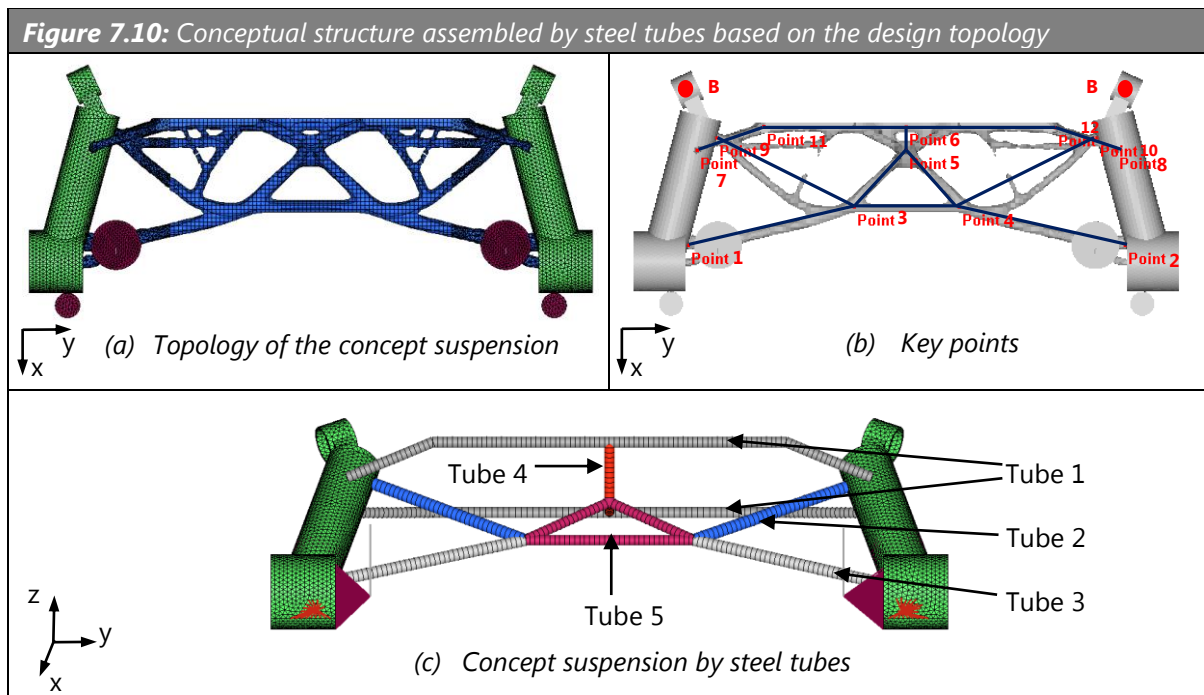
For the size optimization, the objective is to find an optimal element size by which the design satisfies the constraints with a minimized mass. The dimensions of cross sections of the tube elements are defined as the design variables i.e. the outer diameter D_{i_outer} and the inner diameter D_{i_inner} of the tube elements. The load cases, responses and constraints are kept the same as the definition of topology optimization (definition 1). In the size optimization, the element density ρ keeps constant; the design variable i.e. tube diameters vector \mathbf{D} is constrained in a scope \mathbf{Z} . The K&C of the concept suspension and structure geometric non-linearity are also considered. Thus, the optimization problem is formulated as follows.

$$\begin{aligned}
 &\text{Find} && \mathbf{D} \in \mathbf{Z} && (7-15) \\
 &\text{to} && \min_{\mathbf{D} \in \mathbf{Z}} \sum_{i=1}^{n_{tube}} \rho_i v_i(D_i)
 \end{aligned}$$

$$\begin{aligned}
 &D_{i_outer_min} \leq D_{i_outer} \leq D_{i_outer_max} \\
 &D_{i_inner_min} \leq D_{i_inner} \leq D_{i_inner_max} \\
 & i = 1, \dots, n_{tube} \\
 \text{s.t.} \quad &h_i(\mathbf{e}, \mathbf{u}) = 0, i \in E \\
 &g_i(\mathbf{e}, \mathbf{u}) \leq 0, i \in I
 \end{aligned}$$

7.4.2 Implementation

The size optimization is implemented on the basis of the structure topology. In the preliminary size optimization, the key points picked from the structural topology are used to define the geometries of the suspension structure as shown in Figure 7.10 (b). The pivot points B are the anchor points. The points 13, 14, 15, 16 and 17 are not indicated in this picture. They are the symmetric points of 11, 12, 8, 7 and 6 about the x-y plane, respectively.



On the basis of the keypoint position, steel tubes are utilized as the basic components to assemble the suspension structure. According to their functions and positions, the tubes are divided into five groups with different thickness of their cross sections (Figure 7.10 (c)). The dimensions of the cross sections are set as the design variables. At initial design, the dimensional variables can be arranged with a wide range so as to fulfill the requirements. The preliminary size optimization on the basis of previous topological

optimization probably produces a result that meets all the constraints but with unfeasible dimensions, for example the thickness of the tubes maybe is too thin. In this case, the cross section dimensions and thickness of the tubes can be further optimized by size optimization with a tight range, until achieve an appreciate result.

Figure 7.11: Iteration histories of objective function and constraint violation in size optimization

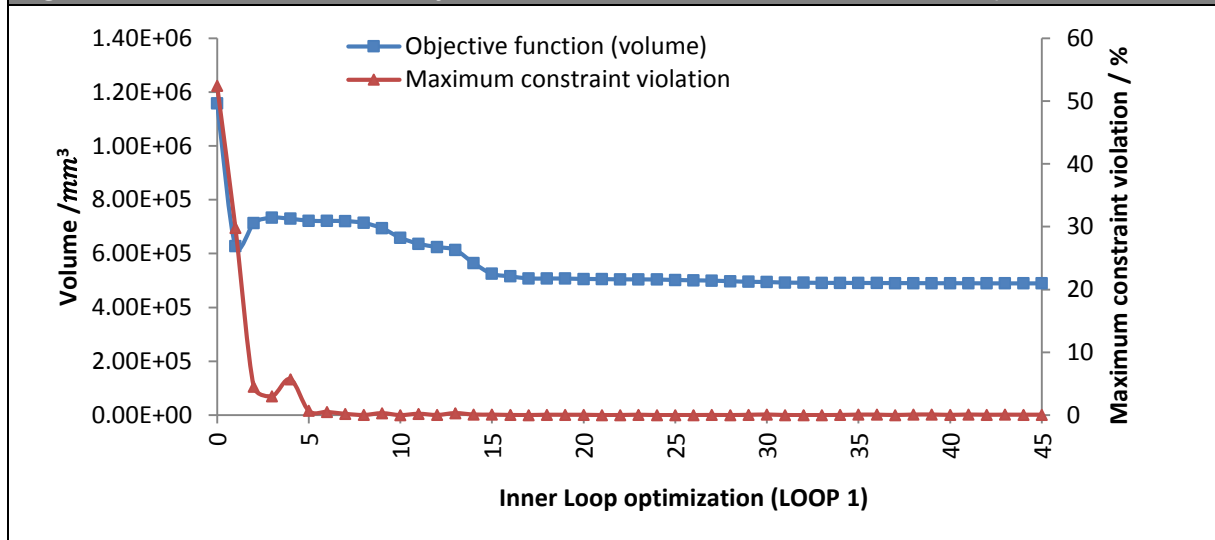
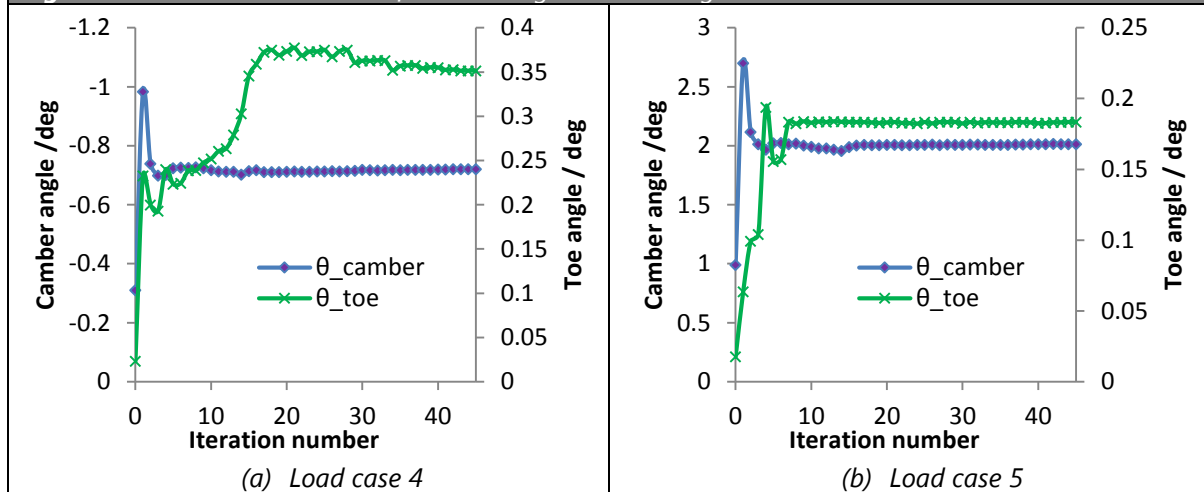


Figure 7.12: Iteration histories of camber angle and toe angles



The iteration histories of the objective function and constraint violation in the optimization are shown in Figure 7.11. The optimization process lasts only one loop. The red curve shows that the optimization result meets all the constraint requirements. The feasible result is given in Table 7.4. The total mass of the resultant structure is 3.76 kg. The center beam of the reference twist beam axle equipped in the benchmark car

weights 8 kg. The concept suspension linkage with the new structural topology is 53% lighter than the center beam of the reference suspension.

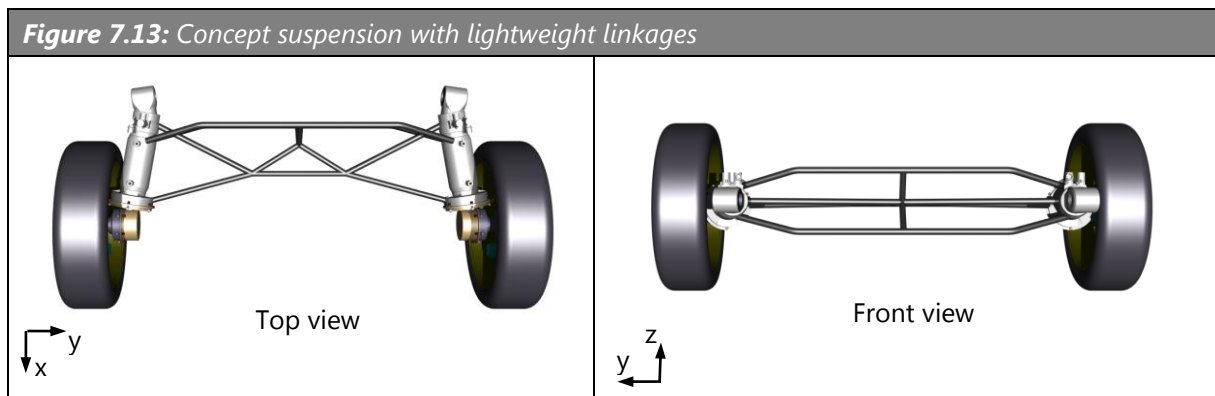
The iteration histories of the camber and toe angles under load case 4 and load case 5 in the size optimization are shown in Figure 7.12, from which we can know both the camber angle and the toe angle converge inside the constraints.

Table 7.4: Results of the size optimization

	Outer radius (mm)	Thickness (mm)	Mass (kg)
Tube 1	12.1	1.2	1.35
Tube 2	12.1	1.1	0.43
Tube 3	11.5	3.0	1.14
Tube 4	13.7	2.7	0.36
Tube 5	11.8	1.2	0.48


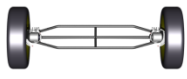
7.5 Result comparisons

According to the size optimization results, the concept suspension with lightweight linkages is constructed (see Figure 7.13).



The concept suspensions are compared with the reference suspension in terms of mass and K&C characteristics. The K&C analysis results of the suspension structures are presented in Table 7.5. From this table we can see that in case 1, case 2, case 3 and case 5, the structure stiffness of the concept structure is stronger than that of the reference suspension. In case 4, the kinematics characteristics of the concept structure perform better than those of the reference suspension.

Table 7.5: Comparison of K&C characteristics of reference and concept suspensions

Items		Reference suspension	Concept suspension 1
Structure			
Mass of the center Linkage	m	8 kg	3.76 kg
Case 1: Compliance under lateral parallel forces 3000 N	$ \Delta y $	0.81 mm	0.75 mm
	$ \Delta x $	0.5 mm	0.34 mm
Case 2: Compliance under lateral opposite forces 3000 N	$ \Delta y $	0.51 mm	0.20 mm
	$ \Delta x $	0.47 mm	0.09 mm
Case 3: Compliance under longitudinal forces 3000 N	$ \Delta x $	0.48 mm	0.06 mm
	$ \Delta y $	0.5 mm	0.11 mm
Case 4: Kinematics under one side fixed and one side vertical force 2500 N	$ \Delta z $	75.4 mm	69.3 mm
	$ \Delta x $	7.18 mm	5.04 mm
	$ \Delta y $	1.38 mm	1.33 mm
	$ \theta_{\text{camber}} $	3.497°	0.721°
	$ \theta_{\text{toe}} $	0.579°	0.351°
Case 5: Kinematics under opposite vertical forces 1800 N	$ \Delta z $	-68.9 mm	-75 mm
	$ \Delta x $	5.36 mm	5.64 mm
	$ \Delta y $	1.45 mm	2.28 mm
	$ \theta_{\text{camber}} $	2.120°	2.01°
	$ \theta_{\text{toe}} $	0.183°	0.183°
Case 6: Compliance under parallel vertical forces 1670 N	$ \Delta z $	0.38 mm	0.35 mm
	$ \Delta y $	0.18 mm	0.03

In case 5, the displacements under torsion of the concept structure in x-axis and y-axis are larger than those of the reference suspension. From this aspect the concept structure is worse. However, the changes in the camber angle and the toe angle of the concept structure are smaller than those of the reference suspension. This means that from this aspect the concept structures are better. The wheel alignment angles are more significant parameters than the displacements in suspension kinematics. Therefore, the concept structures have better K&C characteristics than the reference structure does in case 5.

From the comparisons it can be concluded that the concept suspension linkages obtained by the developed approach are lighter than the reference structure; furthermore, the K&C characteristics of the concept suspensions do not deteriorate because of the mass reduction.

8 Modelling and analyzing ride dynamics of the concept suspension

This chapter deals with the issue of modelling and analysis of the concept suspension with regard to ride dynamics under stochastic road inputs. This model offers the opportunity to explore design variables of the concept suspension with numerical results. The influence of the concept suspension parameters on vehicle ride and road-holding performance should be investigated.

In this chapter, the following problems are solved:

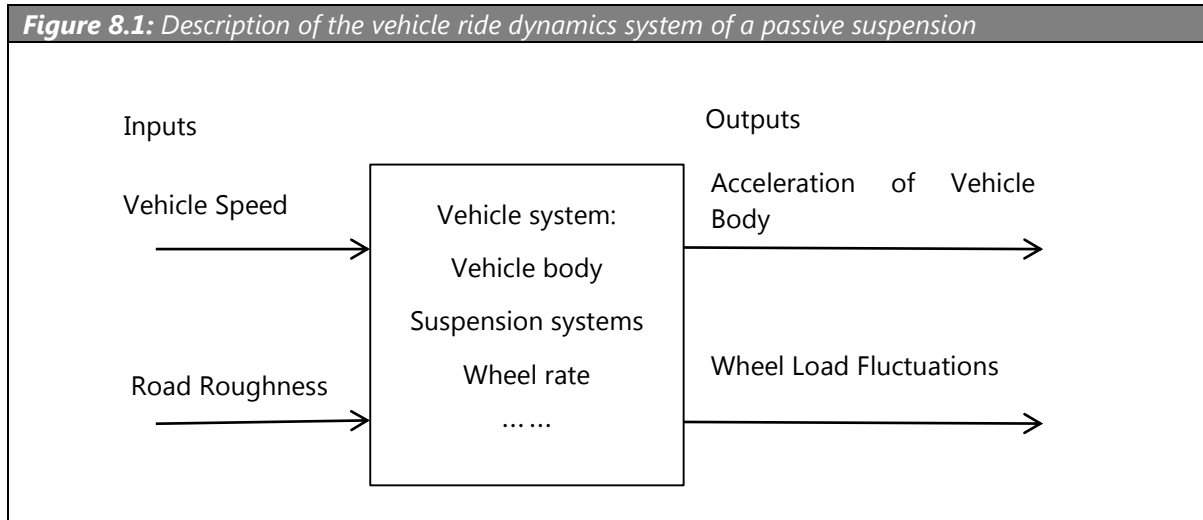
The analytical models of the concept and reference suspensions are developed, respectively. These models incorporate not only the parameters of mass-spring-damper system but also axle geometries and the torsional stiffness of suspension linkages.

The double lane models of road irregularity are built to simulate the road surface roughness which is stochastic excitation of the vehicle system in terms of ride dynamics when the vehicle drives on the road.

The simulations of the concept suspension under the excitation from the road of different roughness are carried out. The vehicle simulation results with the concept suspension are compared to that with reference suspensions in terms of the ride dynamics.

8.1 Ride dynamics system

The diagram in Figure 8.1 illustrates the ride dynamics system of a passive suspension. The inputs of this system are road irregularities and vehicle speed which are the major factors generating the acceleration of vehicle body. The system is vehicle characteristics such as suspension systems, the vehicle body and tires. The outputs are simulation results expressing ride comfort and stability, for example vehicle body accelerations and wheel load fluctuations.



In the Table 2.1, the usual modelling and simulation methods are summarized. Both the analysis model and MBS model are available for the simulation of vehicle ride dynamics with road excitation. However, MBS modelling and further modification are time-consuming and more suitable for the detailed design (see Figure 1.7) when most of the system parameters are determined. In the initial conceptual design phase, an accurate and flexible analysis model with rapid response is appropriate. Therefore, an analytical dynamic model without the complexity of multi-body codes while still capturing the basic vibration modes of rigid-body sprung and unsprung masses is introduced in this chapter.

The vehicle dynamic system can be assumed to be a linear, time-invariant system. In a linear, time-invariant system there is a certain relationship between the input and output signals. In a mathematical view, the dynamic system for vibration with n degrees of freedom can be generally expressed by the following second order linear inhomogeneous differential equations (Wijker, 2004). In a general form is

$$[M]\{\ddot{x}\} + [K]\{\dot{x}\} + [C]\{x\} = \{y\} \quad (8-1)$$

Where, M is the mass matrix; K is the damping matrix; C is the stiffness matrix; y is the system excitation and x is the system response.

For a second order non-homogeneous linear differential equation, the solution is composed of a general solution x_{hom} which is its homogenous differential equation

and a particular solution x_{part} , which is written as follows (Mitschke & Wallentowitz, 2004):

$$x = x_{hom} + x_{part} \quad (8-2)$$

where, x_{hom} is associated with the property of the system; x_{part} is associated with the input signals. According to the characteristics of linear systems, the frequency distribution of system response should be the same as the input signals. Therefore, the frequency range of the system response is equal to the statistical data of the road surface. A periodic function or impulse function cannot completely reflect road characteristics. Only if the input signals completely describe the road irregularity in the frequency domain, the characteristics of the system vibration can be investigated thoroughly.

Power spectrum density (PSD) in the frequency domain is normally used to express the random signals in time domain (Oppenheim & Verghese, 2015). The PSD describes the energy distribution of signals in frequency. The Fourier transform is used for the process of signals converting from an arbitrary form in the time domain to a harmonious form in the frequency domain.

$$F(\omega) = \int_{-\infty}^{+\infty} f(t)e^{-j\omega t} dt \quad (8-3)$$

Where, t means time variable; ω ($\omega = 2\pi f$; f is time frequency) is angular frequency, rad/s ; $f(t)$ is a time signal and $F(\omega)$ is its corresponding frequency signal. The inverse Fourier transform can be written as follows.

$$f(t) = \frac{1}{2\pi} \int_{-\infty}^{+\infty} F(\omega)e^{j\omega t} d\omega \quad (8-4)$$

The mathematic definition of the PSD is given the following equation (Brandstätter, 2013).

$$\Phi(\omega) = \lim_{T \rightarrow \infty} \frac{1}{T} |F_T(\omega)|^2, \quad (-\infty < \omega < +\infty) \quad (8-5)$$

where T means the time duration, which is used to truncate the indefinite stationary random signal (assuming the road profile statistics is a stationary random process) and thus the signals in this time interval contains all the frequency composition; $F_T(\omega)$ is the Fourier transform of the signal in the time duration T .

8.2 Ride dynamics model

8.2.1 Analytical models of vehicle ride dynamics

A simple and most commonly used model for vehicle ride dynamics is the quarter-car suspension system (Fongue, et al., 2014) (Kurzeck & Kaiser, 2013) (Agostinacchio, et al., 2013) (see Figure 8.2 (a)). This model can be expressed by the following equations (Mitschke & Wallentowitz, 2004).

$$m_2 \ddot{z}_2 + k_2(\dot{z}_2 - \dot{z}_1) + c_2(z_2 - z_1) = 0 \quad (8-6)$$

$$m_1 \ddot{z}_1 - k_2(\dot{z}_2 - \dot{z}_1) - c_2(z_2 - z_1) = c_1(\dot{h} - \dot{z}_1) \quad (8-7)$$

In this equation, h is the road excitation related to the vehicle speed; \ddot{z}_2 is the vertical acceleration of the vehicle body that is relevant to the ride comfort; \dot{z}_2 is the vertical vibration speed of the vehicle body; z_2 is the vertical displacement of the vehicle body; \ddot{z}_1 is the vertical acceleration of the wheel that is relevant to the wheel load fluctuation and significant parameter to assess drive stability; \dot{z}_1 is the vertical vibration speed; z_1 is the vertical vibration displacement; m_1 is the unsprung mass; m_2 is the sprung mass; k_2 is the suspension damping; c_2 is the suspension stiffness and c_1 is the wheel stiffness. However, this model contains no information of the geometrical parameters of suspension axles.

Half vehicle simulation models can be classified to pitch plane and roll plane models (Cao, et al., 2010). The pitch plane model is mainly applied for stiffness tuning of front-rear vehicle suspensions under driving and braking maneuvers (Odhams & Cebon, 2006) (Cao, et al., 2008). The roll plane model is usually used in the analysis of the vehicle ride and roll performance (Cao, et al., 2010). The enhancement of the roll-stability using the anti-roll bar is at the cost of ride comfort deterioration (Cole, 2000).

The suspension axle geometry and K&C also strongly influence the roll dynamics (Sharp, 2001). The influence analysis of the axle geometries on vehicle roll motion and ride quality could provide certain insights on axle geometry design.

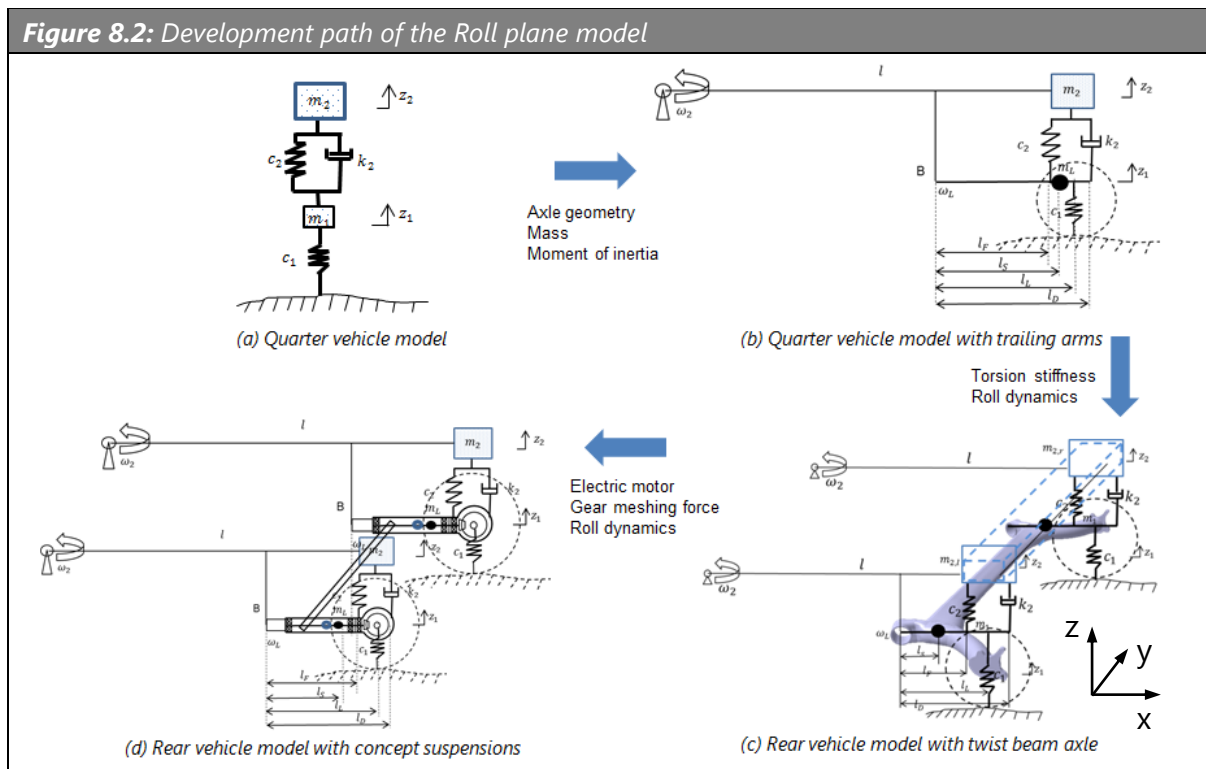
Full vehicle simulation model under the road excitations involves more information of vehicle motions, including four vibration modes: bounce, roll, pitch and warp (Wilde, et al., 2005). Therefore, the vertical, pitch and roll dynamics can be investigated by full vehicle model. For example, a roll- and pitch-plane coupled hydro-pneumatic suspension was modeled and simulated by the full vehicle model with response prediction of full vehicle motions (Cao, et al., 2010) (Cao, et al., 2010) (Cao, 2008). The effect of anti-roll bars on the roll dynamics was explained in a full vehicle simulation, which indicates that the torsional stiffness should not be neglected in the vehicle comfort analysis involving roll dynamics (Iliev, 2011).

8.2.2 Modelling of the concept suspension

Figure 8.2 shows the process of modeling the concept suspension with regard to ride dynamics under stochastic road inputs. The target vehicle is assumed to be symmetrical laterally and longitudinally, and movements of front and rear axles are independent. The quarter vehicle model (see Figure 8.2 (a)) has no axle geometry information and the quarter model with a trailing arm was introduced by Mitschke and Wallentowitz (Mitschke & Wallentowitz, 2004) (see Figure 8.2 (b)) to consider the geometry of the trailing arm in longitudinal direction. Because the left and right wheels of the concept suspension are connected by the lightweight linkage i.e. the motions on one side affect the motions on the other side, the quarter models are insufficient to investigate the effect of the torsional stiffness of the linkage on ride dynamics.

The ride dynamics models of the rear vehicle equipped with the reference and concept suspensions are illustrated in Figure 8.2 (c) and Figure 8.2 (d), respectively. They are used to simulate and compare the vertical and roll dynamics of the reference and concept suspensions. In modelling the concept suspension, axle parameters (including axle geometry, mass and moment of inertia), torsion stiffness and electric motor

parameters (including motor reaction force and motor vibration force) are taken into account. The double lane road is stochastic excitation of vehicle ride dynamics. The influence of conceptual suspension parameters on ride quality and road-holding performance should be investigated. This offers the opportunity to explore design variables of the conceptual suspension with numerical results. Vertical acceleration of vehicle body, roll acceleration, wheel load fluctuation and suspension travel are the critical performance when comparing ride dynamics.



Considering the structure symmetry of the left and right side, the suspension of single side is treated as the study object (see Figure 8.3). The sprung mass m_2 locates on the rear axle and rotates around the front axle with the rotational speed ω_2 . The trailing arm integrated with the electric motor rotates around pivot point B of the vehicle body with rotation speed ω_L , in addition to which it also carries out the motion due to that of the vehicle body. The total mass of the trailing arm, electric motor, gears and other parts fixed to the arm (such as calipers of the disc brake) is expressed by m_L . The parts fixedly connected with the wheel (the tire, the wheel hub and the brake disc) amount to the mass m_R .

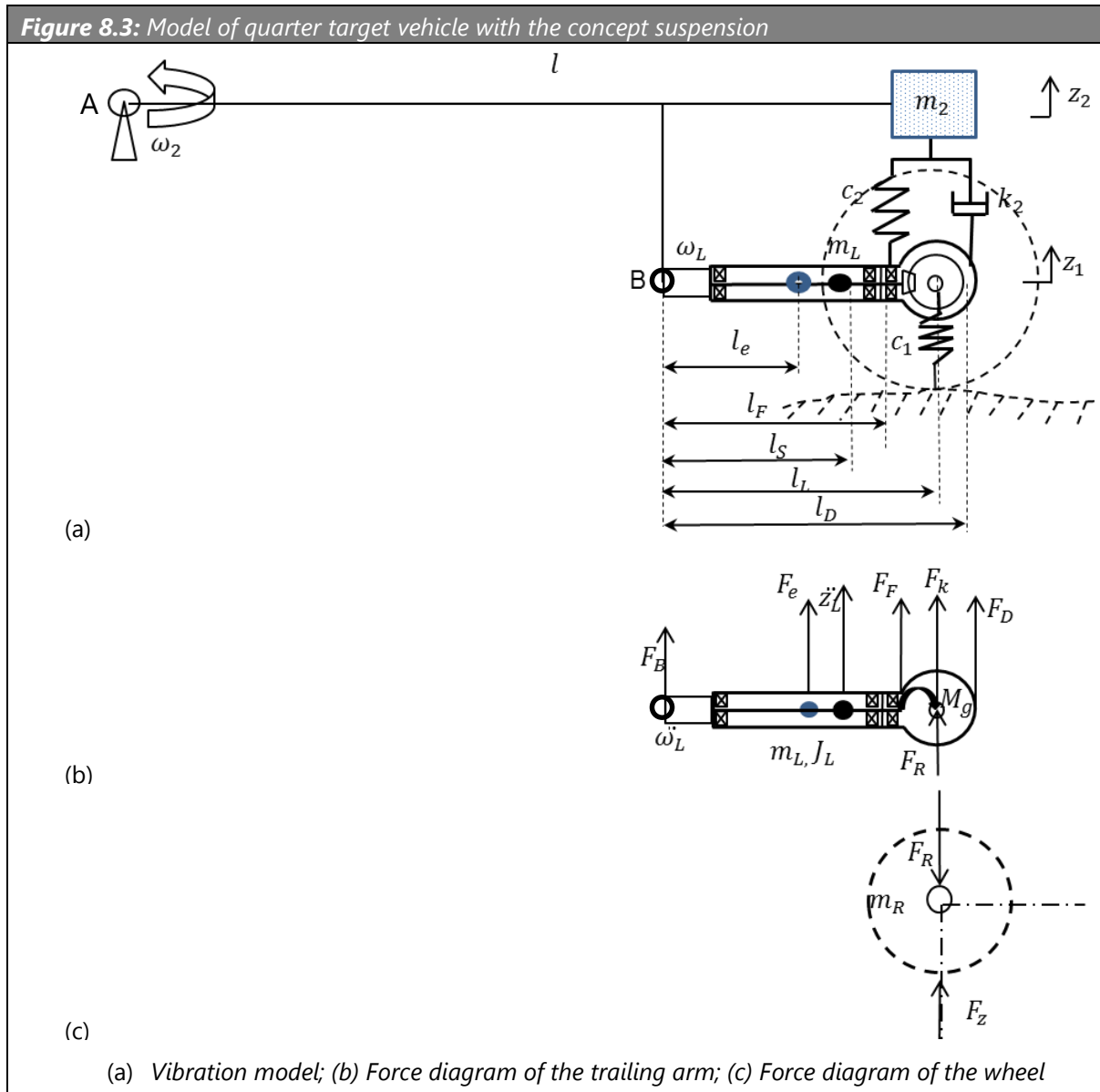
The torque equation around the front axle denoted by the pivot A can be written as equation (8-8).

$$m_2 l^2 \ddot{\omega}_2 = -F_F(l - l_L + l_F) - F_D(l - l_L + l_D) - F_B(l - l_L) \quad (8-8)$$

The vertical dynamic equation of the trailing arm can be as follows.

$$m_L \ddot{z}_L = F_F + F_D + F_B + F_R + F_k + F_e \quad (8-9)$$

where, F_F is the spring force, F_D is the damping force, F_B is the force on the pivot point B, F_R is the reaction force from the wheel center, F_k is the force caused by the torsion stiffness due to irregular travel displacements of the left and right wheels, F_e is the vibration force from the electric motor.



The spring force can be written as follows.

$$F_F = c_2 \frac{l_F}{l_L} (z_2 - z_1) \quad (8-10)$$

where, z_1 is the vertical displacement of the wheel center.

The vertical force generated by the damper can be written in (8-11).

$$F_D = k_2 \frac{l_D}{l_L} (\dot{z}_2 - \dot{z}_1) \quad (8-11)$$

The force on the left side of the suspension due to torsion stiffness can be modeled as follows.

$$F_{k,l} = -c_k \left[\left(z_{1,l} - \frac{l-l_L}{l} z_{2,l} \right) - \left(z_{1,r} - \frac{l-l_L}{l} z_{2,r} \right) \right] / 2 \quad (8-12)$$

where, c_k is the torsion stiffness of the suspension structure, and the difference of the vertical displacement of the left and right wheel center is expressed by the following equation.

$$s_{k,l} = \left(z_{1,l} - \frac{l-l_L}{l} z_{2,l} \right) - \left(z_{1,r} - \frac{l-l_L}{l} z_{2,r} \right) \quad (8-13)$$

The force F_e produced by the vibration of the electric motor in the vertical direction can be simulated depending on ISO standard (ISO 1940-1:1986, 1986).

$$F_e = m_{Rotor} e \omega^2 \sin \omega t \quad (8-14)$$

where, e refers to eccentricity of the rotor, and m_{Rotor} is the mass of the rotor.

The torque dynamic equation to the trailing arm can be written as equation (8-15).

$$J_L \ddot{\omega}_L = F_R(l_L - l_S) + F_D(l_D - l_S) + F_F(l_F - l_S) - F_B l_S + F_k(l_L - l_S) - F_e(l_S - l_e) - M_g \quad (8-15)$$

where, l_S is the longitudinal distance from the gravity center of the trailing arm to the pivot B, l_e is the longitudinal distance from the gravity center of the electric motor to the pivot B, and M_g is the reaction rotational torque on the gear box produced in the gear meshing.

$$M_g = F_g l_g \quad (8-16)$$

where, F_g is the vertical force on gear meshing; l_g is the longitudinal distance between the driving gear center and driven gear center. The gear meshing force can be roughly calculated as follows.

$$F_g = F_d \frac{R_w}{R_g} \quad (8-17)$$

where, F_d is driving force on the wheel; R_w is radius of the wheel; R_g is gear pitch circle of the driven bevel gear.

The vertical dynamic equation about the wheel can be written as follows.

$$m_R \ddot{z}_1 = F_Z - F_R \quad (8-18)$$

In this equation, F_Z is the vertical force caused by the wheel rolling on the uneven ground. It can be written as follows.

$$F_Z = c_1(h - z_1) \quad (8-19)$$

According to the kinematic relationship, the vertical motion z_2 of unsprung mass m_2 can be expressed by the rotational angle φ_2 .

$$z_2 = l\varphi_2 \quad (8-20)$$

The vertical motion z_l of the gravity center of the trailing arm can be expressed by the motions z_2 and z_1 .

$$z_l = \frac{l_s}{l_L} z_1 + \left(1 - \frac{l_s}{l_L}\right) \frac{l - l_L}{l} z_2 \quad (8-21)$$

The rotational angle of the trailing arm can be expressed by the motions z_2 and z_1 .

$$\varphi_L = \frac{1}{f_L} \left(z_1 - \frac{l - l_L}{l} z_2 \right) \quad (8-22)$$

From the equation (8-8), (8-9), (8-15) and (8-18), a set of 2 degrees of freedom differential equations of the rear vehicle can be built as the equation (8-16) and (8-17).

$$\begin{aligned}
& \left[m_2 + m_a \left(\frac{l-l_L}{l} \right)^2 \left(1 - \frac{f_{Sges}}{l_L} \frac{1}{H} \right) \right] \ddot{z}_2 \\
& + k'_2 \left(\frac{l_D}{l_L} \right)^2 \left[\frac{1}{H} + \frac{l_L}{l} \left(1 - \frac{1}{H} \right) \right] (\dot{z}_2 - \dot{z}_1) \\
& + c'_2 \left(\frac{l_F}{l_L} \right)^2 \left[\frac{1}{H} + \frac{l_L}{l} \left(1 - \frac{1}{x} \right) \right] (z_2 - z_1)
\end{aligned} \tag{8-23}$$

$$\begin{aligned}
& = c_1 \left[\frac{l-l_L}{l} \left(1 - \frac{1}{H} \right) \right] (h - z_1) + \frac{F_k(l-l_L)}{l} - F_k \left(\frac{l-l_L}{l} \right) \frac{1}{H} \\
& + \frac{F_e(l-l_L)}{l} - F_e \frac{l_e}{l_L} \left(\frac{l-l_L}{l} \right) \frac{1}{H} + \frac{M_g}{l_L} \left(\frac{l-l_L}{l} \right) \frac{1}{H} \\
& m_a \left(\frac{i_B}{l_L} \right)^2 \ddot{z}_1 - m_a \left(\frac{i_B}{l_L} \right)^2 \left[\frac{l-l_L}{l} \left(1 - \frac{1}{H} \right) \right] \ddot{z}_2 - k'_2 \left(\frac{l_D}{l_L} \right)^2 (\dot{z}_2 - \dot{z}_1) \\
& - c'_2 \left(\frac{l_F}{l_L} \right)^2 (z_2 - z_1) = c_1(h - z_1) + \frac{F_e l_e}{l_L} + \frac{F_k l_L}{l_L} - \frac{M_g}{l_L}
\end{aligned} \tag{8-24}$$

where, the mass m_a includes the combined trailing arm mass m_L and the wheel mass m_R .

$$m_a = m_L + m_R \tag{8-25}$$

f_{Sges} means the distance from the total gravity center of the arm and wheel to the point B;

$$f_{Sges} = \frac{m_L l_S + m_R l_L}{m_L + m_R} \tag{8-26}$$

In order to show the relationship clearly, here introduce a correlative coefficient H .

$$H = \frac{J_B}{m_a l_{Sges} l_L} = \frac{i_B^2}{l_{Sges} l_L} \tag{8-27}$$

where, J_B is the total moment of inertia of the arm and wheel around axis y at point B; i_B is the radius of gyration of the link and wheel around axis y at point B.

$$J_B = m_a i_B^2 = J_L + m_R l_L^2 + m_L l_S^2 \tag{8-28}$$

8.2.3 Modelling of the reference suspension

The method of modelling the benchmark suspension is analogous to the above concept suspension, see Figure 8.4. The trailing arm of the referential suspension is not

combined with an electric motor. Comparing Figure 8.4 (b) to Figure 8.3 (b), there is no torque M_g produced from gear meshing and no electric motor force F_e .

The torque equation around pivot point A:

$$m_2 l^2 \ddot{\omega}_2 = -F_F(l - l_L + l_F) - F_D(l - l_L + l_D) - F_B(l - l_L) \quad (8-29)$$

The vertical dynamic equation to the trailing arm:

$$m_L \ddot{z}_L = F_F + F_D + F_B + F_R + F_k \quad (8-30)$$

The torque dynamic equation to the trailing arm:

$$J_L \ddot{\omega}_L = F_R(l_L - l_S) + F_D(l_D - l_S) - F_F(l_S - l_F) - F_B l_S + F_k(l_L - l_S) \quad (8-31)$$

The vertical dynamic equation to the wheel:

$$m_R \ddot{z}_1 = F_Z - F_R \quad (8-32)$$

Kinematic relationship of the motions can be expressed as follows:

$$z_2 = l\varphi_2 \quad (8-33)$$

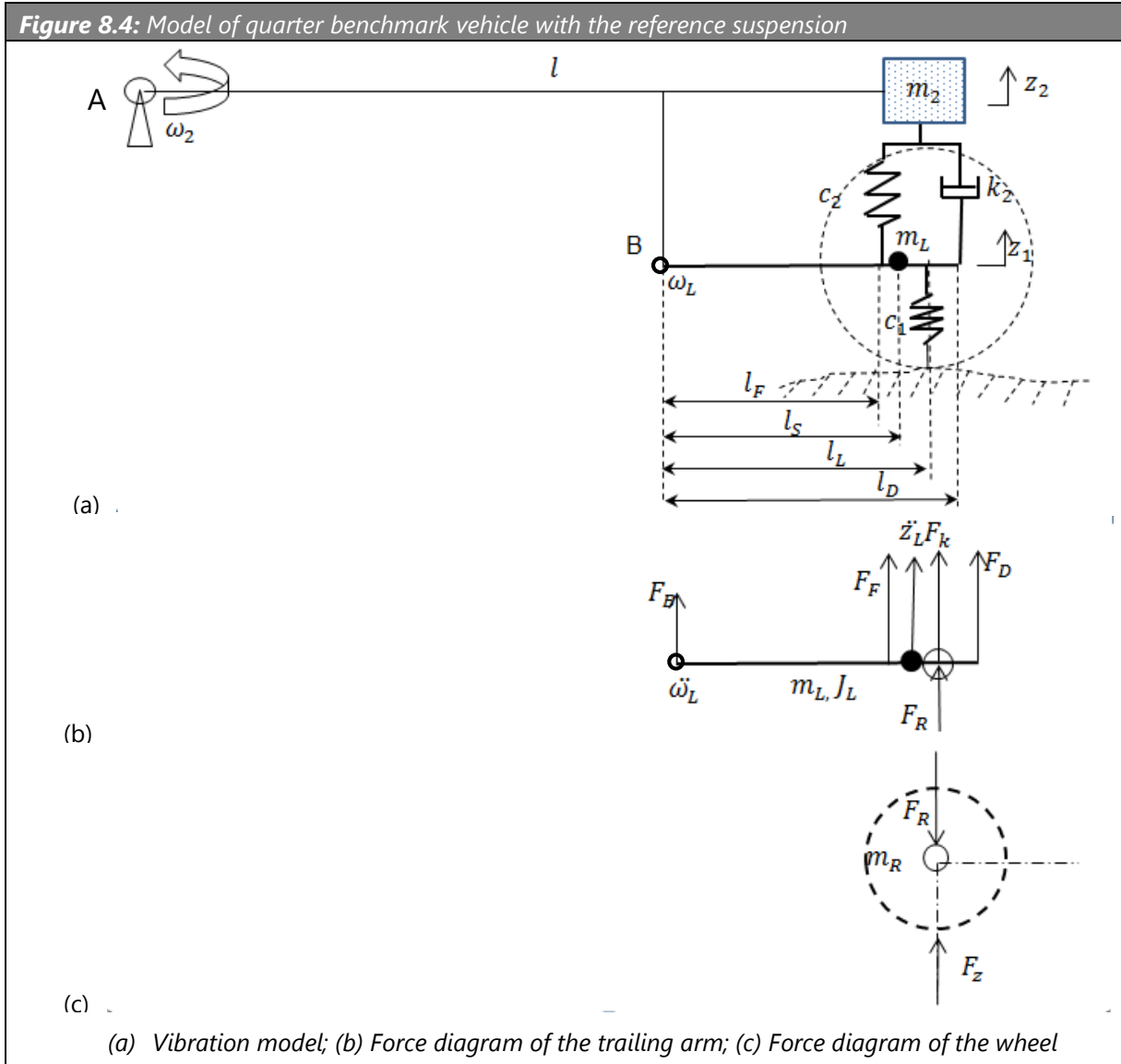
$$z_l = \frac{l_S}{l_L} z_1 + \left(1 - \frac{l_S}{l_L}\right) \frac{l - l_L}{l} z_2 \quad (8-34)$$

$$\varphi_L = \frac{1}{f_L} \left(z_1 - \frac{l - l_L}{l} z_2 \right) \quad (8-35)$$

The differential equations (8-36) and (8-37) representing the vehicular ride dynamics can be deduced from the equation (8-29), (8-30), (8-31) and (8-32).

$$\begin{aligned} & \left[m_2 + m_a \left(\frac{l - l_L}{l} \right)^2 \left(1 - \frac{f_{Sges}}{l_L} \frac{1}{H} \right) \right] \ddot{z}_2 \\ & + k'_2 \left(\frac{l_D}{l_L} \right)^2 \left[\frac{1}{H} + \frac{l_L}{l} \left(1 - \frac{1}{H} \right) \right] (\dot{z}_2 - \dot{z}_1) \\ & + c'_2 \left(\frac{l_F}{l_L} \right)^2 \left[\frac{1}{H} + \frac{l_L}{l} \left(1 - \frac{1}{H} \right) \right] (z_2 - z_1) \\ & = c_1 \left[\frac{l - l_L}{l} \left(1 - \frac{1}{H} \right) \right] (h - z_1) + \frac{F_k(l - l_L)}{l} - F_k \left(\frac{l - l_L}{l} \right) \frac{1}{H} \end{aligned} \quad (8-36)$$

$$\begin{aligned}
 m_a \left(\frac{l_B}{l_L}\right)^2 \ddot{z}_1 - m_a \left(\frac{l_B}{l_L}\right)^2 \left[\frac{l-l_L}{l} \left(1 - \frac{1}{H}\right)\right] \ddot{z}_2 - k'_2 \left(\frac{l_D}{l_L}\right)^2 (\dot{z}_2 - \dot{z}_1) \\
 - c'_2 \left(\frac{l_F}{l_L}\right)^2 (z_2 - z_1) = c_1(h - z_1) + \frac{F_k l_L}{l_L}
 \end{aligned}
 \tag{8-37}$$



The mathematic models expressed by the equations (8-23) (8-24) and (8-36) (8-37) are respectively a set of three by two nonhomogeneous linear differential equations. In system dynamics, the transfer functions between input and outputs signals in the frequency domain is utilized to investigate the system characteristics. Considering the system complexity, a Simulink model is built to simulate the system ride dynamics in vertical direction. The graphical block diagram of the Simulink model and its interface with Matlab library facilitates the engineer to use and adjust it.

8.2.4 Simulink model

A complete dynamic system consists of three parts: the input, output and processing part. The construction of the Simulink model is on the basis of the schematic in

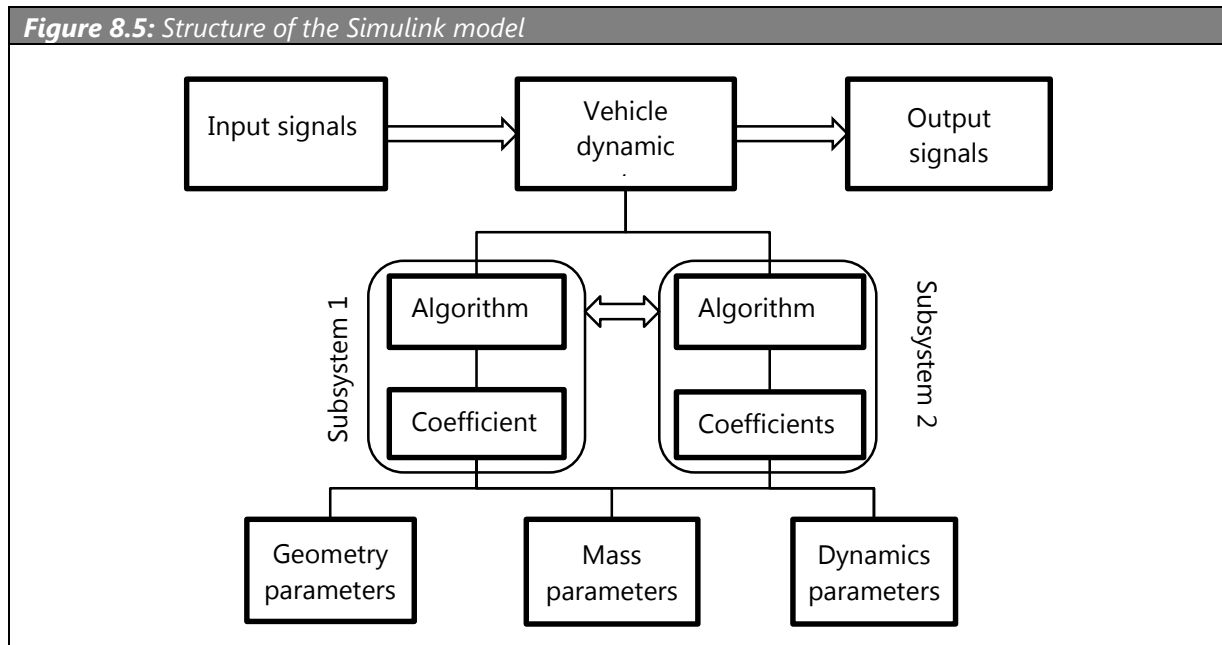


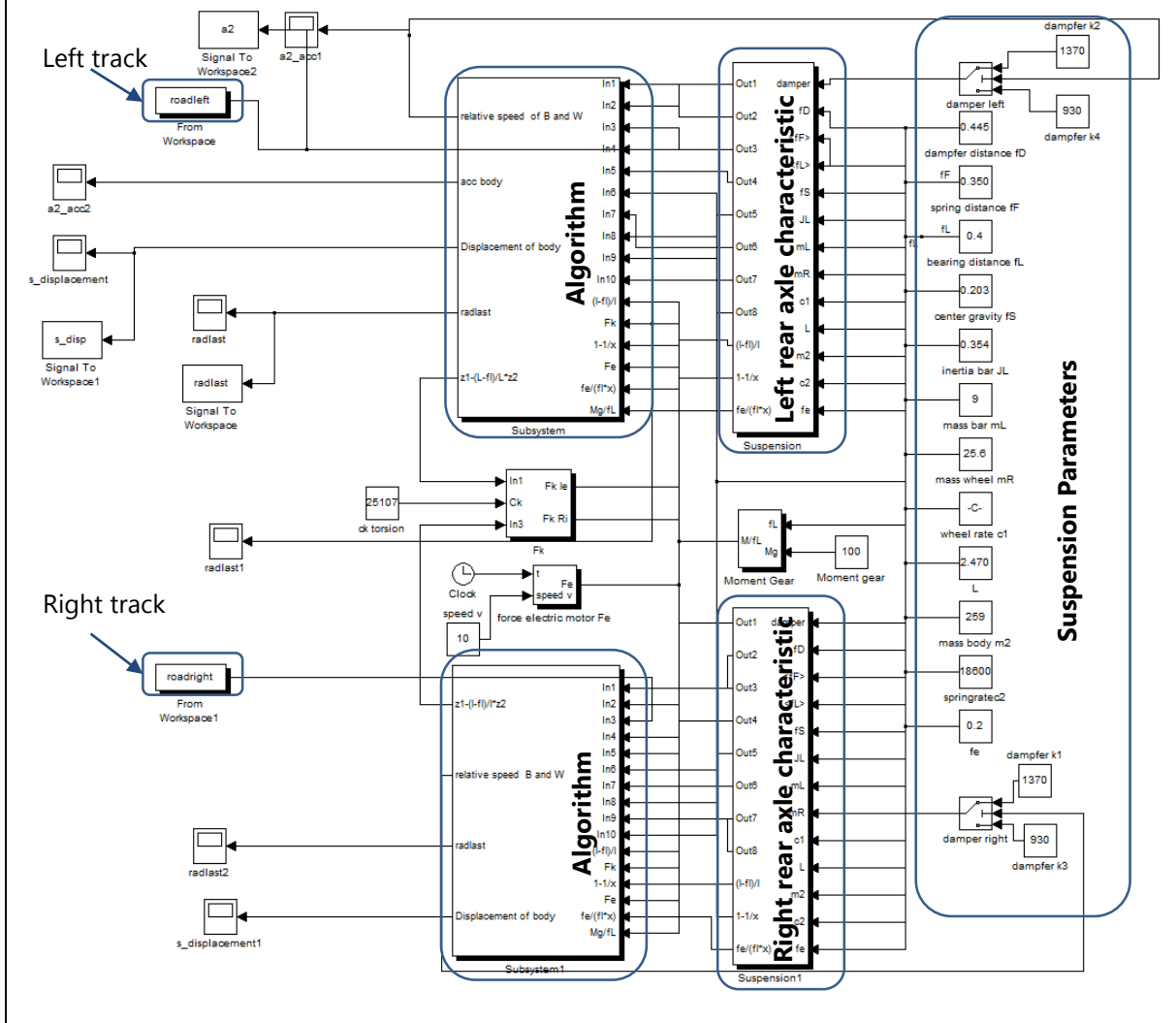
Figure 8.5. The input signals come from road roughness and vehicle speed. The output signals are the vehicle ride dynamics response. The dynamic system comprises three layers. The basic parameters in the ground layer of the system are classified into geometry, mass and dynamics parameters listed in the Table 8.1. These parameters constitute the subsystems representing the suspension dynamic systems on the left and right sides. The system is described through the differential equations in the second layer, which is simulated through the Simulink integrator block. An overview of the Simulink model is shown in Figure 8.6. The suspension parameters are positioned in the right side; the input and outputs signals are in the left side; and the subsystem and algorithms are arranged in the middle area.

The suspension parameters in this Simulink model can be treated as the variable of the system, so the sensitivity analyses of the parameters to the system characteristics are available to be investigated.

Table 8.1: Key model parameters of vehicle dynamics

Geometry parameters	Mass parameters	Dynamics parameters
l_L : Longitudinal distance between wheel center and the bushing center B,	m_2 : Sprung mass,	c_2 : Spring stiffness,
l_p : Distance between spring and the bushing center B,	m_L : Mass of the single rear arm,	k_1 : Damping of the shock absorber,
l_D : Distance between the damper and the bushing center B,	m_R : Mass of the wheel,	c_k : Torsion stiffness,
l_s : Distance between the gravity center of suspension arm and the bushing center B,		c_1 : Tire stiffness,
s : Wheel track,		J_L : Moment of inertia of the longitudinal arm,
l : Wheel base,		v : Vehicle speed

Figure 8.6: Overview of the Simulink model



8.3 Road surface profile Model

The recording of the road surface roughness with laser profilometers is expensive and time-consuming (Feng, et al., 2013). The modelling of road surface roughness is a feasible option to simulate the excitation.

The measured statistical data of road surface roughness are generally described by the stochastic models. There are a variety of methods to model and simulate the road irregularities. For vehicle fatigue assessment long road pavements are usually described as the homogenous Laplace process, non-homogeneous Laplace process and hybrid model combining Gaussian and Laplace modeling (Bogsjö, et al., 2012) (Johannesson, et al., 2014). For the evaluation of vehicle comfort and tuning of suspension parameters the statistical data of vertical road profile is treated as stationary Gaussian process model and the characteristics is described by Power Spectral Density (PSD) (Dodds & Robson, 1973) (Mucka, 2004).

8.3.1 The description of the stochastic road irregularities

In ISO 8608, random pavement profiles are compiled and classified with the hypothesis that the statistical data are a sequence of random stationary ergodic Gaussian processes. From the view of mathematics, stationary means statistical properties of the random process does not change with the time or its distribution dimension; ergodicity means that an enough long sample can reflect the statistical properties of the whole process (Peebles, 2001). A Gaussian process can be expressed by its expectation and standard deviations. The data and classification of the road based on the Gaussian model in terms of displacement power spectral can be found in Table 8.2 (ISO 8608: 1995(E), 1995). It has been well established for the characterizing and simulation of measured vertical road profile data.

Table 8.2: Road classification (ISO 8608: 1995(E), 1995)

Road class	Degree of roughness		
	Lower limit	Geometric mean	Upper limit
A	-	16	32
B	32	64	128
C	128	256	512
D	512	1 024	2 048
E	2 048	4 096	8 192
F	8 192	16 384	32 767
G	32 768	65 536	131 072
H	131 072	262 144	-

According to the standard ISO 8608, the degree of road roughness in the special frequency range from 0.011 to 2.83 m^{-1} is described into different classes by its fitted vertical displacement PSD $G_q(n_0)$ at the reference spatial frequency ($n_0 = 0.1 \text{ m}^{-1}$). The Fitted PSD of each class can be approximated in a general form as follows:

$$G_q(n) = G_q(n_0) \cdot \left(\frac{n}{n_0}\right)^{-w} \quad (8-38)$$

where n is the spatial frequency (m^{-1}) from 0.011 to 2.83 m^{-1} , $G_q(n)$ is the spatial PSD (m^2/m^{-1}), w is undulation exponent and $G_q(n_0)$ represents different road quality levels range from A (very good) to H (very poor). The graphed classification is shown in appendix E.

8.3.2 Coherence of two road lanes

Since the road is assumed as isotropic, the statistical properties of the left and right road path are the same. To simulate the irregularity of the two road lanes, the coherence function (equation (8-39)) are used to describe the statistical relationship of the left and right lanes (Mitschke & Wallentowitz, 2004) (Brandstätter, 2013) (Braun, 1969).

$$\gamma_h^2(\Omega) = \frac{|\Phi_{hlr}(\Omega)|^2}{\Phi_{hrr}(\Omega) \cdot \Phi_{hll}(\Omega)} \quad (8-39)$$

where, $\Phi_{lr}(\Omega)$ is the cross spectral density (CSD) of the left and right road statistical data, $\Phi_{hrr}(\Omega)$ and $\Phi_{hll}(\Omega)$ is the auto-PSD of the right and left road, respectively, and Ω ($\Omega = 2\pi n$) is angular spatial frequency, *rad/m*.

The angular spatial frequency Ω and angular frequency ω can be connected by the vehicle velocity v .

$$\omega = v \cdot \Omega \quad (8-40)$$

The auto-PSD of the right road lane

$$\Phi_{hrr}(\Omega) = \lim_{L \rightarrow \infty} \frac{1}{L} [H_{hr}^*(\Omega) H_{hr}(\Omega)] \quad (8-41)$$

where, $H_{hr}(\Omega)$ is the displacement spectrum of the road irregularity $h_r(l_r)$ on the right side, according to formula (8-3), $H_{hr}^*(\Omega)$ is the complex conjugates of the displacement spectrum $H_{hr}(\Omega)$, and L is the road distance.

The CSD of left and right road is defined by the following equation.

$$\Phi_{hrl}(\Omega) = \lim_{L \rightarrow \infty} \frac{1}{L} [H_{hr}^*(\Omega)] [H_{hl}(\Omega)] \quad (8-42)$$

The value of the coherence represents the degree of the correlation between two signals. When $\gamma_h = 1$, it means the two signals are linear correlation. In contrast, when $\gamma_h = 0$, it means the two signals are unrelated. Ammon introduced an approximated formula to express the mathematic relationship of the left and right road paths (Ammon, 1992) (Ammon & Bormann, 1991) according to their statistical data.

$$\gamma_h(\Omega, s) = \left[1 + \left(\frac{\Omega}{\Omega_p} \left(\frac{s}{s_0} \right)^a \right)^w \right]^{-p} \quad (8-43)$$

where, Ω_p is the reference angular frequency, p and a are given constant value, s is the width of the left and right tracks, the reference of wheel track is $s_0 = 1$, and w is the above called undulation exponent. Considering the relationship of Ω and ω in formula (8-40), the coherence function can be rewritten as follows.

$$\gamma_h(\omega, s) = \left[1 + \left(\frac{\omega}{v \cdot \Omega_p} \left(\frac{s}{s_0} \right)^a \right)^w \right]^{-p} \quad (8-44)$$

8.3.3 Modelling of two road lanes

In the conceptual phase of design, the simulation of suspensions in time domain is appropriate way to investigate the ride dynamics.

One track model of the road profile

The simulation of the road roughness in time domain for the quarter car model has already been well studied. A number of methods can be found in the literatures, such as the harmony superposition method (Grigoriu, 1993), the white noise filtration method (Heath, 1987), ARMA method (linear filtering or auto-regressive and moving average method) (Samaras, et al., 1985) (Yoshimura, 1998), and Inverse Fast Fourier Transformation (IFFT) method (Cebon & Newland, 1983) (Cebon, 1993).

In this section, the IFFT method is applied to compose the road signal from the PSD by using Fast Fourier Transformation (FFT).

The first step is to discrete the signal. The road distance is discretized into N segments. The length of each segment is Δl .

$$L = N \cdot \Delta l \quad (8-45)$$

Nyquist–Shannon sampling theorem, the sampling rate is related to the road spatial frequency.

$$N \geq 2 \cdot n_{upper} L \quad (8-46)$$

where, n_{upper} is the upper limit of the road spatial frequency. The frequency at the k^{th} point is denoted by n_k

$$n_k = k \cdot \Delta n \quad (8-47)$$

Based on the formula (8-3), the discrete Fourier transform (DFT) of the road profile with a length L is

$$H_L(n_k) = \int_0^L h(l)e^{-j2\pi n_k l} dl = \sum_{m=0}^{N-1} h(m\Delta l)e^{-j2\pi n_k m\Delta l} \Delta l = H_k \Delta l \quad (8-48)$$

In this equation, $\sum_{m=0}^{N-1} h(m\Delta l)e^{-j2\pi n_k m\Delta l}$, simplified as the form of $\sum_{m=0}^{N-1} h(m\Delta l)e^{\frac{-j2\pi km}{N}}$, is denoted by H_k , which is the DFT (discrete Fourier transform) of the road profile h_m , i.e. $h(m\Delta l)$.

According to the equation (8-5), the one side PSD of the road irregularity of one track is written as the following form with the assumption that the sample road is with a limited length L . Compared to two side PSD, the one side PSD must multiple the coefficient 2.

$$G_q(n_k) = \frac{2}{N \cdot \Delta l} |H_L(n_k)|^2 = \frac{2}{N\Delta l} |H_k \Delta l|^2 = \frac{2\Delta l}{N} |H_k|^2 \quad (8-49)$$

Then the DFT can be computed by the PSD.

$$|H_k| = \sqrt{G_q(n_k) \frac{N}{2\Delta l}} \quad (8-50)$$

Using the equation (8-50), the amplitude spectrum of single road track can be obtained by its PSD. The phase information is compensated by a series of random phase angles φ_k distributed in the scope $[0, 2\pi]$.

$$H_k = |H_k| e^{j\varphi_k} \quad (8-51)$$

The random road roughness of on single track in space domain can be obtained by the IFFT of H_k .

$$h_m = \frac{1}{N} \sum_{k=0}^{N-1} H_k e^{\frac{j2\pi km}{N}} \quad (8-52)$$

The road roughness in time domain can be derived from the space domain by vehicle speed v .

$$h(t) = h\left(\frac{l}{v}\right) \quad (8-53)$$

Parallel track model of the road profile

In this section, the road model of another road lane is derived by using the coherence relationship equation (8-43) and (8-44) (see the blue curve Figure 8.10). From the literature (Ammon & Bormann, 1991), the range of the γ_h in the coherence function is

$$0 < \gamma_h < 1 \quad (8-54)$$

In the low frequency, the value γ_h approximates to 1, which means the left and right road signals are high linear related. In the higher frequency, the value γ_h approximates to 0, which means the left and right road signals are nearly irrelative.

The road roughness of the left side in time domain is defined as $h_l(t)$, and the right side in time domain is defined as $h_r(t)$. Based on the knowledge of signal processing, if the coherence of the two signals is between 0 and 1, it indicates that noise is included in the signals $h_l(t)$ and $h_r(t)$ and they are non-linear.

The $h_l(t)$ can be considered as an output signal of $h_r(t)$ and consists of two parts, output signal $n_l(t)$ from $h_r(t)$ and noise signal $u_l(t)$.

$$h_l(t) = n_l(t) + u_l(t) \quad (8-55)$$

This system only changes the signal amplitudes without changing its phase. The right lane signal $h_r(t)$ and the noise signal of the left lane $u_l(t)$ are irrelative. The signal $n_l(t)$ and noise signal $u_l(t)$ are also irrelative.

Since the Fourier transform is a linear transform, the above equation can be written as.

$$H_{lh}(\omega) = H_{ln}(\omega) + H_{lu}(\omega) \quad (8-56)$$

The auto-PSD of $h_l(t)$ according formula (8-41) is

$$G_{ll}(\omega) = G_{lnn}(\omega) + G_{lnu}(\omega) + G_{lun}(\omega) + G_{luu}(\omega) \quad (8-57)$$

As above mentioned, $n_l(t)$ and noise signal $u_l(t)$ are unrelated, so we can obtain that:

$$G_{lnu}(\omega) = G_{lun}(\omega) = 0.$$

$$G_{ll}(\omega) = G_{lnn}(\omega) + G_{luu}(\omega) \quad (8-58)$$

Analogous to the above process, because the right road lane signal $h_r(t)$ and the left road noise signal $u_l(t)$ are unrelated, the cross-PSD between $h_l(t)$ and $h_r(t)$ can be obtained.

$$G_{rl}(\omega) = G_{rln}(\omega) \quad (8-59)$$

The denotation of auto-PSD in the right road lane is $G_{rr}(\omega)$.

Because the signal $n_l(t)$ is assumed to be an output signal in a linear system by which the input signal is the road roughness of the right road lane $h_r(t)$, their coherence functions can be written as follows, referring to (8-39).

$$\frac{|G_{rln}(\omega)|^2}{G_{lnn}(\omega) \cdot G_{rr}(\omega)} = 1 \quad (8-60)$$

The coherence function between the $h_l(t)$ and the $h_r(t)$ is written as the following form.

$$\gamma_h^2(\omega) = \frac{|G_{rln}(\omega)|^2}{[G_{lnn}(\omega) + G_{luu}(\omega)] \cdot G_{rr}(\omega)} \quad (8-61)$$

Substituting (8-60) into (8-61), the (8-61) is rewritten as follows.

$$\begin{aligned} \gamma_h^2(\omega) &= \frac{|G_{rln}(\omega)|^2}{[G_{lnn}(\omega) \cdot G_{rr}(\omega)] \frac{[G_{lnn}(\omega) + G_{luu}(\omega)] \cdot G_{rr}(\omega)}{[G_{lnn}(\omega) \cdot G_{rr}(\omega)]}} \\ &= \frac{G_{lnn}(\omega)}{G_{lnn}(\omega) + G_{luu}(\omega)} = \frac{G_{lnn}(\omega)}{G_{ll}(\omega)} \end{aligned} \quad (8-62)$$

$G_{lnn}(\omega)$ and $G_{luu}(\omega)$ can be obtained by the following equation.

$$G_{lnn}(\omega) = G_{ll}(\omega)\gamma_h^2(\omega) \quad (8-63)$$

$$G_{luu}(\omega) = G_{ll}(\omega)[1 - \gamma_h^2(\omega)] \quad (8-64)$$

They can be written as the form of spatial frequency.

$$G_{lnn}(n) = G_{ll}(n)\gamma_h^2(n) \quad (8-65)$$

$$G_{luu}(n) = G_{ll}(n)[1 - \gamma_h^2(n)] \quad (8-66)$$

The $G_{ll}(n)$ and $G_{rr}(n)$ are equal to the standard road PSD $G_q(n)$ given in ISO 8608.

$$G_{rr}(n) = G_q(n) \quad (8-67)$$

$$G_{lnn}(n) = G_q(n)\gamma_h^2(n) \quad (8-68)$$

$$G_{luu}(n) = G_q(n)[1 - \gamma_h^2(n)] \quad (8-69)$$

The corresponding road irregularity $h_r(t)$, $n_l(t)$ and $u_l(t)$ can be computed using the equation (8-50) to (8-53).

The steps to construct the road roughness can be concluded as follows.

Step 1: determine the road model parameters: the $G_q(n_0)$, the frequency scope, the sampling rate, the coherence function γ_h and the vehicle speed v .

Step 2: calculate the PSD of road roughness $G_{rr}(n)$ according equation (8-67). The corresponding PSD $G_{lnn}(n)$ and noise PSD $G_{luu}(n)$ are calculated by equation (8-68) and (8-69).

Step 3: the road roughness $h_r(t)$ of one lane, road roughness $n_l(t)$ and noise $u_l(t)$ of the other lane are calculated according to auto-PSD equation (8-50) to (8-53). The full road roughness on the other side is calculated by equation (8-55).

8.3.4 Program and validation of road surface model

The simulated road model in time domain functions as excitation on the wheels when the vehicle drives on the road under a specified velocity.

The standard PSD of the C-level road is calculated by equation (8-38) with parameters: $G_q(n_0) = 256 \times 10^{-6} m^3$, undulation exponent $w = 2$ and frequency range $n = [0.011, 2.83] m^{-1}$ (ISO 8608: 1995(E), 1995). The standard PSD of the C-level road $G_q(n)$, the PSD of the right road lane $G_{rr}(n)$, the related PSD $G_{lnn}(n)$ and the unrelated PSD $G_{luu}(n)$ of the other lane are illustrated in Figure 8.7.

The coherence function of C level road is specified with parameters (Ammon & Bormann, 1991): wheel track $s = 1.456 m$, $\Omega_p = 0.99$, $a = 0.94$, and $p = 0.50$.

Figure 8.7: Road PSDs of C-level road roughness on the left and right sides

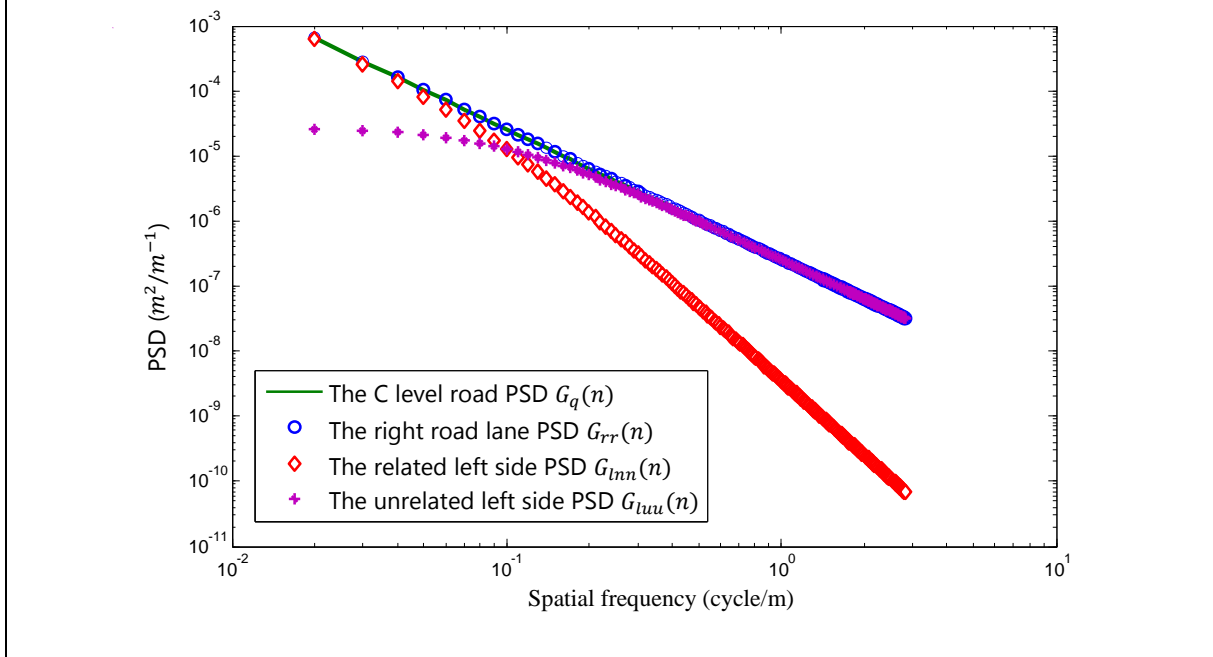
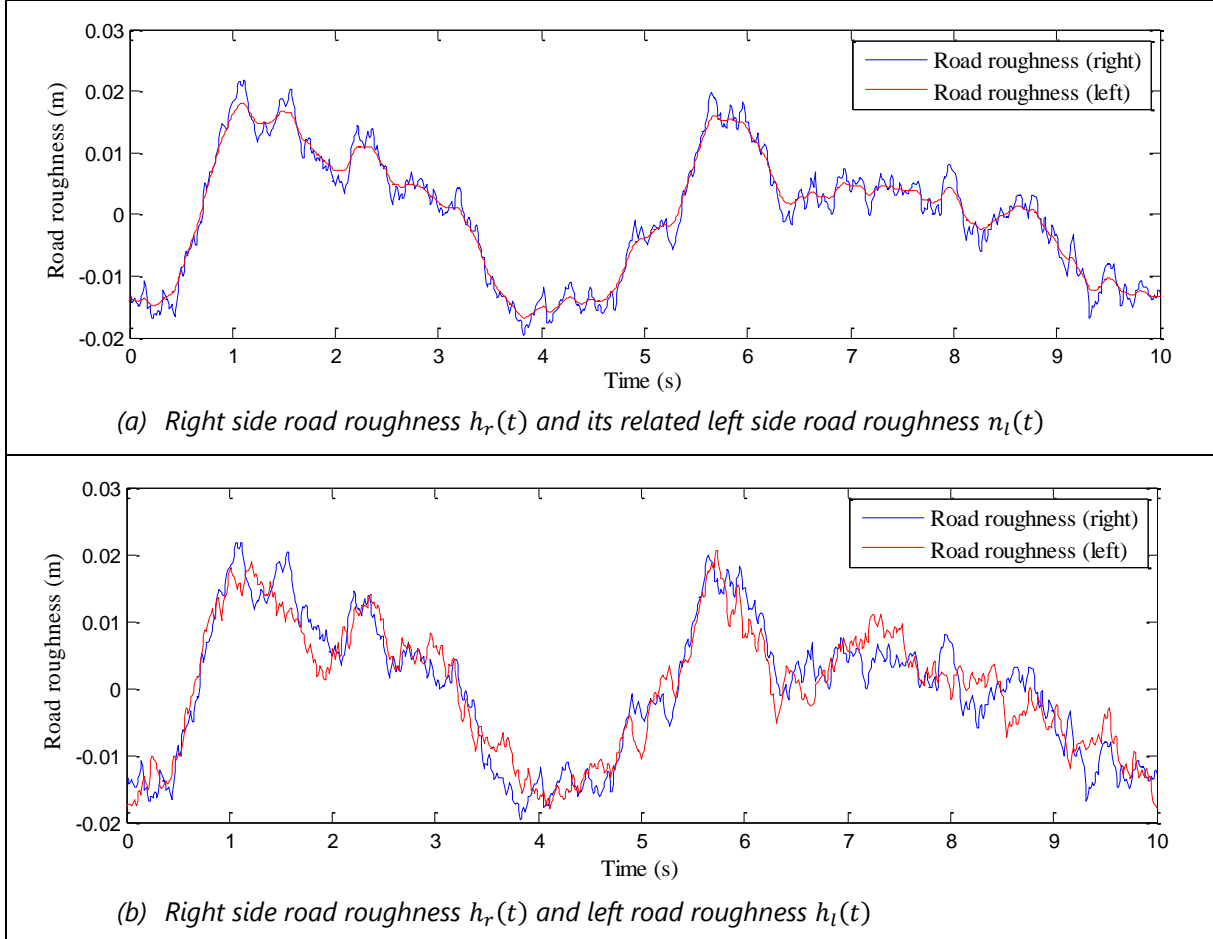


Figure 8.8: Time domain road profile of the left and right tracks



When the vehicle speed is $v = 10 \text{ m/s}$, the right side road roughness $h_r(t)$ and its related left side road roughness $n_l(t)$ in time domain are shown in Figure 8.8 (a) with different curves. It can be observed that the $n_l(t)$ is coincide with the road roughness

$h_r(t)$, but $n_l(t)$ is relatively smoother as lack of high-frequency components. The composed full left road roughness $h_l(t)$ is shown in Figure 8.8 (b). The high-frequency component is established by composition of the $u_l(t)$.

The computed road roughness signals are validated through the comparison of the auto-PSDs and coherence function in frequency domain. The equations are given in (8-70), (8-71) and (8-72). The comparisons are shown in Figure 8.9 and Figure 8.10.

$$G_{rr}(n) = \frac{2\Delta l}{N} |FFT[h_r(t \cdot v)]|^2 \quad (8-70)$$

$$G_{ll}(n) = \frac{2\Delta l}{N} |FFT[h_l(t \cdot v)]|^2 \quad (8-71)$$

$$\gamma_h(n) = \frac{|G_{rl}(n)|}{\sqrt{G_{rr}(n) \cdot G_{ll}(n)}} \quad (8-72)$$

Figure 8.9: Comparison of the road PSDs of B-level road simulated on the left and right sides with the ISO 8608 standards

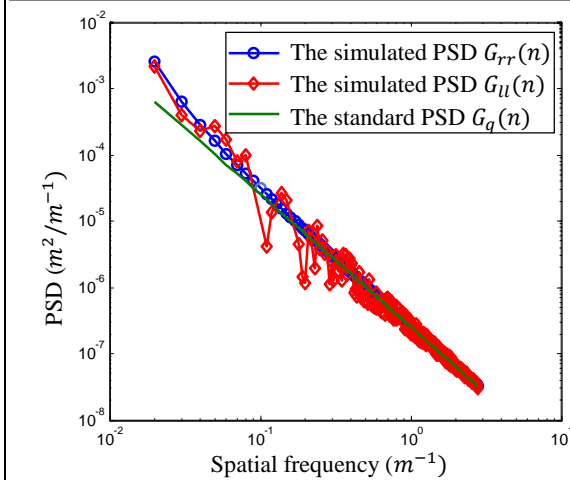
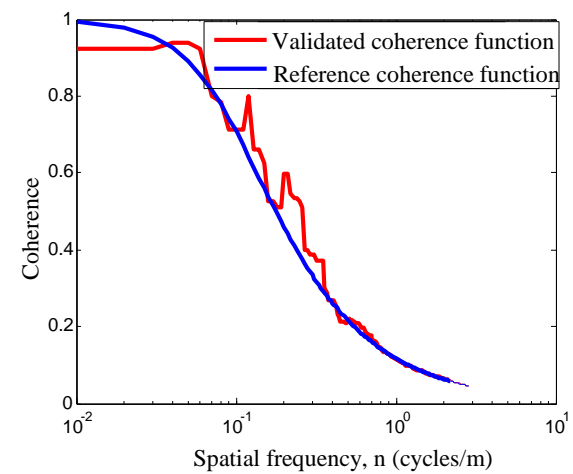


Figure 8.10: Validation of the coherence of the C-level road with the specified coherence function



8.4 Ride dynamics analysis

The ride dynamic of the rear vehicle with the concept suspension is investigated with regard to ride comfort and wheel load fluctuations. The performance is compared with the benchmark car with the reference suspension.

8.4.1 Setting model parameters

As the left and right side symmetry of the car, the data of the benchmark car and left side suspension are provided in Table 8.3. The spring constant k of the benchmark car is calculated as follows:

$$c_2 = \frac{Gd^4}{8i_f D_m^3} \quad (8-73)$$

in which, G is Shear Modulus, N/mm^2 , d is wire diameter, mm , i_f is number of active coils, and D_m means coil diameter, mm .

Symbol	Value	Unit	Description
m_v	1050	kg	Vehicle mass
i	62:38		Front/rear mass distribution
$m_{R,l}$	25.6	kg	Mass of the left wheel
$m_{L,l}$	9	kg	Mass of the left trailing arm
l_L	0.384	m	Longitudinal distance between wheel center and bushing bearing center B
l_F	0.345	m	Distance between spring and bearing center B
l_D	0.445	m	Distance between damper and bearing center B
l_s	0.203	m	Distance between gravity center of arm and bearing center B
J_L	0.354	$kg \cdot m^2$	Rotational inertia of longitudinal arm
s	1.456	m	Wheel track
l	2.47	m	Wheel base
c_k	25107	N/m	Torsion stiffness of the twist beam
$c_{1,l}/c_{1,r}$	200000	N/m	Left/right vertical tire stiffness (Engelmann, 2013) (Reimpell & Betzler, 2005)
$c_{2,l}/c_{2,r}$	18600	N/m	Left/right spring stiffness
$k_{2,l}/k_{2,r}$	1000, $\dot{z}_2 - \dot{z}_1 > 0$ 620, $\dot{z}_2 - \dot{z}_1 < 0$	$N \cdot s/m$	Left/right damping of shock absorber (Engelmann, 2013)

The damping of the shock absorber is based on a test result in the literature (Engelmann, 2013). The non-linear damping characteristic of the shock absorber is

approximated by a piecewise linear expression. The geometry and the mass of the reference axle are from the CATIA model.

The calculation of the natural frequency and damping ratio of the benchmark car is carried out with the equivalent spring stiffness c'_2 , equivalent damping k'_2 , unsprung mass m_1 and sprung mass m_2 . The c'_2 and k'_2 are calculated as follows.

$$c'_2 = c_2 \cdot \left(\frac{l_F}{l_L}\right)^2 = 14940 \text{ N/m} \quad (8-74)$$

$$k'_2 = k_2 \cdot \left(\frac{l_D}{l_L}\right)^2 = \begin{cases} 1342 \text{ N} * \frac{\text{S}}{\text{m}}, & \dot{z}_2 - \dot{z}_1 > 0 \\ 832 \text{ N} * \frac{\text{S}}{\text{m}}, & \dot{z}_2 - \dot{z}_1 < 0 \end{cases} \quad (8-75)$$

The m_1 is calculated to 30.4 kg and m_2 is 169.1 kg (see Appendix 0).

The natural frequency λ_p and damping ratio η_p of suspension system are calculated by formula (8-76) and (8-77).

$$\lambda_p = \frac{1}{2\pi} \sqrt{\frac{c'_2}{m_2}} = 1.49 \quad (8-76)$$

$$\eta_p = \frac{k'_2}{2\sqrt{c'_2 m_2}} = \begin{cases} = 0.42, & \dot{z}_2 - \dot{z}_1 > 0 \\ = 0.26, & \dot{z}_2 - \dot{z}_1 < 0 \end{cases} \quad (8-77)$$

The parameters of the target vehicle are given in Table 8.4. Because the target car is set to be an electric car, the vehicle mass is possibly distributed in target way 50:50. The geometry and mass parameters of the concept suspension are obtained from the CATIA model. In order to achieve an equivalent ride dynamic performance to the benchmark car, the initial natural frequency and damping ratio of the concept suspension are set to be consistent with the reference suspension.

The unsprung mass and sprung mass of the target vehicle are $m_1 = 39.8 \text{ kg}$ and $m_2 = 222.7 \text{ kg}$ respectively (see appendix 0).

The suspension rate and damping are calculated as follows.

$$c_2 = (2\pi\lambda_p)^2 m_2 \left(\frac{l_L}{l_F}\right)^2 \quad (8-78)$$

$$k_2 = 2\sqrt{c_2' m_2} \cdot \eta_p \cdot \left(\frac{l_L}{l_D}\right)^2 \quad (8-79)$$

in which, $\lambda_p = 1.49$; when $\dot{z}_2 - \dot{z}_1 > 0$, $\eta_p = 0.42$; when $\dot{z}_2 - \dot{z}_1 < 0$, $\eta_p = 0.26$.

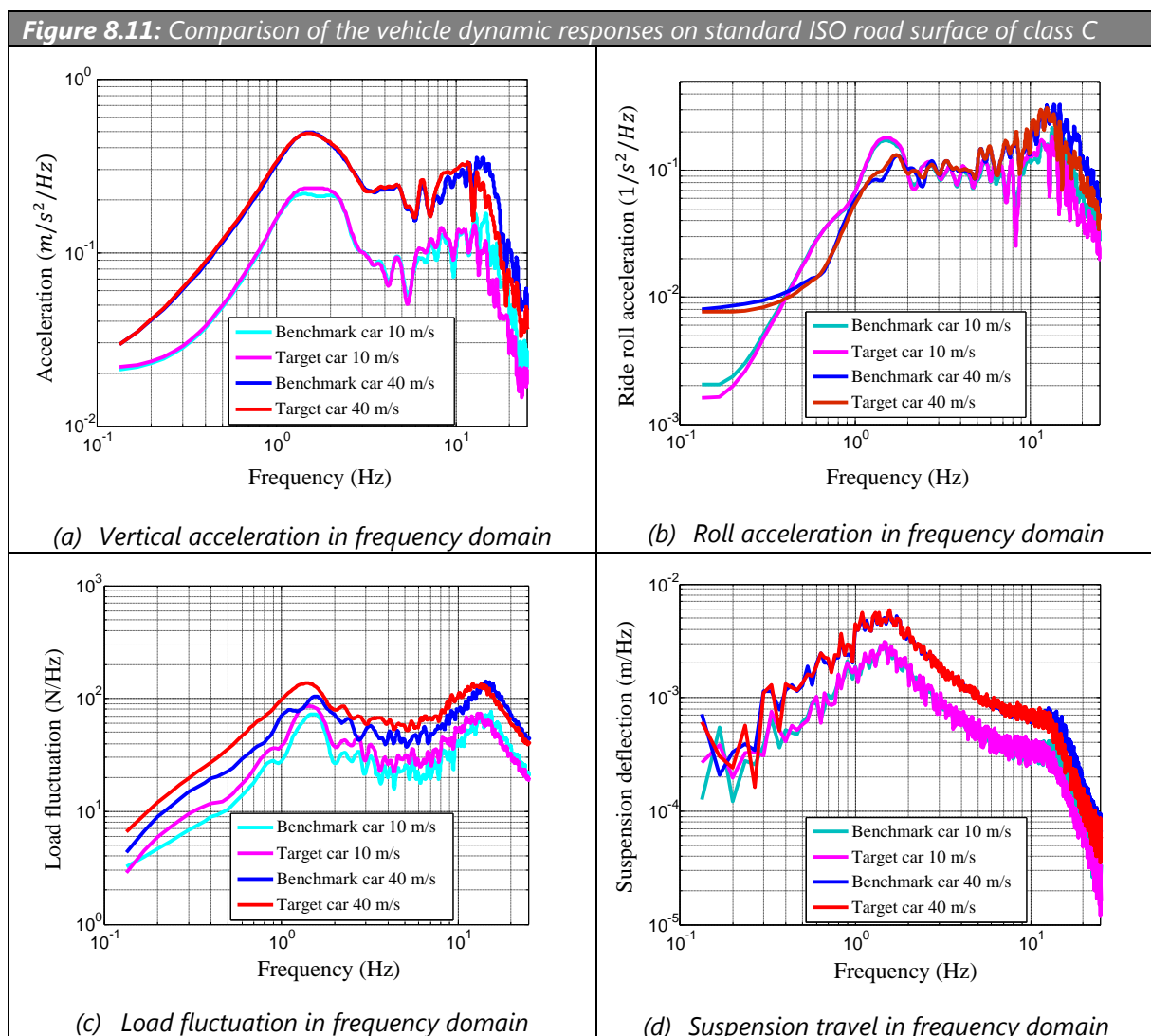
Table 8.4: Parameters of the target car			
Symbol	Value	Unit	Description
m_v	1050	kg	Vehicle mass
i	50:50		Front/Rear mass distribution
$m_{R,l}$	25.6	kg	Mass of the left wheel
$m_{L,l}$	22.4	kg	Mass of the left trailing arm
l_L	0.427	m	Longitudinal distance between wheel center and bearing center B
l_F	0.396	m	Distance between spring and bearing center B
l_D	0.501	m	Distance between damper and bearing center B
l_s	0.270	m	Distance between gravity center of arm and bearing center B
l_e	0.210	m	Distance between vibration center of electric motor and bearing center B
J_L	0.5	kg · m ²	Rotational inertia of longitudinal arm
s	1.456	m	Wheel track
l	2.47	m	Wheel base
c_k	25107	N/m	Torsion stiffness
$c_{1,l}/c_{1,r}$	200000	N/m	Left/right vertical tire stiffness
$c_{2,l}/c_{2,r}$	22694	N/m	Left/right spring stiffness
$k_{2,l}/k_{2,r}$	1272, $\dot{z}_2 - \dot{z}_1 > 0$	N · s/m	Left/right damping force of shock absorber
	788, $\dot{z}_2 - \dot{z}_1 < 0$	N · s/m	

8.4.2 Comparison of the ride dynamic response

The ride dynamic response of the benchmark vehicle and target vehicle (equipped with reference suspension and concept suspension respective) are compared in terms of vehicle body vertical and roll ride response, wheel load fluctuation and suspension

travel described in equations (8-23) (8-24) and (8-36) (8-37). The benchmark vehicle and target vehicle on standard roads are simulated under the road random inputs and vehicle speeds. While the properties of the reference and the concept suspensions are defined from the parameters in the Table 8.3 and Table 8.4.

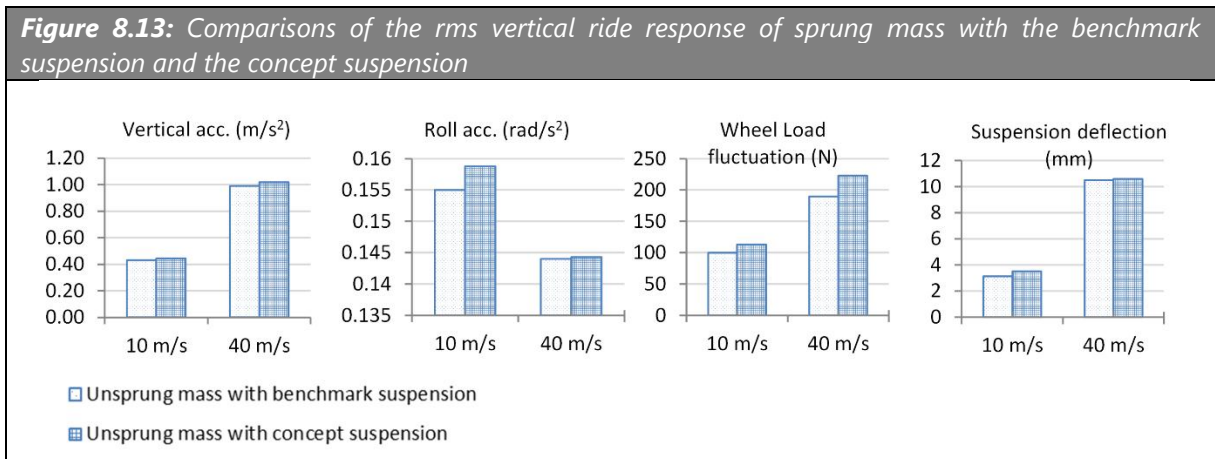
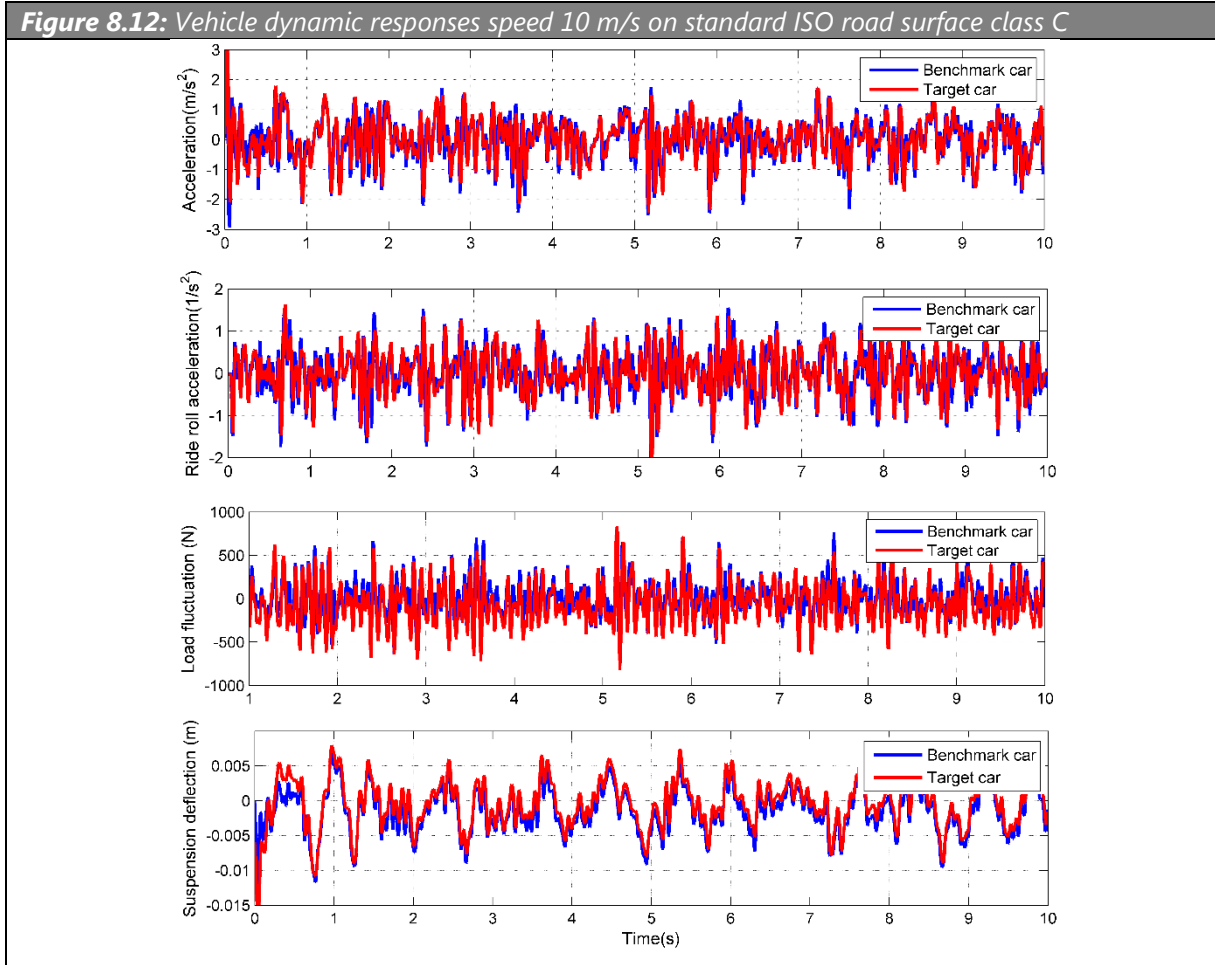
In order to compare their dynamic responses at low speed and high speed, the simulation is carried out at low speed and high speed, 10 m/s and 40 m/s, respectively. The C-level road is selected as the simulation input. The amplitude spectrums of those responses in the frequency range 0-25 Hz are shown in Figure 8.11.



The simulation results of vertical ride response are graphed in Figure 8.11. The vertical acceleration in Figure 8.11 (a) of the benchmark car and target car in the vicinity of the first vibration peak are identical, because their natural frequencies of the vehicles are

set as the same value. However, the vertical ride responses in the vicinity of the second vibration peak are different; the second peaks of the target car curves shift to the left. The reason is that the natural frequency of the wheel on the target car is reduced because of the increased unsprung mass. Figure 8.11 (b) shows curves of roll acceleration between the benchmark car and target car, which illustrates that their curves in frequency domain have the similar trends as the curves of vertical acceleration. These curves representing wheel load fluctuations show significant difference in Figure 8.11 (c). The target car curves are higher than the benchmark car curves and the second peaks in the curves shift to the left. One of the reasons is attribute to the load generated by the driving unit, i.e. the electric motor and the gears; another reason could be the increased unsprung mass. The curves in Figure 8.11 (d) are the amplitude spectrum of suspension deflection. The suspension deflection reflects the rattle space changing between the wheel and vehicle body when the car drives on the road. It can be concluded from this figure that the benchmark car and the target car have nearly the same spectrum of suspension deflection.

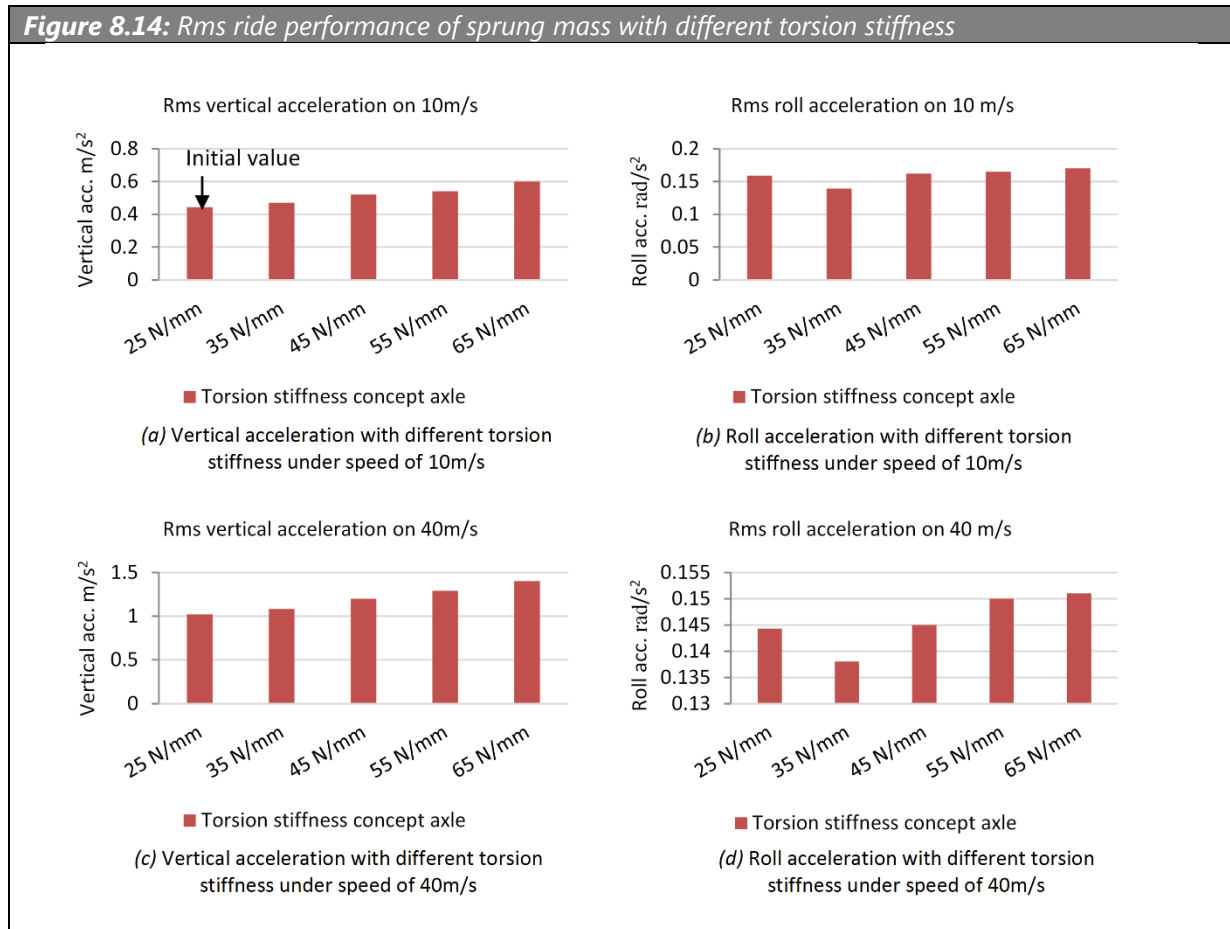
The root mean squares (rms) of the vertical ride response are calculated to compare the relative ride performance of the benchmark car and the target car. Figure 8.12 shows the ride response performance of the benchmark car and the target car with the speed of 10 m/s in time domain. Figure 8.13 compares the rms ride dynamic response of the benchmark car with the twist beam axle and the target with the concept suspension. The result shows that the target car with the concept suspension has comparable acceleration in vertical and roll direction to the benchmark car with twist beam axle. Due to the increased sprung mass, the wheel load fluctuation of the target car is increased dramatically compared to the benchmark car with twist beam axle. The suspension travels of the benchmark suspension and target suspension show comparable results.



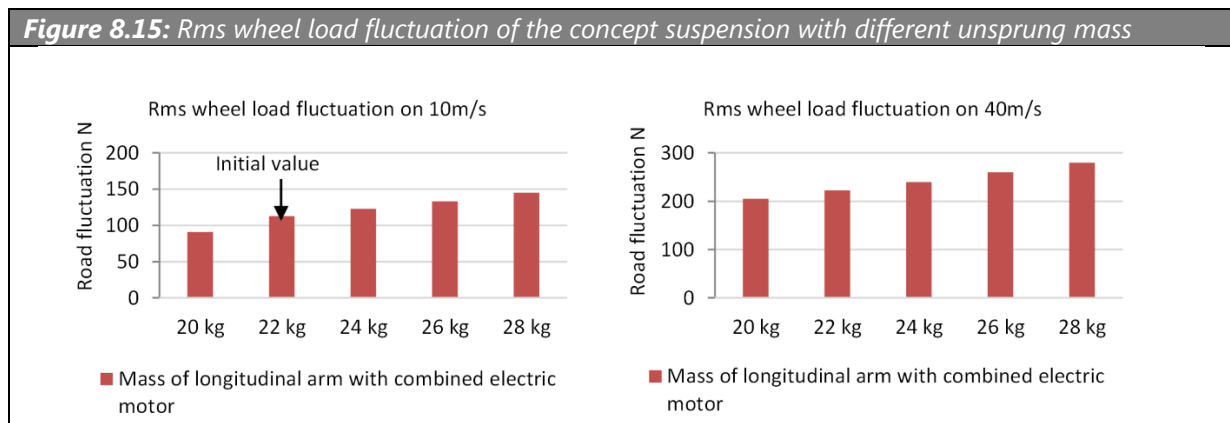
8.4.3 Parameter sensitivity to vertical ride response

The sensitivity of the concept suspension parameters to vertical ride response of the sprung mass is studied. For the target vehicle, the sensitivity of vertical acceleration and ride roll acceleration of sprung mass to torsion stiffness of the conceptual suspension axle is illustrated in Figure 8.14, by which the diagrams show the simulation

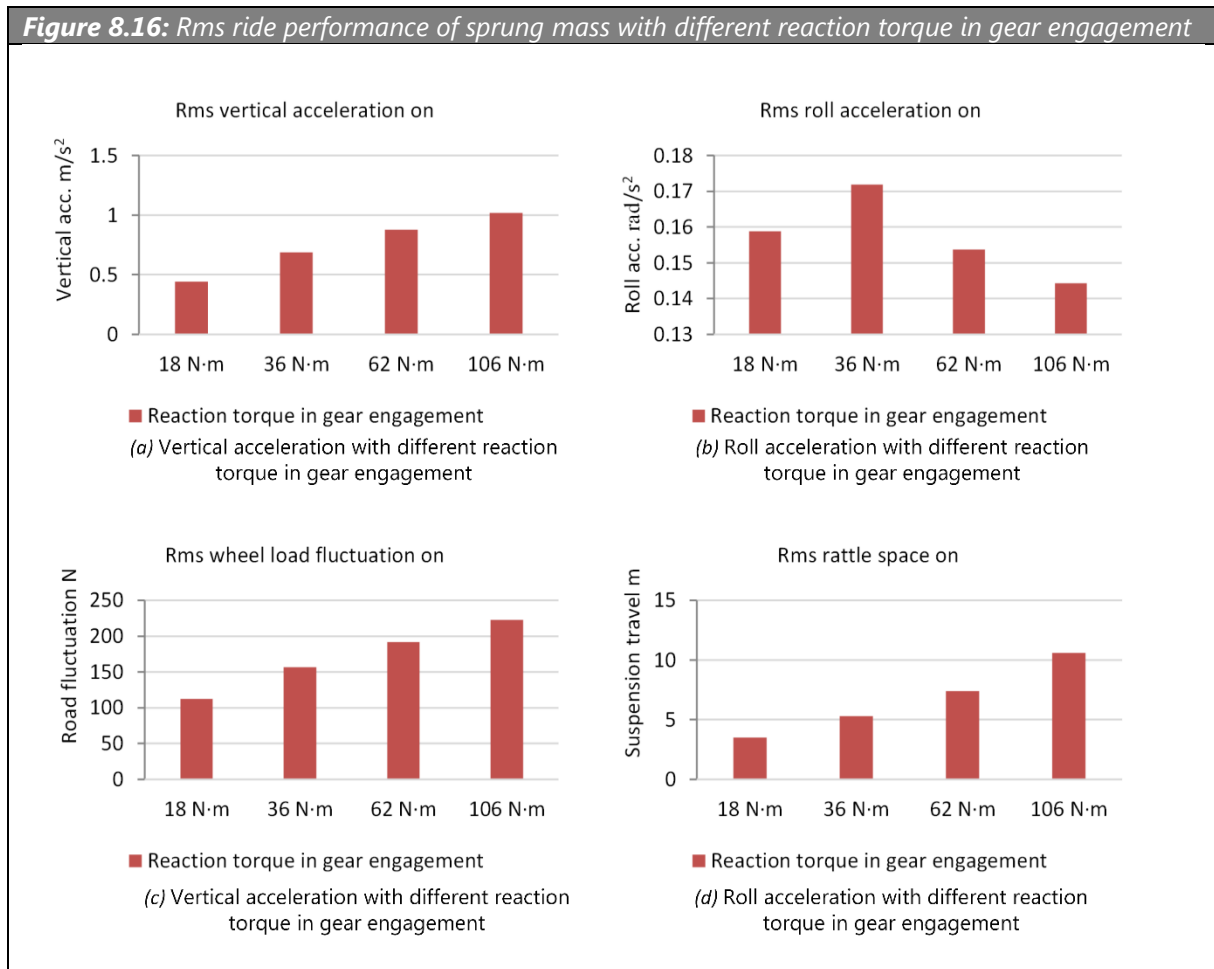
result of the target vehicle driving on the standard ISO road surface of roughness class C with speeds of 10 m/s and 40 m/s respective.



The unsprung mass of the concept suspension is raised by the combined electric motors significantly. The resultant load fluctuation caused by the mass of the longitudinal arm with combined electric motors is investigated. Target vehicle with the concept suspension mass is simulated on the standard ISO class C road surface with speed of 10 m/s and 40 m/s, and the result is illustrated in Figure 8.15.



In contrast with the reference twist beam axle, the motors combined in concept axle not only generate driving force but also influence ride dynamic response, which is caused primarily by the reaction rotational torque on the gear box in the gear engagement M_g and vibration of the electric motor in the vertical direction F_e . Although the reaction rotational torque M_g and vibrational force F_e of electric motors are associated with the vehicle driving status, in order to investigate their influence on ride dynamics, the target vehicle with reaction torques 25 N·m, 35 N·m, 45 N·m, 55 N·m and 65 N·m in gear engagement of each driven wheel is simulated respectively and in each speed the influence of different M_g variants on ride dynamics is illustrated on Figure 8.16.



8.5 Conclusion

In this chapter, an analytical model for vehicle ride dynamics was built with the consideration of the axle geometry and combined driving units. The ride performance

of the target car with concept suspension is calculated. The simulation results are compared with the reference suspension. It indicated the concept suspension for the target vehicle achieves an equivalent ride dynamic performance to the reference suspension. The influences of the electric parameters on ride dynamics are analyzed. The top view and front view of the suspension concept is shown in Figure 8.17 and Figure 8.18, respectively.

In the future, this model can also be applied to the tuning analysis of the spring rate and damping of suspensions to vehicle ride dynamics. The optimization of the suspension parameters will be carried out with full consideration of the driving dynamics and ride performance.

Figure 8.17: Top view of the whole suspension concept

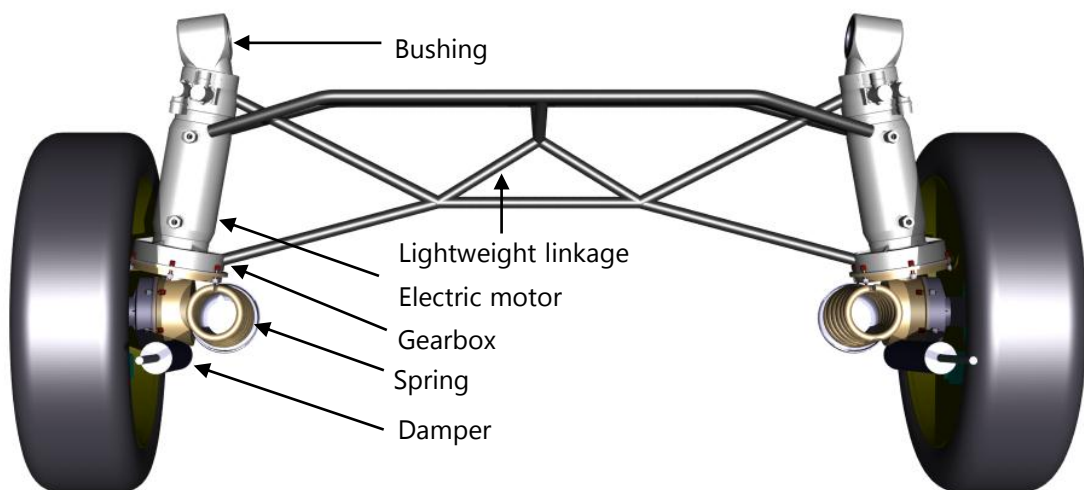
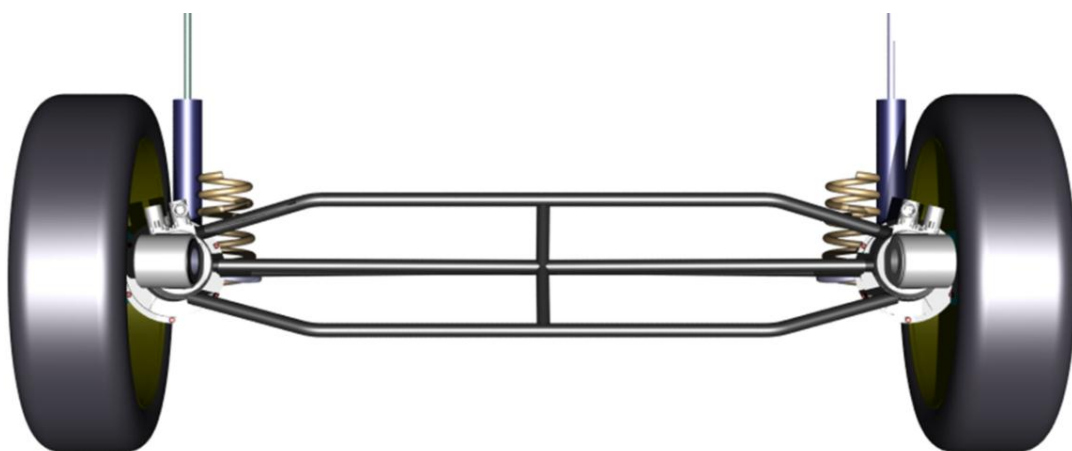


Figure 8.18: Front view of the concept suspension



9 Conclusions and recommendations

9.1 Conclusions

Combining two systems by integrating their common functions is an effective way to achieve a lightweight design. For the purpose of reducing the vehicle mass, an available way is to combine vehicle suspension and electric motor systems. However, successfully combining two systems by the conventional way is strongly dependent on engineering experience and specialized knowledge of the participants on the two systems, especially when the functions of two systems are complex. The mutual effects between the two systems may cause undesirable performance of the combined system.

This thesis has presented a systematic methodology for the new suspension conceptual design by which the electric motor was combined to suspension links. This methodology has a range of topics in mechanical and automotive engineering, from approaches for concept generation and evaluation, suspension structure/linkage design, topological optimization to vehicle vertical dynamics modelling and simulation.

The main problems solved in the development are concluded as follows.

1. *How to successfully generate new concepts through functional integration and evaluate the functionality of the new concepts? Concept suspensions have a large number of design variables, how to determine the design sequence of the design variables?*

A method based on the AD method was proposed to formulate the functional integration process of independent systems. This method expressed the integration process using mathematic matrix equations. The functions of the two systems were mapped into their physical parameters by matrix coefficients, respectively. Thus, in the functional integration design, the relationship between functions and parameters were explicit. Moreover, the functionality of the new concept was evaluated by its matrix coefficient depending on the Axioms proposed in the AD method. The elements in the

design matrix were rearranged to form a lower triangular matrix and as close as possible to the diagonal. According to the way of solving matrix equations, the design sequence of the suspension parameters was determined the same as the equation solving sequence.

2. How to efficiently design a lightweight suspension structure for the new concept suspension without decreasing its K&C performance?

A structure design approach for suspension based on structure optimization was developed. The stiffness and K&C requirements were used as the design conditions. The size optimizations of tube elements were carried out on the basis of the structure topology. In the optimization, the K&C performance was constantly under control. By this way, the complicated iterative design process between structure topology and conceptual structure is substantially avoided.

3. How to design and investigate the vertical dynamics of the target car with the concept suspension?

An analytical model with the main relevant suspension parameters was built for the vertical dynamics of the target car with the concept suspension. In order to simulate the car ride comfort on random road, standard road models of double lanes with stochastic irregularities were built. These models were programmed in MATLAB/Simulink. The spring rate and damping of the concept suspension were defined with reference to the natural frequency and damping ratio of the reference suspension. The vertical dynamics of the target car with the concept suspension were calculated and compared with the benchmark car.

9.2 Scientific contributions

Three main scientific contributions of this research are summarized as follows.

1. A method based on AD method is developed to formulate and guide the functional integration process. This method enables the conceptual design a systematic and

explicit way in combining two independent systems by way of functional integration. The functionalities of the generated concepts are able to be evaluated by its matrix coefficient. The design sequence of the concept variables is able to be defined by the element positions in the design matrix. This method can be applied not only to the combining of suspensions and electric motors but also to other concept or lightweight designs which aim to integrate common functions of two independent systems (see chapter 3 and 4).

2. A topological design approach for the design of suspension structure is proposed. This approach is different from the topological optimization of a single suspension link which is based on strength. This approach aims to the whole axle design. The optimal structure topology can be achieved with consideration of strength and suspension K&C performance. Based on the topology, the keypoints and linkage of suspension can be designed rationally. This approach can also be applied to the structure design of other concept suspensions (see chapter 7).
3. An analytical model for the vertical dynamics of the concept suspension is presented. Unlike the simple quarter vehicle model, this rear-axle vehicle model incorporates the parameters about geometric and mass of suspension links, torsion stiffness, spring stiffness, suspension damping and vibration of the electric motor. This model can be used to investigate the influence of these above parameters on vehicle vertical dynamics. It can also be used to optimize these parameters (see chapter 8).

9.3 Recommendations

The following works are proposed for the future research.

- For the methodology
 1. Further develop the design matrix of the concept suspension in detail in order to assist the detail design.
 2. In the topological optimization, take the bushing elements into account.

3. Develop dynamics model for the whole car in order to investigate the whole car ride performance with the concept suspension on road with stochastic irregularities.
- For the development of the concept suspension
 - A. The connection of the suspension linkage and electric motors should be designed and developed.
 - B. The crash test or crash simulation should be carried out to investigate the concept suspension safety performance.
 - C. Durability analysis of the suspension should be carried out to investigate the fatigue life of the suspension linkage.
 - D. The suspension parameters related to the vehicle ride dynamics should be optimized on the basis of the analytical model.

Bibliography

AC Propulsion, 2013. *Products & Services: Drive Systems*. [Online] Available at: <http://www.acpropulsion.com/index.html> [Accessed 2014]

Agostinacchio, M., Ciampa, D. & Olita, S., 2014. The Vibrations Induced by Surface Irregularities in Road Pavements – a Matlab Approach. *European Transport Research Review*, 6(3), p. 267–275. DOI: 10.1007/s12544-013-0127-8

Altair Engineering Inc., 2014. *HyperWorks Online Help Version 13.0*, s.l.: Altair Engineering Inc..

Altair Engineering Inc., April, 2009. *Altair OptiStruct: Concept Design with Topology and Topography Optimization*, s.l.: Altair Engineering Inc..

Altidis, P. & Warner, B., 2005. *Analyzing Hyperelastic Materials*, s.l.: IMPACT Engineering Solutions, Inc..

AMK Antriebs- und Steuerungstechnik GmbH Co. KG, 2012. *Motor-Datenblatt*, Germany.

Ammon, D., 1992. Problems in Road Surface Modelling. *Vehicle System Dynamics*, 20(sup1), p. 28–41. DOI: 10.1080/00423119208969386

Ammon, D. & Bormann, V., 1991. *Zur Kohärenz zwischen den Unebenheitsanregungen an linker und rechter Fahrspur*, VDI-Berichte Nr.877, pp. 103-118.

Anon., 2013. *Chevrolet Spark EV*. [Online] Available at: <http://www.autobild.de/artikel/chevrolet-spark-ev-preis-usa-4218490.html> [Accessed 2013]

Anon., 2014. *Chevrolet Product Information: 2014 CHEVROLET SPARK EV*. [Online] Available at: <http://media.gm.com/content/media/us/en/chevrolet/vehicles/spark->

[ev/2014/jcr_content/iconrow/textfile/file.res/14-PG-Chevrolet-Spark-EV-07-12-13.pdf](#) [Accessed 2018]

Audi AG, 2011. *Audi Technology Portal*. [Online] Available at: <http://www.audi-technology-portal.de/> [Accessed 2014]

Bae, S. et al., 2003. Axiomatic Approach to the Kinematic Design of an Automotive Suspension System with the McPherson Strut Type. *International Journal of Vehicle Design*, 31(1), pp. 58-70. DOI: 10.1504/IJVD.2003.002047

Bae, S., Lee, J. M. & Chu, C. N., 2002. Axiomatic Design of Automotive Suspension Systems. *CIRP Annals - Manufacturing Technology*, 51(1), pp. 115-118. DOI: 10.1016/S0007-8506(07)61479-6

Barthel, M. & Lingnau, G., 1986. *100 Jahre Daimler-Benz Die Technik*, Ludwigsburg: Hase & Koehler. Mainz. ISBN: 3775811192

Baxter, M., 1995. *Product Design*. USA: CRC press. ISBN-13: 978-1138442863

Beeh, E. et al., 2013. *Crashsicherheitspotentiale durch leichte, funktionsintegrierte Fahrzeugstrukturen*. ATZ live. Springer Vieweg, Springer Fachmedien Wiesbaden GmbH. [Online] Available at: <https://elib.dlr.de/87217/> [Accessed 2019]

Beer, F. P., Johnston, E. R. & Johnston, E. R., 1987. *Mechanics for Engineers: Statics and Dynamics*. s.l.:McGraw-Hill Companies. ISBN-13: 978-0070045842

Beggs, J. S., 1983. *Kinematics*. Los Angeles: Taylor & Francis. ISBN-13: 978-3540125853

Beitz, W. & Grote, K.-H., 2000. Mechanische Konstruktionselemente. In: *Dubbel: Taschenbuch für den Maschinenbau*. s.l.:Springer, p. 142. ISBN: 3540677771

Bendsoe, M., 1989. Optimal Shape Design as a Material Distribution Problem. *Structural Optimization*, 1(4), p. 193–202. DOI: 10.1007/BF01650949

BMW AG, 2013. *The Double-wishbone Front Axle on the BMW X6*. [Online] Available at: <http://www.bmw.com> [Accessed 2014]

BMW AG, 2014. *BMW i3 Technical Data*. [Online] Available at: <https://www.bmw.de/de/neufahrzeuge/bmw-i/i3/2020/bmw-i3-technische-daten.html#tab-0> [Accessed 2019]

Bogsjö, K., Podgorski, K. & Rychlik, I., 2012. Models for Road Surface Roughness. *Vehicle System Dynamic*, 50(5), pp. 725-747. DOI: 10.1080/00423114.2011.637566

BorgWarner Inc., 2016. *HVH250 Series Electric Motors Specifications*. [Online] Available at: <https://www.borgwarner.com/technologies/electric-drive-motors/hvh-series-electric-motor> [Accessed 2019]

Bormann, A., 2005. *Elastomerringe zur Schwingungsberuhigung in der Rotordynamik Theorie, Messungen und optimierte Auslegung*. Berlin: Technischen Universität Berlin. Dissertation. DOI: 10.14279/depositonce-1243

Bowen, R., 2013. *BMW 3-Series (E30) Performance Guide 1982-1994*. United States: CarTech Inc. ISBN-13 : 978-1934709863

Braess, H.-H. & Seiffert, U., 2013. *Vieweg Handbuch Kraftfahrzeugtechnik*. s.l.:Springer Vieweg, Wiesbaden. ISBN: 978-3-658-01691-3; DOI: 10.1007/978-3-658-01691-3

Brand, R., 2012. *Power Train: The sportier side of electric vehicles*. [Online] Available at: http://www.automotive-eetimes.com/en/the-sportier-side-of-electric-vehicles.html?cmp_id=71&news_id=222902525 [Accessed 2014]

Brandstätter, M., 2013. *Tieffrequente Geräusche in einem Kraftfahrzeug bei Unebenheitsanregung*. Berlin: Technischen Universität Berlin, Dissertation. DOI: 10.14279/depositonce-3888

Branke, D., 2014. *BMW i3 / Kia Soul EV: Test*. [Online] Available at: <http://www.autobild.de/artikel/bmw-i3-kia-soul-ev-test-5394038.html> [Accessed 2014]

Braun, H., 1969. *Untersuchung von Fahrbahnunebenheiten und Anwendung der Ergebnisse*. Braunschweig: Technische Universität Carolo-Wilhelmina zu Braunschweig.

Buchmeier, R., 2014. *ZF präsentiert Elektroantriebe für Pkw*. [Online] Available at: http://www.autokon.de/home/-/article/33673047/39007608/Emissionsfreie-Zukunft/art_co_INSTANCE_0000/maximized/ [Accessed 2019]

Calvel, S. & Mongeau, M., 2007. Black-box Structural Optimization of a Mechanical Component. *Computers & Industrial Engineering*, 53(3), pp. 514-530. DOI: 10.1016/j.cie.2007.05.009

Cao, D., 2008. *Theoretical Analyses of Roll and Pitch Coupled Hydro Pneumatic Strut Suspensions*. Canada: Concordia University, Dissertation. ISBN: 978-0-494-37763-5

Cao, D., Rakheja, S. & C.-Y. Su, 2008. Heavy Vehicle Pitch Dynamics and Suspension Tuning. Part I: Unconnected Suspension. *Vehicle System Dynamic*, 46(10), p. 931–953. DOI: 10.1080/00423110701732899

Cao, D., Rakheja, S. & Su, C.-Y., 2010. Roll- and Pitch-Plane Coupled Hydro-Pneumatic Suspension: Part 1: Feasibility Analysis and Suspension Properties. *Vehicle System Dynamics*, 48(3), pp. 361-386. DOI: 10.1080/00423110902883251

Cao, D., Rakheja, S. & Su, C.-Y., 2010. Roll- and Pitch-Plane-Coupled Hydro-Pneumatic Suspension. Part 2: Dynamic Response Analyses. *Vehicle System Dynamics*, 48(4), pp. 507-528. DOI: 10.1080/00423110902923461

Cao, D., Song, X. & Ahmadian, M., 2010. Editors' Perspectives: Road Vehicle Suspension Design, Dynamics, and Control. *Vehicle System Dynamics: International Journal of Vehicle Mechanics and Mobility*, 49(1-2), p. 3–28. DOI: 10.1080/00423114.2010.532223

Cebon, D., 1993. Interaction Between Heavy Vehicles and Roads. *SAE Technical Paper*, Volume 930001. ISBN: 1-56091-336-3

Cebon, D. & Newland, D., 1983. Artificial Generation of Road Surface Topography by the Inverse F.F.T. Method. *Vehicle System Dynamics*, 12(1), pp. 160-165. DOI: 10.1080/00423118308968747

Chan, C. C. & Chau, K. T., 2001. *Modern Electric Vehicle Technology*. Oxford Science Publications. ISBN: 0198504160, 9780198504160

Chen, X. et al., 2013. 一体化单摆臂悬架-同步带传动轮边电驱动系统的设计与分析. *机械传动*, 37(8), pp. 60-71. ISSN: 1004-2539

Chen, Y. C., Tsai, P. Y. & Lai, I. A., 2012. Kinematic Analysis of Roll Motion for a Strut/SLA Suspension System. *World Academy of Science, Engineering and Technology*, Volume 6, pp. 1170-1174. DOI: 10.5281/zenodo.1076022

Chiandussi, G., Gaviglio, I. & Ibba, A., 2004. Topology Optimisation of an Automotive Component without Final Volume Constraint Specification. *Advances in Engineering Software*, 35(10-11), p. 609–617. DOI: 10.1016/j.advengsoft.2003.07.002

Cole, D . Evaluation of design alternatives for roll-control of road vehicles. In: Proceedings of 5th International Symposium on Advanced Vehicle Control, AVEC 2000, Ann Arbor, MI, 22–24 August 2000, pp. 561–567.

Commission of the European Communities, 1999. *Case No COMP/M.1406 - Hyundai / Kia: Regulation (EEC) No 4064/89 Merger Procedure: Article 6(1)(b)*, Luxembourg: s.n. https://ec.europa.eu/competition/mergers/cases/decisions/m1406_en.pdf [Accessed 2019]

Czajka, G., 2014. *BMW i3-Nissan Leaf-VW E-Golf: Test*. [Online] Available at: <http://www.autobild.de/artikel/bmw-i3-nissan-leaf-vw-e-golf-test-5117168.html>

Daimler AG, 2005. *Autobilder: Mercedes-Benz B150*. [Online] Available at: <http://www.autobilderweb.com/bilder-mercedes-benz-b150> [Accessed 2019]

Daimler AG, 2008. *From Independent to Active Suspension*, Stuttgart: Daimler Communications. <https://media.daimler.com/marsMediaSite/ko/en/9361881> [Accessed 2019]

Daimler AG, 2013. *Mercedes-Benz CLA-Klasse: Das Fahrwerk des CLA verfügt über eine McPherson- Vorderachse und eine Raumlener-Hinterachse*. [Online] Available at: <https://media.daimler.com/marsMediaSite/de/instance/ko/CLA.xhtml?oid=9266868> [Accessed 2019]

Daimler AG, 2019. *Suspension: A Focus on Comfort*. [Online] Available at: <https://media.daimler.com/marsMediaSite/ko/en/9904520> [Accessed 2019]

Deo, H. & Suh, N. P., 2004. Axiomatic Design of Automobile Suspension and Steering Systems: Proposal for a Novel Six-Bar Suspension. *SAE Technical Paper*, Volume 2004-01-0811, pp. 189-198. ISSN: 0148-7191. DOI: <https://doi.org/10.4271/2004-01-0811>

Deo, H. V., & Suh, N. P., 2004. Axiomatic design of customizable automotive suspension. In: *Anais do ICAD2004-the 3rd International Conference on Axiomatic Design*. [Online] Available at: <https://axiomaticdesign.com/technology/icad/icad2004/icad-2004-38.pdf> [Accessed 2019]

Dodds, C. J. & Robson, J. D., 1973. The Description of Road Surface Roughness. *Journal of Sound and Vibration*, Volume 31, p. 175–183. DOI: 10.1016/S0022-460X(73)80373-6

Dym, C. L., 1994. *Engineering Design: A Synthesis of Views*. New York: Cambridge University. ISBN: 0-521-47760-3

Eckert, A., Eckstein, L., Gutzmer, P. & Jagt, P., 2018. Radnabenantriebe Wegbereiter für Raumeffizienz und Fahrdynamik. *MTZ - Motortechnische Zeitschrift*, 79(6), p. 48–55. DOI: <https://doi.org/10.1007/s35146-018-0033-7>

Eckstein, L., Göbbels, R. & Wohlecker, R., 2011. Benchmarking des Elektrofahrzeugs Mitsubishi i-MiEV. *ATZ - Automobiltechnische Zeitschrift*, Issue 11. DOI: <https://doi.org/10.1365/s35148-011-0223-9>

EMRAX d.o.o., 2014. *Technical Data and Manual for EMRAX Motors / Generators*. [Online] Available at: https://emrax.com/wp-content/uploads/2017/10/user_manual_for_emrax_motors.pdf [Accessed 2019]

Engelmann, S., 2013. *Simulation von fahrwerkdominierten Misuse-Lastfällen zur Unterstützung der virtuellen Crashsensorik*. Dissertation ed. Hamburg: Helmut-Schmidt-Universität /Universität der Bundeswehr Hamburg. ISBN: 978-3-18-092169-3

Falk, A., 2011. *BYD e6 (2010)*. [Online] Available at: <http://www.automativ.de/byd-e6-2010-id-395.html> [Accessed 2018]

Feng, J. et al., 2013. A Frequency Compensation Algorithm of Four-Wheel Coherence Random Road. *Mathematical Problems in Engineering*, Volume 2013. DOI: 10.1155/2013/986584

Fischer, R., 2014. *Flinker in der Stadt: Radnabenantriebe von Schaeffler*. Baden-Baden, Schaeffler Kolloquium.

Fongue, W. A., Kieserling, J. & Pelz, P. F., 2014. *Air Spring Damper, on the Way to Exceptional Sliding: Modeling, Development and Optimization of an Air Spring Damper with Regard to Ride Comfort and Handling*. Munich. ISBN: 978-3-658-05977-4. DOI: 10.1007/978-3-658-05978-1_19

Ford Motor Company, 2015. *Ford Focus-Specifications & Options*. [Online] Available at: <https://www.ford.com.au/cars/focus/compare-models/> [Accessed 2019]

Friedrich, H. E., 2013. Konzeptleicht. In: *Leichtbau in der Fahrzeugtechnik*. Stuttgart: Springer Vieweg, pp. 68-70. ISBN: 978-3-8348-2110-2. DOI: 10.1007/978-3-8348-2110-

- Gadd, K., 2011. *TRIZ for Engineers*. United Kingdom: Wileys. ISBN: 978-0-470-74188-7
- Gaertner, T., Terstegen, S. & Schlick, C. M., 2015. Applying DSM Methodology to Improve the Scheduling of Calibration Tasks in Functional Integration Projects in the Automotive Industry. *The Journal of Modern Project Management*, Volume Special Issue DSM Conference 2014, pp. 47-55. DOI: 10.3139/9781569904923.027
- Gebala, D. A. & Suh, N. P., 1992. An Application of Axiomatic Design. *Research in Engineering Design*, 3(3), pp. 149-162. DOI: 10.1007/BF01580517
- Geis, C. & Birkhofer, H., 2010. *Classification and Synthesis of Design Theories*. In: *DS 60: Proceedings of DESIGN 2010, the 11th International Design Conference*. Dubrovnik, Croatia.
- Gillespie, T. D., 1992. *Fundamentals of Vehicle Dynamics*. United States: SAE International. ISBN of 978-1-56091-199-9
- Glaser, H. & Schweizer, R., 2007. Das Dynamikfahrwerk des neuen Audi A4. *ATZ Extra*, 12(1), pp. 102-103. DOI: 10.1365/s35778-007-0020-y
- Gombert, B., November 2007. *Technologie- und Innovationstrends aus der Zuliefer-Perspektive: Neue Fahrzeugkonzepte erfordern einen ganzheitlichen Ansatz in der Integrationsstrategie*. Munich, Siemens VOD Automotive AG. [Online] Available at: https://www.munichnetwork.com/fileadmin/user_upload/konferenzen/mobilitaetsforum-2/071128MUN_Gombert_Bernd.pdf [Accessed 2019]
- Grabianowski, E., 2006. *Tesla Roadster Motor and Other Features*. [Online] Available at: <http://auto.howstuffworks.com/tesla-roadster1.htm> [Accessed 2019]
- Griffin, M. J., 1990. *Handbook of Human Vibration*. London: Academic Press. ISBN: 978-0-12-303040-5. DOI: 10.1016/C2009-0-02730-5
- Grigoriu, M., 1993. On the Spectral Representation Method in Simulation. *Probabilistic Engineering Mechanics*, 8(2), p. 75–90. DOI: 10.1016/0266-8920(93)90002-D

Gumpinger, T. & Krause, D., 2008. *Potenziale der Methode Funktionsintegration beim Leichtbau von Flugzeugküchen*. Erlangen, Germany. Corpus ID: 185261387

Gysen, B., Paulides, J., Janssen, J. & Lomonova, E., 2010. Active Electromagnetic Suspension System for Improved Vehicle Dynamics. *Vehicular Technology, IEEE Transactions*, 59(3), pp. 1156 - 1163. ISSN: 0018-9545. DOI: 10.1109/TVT.2009.2038706

HAĆ, A., 2010. Adaptive Control of Vehicle Suspension. *Vehicle System Dynamics*, 16(2), pp. 57-74. DOI: 10.1080/00423118708968870

Harkort, C. et al., 2018. *Mobile in the City of Tomorrow - The Fusion of Drive and Chassis*. [Online] Available at: <http://schaeffler-events.com/symposium/lecture/c1/index.html> [Accessed 2019]

Hatchuel, A., 1996. *Théories et modèles de la conception, Cours d'ingénierie de la conception*. Paris: École des Mines de Paris.

Heath, A., 1987. Application of the Isotropic Road Roughness Assumption. *Journal of Sound and Vibration*, 115(1), p. 131–144. DOI: 10.1016/0022-460X(87)90495-0

Heißing, B. & Ersoy, M., 2007. *Fahrwerkhandbuch-Grundlagen, Fahrdynamik, Komponenten, Systeme, Mechatronik, Perspektiven*. 2 ed. Germany: Vieweg+Teubner Verlag. ISBN: 978-3-8348-0444-0. DOI: <https://doi.org/10.1007/978-3-8348-9493-9>

Heißing, B., Ersoy, M. & Gies, S., 2013. *Fahrwerkhandbuch: Grundlagen Fahrdynamik Komponenten Systeme Mechatronik Perspektiven*. 4 ed. s.l.:Springer Vieweg. ISBN: 978-3-658-01992-1. DOI: 10.1007/978-3-658-01992-1

Henker, E., 1993. *Fahrwerktechnik: Grundlagen, Bauelemente, Auslegung*. s.l.:Vieweg+Teubner Verlag. ISBN: 978-3-322-93854-1. DOI: 10.1007/978-3-322-93854-1

Henning, F. & Moeller, E., 2010. *Handbuch Leichtbau - Methoden, Werkstoffe und Fertigung*. s.l.:Carl Hanser Verlag GmbH & Co. KG. ISBN: 978-3-446-42267-4

Hieronimus, K., 1990. *Anforderungen an Schwingung- und Akustikberechnungen*, Düsseldorf: VDI-Bericht Nr.186. DOI: https://doi.org/10.1007/978-3-663-13955-3_4

Hughes, A. & Drury, B., 2013. *Electric Motors and Drives - Fundamentals, Types and Applications*. 4 ed. s.l.:Newnes. ISBN: 9780080993683

Husain, I., 2010. *Electric and Hybrid Vehicles Design Fundamentals*. USA: CRC Press. ISBN: 1439811784, 9781439811788

Iliev, V., 2011. *Systemansatz zur anregungsunabhängigen Charakterisierung des Schwingungskomforts eines Fahrzeugs*. Karlsruhe: Karlsruher Institut für Technologie. ISBN: 9783866446816

ISO 1940-1:1986, 1986. *Mechanical Vibration - Balance Quality Requirements of Rigid Rotors - Part 1: Determination of Permissible Residual Unbalance*, Switzerland: ISO copyright office.

ISO 4130: 1978, 1978. *Road vehicles-Three-dimensional reference system and fiducial marks- Definitions*. [Online] Available at: <https://www.iso.org/standard/9886.html> [Accessed 2019]

ISO 8608: 1995(E), 1995. *Mechanical Vibration - Road Surface Profiles - Reporting of Measured Data*. [Online] Available at: <https://www.iso.org/standard/15913.html> [Accessed 2019]

Jänsch, J. & Birkhofer, H., 2006. *The Development of the Guideline VDI 2221- the Chance of Direction*. In: *International Design Conference – Design 2006*. Croatia. ISBN: 953-6113-78-2

Jin, Y., Li, W. & Lu, S. C.-Y., 2005. A Hierarchical Co-Evolutionary Approach to Conceptual Design. *Annals of the CIRP*, 54(1), pp. 155-158. DOI: [https://doi.org/10.1016/S0007-8506\(07\)60072-9](https://doi.org/10.1016/S0007-8506(07)60072-9)

Johannesson, P., Podgórski, K. & Rychlik, I., 2014. *Modelling Roughness of Road Profiles on Parallel Tracks using Roughness Indicators*. Gothenburg Sweden: Chalmers University of Technology and University of Gothenburg. ISSN 1652-9715

Jungmann, T., 2006. *Hybrid-Antrieb nur Zwischenlösung auf dem Weg zu eCorner*. [Online] Available at: <http://www.springerprofessional.de/hybrid-antrieb-nur-zwischenloesung-auf-dem-weg-zu-ecorner-5422/3940612.html> [Accessed 2019]

Kim, J. H., Kim, K. S. & Kang, Y. J., 2007. Ride Comfort Evaluation and Suspension Design Using Axiomatic Design. *Journal of Mechanical Science and Technology*, 21(7), pp. 1066-1076. DOI: <https://doi.org/10.1007/BF03027656>

Kiyota, K. & Chiba, A., 2012. Design of Switched Reluctance Motor Competitive to 60 kW IPMSM in Third Generation Hybrid Electric Vehicle. *IEEE Transactions on Industry Applications*, 48(6), pp. 2303 - 2309. DOI: 10.1109/TIA.2012.2227091

Klein, B., 2009. Leichtbauweisen. In: *Leichtbau-Konstruktion: Berechnungsgrundlagen und Gestaltung*. Wiesbaden: Vieweg+Teubner, pp. 17-20. ISBN: 978-3-8348-9965-1. DOI: 10.1007/978-3-8348-9965-1

Koch, G., 2010. *Adaptive Control of Mechatronic Vehicle Suspension Systems*. Munich: TU München. ISBN: 3844000208, 9783844000207

Koller, R., 1998. *Konstruktionslehre für den Maschinenbau: Grundlagen zur Neu- und Weiterentwicklung technischer Produkte mit Beispielen*. Berlin: Springer Verlag. ISBN: 978-3-642-80417-5. DOI: 10.1007/978-3-642-80417-5

Konica Minolta Sensing Inc, 2004-2006. *Non-contact 3D Digitizer Vivid 9i/VI-9i-Instruction Manual*, Japan.

Kopp, G., Friedrich, H. E., Kuppinger, J. & Henning, F., 2009. Innovative Sandwichstrukturen für den funktionsintegrierten Leichtbau. *ATZ Automobiltechnische Zeitschrift*, 111(4), p. 298–305. DOI: <https://doi.org/10.1007/BF03222069>

- Kota, S., Londal, G. F. & Flynn, M. S., 1998. *Automotive Product Design and Development Delphi: Forecast and Analysis of the North American Auto Industry Trends Through 2007*. Michigan, USA: Office for the Study of Automotive Transportation, University of Michigan, Transportation Research Institute. [Online] Available at: <https://deepblue.lib.umich.edu/handle/2027.42/1260> [Accessed 2019]
- Kranzeder, J., 2013. *OptiStruct Optimization: Concept and Fine-Tuning Design*. s.l.:Altair Engineering, Inc. [Online] Available at: <https://altairhyperworks.de/solution/Optimization> [Accessed 2019]
- Kunz, J. & Studer, M., 2006. Druck-Elastizitätsmodul über Shore-A-Härte ermitteln. *Kunststoffe*, Volume 6, pp. 92-94. München: Carl Hanser Verlag.
- Kurata, F., *Suspension System for Electric Vehicle*. USA, Patent No. US20060225931A1, Assignee: Toyota Jidosha Kabushiki Kaisha, Publication date: Oct. 12, 2006
- Kurzeck, B. & Kaiser, I., 2013. Running Dynamics Concept with Mechatronic Guidance. *Rail Technology Review (RTR)*, pp. 30-36. ISBN 978-3-7771-0435-5. ISSN 1869-7801
- Lee, D. & Yang, C., 2013. An Analytical Approach for Design and Performance Evaluation of Torsion Beam Rear Suspension. *Finite Elements in Analysis and Design*, Volume 63, p. 98–106. DOI: <https://doi.org/10.1016/j.finel.2012.09.002>
- Lee, H.-A. & Park, G.-J., 2012. Topology Optimization for Structures With Nonlinear Behavior Using the Equivalent Static Loads Method. *Journal of Mechanical Design*, 134(3). DOI: 10.1115/1.4005600
- Lee, S.-I. et al., 2007. Integrated Process for Structural–Topological Configuration Design of Weight-Reduced Vehicle Components. *Finite Elements in Analysis and Design*, 43(8), pp. 620-629. DOI: 10.1016/j.finel.2007.01.003
- Linning, W. et al., 2009. Die Verbundlenkerhinterachse Auslegung, Materialien, Prozesse und Konzepte. *ATZ*, 111(2), pp. 100-109. DOI: 10.1007/BF03222050

Li, W., 2006. *A Hierarchical Co-evolutionary Approach to Conceptual Design*. Los Angeles: University of Southern California, Ph.D thesis. [Online] Available at: <http://digitallibrary.usc.edu/cdm/compoundobject/collection/p15799coll16/id/584578/rec/1> [Accessed 2019]

Luan, Y., 2012. *Development of Chang'An E30 Electric Vehicle*, Washinton, USA: United Nations Economic Commission for Europe. [Online] Available at: <https://www.unece.org/fileadmin/DAM/trans/doc/2012/wp29grsp/EVS-1-09.pdf> [Accessed 2019]

Magrab, E. B., Gupta, S. K., McCluskey, F. P. & Sandborn, P., 2009. *Integrated Product and Process Design and Development: The Product realization process*. USA: Taylor & Francis. ISBN 9780367385378

Mair, U., Heimann, J. & Pollmeyer, S.. *Antriebsvorrichtung zum Antreiben eines Rades für ein elektrisch antreibbares Fahrzeug*. Germany, Patent No. DE 102011005618 A1. Assignee: ZF Friedrichshafen AG. Publication date: Sep. 20, 2020

Maydell, M., 2012. *Audi A1 E-Tron im Fahrbericht: Wankelmutig über 250 Kilometer*. [Online] Available at: <http://www.auto-motor-und-sport.de/fahrberichte/audi-a1-e-tron-wankelmutig-ueber-250-kilometer-5243744.html> [Accessed 2019]

Maydell, M., 2011. *Mercedes A-Klasse E-Cell: Kompaktwagen mit Elektroantrieb*. [Online] Available at: <http://www.auto-motor-und-sport.de/fahrberichte/mercedes-a-klasse-e-cell-test-kompaktwagen-mit-elektroantrieb-3921446.html> [Accessed 2019]

Mercedes-Benz USA, LLC, 2014. *Electric Drive Features and Specifications*. [Online] Available at: <http://www.smartusa.com/models/electric-drive/overview.aspx#/module/range> [Accessed 2019]

Mitschke, M. & Wallentowitz, H., 2004. *Dynamik der Kraftfahrzeuge*. Berlin: Springer-Verlag Berlin Heidelberg. ISBN: 978-3-662-06802-1. DOI: 10.1007/978-3-662-06802-1

- Ecomento.de, 2019. Mitsubishi Electric Vehicle (i-MiEV). [Online] Available at: <https://www.mitsubishi-motors.ch/modelle/i-miev/> [Accessed 2019]
- Mucka, P., 2004. Road Waviness and the Dynamic Tyre Force. *International Journal of Vehicle Design*, 36(2-3), p. 216–232. DOI: 10.1504/IJVD.2004.005357
- Müller, G. & Ponick, B., 2005. *Grundlagen elektrischer Maschinen*. s.l.:WILEY-VCH. ISBN: 978-3-527-40524-4
- Mun, K.-J., Kim, T.-J. & Kim, Y.-S., 2010. Analysis of the Roll Properties of a Tubular-type Torsion Beam Suspension. *Proceedings of the Institution of Mechanical Engineers, Part D: Journal of Automobile Engineering*, 224(1), pp. 1-13. DOI: 10.1243/09544070JAUTO1229
- Odhams, A. & Cebon, D., 2006. An Analysis of Ride Coupling in Automobile Suspensions. *Proceedings of the Institution of Mechanical Engineers, Part D: Journal of Automobile Engineering*, 220(8), p. 1041–1061. DOI: 10.1243/09544070D18404
- Ogando, J., 2005. *Electric Racer*. [Online] Available at: <http://www.designnews.com> [Accessed 2014]
- Ogden, R. W., 1997. *Non-linear Elastic Deformations*. New York: Dover Publications. ISBN-10 : 0486696480
- Oppenheim, A. V. & Verghese, G. C., 2010. *Signals, Systems, and Inference*, Cambridge: Massachusetts Institute of Technology. ISBN-10 : 0133943283
- Oswald, W., 1987. *Mercedes-Benz Personenwagen 1886–1986*. Stuttgart: Motorbuch Verlag. ISBN: 3613011336 / 3-613-01133-6
- Overholser, R., 2006. *997.1 GT3 Cup Homologation*. [Online] Available at: <http://www.gt3r.com/06gt3.html> [Accessed 2019].

Pahl, G., Beitz, W., Feldhusen, J. & Grote, K., 2007. *Engineering Design: A Systematic Approach*. 3 ed. London: Springer. ISBN: 978-1-84628-319-2. DOI: 10.1007/978-1-84628-319-2

Park, G.-J., 2007. *Analytic Methods for Design Practice*. London: Springer-Verlag. ISBN: 978-1-84628-473-1. DOI: 10.1007/978-1-84628-473-1

Park, G.-J., 2014. *Recent Advances in Nonlinear Response Structural Optimization Using the Equivalent Static Loads Method*. Monterey, USA. [Online] Available at: https://www.vrand.com/sites/default/files/pub/VRD-2014UConf_GJPark_Keynote2_HanyangU.pdf [Accessed 2019]

Peebles, P. Z., 2001. *Probability, Random Variables and Random Signal Principles*. Boston: McGraw-Hill Inc. ISBN: 0073660078, 9780073660073

Phillips, D., 2004. *Report: S197 Ford Mustang could Have Had Independent Rear Suspension for \$100 per Car*. [Online] Available at: <http://www.autoblog.com> [Accessed 2019].

Poetter, M., 2013. *Elektromobilität: Forschungsprojekt FAIR verlegt Antrieb ins Rad*. [Online] Available at: http://www.dlr.de/dlr/presse/desktopdefault.aspx/tabid-10310/473_read-6724/year-all/#/gallery/9297 [Accessed 2019]

Priest, J. & Sanchez, J., 2001. *Product Development and Design for Manufacturing: A Collaborative Approach to Producibility and Reliability*. Basel: CRC Press. ISBN 10: 0824799356 ISBN 13: 9780824799359

Protean Electric Ltd, 2016. *Understanding the Challenges of Integrating In-Wheel Motors*, United Kingdom. [Online] Available at: https://www.proteanelectric.com/f/2018/04/2016-03-28_TMC2016-SAE-2.pdf [Accessed 2019]

Protean Electric, 2010. *Hi-Pa Drive*. [Online] Available at: <http://www.proteanelectric.com/en/> [Accessed 2019]

Pruckner, A., Davy, E., Schlichte, D. & Kaspar, S., March 2014. Electric Single Wheel Drive Optimised Installation Space at Maximum Vehicle Dynamics. *ATZ worldwide*, Volume 116, pp. 28-33. DOI: 10.1007/s38311-014-0150-y

Pudenz, K., 29. Juli 2013. "Born electric": BMW i3 Weltpremiere in New York, London und Peking. [Online] Available at: <https://www.springerprofessional.de/automobil---motoren/batterie/born-electric-bmw-i3-weltpremiere-in-new-york-london-und-peking/6562128> [Accessed 2019]

Rahman, Z., Ehsani, M. & Butler, K. L., August, 2000. *An Investigation of Electric Motor Drive Characteristics for EV and HEV Propulsion Systems*. USA: SAE Technical Paper. ISSN: 0148-7191. DOI: <https://doi.org/10.4271/2000-01-3062>

Rautaruukki Corporation, 2014. *Boron Steel 22MnB5*. [Online] Available at: <http://www.ruukki.com/Steel/Cold-rolled-steels/Hardenable-steels/Boron-steel-22MnB5> [Accessed 2019].

Reimpell, J. & Betzler, J. W., 2005. *Fahrwerktechnik: Grundlagen*. Würzburg: Vogelbuchverlag. ISBN-13: 978-3-8343-3031-4

Reimpell, J., Stoll, H. & Betzler, J. W., 2001. *The Automotive Chassis: Engineering Principles*. Würzburg: Elsevier Science. ISBN: 9780080527734

Samaras, E., Shinzuka, M. & Tsurui, A., 1985. ARMA Representation of Random Processes. *Journal of Engineering Mathematics*, 111(3), p. 449–461. DOI: [https://doi.org/10.1061/\(ASCE\)0733-9399\(1985\)111:3\(449\)](https://doi.org/10.1061/(ASCE)0733-9399(1985)111:3(449))

Schindler, T., 2013. *Multi-Body Simulation*. München: Technische Universität München. [Online] Available at: <https://campus.tum.de/tumonline/wbLv.wbShowLVDetail?pStpSpNr=950092538&pSpracheNr=2> [Accessed 2019]

Sessions, R., 2013. *2013 Honda Fit EV*. [Online] Available at: <http://www.caranddriver.com/reviews/2013-honda-fit-ev-test-review> [Accessed 2019]

Sharp, R., 2001. Fundamentals of the Lateral Dynamics of Road Vehicles. In: *Mechanics for a New Millennium*. Dordrecht: Springer, p. 127–146. ISBN: 978-0-306-46956-5. DOI: https://doi.org/10.1007/0-306-46956-1_9

Sokolowski, J. & Zolesio, J., 1992. *Introduction to Shape Optimization: Shape Sensitivity Analysis*. s.l.:Springer-Verlag Berlin Heidelberg. ISBN 10: 3540541772 ISBN 13: 9783540541776

Steel Market Development Institute, 2013. *Lightweight Twist Beam Final Report*, Southfield, Michigan, USA. [Online] Available at: <https://studylib.net/doc/18710728/lightweight-steel-twist-beam-achieves-30-percent-mass> [Accessed 2019]

Sterbak, R., 2007. *Technology for the Environment – Environmentally Friendly Transportation Lowering Emissions*. [Online] Available at: http://www.siemens.com/innovation/en/publikationen/publications_pof/pof_spring_2007/technology_for_the_environment/green_transportation.htm [Accessed 2019]

Steward, D., 1981. The Design Structure System: a Method for Managing the Design of Complex Systems. *IEEE Transactions on Engineering Management*, 28(3), pp. 71-74. DOI: 10.1109/TEM.1981.6448589

Suh, N. P., 1990. *The Principles of Design*. New York: Oxford University Press. ISBN: 9780195043457

Suh, N. P., 2001. *Axiomatic Design: Advances and Applications*. Oxford University Press. ISBN 0-19-513466-4

Sushkov, V., Mars, N. & Wognum, P., 1995. Introduction to TIPS: a Theory for Creative Design. *Artificial Intelligence in Engineering*, 9(3), pp. 177-189. DOI: [https://doi.org/10.1016/0954-1810\(95\)00002-Z](https://doi.org/10.1016/0954-1810(95)00002-Z)

Tang, D., Zhang, G. & Dai, S., 2008. Design as Integration of Axiomatic Design and Design Structure Matrix. *Robotics and Computer-Integrated Manufacturing*, Volume 25, pp. 610-619. DOI: 10.1016/j.rcim.2008.04.005

Tobisch, K., 1981. Über den Zusammenhang zwischen Härte und Elastizitätsmodul. *Kautschuk+Gummi Kunststoffe*, 34(02), pp. 105-109.

Torrance, C., 2009. *2009 Honda Pilot: Chassis*. [Online] Available at: <http://hondanews.com/channels/honda-automobiles-pilot> [Accessed 2008].

VDI-Guideline 2221, 1993. *Systematic Approach to the Design of Technical Systems and Products*, Düsseldorf: VDI Gesellschaft für Entwicklung Konstruktion Vertrieb. [Online] Available at: <https://www.vdi.de/richtlinien/details/vdi-2221-methodik-zum-entwickeln-und-konstruieren-technischer-systeme-und-produkte> [Accessed 2019]

Vijayenthiran, V., 2008. *Michelin's Active Wheel technology in detail*. [Online] Available at: http://www.motorauthority.com/news/1030025_michelins-active-wheel-technology-in-detail [Accessed 2019]

Vogt, K. A., 1996. *Berechnung Elektrischer Maschinen*. Wiley-VCH Verlag GmbH: Weinheim. ISBN-10 : 3527283919. ISBN-13 : 978-3527283910

Volkswagen AG, 1996. *Semi-Trailing Arm Suspension*. [Online] Available at: <http://en.volkswagen.com/en/innovation-and-technology> [Accessed 2019].

Volkswagen AG, 2013. *Torsion Beam Rear Suspension*. [Online] Available at: <http://en.volkswagen.com/en/innovation-and-technology> [Accessed 2014].

Volkswagen AG, 2019. *Volkswagen UK Technology Glossary*. [Online] Available at: http://www.vwgolf.org/overview_rear_axle_multi_link_suspension-1906.html [Accessed 2019].

- Wallentowitz, H. & Freialdenhoven, A., 2011. *Strategien zur Elektrifizierung des Antriebsstranges*. Deutschland: ATZ/MTZ-Fachbuch. ISBN: 978-3-8348-9910-1. DOI: 10.1007/978-3-8348-9910-1
- Wijker, J., 2004. *Mechanical Vibrations in Spacecraft Design*. Springer-Verlag Berlin Heidelberg. ISBN: 978-3-662-08587-5. DOI: 10.1007/978-3-662-08587-5
- Wilde, J., Heydinger, G., Guenther, D. & Mallin, T., 2005. Experimental Evaluation of Fishhook Maneuver Performance of a Kinetic Suspension System. *SAE Technical Paper*, Volume 2005-01-0392. DOI: <https://doi.org/10.4271/2005-01-0392>
- Winterkorn, M. & König, H., 2001. Der neue VW Polo. *ATZ - Automobiltechnische Zeitschrift*, 103(12), p. 1116–1127. DOI: <https://doi.org/10.1007/BF03223466>
- Wöstmann, F., 2011. *Neues Konzept für Radnabenmotoren mit gesteigerter leistungsdichte und Notlaufeigenschaften – Material, Auslegung, Fertigung und Regelung*. Fraunhofer-Institute for Manufacturing and Advanced Materials IFAM. DOI: <https://doi.org/10.2314/GBV:679566368>
- Wriggers, P., 2008. *Nonlinear Finite Element Methods*. Springer-Verlag Berlin Heidelberg. ISBN: 978-3-540-71001-1. DOI: 10.1007/978-3-540-71001-1
- Xue, S., 2009. *电动车双纵臂悬架—轮边驱动系统的设计与研究*. Shanghai: Tongji University, Master thesis.
- Xue, X. D., Cheng, K. & Cheung, N. C., 2008. *Selection of Electric Motor Drives for Electric Vehicles*. Sydney, NSW, Australia, IEEE. ISBN: 978-0-7334-2715-2
- Yamada, T., Izui, K., Nishiwaki, S. & Takezawa, A., 2010. A Topology Optimization Method based on the Level Set Method Incorporating a Fictitious Interface Energy. *Computer Methods in Applied Mechanics and Engineering*, 199(45–48), p. 2876–2891. DOI: 10.1016/j.cma.2010.05.013

Yang, X., Xie, Y., Steven, G. & Querin, O., 1999. Topology Optimization for Frequencies Using an Evolutionary Method. *Journal of Structural Engineering*, 125(12), p. 1432–1438. DOI: [https://doi.org/10.1061/\(ASCE\)0733-9445\(1999\)125:12\(1432\)](https://doi.org/10.1061/(ASCE)0733-9445(1999)125:12(1432))

YASA Motors, 2014. *YASA Motors: Powering the Future*. [Online] Available at: <http://www.yasamotors.com/> [Accessed 2019].

Yoshimura, T., 1998. A Semi-active Suspension of Passenger Cars using Fuzzy Reasoning and the Field Testing. *International Journal of Vehicle Design*, 19(2), pp. 150-166. DOI: 10.1504/IJVD.1998.062100

Zandbergen, P., 2004. *A Composite Beam as a Multifunctional Suspension Component*. Netherlands: Universiteit Twente. ISBN: 90-365-2104-1

Zeller, P., 2009. *Handbuch Fahrzeugakustik-Grundlagen, Auslegung, Berechnung, Versuch*, s.l.: Vieweg+Teubner Verlag. ISBN: 978-3-8348-8657-6. DOI: 10.1007/978-3-8348-8657-6

Zhang, X., 2006. *NPD in Indigenous Chinese Companies and its Deployment within the Chinese Economy*. Florida: University of Salford Salford, Dissertation. ISBN: 158112340X, 9781581123401

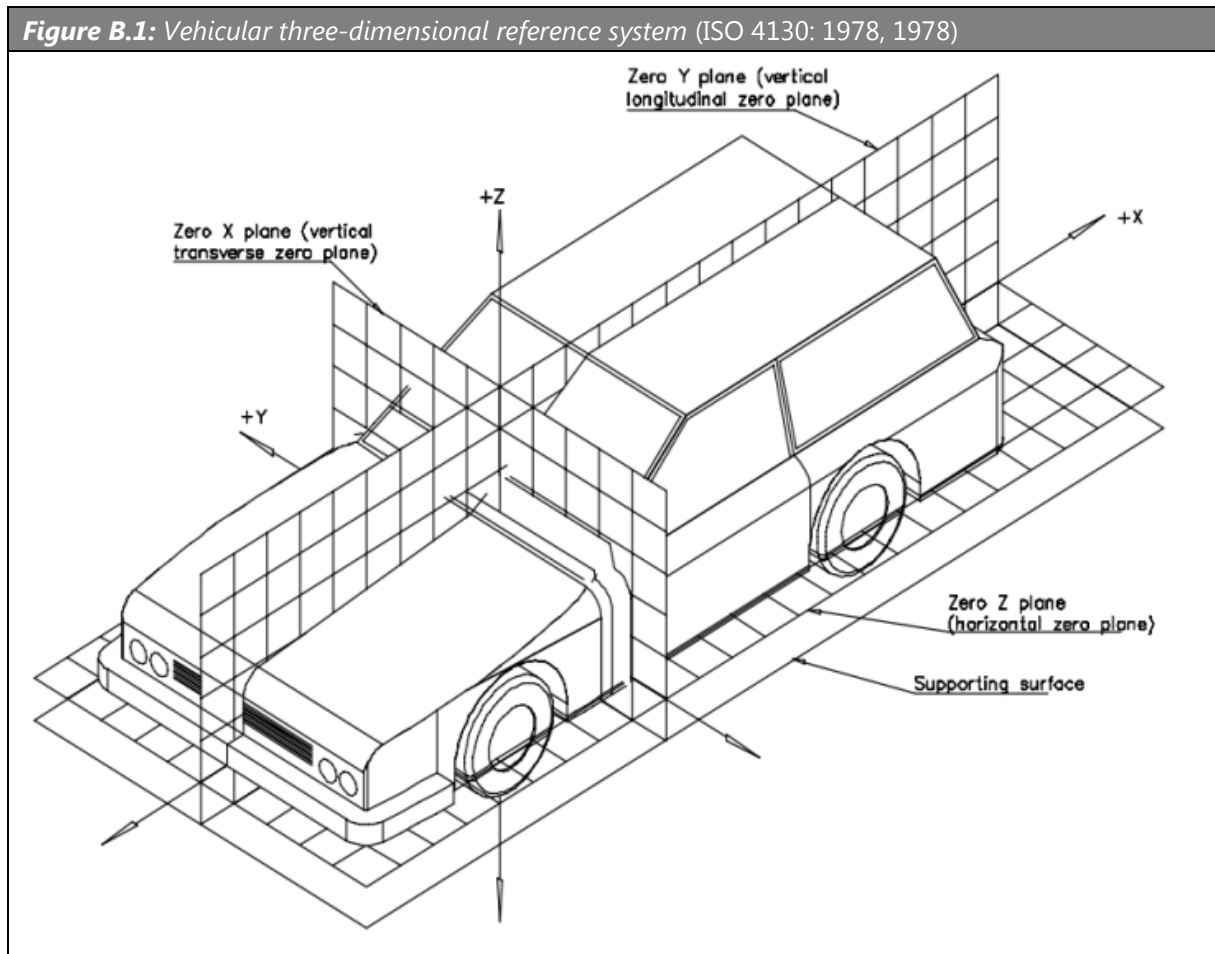
Ziebart, J. R., 2012. *Ein konstruktionsmethodischer Ansatz zur Funktionsintegration, Dissertation, TU Braunschweig*. München: Verlag Dr. Hut. ISBN: 9783843905671 3843905673

Appendices

A. Data of economic EVs in the market and concepts

<i>Table A.1: Investigation of economic EVs in the market and concepts</i>					
EVs	Acceleration / 0-100 km/h / s	Top speed / km/h	Power / kW	Torque / Nm	Weight / kg
Mitsubishi i-MiEV (Ecomento.de, 2019)	15.9	130	49	180	1185
Nissan Leaf (Czajka, 2014)	11.3	144	80	254	1523
HONDA Fit EV (Sessions, 2013)	8.7	143	93	256	1468
Kia Soul EV (Branke, 2014)	11.2	145	81	285	1565
BYD e6 (Falk, 2011)	14	140	90	450	2380
Chang'An E30 (Luan, 2012)	12	125	85	280	1610
Chevrolet Spark EV 1.0 (Anon., 2013) (Anon., 2014)	8.5	130	105	542	1346
E-Golf (Czajka, 2014)	10.2	140	85	270	1518
Smart Fortwo (Mercedes-Benz USA, LLC, 2014)	11.5	125	55	130	900
Audi A1 e-tron (Maydell, 2012)	10.4	130	75	240	1410
BMW i3 (BMW AG, 2014)	7.2	150	125	250	1270
Mercedes A-Klasse E- Cell (Maydell, 2011)	11.8	150	70	290	1591

B. Vehicular three-dimensional reference system



Information:

Roll dynamics means the rotational dynamics around the axis X;

Yaw dynamics means the rotational dynamics around the axis Z;

Pitch dynamics means the rotational dynamics around the axis Y.

C. Data of the electric motor AMK DT5-26-10-POW

Figure C.1: Technology performance of the AMK DT5-26-10-POW (AMK Antriebs- und Steuerungstechnik GmbH Co. KG, 2012)

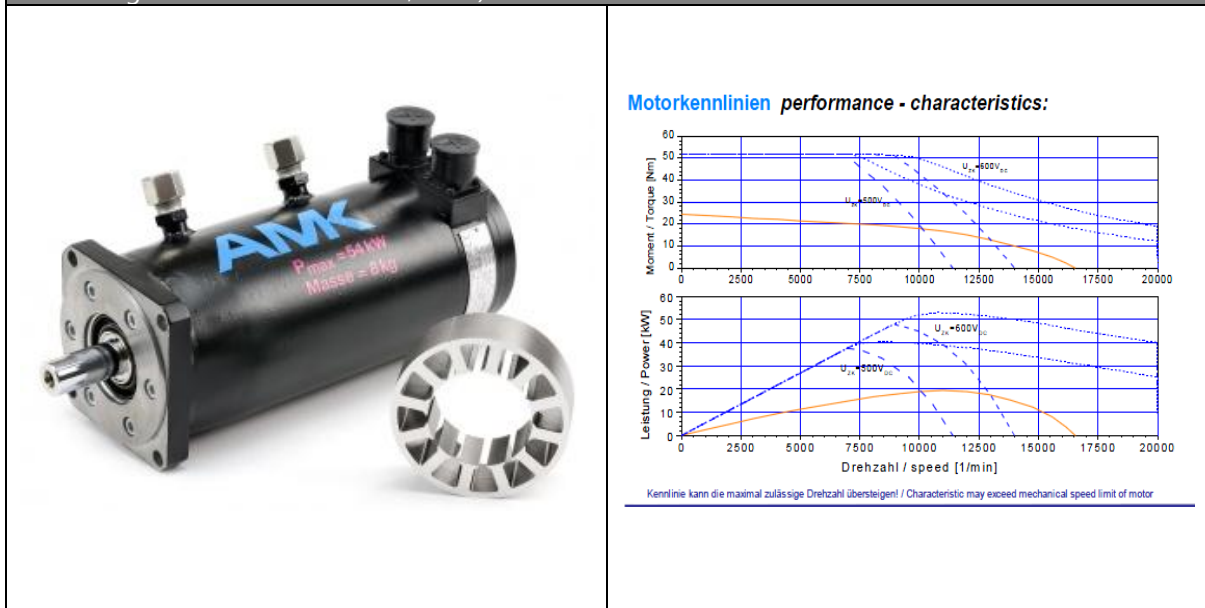


Table C.1: Motor specification of the AMK DT5-26-10-POW (AMK Antriebs- und Steuerungstechnik GmbH Co. KG, 2012)

Type	Synchronous
Cooling type:	Water cooling
Maximum torque	51.3 Nm
Rated torque	18 Nm
Maximum power	52 kW
Rated power	19 kW
Number of poles	10
Rated speed	10000 rpm
Motor mass with case	8 kg
Motor mass without case	6 kg
Moment of inertia	5.2 kg · cm ²

D. Functional integration in case 2 and case 3

Case 2

In case 2, one of the systems to be combined is a decoupled design. Assuming system 1 is the decoupled design expressed by equation ((D-1), in this system, FR_1 to be integrated is impacted by both DP_1 and DP_3 .

$$\begin{Bmatrix} FR_1 \\ FR_2 \\ FR_3 \end{Bmatrix} = \begin{bmatrix} \times & 0 & \times \\ 0 & \times & 0 \\ 0 & 0 & \times \end{bmatrix} \begin{Bmatrix} DP_1 \\ DP_2 \\ DP_3 \end{Bmatrix} \quad (D-1)$$

System 2 is an uncoupled system.

$$\begin{Bmatrix} FR'_1 \\ FR'_2 \\ FR'_3 \end{Bmatrix} = \begin{bmatrix} \times & 0 & 0 \\ 0 & \times & 0 \\ 0 & 0 & \times \end{bmatrix} \begin{Bmatrix} DP'_1 \\ DP'_2 \\ DP'_3 \end{Bmatrix} \quad (D-2)$$

FR_1 and FR'_1 are the common functions of two different systems. The difference with case 1 is that in case 2 the DPs are in the physical domain, not only the feasibility combining DP_1 and DP'_1 but also the effect of DP_3 should be considered. The process combining the two matrices of the systems is likewise executed as that in case 1. The equation (D-1) and equation (D-2) are unified in equation.

$$\begin{Bmatrix} FR_1 \\ FR_2 \\ FR_3 \\ FR'_1 \\ FR'_2 \\ FR'_3 \end{Bmatrix} = \begin{array}{c} \begin{array}{cc} P_1 & P_2 \end{array} \\ \begin{array}{|ccc|ccc|} \hline \times & 0 & \times & ? & ? & ? \\ \hline 0 & \times & 0 & ? & ? & ? \\ \hline 0 & 0 & \times & ? & ? & ? \\ \hline \end{array} \\ \begin{array}{cc} P_3 & P_4 \end{array} \end{array} \begin{Bmatrix} DP_1 \\ DP_2 \\ DP_3 \\ DP'_1 \\ DP'_2 \\ DP'_3 \end{Bmatrix} \quad (D-3)$$

To define the rows representing the effect on the common FRs in the DM of the system 1 and system 2, like case 1, DP_1 has an effect on FR_1 , so it has also a cross effect on FR'_1 in the combination; DP_2 has no effect on FR_1 , then it has no cross effect on FR'_1 ; DP_3 has an effect on FR_1 , so it has an effect on FR'_1 ; so do the cross effects of DP'_1 , DP'_2 and DP'_3 .

To define the columns representing the effect of the DPs to be combined in the DM of the system 1 and system 2, if either DP_1 and DP'_1 has an effect on an FR , after combination the DP''_1 must have an effect on this FR .

$$\begin{Bmatrix} FR_1 \\ FR_2 \\ FR_3 \\ FR'_1 \\ FR'_2 \\ FR'_3 \end{Bmatrix} = \begin{bmatrix} \times & 0 & \times & \times & 0 & 0 \\ 0 & \times & 0 & ? & ? & ? \\ 0 & 0 & \times & ? & ? & ? \\ \times & 0 & \times & \times & 0 & 0 \\ ? & ? & ? & 0 & \times & 0 \\ ? & ? & ? & 0 & 0 & \times \end{bmatrix} \begin{Bmatrix} DP_1 \\ DP_2 \\ DP_3 \\ DP'_1 \\ DP'_2 \\ DP'_3 \end{Bmatrix} \quad (D-4)$$

The combined DM is expressed in equation (D-5) with the unknown elements which should be defined depending on the specific situation.

$$\begin{Bmatrix} FR''_1 \\ FR_2 \\ FR_3 \\ FR'_2 \\ FR'_3 \end{Bmatrix} = \begin{bmatrix} \times & 0 & \times & 0 & 0 \\ ? & \times & 0 & ? & ? \\ ? & 0 & \times & ? & ? \\ ? & ? & ? & \times & 0 \\ ? & ? & ? & 0 & \times \end{bmatrix} \begin{Bmatrix} DP''_1 \\ DP_2 \\ DP_3 \\ DP'_2 \\ DP'_3 \end{Bmatrix} \quad (D-5)$$

Case 3

In this case, system 1 is assumed to be a decoupled design described by equation (D-6) where the DP_1 to be combined has an effect on both FR_1 and FR_3 .

$$\begin{Bmatrix} FR_1 \\ FR_2 \\ FR_3 \end{Bmatrix} = \begin{bmatrix} \times & 0 & 0 \\ 0 & \times & 0 \\ \times & 0 & \times \end{bmatrix} \begin{Bmatrix} DP_1 \\ DP_2 \\ DP_3 \end{Bmatrix} \quad (D-6)$$

System 2 is assumed to be an uncoupled design expressed as follows.

$$\begin{Bmatrix} FR'_1 \\ FR'_2 \\ FR'_3 \end{Bmatrix} = \begin{bmatrix} \times & 0 & 0 \\ 0 & \times & 0 \\ 0 & 0 & \times \end{bmatrix} \begin{Bmatrix} DP'_1 \\ DP'_2 \\ DP'_3 \end{Bmatrix} \quad (D-7)$$

FR_1 and FR'_1 are the common functions to be merged. DP_1 and DP'_1 are the corresponding parameters in the physical domain.

The combination of the two rows representing the effect on the common functions in the DM of the equation (D-8) is implemented in the same way as in case 1 and case 2.

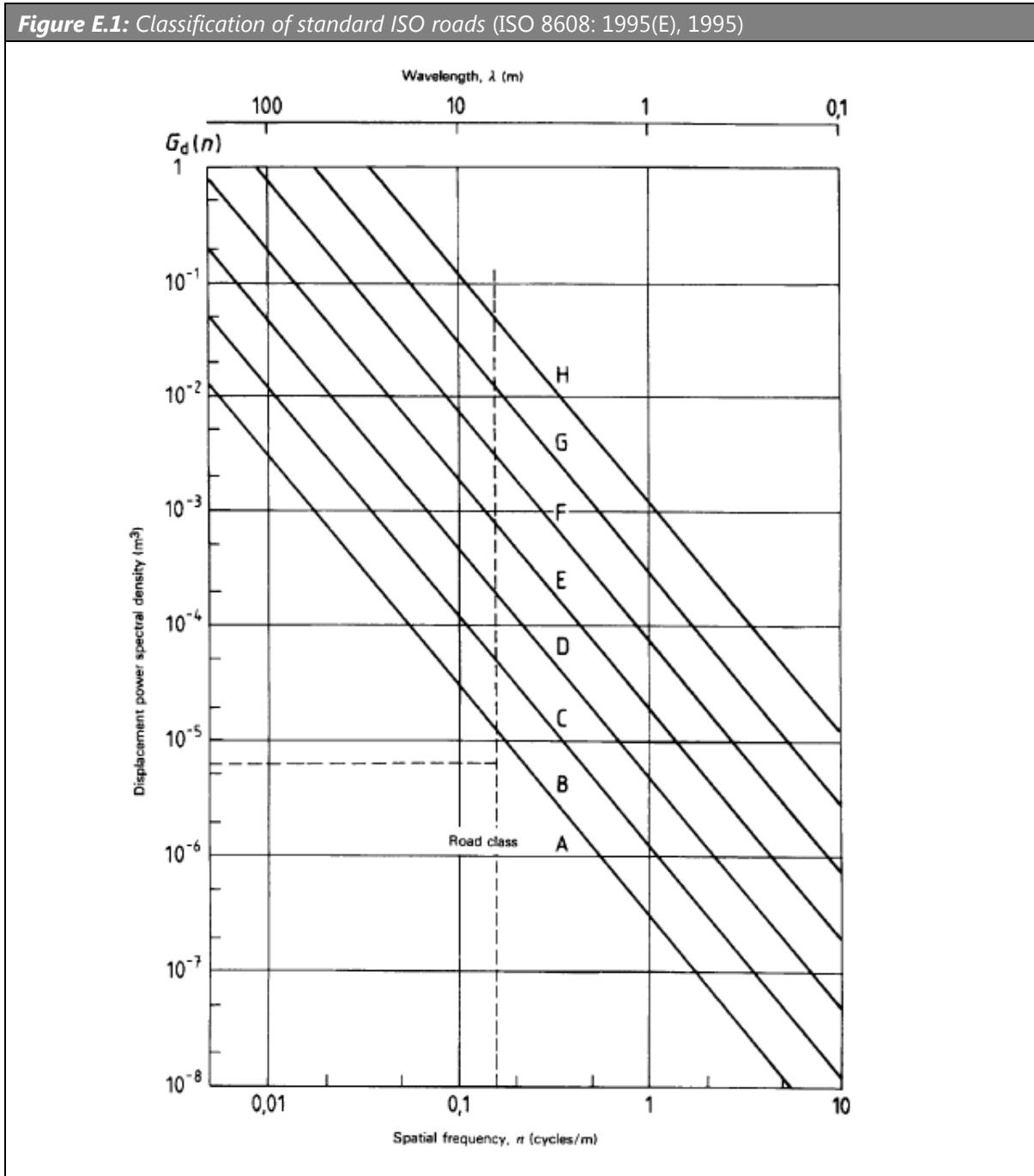
Defining the columns in the red vertical rectangles in equation (D-8) follows the principle that if either of the two combined DP s has an effect on an FR , the combined DP must have an effect on the FR . Because DP_1 has an effect on FR_3 in system 1, although the cross effect of DP'_1 on FR_3 is still unknown, it is determined that the combined DP''_1 has an effect on the FR_3 in the new system. The definition of other elements is the same as case 1 and 2.

$$\begin{array}{c}
 \left. \begin{array}{l} FR_1 \\ FR_2 \\ FR_3 \end{array} \right\} = \begin{array}{cc} & \begin{array}{ccc} P_1 & & P_2 \end{array} \\ \begin{array}{ccc} \times & 0 & 0 \\ 0 & \times & 0 \\ \times & 0 & \times \end{array} & \begin{array}{ccc} ? & ? & ? \\ ? & ? & ? \\ ? & ? & ? \end{array} \\ & \begin{array}{ccc} P_3 & & P_4 \end{array}
 \end{array} \left. \begin{array}{l} DP_1 \\ DP_2 \\ DP_3 \\ DP'_1 \\ DP'_2 \\ DP'_3 \end{array} \right\} \quad (D-8)
 \end{array}$$

After combination, the equation is written in the form of ((D-9).

$$\begin{array}{c}
 \left. \begin{array}{l} FR''_1 \\ FR_2 \\ FR_3 \end{array} \right\} = \begin{array}{cc} & \begin{array}{ccc} P_1 & & P_2 \end{array} \\ \begin{array}{ccc} \times & 0 & 0 \\ ? & \times & 0 \\ \times & 0 & \times \end{array} & \begin{array}{ccc} 0 & 0 & 0 \\ ? & ? & ? \\ ? & ? & ? \end{array} \\ & \begin{array}{ccc} P_3 & & P_4 \end{array}
 \end{array} \left. \begin{array}{l} DP''_1 \\ DP_2 \\ DP_3 \\ DP'_2 \\ DP'_3 \end{array} \right\} \quad (D-9)
 \end{array}$$

E. Graphed classification of standard ISO roads



F. Data of the suspension mass

Table F.1: Data of suspension mass		
Item	Mass / kg	Concept / kg
Wheel bearing m_b	1.65	1.65
Wheel spindle m_s	0.8	0.8
Wheel m_w	17	17
Spring m_{spring}	1.8	1.8
Damper m_{damper}	1.5	1.5
m_{brake}	Brake calipers	1.5
	Brake disc	3
Twist beam axle m_{axle}	Beam	8
	Arm	4.3
	Spring and damper supporter	0.7

Calculation of the unsprung mass

Reference suspension:

$$m_1 = m_b + m_s + m_w + m_{brake} + \frac{1}{2}(m_{spring} + m_{damper}) + \frac{1}{2}m_{axle} \frac{l_s}{l_L} \quad (\text{F-1})$$

$$= 30.4 \text{ kg}$$

Concept suspension:

$$m_1 = m_b + m_s + m_w + m_{brake} + \frac{1}{2}(m_{spring} + m_{damper}) + \frac{1}{2}m_{axle} \frac{1}{2} = 36.8 \text{ kg} \quad (\text{F-2})$$

Publication

Papers

M. Wang, A. Höfer, E. Beeh, P. Zhou, H. E. Friedrich, "Concept design and dynamics analysis of a novel lightweight vehicle suspension combined with driving units", *Proceedings of the Institution of Mechanical Engineers, Part D: Journal of Automobile Engineering*. 2019

M. Wang, A. Höfer, H. E. Friedrich, "Conceptual Design of Suspensions with Integrated Electric Motors on the basis of DSM", *DSM 2018-20th International DSM Conference*. 2018

M. Wang, A. Höfer, E. Beeh, H. E. Friedrich, "Function Integration for Lightweight Chassis based on Axiomatic Design and Design Structure Matrix", *International Journal of Automotive Technology*. 2018

M. Wang, E. Beeh, D. Krüger and H.E. Friedrich, "Topological optimization of a suspension concept considering the kinematics and compliance performance and the geometric non-linearity", *Proceedings of the Institution of Mechanical Engineers, Part D: Journal of Automobile Engineering*. 2017

P. Zhou, E. Beeh, M. Wang and H.E. Friedrich, "Dynamic tensile behaviors of AZ31B magnesium alloy processed by twin-roll casting and sequential hot rolling", *Elsevier: Transactions of Nonferrous Metals Society of China*. 2016

A. Höfer, D. Schlamp, M. Wang G. Kopp, G. Kopp, and H. Friedrich, "Development and Performance of An In-Wheel Suspension Concept with An Integrated E-Drive". FISITA 2016 World Automotive Congress, 2016, BEXCO, Busan, Korea.

Patents

DE102017205358 (A1). "Fahrwerksachse und Fahrzeug". M. Wang, E. Beeh, A. Höfer, O. Deißer. 2018-10-04

DE202017001665 (U1). "Fahrwerksbauteil und Kraftfahrzeug", M. Wang, E. Beeh, A. Höfer. 2018-07-02

DE102016203279(A1). "Fahrwerk für ein straßengebundenes Fahrzeug". M. Wang, E. Beeh. 2017-08-31

WO2017148692 (A1). "Twist-beam rear suspension with brace structure between the trailing arms". M. Wang, E. Beeh. 2017-09-08

Declaration

Ich versichere,

dass ich die Arbeit selbstständig verfasst habe, dass ich keine anderen als die angegebenen Quellen benutzt habe und ich alle wörtlich oder sinngemäß aus anderen Werken übernommenen Aussagen als solche gekennzeichnet habe, dass die eingereichte Arbeit weder vollständig noch in wesentlichen Teilen Gegenstand eines anderen Prüfungsverfahrens gewesen ist, dass ich die Arbeit noch nicht veröffentlicht habe und dass das elektronische Exemplar mit dem gedruckten Exemplar übereinstimmt.

Stuttgart, den 27.06.2019

Meng Wang

Meng Wang